Multichromophoric Arrays of Perylene Bisimide Dyes – Synthesis and Optical Properties

Dissertation zur Erlangung des
naturwissenschaftlichen Doktorgrades
der Bayerischen Julius-Maximilians-Universität Würzburg

vorgelegt von

Catharina Hippius

aus Jena

Würzburg 2007

Eingereicht am: _____

bei der Fakultät für Chemie und Pharmazie

1. Gutachter: _____

2. Gutachter: _____

der Dissertation.

1. Prüfer: _____

2. Prüfer: _____

3. Prüfer: _____

des öffentlichen Promotionskolloquiums.

Tag des öffentlichen Promotionskolloquiums:

_____

Doktorurkunde ausgehändigt am: _____

List of Abbreviations

A	(energy or electron) acceptor
Boc	*tert*-Butyloxycarbonyl
CR	charge recombination
CS	charge separation
CT	charge transfer
CV	cyclic voltammetry/voltammogram
D	(energy or electron) donor
EADS	evolution associated difference spectra
ESI	electro-spray ionization
FRET	fluorescence resonance energy transfer
HOMO	highest occupied molecular orbital
HPLC	high pressure liquid chromatography
IRF	instrument response function
LHS	light-harvesting system
LUMO	lowest unoccupied molecular orbital
MALDI	matrix-assisted laser desorption injection
NIR	near infrared
NP	normal phase
PET	photoinduced electron transfer
PBA	perylene-3,4:9,10-tetracarboxylic acid bisanhydride (perylene bisanhydride)
PBI	perylene-3,4:9,10-tetracarboxylic acid bisimide (perylene bisimide)
PMI	perylene-3,4:9,10-tetracarboxylic acid monoanhydride monoimide (perylene monoimide)
RT	room temperature
SADS	species associated difference spectra
TBAHFP	tetrabutylammoniumhexafluorophosphate
TLC	thin layer chromatography
UV	ultraviolet
vis	visible

Table of Contents

Aim of this Thesis

The light-driven reactions of photosynthesis are the means by which nature converts energy of light into a stable electrochemical potential, and accordingly, photosynthesis represents one of the most important processes in biological systems. It has been demonstrated that, for example, in purple bacteria in the early steps of photosynthesis the light energy is absorbed by a network of so-called antenna pigment proteins and very efficiently transported through energy transfer to the photochemical reaction center where the energy is converted through a sequence of electron transfer reactions.[1] Key requirement for the high efficiency of this process is the defined organization of a multitude of chromophores in space. Inspired by these biofunctional systems many organic chemists aim at artificial structures containing multiple chromophores that provide sequential energy transfer, but the realization of high efficiency and directionality remains a challenging task. On the one hand, this is due to the synthetic challenge to position dyes at predefined spatial positions and, on the other hand, competing processes like photoinduced electron transfer may take place between photoexcited dyes located in close proximity.[2] To date the majority of covalent multichromophoric architectures showing efficient directional energy transfer are either based on dendrimers[3,4] (in general, with energy transfer from peripheral chromophores to the core dye) or linear arrays of chromophores that are mostly linked by rigid π–conjugated spacers.[5,6]

Numerous classes of functional dyes have been employed in multichromophoric architectures among which, particularly, perylene bisimides (PBIs)[7] became popular to investigate the basic light-harvesting energy transfer processes.[8] Perylene bisimides are especially suitable for this purpose due to their bright photoluminescence with quantum yields up to unity, chemical inertness, and exceptional photostability.[7,9,10] Moreover, perylene bisimides show excellent n-type semiconductivity,[11] and have been applied widely as industrial pigments, laser dyes,[9,12] probes for single molecule spectroscopy,[4a,13] organic thin film transistors,[14] and solar cells.[15] Recently, their ability to form

supramolecular light-harvesting architectures by $\pi-\pi$-stacking, hydrogen-bonding or metal-ion-coordination has been explored.[7,16,17]

Calixarenes are supramolecular building blocks with distinct complexation capabilities that are obtained from the condensation of formaldehyde with *para*-alkylphenols under alkaline conditions.[18] They usually consist of phenolic units that are separated by methylene bridging groups. The name *calix* which means *beaker* in Latin and Greek was suggested by the bowl- or beakerlike shape of the cyclic tetramer in the *cone* conformation. Calixarenes are readily available in larger quantities by simple one-pot procedures[19] and are easily modified in various ways by reactions that can be independently carried out at the *narrow rim* (the phenolic hydroxy groups) and at the *wide rim* (the aromatic positions *para* to the phenolic hydroxy groups).[18,19] Consequently, they represent an ideal scaffold on which to assemble various desired functionalities such as nonlinear optical dyes,[20] electrophores,[21] and fluorophores.[22] Calixarenes have been also used as versatile building blocks for the construction of larger species through self-assembly by, for example, hydrogen bonding,[23] or metal-ion-coordination.[24] A covalent linkage of calix[4]arenes with perylene bisimides affords conjugates that combine the interesting properties of the individual building blocks.[25]

Aim of this thesis was the synthesis of calix[4]arene functionalized perylene bisimide dye arrays containing variate chromophoric units. Accordingly, a variety of multichromophoric conjugates composed of up to three different types of perylene bisimide chromophores (orange, red, and green PBIs) connected to each other by calix[4]arene spacers was envisioned, as well as their monochromophoric reference compounds. The obtained conjugates should be characterized with respect to their photochemical properties and light-harvesting ability by means of several steady state and time-resolved spectroscopic techniques. In this context, a new design principle for artificial light-harvesting architectures has been realized aiming at a zigzag-type of arrangements of perylene bisimide chromophoric units (for details see Chapter 4) which is exemplified in the schematic representation of a newly synthesized PBI-calix[4]arene light-harvesting array depicted in Figure 1. Furthermore, PBI-Calix[4]arene arrays composed of identical chromophores should be synthesized to elucidate intramolecular $\pi-\pi$-interactions of the PBI moieties.
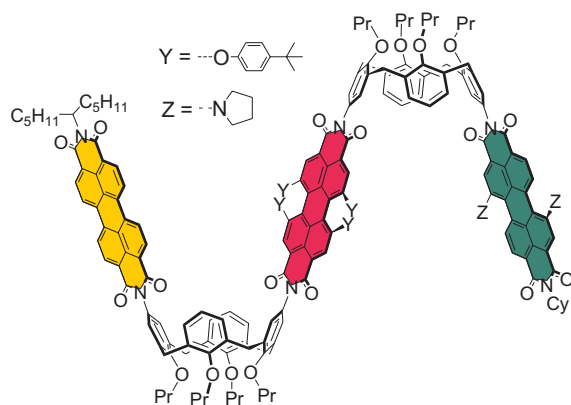
Figure 1. Schematic representation of a zigzag-type PBI-calix[4]arene light-harvesting array.

Chapter 1 gives a short overview of several architectures of artificial light-harvesting systems containing perylene bisimides. Furthermore, an introduction into the field of calix[4]arenes is given and important concepts of photoinduced processes are discussed briefly.

In *Chapter 2* the experimental techniques that have been applied are described shortly.

In *Chapter 3* the synthesis of a series of mono- and biscalix[4]arene substituted PBI chromophores is described employing orange, red, and green perylene bisimide units. For the orange calix[4]arene-PBI systems photoinduced fluorescence quenching of the perylene bisimide chromophore is observed. The excited state processes are investigated by femtosecond transient absorption spectroscopy, streak camera measurements, and spectroelectrochemistry, and the excited state processes are evaluated by means of global and target analysis revealing a very efficient photoinduced electron transfer process from the electron-rich calix[4]arene moiety to the PBI core.

Chapter 4 describes the construction of a variety of multichromophoric perylene bisimide arrays composed of orange, red, and green PBI units that are linked by calix[4]arene spacers and between which very efficient energy transfer processes are observed. The latter are investigated by UV/vis absorption and steady state and time-resolved fluorescence spectroscopy as well as femtosecond transient absorption measurements. An excellent agreement of the experimentally obtained rate constants of the energy transfer with those calculated from the Förster theory is found.

Chapter 5 provides details on synthesis and opical properties of a series of orange, red, and green perylene bisimide dimers linked by a calix[4]arene spacer. An equilibrium between

the two possible *pinched cone* conformations of the calix[4]arene unit is observed which is influenced by solvent polarity and sterical hindrance of the respective PBI substituents. The effects in various solvents are discussed by means of UV/vis absorption, steady state and time-resolved fluorescence spectroscopy, and femtosecond transient absorption spectroscopy.

The thesis concludes with summaries in English (*Chapter 6*) and German (*Chapter 7*).

References

(1)   (a) Huber, R. *Angew. Chem., Int. Ed. Engl.* **1989**, *28*, 848–869. (b) Pullerits, T.; Sundström, V. *Acc. Chem. Res.* **1996**, *29*, 381–389. (c) Ritz, T.; Damjanović, A.; Schulten, K. *ChemPhysChem* **2002**, *3*, 243–248. (d) Hu, X.; Ritz, T.; Damjanović, A.; Autenrieth, F.; Schulten, K. *Q. Rev. Biophys.* **2002**, *35*, 1–62. (e) *Molecular Mechanisms of Photosynthesis*; Blankenship, R. E.; Blackwell Science: Oxford, 2002. (f) Cogdell, R. J.; Lindsay, J. G. *New Phytol.* **2000**, *145*, 167–196. (g) Holzwarth, A. R. In *Series on Photoconversion of Solar Energy*; Archer, M. D., Barber, J., Eds.; Imperial College Press: London, UK, 2002; pp 43–115. (h) Katz, J. J. *Photosynth. Res.* **1990**, *26*, 143–160.

(2)   (a) Paddon-Row, M. N. In *Stimulating Concepts in Chemistry*; Vögtle, F., Stoddart, J. F., Shibasaki, M., Eds.; Wiley-VCH: Weinheim, Germany, 2000; pp 267–291. (b) Armaroli, N. *Photochem. & Photobiol. Sci.* **2003**, *2*, 73–87. (c) Barigelletti, F.; Flamigni, L. *Chem. Soc. Rev.* **2000**, *29*, 1–12. (d) Guldi, D. M. *Chem. Soc. Rev.* **2002**, *31*, 22–36. (e) Holten, D.; Bocian, D. F.; Lindsey, J. S. *Acc. Chem. Res.* **2002**, *35*, 57–69. (f) Prodi, A.; Indelli, M. T.; Kleverlaan, C. J.; Alessio, E.; Scandola, F. *Coord. Chem. Rev.* **2002**, *229*, 51–58. (g) Harriman, A.; Sauvage, J.-P. *Chem. Soc. Rev.* **1996**, *25*, 41–48. (h) Nakamura, Y.; Hwang, I.-W.; Aratani, N.; Ahn, T. K.; Ko, D. M.; Takagi, A.; Kawai, T.; Matsumoto, T.; Kim, D.; Osuka, A. *J. Am. Chem. Soc.* **2005**, *127*, 236–246. (i) Balzani, V.; Juris, A. *Coord. Chem. Rev.* **2001**, *211*, 97–115. (j) Wasielewski, M. R. *Chem. Rev.* **1992**, *92*, 435–461. (k) Gust, D.; Moore, T. A.; Moore, A. L. *Acc. Chem. Res.* **2001**, *34*, 40–48. (l) Wasielewski, M. R. *J. Org. Chem.* **2006**, *71*, 5051–5066. (m) Scandola, F.; Indelli, M. T.; Chiorboli, C.; Bignozzi, C. A. *Top. Curr. Chem.* **1990**, *158*, 73–149. (n) Choi, M.-S.; Yamazaki, T.; Yamazaki, I.; Aida, T. *Angew. Chem., Int. Ed. Engl.* **2004**, *43*, 150–158.

(3)   For general examples on light-harvesting dendrimers, see: (a) Dirksen, A.; De Cola, L. *C. R. Chimie* **2003**, *6*, 873–882. (b) *Dendritic Molecules: Concepts, Syntheses, Perspectives*; Newkome, G. R.; Moorefield, C. N.; Vögtle, F., Eds.; VCH: New York, 1996. (c) Balzani, V.; Ceroni, P.; Maestri, M.; Saudan, C.; Vicinelli, V. *Top. Curr. Chem.* **2003**, *228*, 159–191. (d) Venturi, M; Serroni, S.; Juris, A.; Campagna, S.; Balzani, V. *Top. Curr. Chem.* **1998**, *197*, 193–228. (e) Hahn, U.; Gorka, M.; Vögtle, F.; Vicinelli, V.; Ceroni, P.; Maestri, M.; Balzani, V. *Angew. Chem., Int. Ed. Engl.* **2002**, *41*, 3595–3598. (f) Balzani, V.; Ceroni, P.; Maestri, M.; Vicinelli, V. *Curr. Opin. Chem. Biol.* **2003**, *7*, 657–665. (g) Balzani, V.; Campagna, S.; Denti, G.; Juris, A.; Serroni, S.; Venturi, M. *Acc. Chem. Res.* **1998**, *31*, 26–34.

(4)   For light-harvesting dendrimers containing perylene bisimides, see: (a) De Schryver, F. C.; Vosch, T.; Cotlet, M.; Van der Auweraer, M.; Müllen, K.; Hofkens, J. *Acc. Chem. Res.* **2005**, *38*, 514–522. (b) Serin, J. M.; Brousmiche, D. W.; Fréchet, J. M. J. *Chem. Commun.* **2002**, 2605–2607. (c) Serin, J. M.; Brousmiche, D. W.; Fréchet, J. M. J. *J. Am. Chem. Soc.* **2002**, *124*, 11848–11849. (d) Gronheid, R.; Stefan, A.; Cotlet, M.; Hofkens, J.; Qu, J.; Müllen, K.; Van der Auweraer, M.; Verhoeven, J. W.; De Schryver, F. C. *Angew. Chem., Int. Ed. Engl.* **2003**, *42*, 4209–4214. (e) Weil, T.; Reuther, E.; Müllen, K. *Angew. Chem., Int. Ed. Engl.* **2002**, *41*, 1900–1904. (f) Gronheid, R.; Hofkens, J.; Köhn, F.; Weil, T.; Reuther, E.; Müllen, K.; De Schryver, F. C. *J. Am. Chem. Soc.* **2002**, *124*, 2418–2419. (g) Jordens, S.; De Belder, G.; Lor, M.; Schweitzer, G.; Van der Auweraer, M.; Weil, T.; Reuther, E.; Müllen, K.; De Schryver, F. C. *Photochem. Photobiol. Sc.* **2003**, *2*, 177–186.

(5)   For general examples of linear light-harvesting arrays, see: (a) Ziessel, R.; Hissler, M.; El-ghayoury, A.; Harriman, A. *Coord. Chem. Rev.* **1998**, *178-180,* 1251–1298. (b) Aratani, N.; Osuka, A.; Cho, H. S.; Kim, D. *J. Photochem. Photobiol. C* **2002,** *3*, 25–52. (c) Bossart, O.; De Cola, L.; Welter, S.; Calzaferri, G. *Chem. Eur. J.* **2004**, *10*, 5771–5775. (d) Berglund Baudin, H.; Davidsson, J.; Serroni, S.; Juris, A.; Balzani, V.; Campagna, S.; Hammarström, L. *J. Phys. Chem. A* **2002,** *106*, 4312–4319. (e) Chiorboli, C.; Indelli, M. T.; Scandola, F. *Top. Curr. Chem.* **2005**, *257*, 63–102. (f) Harriman, A.; Ziessel, R. *Coord. Chem. Rev.* **1998**, *171,* 331–339. (g) Yang, S. I.; Seth, J.;

Balasubramanian, T. Kim, D. Lindsey, J. S.; Holten, D.; Bocian, D. F. *J. Am. Chem. Soc.* **1999**, *121*, 4008–4018.

(6)   For examples containing perylene bisimides, see: (a) Prathapan, S.; Yang, S. I.; Seth, J.; Miller, M. A.; Bocian, D. F.; Holten, D.; Lindsey, J. S. *J. Phys. Chem. B* **2001,** *105,* 8237–8248. (b) Rybtchinski, B.; Sinks, L. E.; Wasielewski, M. R. *J. Am. Chem. Soc.* **2004**, *126*, 12268–12269. (c) Langhals, H.; Saulich, S. *Chem. Eur. J.* **2002**, *8*, 5630–5643. (d) Ego, C.; Marsitzky, D.; Becker, S.; Zhang, J.; Grimsdale, A. C.; Müllen, K.; MacKenzie, J. D.; Silva, C.; Friend, R. H. *J. Am. Chem. Soc.* **2003**, *125*, 437–443. (e) Loewe, R. S.; Tomizaki, K.-Y.; Youngblood, W. J.; Bo, Z.; Lindsey, J. S. *J. Mat. Chem.* **2002**, *12*, 3438–3451. (f) Schlichting, P.; Duchscherer, B.; Seisenberger, G.; Basché, T.; Bräuchle, C.; Müllen, K. *Chem. – Eur. J.* **1999**, *5*, 2388–2395. (g) Metivier, R.; Nolde, F.; Müllen, K.; Basché, T. *Phys. Rev. Lett.* **2007**, *98*, 047802/1–047802/4. (h) Hinze, G.; Haase, M.; Nolde, F.; Müllen, K.; Basché, T. *J. Phys. Chem. A* **2005**, *109*, 6725–6729.

(7)   Würthner, F. *Chem. Commun.* **2004**, 1564–1579.

(8)   (a) Sautter, A.; Kaletas, B. K.; Schmid, D. G.; Dobrawa, R.; Zimine, M.; Jung, G.; Van Stokkum, I. H. M.; De Cola, L.; Williams, R. M.; Würthner, F. *J. Am. Chem. Soc.* **2005**, *127*, 6719–6729. (b) You, C.-C.; Hippius, C.; Grüne, M.; Würthner, F. *Chem. – Eur. J.* **2006**, *12,* 7510–7519. (c) Flamigni, L.; Ventura, B.; You, C.-C.; Hippius, C.; Würthner, F. *J. Phys. Chem. C* **2007**, *111*, 622–630. (d) Prodi, A.; Chiorboli, C.; Scandola, F.; Iengo, E.; Alessio, E.; Dobrawa, R.; Würthner, F. *J. Am. Chem. Soc.* **2005**, *127*, 1454–1462. (e) Kaletas, B. K.; Dobrawa, R.; Sautter, A.; Würthner, F.; Zimine, M.; De Cola, L.; Williams, R. M. *J. Phys. Chem. A* **2004**, *108*, 1900–1909.

(9)   Gvishi, R.; Reisfeld, R.; Burshtein, Z. *Chem. Phys. Lett.* **1993**, *213*, 338–344.

(10)   Langhals, H. *Heterocycles*, **1995**, *40*, 477–500.

(11)   (a) Schlettwein, D.; Wöhrle, D.; Karmann, E.; Melville, U. *Chem. Mater.* **1994**, *6*, 3–6. (b) Katz, H. E.; Bao, Z.; Gilat, S. L. *Acc. Chem. Res.* **2001**, *34*, 359–369. (c) Dimitrakopoulos, C. D.; Malenfant, P. R. L. *Adv. Mater.* **2002**, *14*, 99–117.

(12)   Sadrai, M.; Hadel, L.; Sauers, R. R.; Husain, S.; Krogh-Jespersen, K.; Westbro, J. D.; Bird, G. R. *J. Phys. Chem.* **1992**, *96*, 7988–7996.

(13)   (a) Zang, L.; Liu, R.; Holman, M. W.; Nguyen, K. T.; Adams, D. M. *J. Am. Chem. Soc.* **2002**, *124*, 10640–10641. (b) Sauer, M. *Angew. Chem. Int. Ed.* **2003**, 42, 1790 – 1793. (c) Han, J. J.; Wang, W.; Li, A. D. Q. *J. Am. Chem. Soc.* **2006**, *128*, 672–673.

(14)   Horowitz, G.; Kouki, F.; Spearman, P.; Fichou, D.; Nogues, C.; Pan, X.; Garnier, F. *Adv. Mater.* **1996**, *8*, 242–245.

(15)   (a) Malenfant, P. R. L.; Dimitrakopoulos, C. D.; Gelorme, J. D.; Kosbar, L. L.; Graham, T. O.; Curioni, A.; Andreoni, W. *Appl. Phys. Lett.* **2002**, *80*, 2517–2519. (b) Tang, C. W. *App. Phys. Lett.* **1986**, *48*, 183–185.

(16)   You, C.-C.; Dobrawa, R.; Saha-Möller, C. R.; Würthner, F. *Top. Curr. Chem.* **2005**, *258*, 39–82.

(17)   *Supramolecular Dye Chemistry*; Würthner, F., Ed.; Topics in Current Chemistry 258, Springer-Verlag: Berlin, 2005.

(18)   (a) *Calixarenes 2001*; Asfari, Z., Böhmer, V., Harrowfield, J., Eds.; Kluwer Academic Publishers: Dordrecht, 2001. (b) *Calixarenes*; Gutsche, C. D.; The Royal Society of Chemistry: Cambridge, 1993. (c) *Calixarenes Revisited*; Gutsche, C. D.; The Royal Society of Chemistry: Letchworth, 1998. (d) Böhmer, V.; *Angew. Chem., Int. Ed. Engl.* **1995**, *34*, 713–745. (e) *Calixarenes in Action*; Mandolini, L., Ungaro, R., Eds.; Imperial College Press: London, 2000.

(19)   (a) Gutsche, C. D.; Iqbal, M. *Org. Synth.* **1990**, *68*, 234–237. (b) Gutsche, C. D.; Dhawan, B.; Leonis, M.; Stewart, D. *Org. Synth.* **1990**, *68*, 238–242. (c) Munch, J. H.; Gutsche, C. D. *Org. Synth.* **1990**, *68*, 243–246.

(20)   Kenis, P. J. A.; Noordman, O. F. J.; Houbrechts, S.; van Hummel, G. J.; Harkema, S.; van Veggel, F. C. J. M.; Clays, K.; Engbersen, J. F. J.; Persoons, A.; van Hulst, N. F.; Reinhoudt, D. N. *J. Am. Chem. Soc.* **1998**, *120*, 7875–7883.

(21)   (a) Zhao, B.-T.; Blesa, M.-J.; Mercier, N.; Le Derf, F.; Sallé, M. *J. Org. Chem.* **2005**, *70*, 6254–6257. (b) Yu, H.-h.; Xu, B.; Swager, T. M. *J. Am. Chem. Soc.* **2003**, *125*, 1142–1143. (c) Scherlis, D. A.; Marzari, N. *J. Am. Chem. Soc.* **2005**, *127*, 3207–3212. (d) Yu, H.-h.; Pullen, A. E.; Büschel, M. G.; Swager, T. M. *Angew. Chem., Int. Ed. Engl.* **2004**, *43*, 3700–3703.

(22)   (a) Schazmann, B.; Alhashimy, N.; Diamond, D. *J. Am. Chem. Soc.* **2006**, *128*, 8607–8614. (b) Souchon, V.; Leray, I.; Valeur, B. *Chem. Commun.* **2006**, 4224–4226. (c) Lee, S. H.; Kim, S. H.; Kim, S. K.; Jung, J. H.; Kim, J. S. *J. Org. Chem.* **2005**, *70*, 9288–9295. (d) Kim, S. K.; Bok, J. H.; Bartsch, R. A.; Lee, J. Y.; Kim, J. S. *Org. Lett.* **2005**, *7*, 4839–4842. (e) Kim, S. K.; Lee, S. H.; Lee, J. Y.; Bartsch, R. A.; Kim, J. S. *J. Am. Chem. Soc.* **2004**, *126*, 16499–16506. (f) Leray, I.; Lefevre, J.-P.; Delouis, J.-F.; Delaire, J.; Valeur, B. *Chem.–Eur. J.* **2001**, *7*, 4590–4598. (g) van der Veen, N.; Flink, S.; Deij, M. A.; Egberink, R. J. M.; van Veggel, F. C. J. M.; Reinhoudt, D. N. *J. Am. Chem. Soc.* **2000**, *122*, 6112–6113. (h) Ji, H.-F.; Dabestani, R.; Brown, G. M.; Sachleben, R. A. *Chem. Commun.* **2000**, 833–834. (i) Ji, H.-F.; Brown, G. M.; Dabestani, R. *Chem. Commun.* **1999**, 609–610. (j) Jin, T.; *Chem. Commun.* **1999**, 2491–2492. (k) Larey, I.; O'Reilly, F.; Habib Jiwan, J.-L.; Soumillion, J.-Ph.; Valeur, B. *Chem. Commun.* **1999**, 795–796. (l) Beer, P. D.; Timoshenko, V.; Maestri, M.; Passaniti, P.; Balzani, V. *Chem. Commun.* **1999**, 1755–1756. (m) Unob, F.; Asfari, Z.; Vicens, J. *Tetrahedron Lett.* **1998**, *39*, 2951–2954. (n) Jin, T.; Monde, K. *Chem. Commun.* **1998**, 1357–1358. (o) Ikeda, A.; Yoshimura, M.; Lhotak, P.; Shinkai, S. *J. Chem. Soc., Perkin Trans. 1*, **1996**, 1945–1950. (p) Grigg, R.; Holmes, J. M.; Jones, S. K.; Norbert, W. D. J. A. *J. Chem. Soc., Chem. Comm.* **1994**, 185–187. (q) Aoki, I.; Sakaki, T.; Shinkai, S. *J. Chem. Soc., Chem. Comm.* **1992**, 730–732. (r) Jin, T.; Ichikawa, K.; Koyama, T. *J. Chem. Soc., Chem. Comm.* **1992**, 499–501.

(23)   (a) Prins, L. J.; Reinhoudt, D. N.; Timmerman, P. *Angew. Chem., Int. Ed. Engl.* **2001**, *40*, 2382–2426. (b) Rebek, J., Jr. *Chem. Commun.* **2000**, 637–643. (c) Böhmer, V.; Vysotsky, M. O. *Aust. J. Chem.* **2001**, *54*, 671–677. (d) Conn, M. M.; Rebek, J., Jr. *Chem. Rev.* **1997**, *97*, 1647–1668.

(24)   (a) Steyer, S.; Jeunesse, C.; Armspach, D.; Matt, D.; Harrowfield, J. Coordination Chemistry and Catalysis. In *Calixarenes 2001*; Asfari, Z., Böhmer, V., Harrowfield, J., Vicens, J., Eds.; Kluwer: Dordrecht, The Netherlands, 2001; pp 513–535. (b) Fochi, F.; Jacopozzi, P.; Wegelius, E.; Rissanen, K.; Cozzini, P.; Marastoni, E.; Fisicaro, E.; Manini, P.; Fokkens, R.; Dalcanale, E. *J. Am. Chem. Soc.* **2001**, *123*, 7539–7552.

(25)   (a) Vysotsky, M. O.; Böhmer, V.; Würthner, F.; You, C.-C.; Rissanen, K. *Org. Lett*. **2002**, *4*, 2901–2904. (b) Van der Boom, T.; Evmenenko, G.; Dutta, P.; Wasielewski, M. R. *Chem. Mater.* **2003**, *15*, 4068–4074.

1

Introduction

Abstract: This chapter gives an overview of covalently and non-covalently constructed artificial light-harvesting architectures containing perylene bisimides. Accordingly, rigid linear arrays, self-assembled molecular squares and dendrimeric structures constructed from PBIs are discussed on the basis of individual examples from the literature. Furthermore, an introduction into the field of calix[4]arenes is given dealing with general nomenclature and conformational aspects, including the differentiation of the various conformers by NMR spectroscopy, as well as the further chemical functionalization strategies of the parent calix[4]arene skeleton. Finally, important concepts of photoinduced processes such as energy transfer mechanisms and basic principles of electron transfer theory are discussed briefly.

1.1   Perylene Bisimides in Artificial Light-Harvesting Architectures

Photoinduced energy transfer processes play a key role in the primary steps of photosynthesis.[1] In the natural photosynthetic systems these transfer processes are performed by extremely complex, highly organized multi-component structures (light-harvesting complexes).[2,3] Accordingly, an antenna or light-harvesting system (LHS) is an arrangement of a multitude of chromophores in space exhibiting distinct absorption and redox properties. Light-harvesting systems absorb the incident solar light and funnel the excitation energy by multi-step directional energy transfer to a common acceptor component. The underlying basic principles are schematically illustrated in Figure 1. In the course of evolution, nature has produced antenna systems that collect a considerable amount of solar energy and redirect it as electronic excitation energy to reaction centers, where subsequent conversion into redox chemical energy takes place.[3,4] Recently, much attention has been devoted to the design and synthesis of molecular or supramolecular species that can function as antennas in *artificial* systems for the photochemical conversion of solar energy.
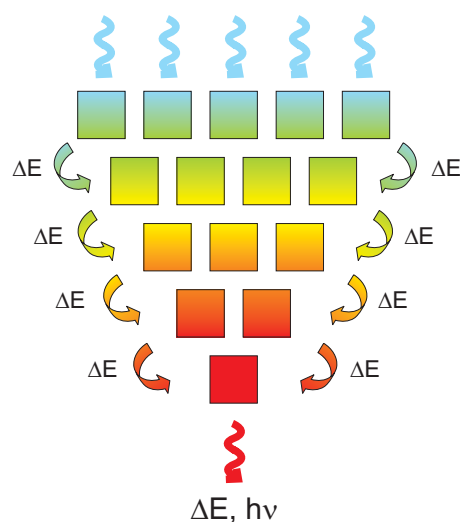
Figure 1. Schematic representation of an artificial light-harvesting antenna system. Absorption of light by an array of chromophores is followed by sequential and directional energy transfer that leads the excitation energy to a reaction center.[1c,h]

Essential properties of light-harvesting systems are, first, the capacity to absorb light over a substantial part of the visible spectral region, and, second, their chemical and photochemical stability. Furthermore, as schematized in Figure 1, in an antenna system the

excitation energy must be delivered to a common acceptor component. This implies the occurrence of a sequence of energy transfer steps along predetermined directions. To ensure a high light-harvesting efficiency, each energy transfer step must successfully compete with the intrinsic decay of the excited state as well as with other excited state deactivation processes, such as electron transfer, and exciplex and excimer formation. Numerous classes of functional dyes have been employed to design multichromophoric architectures among which, particularly, perylene bisimides (PBIs) have been proven to meet these requirements to a high degree due to their strong and furthermore tunable absorption in the visible region, their bright photoluminescence with quantum yields up to unity, their chemical inertness and low triplet yield, and also their exceptional photostability.[5-7] Perylene bisimides have been utilized in various electronic and optical applications such as photovoltaic cells,[8] dye lasers,[5,9] light-emitting diodes,[10] field-effect transistors,[11] electrophotographic devices[12] and solar collectors.[13] Furthermore, their ability to form supramolecular light-harvesting architectures by $\pi-\pi$-stacking, hydrogen-bonding or metal-ion-coordination[7,14] justifies their wide use as building blocks for the design and synthesis of artificial antenna model systems. Accordingly, perylene bisimides (among other classes of functional dyes) have been incorporated successfully into a variety of covalently constructed and self-assembled light-harvesting architectures such as *rigid linear arrays* of chromophores linked by spacer units,[15,16] *molecular squares*[17] as well as *dendrimers* (in general, with energy transfer from peripheral dyes to the core dye).[18,19] In this section, a short survey of literature is given on multichromophoric architectures containing perylene bisimide moieties in which photoinduced energy transfer processes occur.

1.1.1   Linear Light-Harvesting Arrays

Wasielewski and coworkers were pioneering in the study of photoinduced processes in covalently linked perylene bisimide–porphyrin systems.[15a] In their early work, two porphyrin donors rigidly attached to a perylene bisimide moiety (see Figure 2) are designed as a light-intensity dependent molecular biphotonic switch on a picosecond time scale. Excitation of the porphyrins within this molecular switch results in single or double reduction of the acceptor unit depending on the light intensity.[15a]
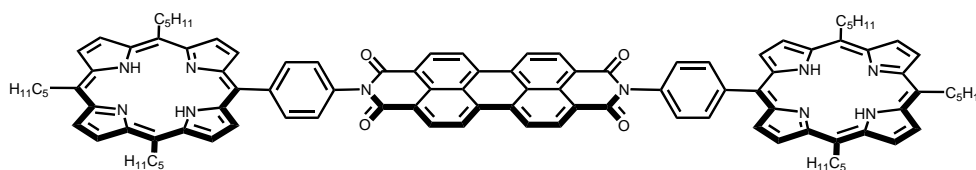
Figure 2. Chemical structure of the porphyrin–perylene bisimide system designed by Wasielewski and coworkers as a light-intensity dependent molecular switch.[15a]

The photophysical properties of a perylene bisimide-zinc porphyrin dyad shown in Figure 3 have been examined by Lindsey and coworkers with the aim of application in molecular photonics.[15b] The dyad consists of a perylene bisimide dye connected to a zinc porphyrin via a diphenylethylene linker (pep). In both polar and nonpolar solvents, the photoexcited perylene unit PBI* decays very rapidly with lifetimes of 2.5 ps in toluene and 2.4 ps in acetonitrile by directional energy transfer to the porphyrin moiety, forming the singlet excited state of the Zn-porphyrin PBI-pep-Zn* in high yields (80% in toluene; 70% in acetonitrile), and a subsequent hole transfer product PBI$^{\bullet-}$-pep-Zn$^{\bullet+}$ in lower yield (20% in toluene; 30% in acetonitrile). This suggests that perylene bisimides have significant potential as accessory pigments in porphyrin-based arrays for light-harvesting and energy-transport applications.
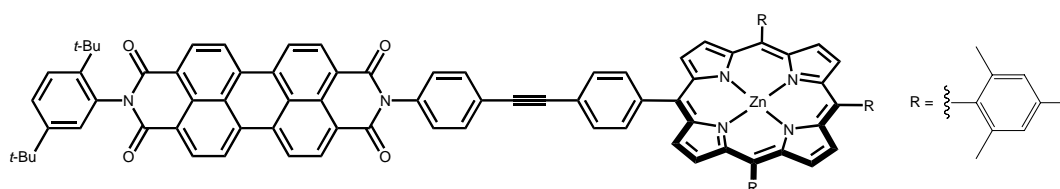
Figure 3. Chemical structure of the perylene bisimide–zinc porphyrin dyad connected via a diphenylethylene linker.[15b]

According to Wasielewski and coworkers the antenna reaction-center array shown in Figure 4 can be prepared by functionalization of a 1,7-dipyrrolidino-perylene bisimide chromophore with four 1,7-(3',5'-di-*tert*-butylphenoxy)-perylene bisimide moieties which self-assembles to form stacked dimers in toluene.[15c] Self-assembly is used here to produce an artificial light-harvesting antenna structure containing a functional special pair unit of two stacked 1,7-pyrrolidino-substituted PBIs (see schematic representation in Figure 4, right). Energy transfer from the 1,7-(3',5'-di-*tert*-butylphenoxy)-perylene bisimide moiety to the 1,7-dipyrrolidino-perylene bisimide unit occurs with τ = 21 ps, followed by ultrafast

and quantitative charge separation due to excited-state symmetry breaking to produce a charge separated state quantitatively with τ = 7 ps consisting of the respective 1,7-dipyrrolidino-perylene bisimide monoanion and -cation. The ion pair recombines with τ = 420 ps. Notably, the electron transfer occurs only in the dimeric system and is not observed in the disassembled monomer, thus mimicking both antenna and special pair function in photosynthesis.
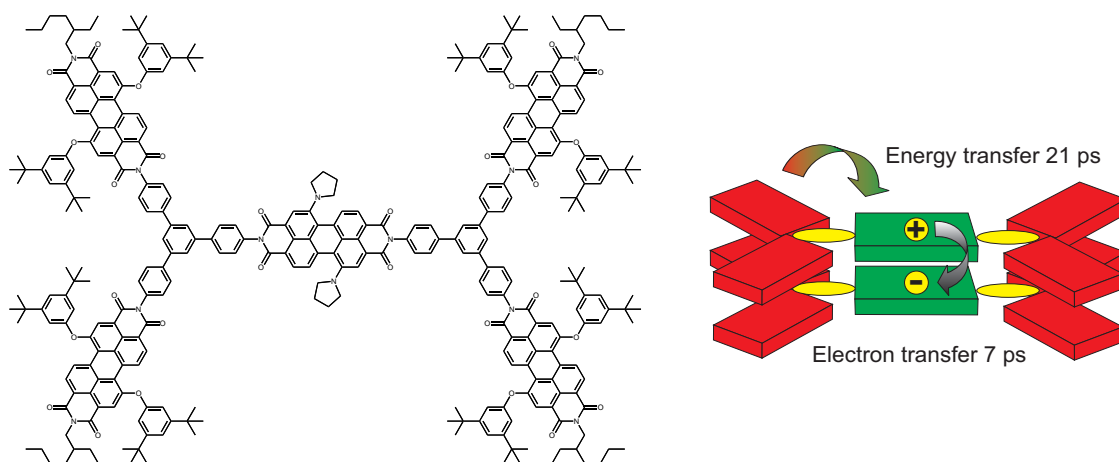
Figure 4. Chemical structure of the antenna reaction-center array obtained by functionalization of a 1,7-dipyrrolidino-perylene bisimide chromophore with four 1,7-(3',5'-di-*tert*-butylphenoxy)-perylene bisimide moieties (left) and schematic representation of the processes occurring in the excited state after photoexcitation (right).[15c]

Unidirectional electronic excitation energy transfer in a dyad consisting of a perylene bisimide donor and a terrylene bisimide acceptor separated at a fixed distance by a rigid *p*-terphenyl spacer (see Figure 5) has also been investigated by means of low temperature high-resolution single molecule spectroscopy by Basché, Müllen and coworkers.[15h] Density-functional theory calculations reveal a nearly linear geometry for this dyad, and the coupling between the two chromophores in the dyad is found to be negligible. Almost quantitative energy transfer is observed, as the lifetime of the perylene bisimide moiety is reduced to 4 ps compared of the value of several nanoseconds observed for the free chromophore. The authors are furthermore able to accurately access static disorder in the donor and acceptor electronic transitions and to calculate the spectral overlap for each couple.
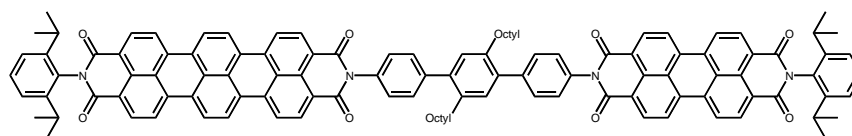
Figure 5. Chemical structure of the perylene bisimide (donor)-terrylene bisimide (acceptor) dyad with a *p*-terphenyl bridge studied by Basché, Müllen and coworkers.[15h]

1.1.2   Light-Harvesting Molecular Square Assemblies

Perylene bisimides have also been incorporated into light-harvesting structures by metal-ion coordination resulting in self-assembled molecular squares. A recent example of such a square incorporating sixteen pyrene chromophores attached to four ditopic *bay*-functionalized perylene bisimide chromophores is shown in Figure 6.[17d] Steady state and time-resolved emission as well as femtosecond transient absorption studies reveal the presence of a highly efficient (> 90%) and fast photoinduced energy transfer with a rate constant of k = 5.0 x 10^9 s^{-1} from the pyrene to the perylene bisimide chromophores, and additionally a very fast and efficient electron transfer (> 94%) with rate constants ranging from k = 5 x 10^{11} up to 43 x 10^{11} s^{-1}. Temperature-dependent time-resolved emission spectroscopy has shown that the acceptor emission lifetime increases with decreasing temperature from which an electron-transfer barrier of $\Delta G^{\#}$ = 0.098 eV is obtained. Likewise, for a similar molecular square bearing naphthalene units instead of pyrene functionalization also very efficient energy transfer (>95%) processes have been observed.[17e] Furthermore, the square scaffold containing in this case aminonaphthalimide antenna dyes instead of pyrene moieties exhibits a more than seven times higher fluorescence quantum yield (Φ_{fl} = 0.37) compared to the pyrene-bearing perylene bisimide-walled square (Φ_{fl} = 0.05).
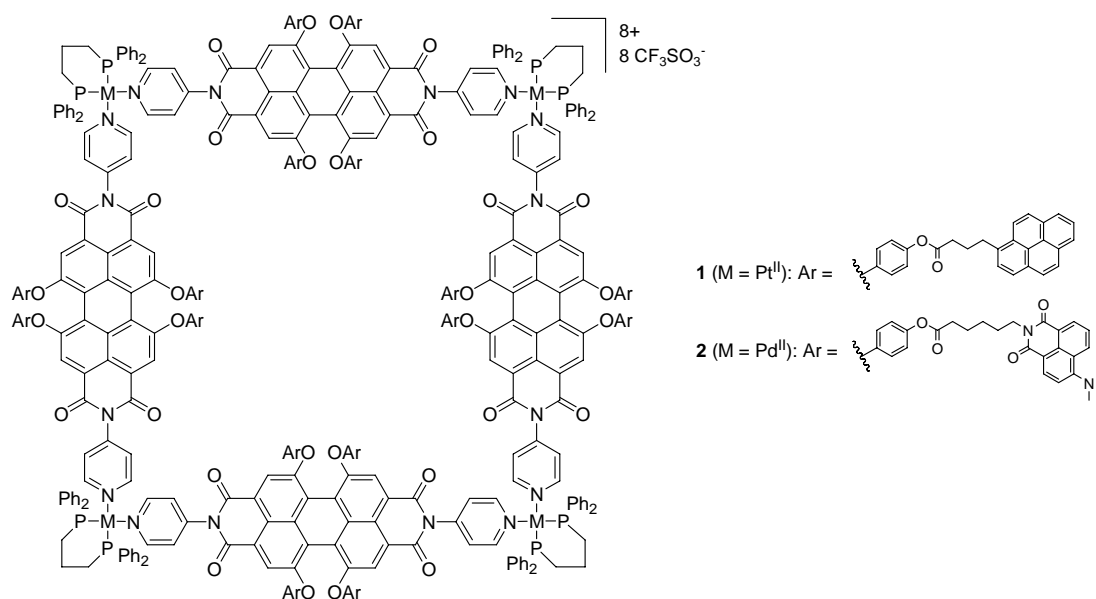
Figure 6. Chemical structures of self-assembled light-harvesting molecular squares containing four perylene bisimide moieties functionalized each with either four pyrene[17d] (compound **1**) or naphthalene[17e] units (compound **2**) in the *bay*-positions.

1.1.3   Dendritic Light-Harvesting Structures

A great variety of the artificial antennas known today are dendrimers, that are characterized by a more or less globular structure and the possibility to arrange selected chemical units in predetermined sites of their structure. A number of fascinating dendritic derivatives have been synthesized and studied by the groups of Müllen and De Schryver.[18a-f] The combination of chemically very stable, shape-persistent polyphenylene dendrimers and perylene imide chromophores opened up the possibility to derive outstanding multichromophoric arrays, in which the relative position and orientation of the chromophores is fixed in space and determined by the synthetic route. For example, the polyphenylenic first generation donor-acceptor dendrimer depicted in Figure 7, left, contains four perylene monoimide units (denoted as P in Figure 7, left) as energy donors on the periphery and one terrylene bisimide unit (denoted as T in Figure 7, left) acting as the acceptor unit in the center of the molecule. In contrast, the respective second generation analogue depicted in Figure 7, right, bears eight perylene monoimide chromophores at the rim.[18d,f] The donor and acceptor units show a good spectral overlap between the fluorescence emission of the donor with the UV/vis absorption of the acceptor

component.[18d] As a consequence, very efficient energy transfer processes are observed, and the fluorescence lifetime of the PMI unit is reduced to ~5 ps within the dendritic structure compared to the value of 4.2 ns observed for the free perylene imide chromophore, in both assembly measurements as well as on single molecule level.[18d,f]
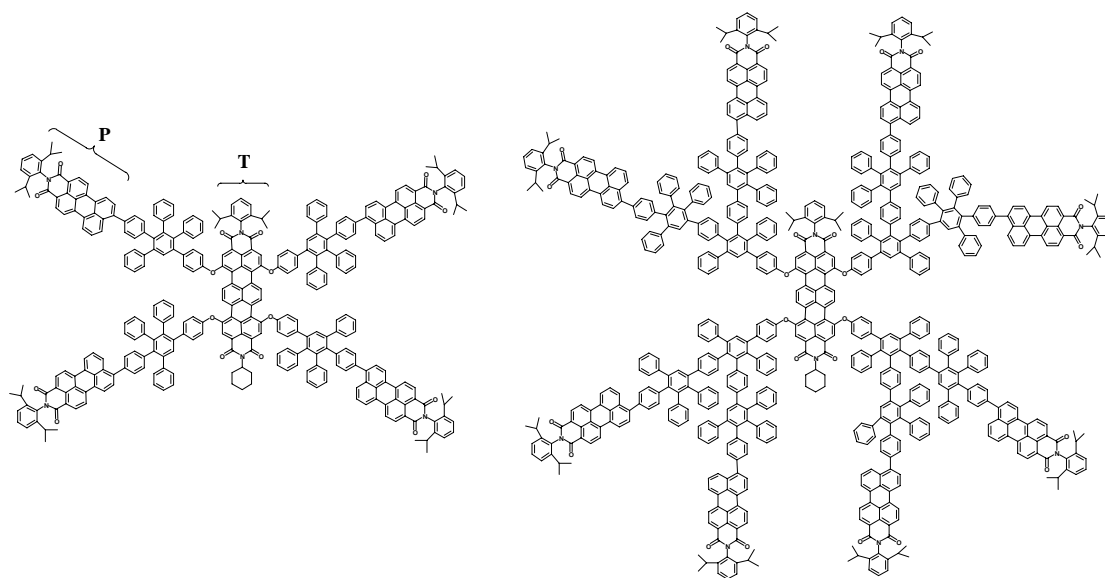
Figure 7. Structures of the first (left) and second (right) generation donor-acceptor dendrimers containing perylene monoimide donor chromophores at the rim and a central terrylene bisimide acceptor unit.[18d,f]

Another example for a dendrimer-type multichromophoric architecture favoring quantitative cascade fluorescence resonance energy transfer without the appearance of undesired chromophore self-quenching interactions is shown in Figure 8.[18g] This compound is particularly interesting, because three different types of properly chosen chromophoric units with different excited state energies are arranged in a certain geometry as the system presents eight coumarin-2 dyes (blue dye residues in Figure 8) and four fluorol 7GA units (green chromophoric moieties in Figure 8) attached to a perylene bisimide core (red center unit in Figure 8). Efficient energy transfer following photoexcitation is observed from the coumarin groups via the fluorol units to the perylene core (> 95%). A cascade directional transfer mechanism from coumarin to fluorol and subsequently to the perylene core is favored over direct energy transfer from the coumarin to the PBI unit because of poor spectral overlap between coumarin fluorescence emission and perylene bisimide UV/vis absorption.
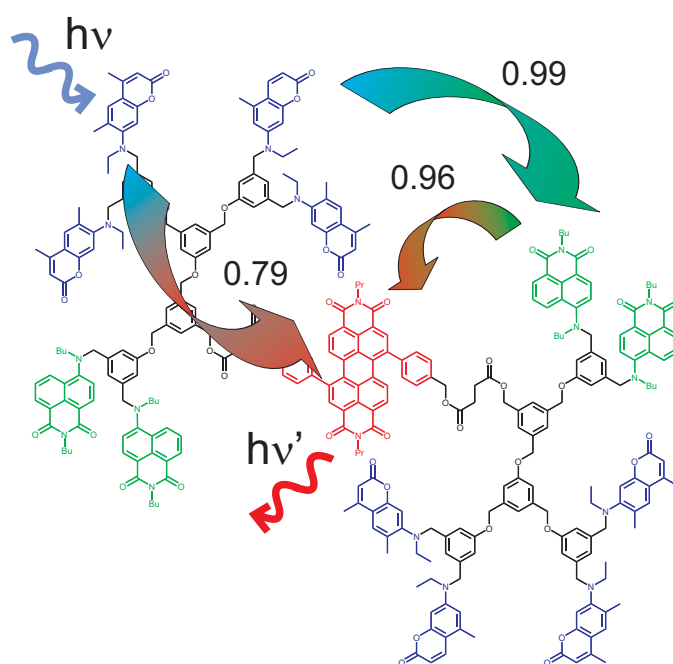
Figure 8. Schematic representation of the trichromophoric cascade energy transfer system studied by Fréchet and coworkers.[18g] Arrows indicate the energy transfer pathways together with their efficiency between the individual subunits.

1.2   Introduction to Calix[4]arenes

1.2.1   Definition and Nomenclature

The name *calixarenes* was introduced by Gutsche for the cyclic oligomers which are obtained from the condensation of formaldehyde with *para*-alkylphenols under alkaline conditions.[20] The use of the word *calix* which means *beaker* in Latin and Greek was suggested by the bowl- or beaker like shape of the cyclic tetramer in the *cone* conformation (see below). Formally, calixarenes are denoted as [1.1.1.1] metacyclophanes or 1_n-metacyclophanes. However, in the following the name calix[n]arene, with [n] representing the number of the aromatic units, will be used. Readily available are cyclic oligomers containing four, five, six, or eight phenol units joined by methylene bridges. Exemplarily, the calix[4]arene skeleton with its systematic numbering is depicted in Figure 9. On a laboratory scale the *tert*-butylcalixarenes are available by alkali-catalyzed condensation of *p-tert*-butylphenol with formaldehyde in a one-pot procedure.[21] By sophisticated control of the reaction conditions (solvent, temperature, base, aldehydes), the total yields of the cyclic oligomers containing tetra-, penta-, hexa- hepta- and octamers are higher than 50%. It is generally accepted that the *tert*-butylcalix[8]arene is the kinetically and the *tert*-butylcalix[4]arene the thermodynamically controlled product, while a template effect seems to enable the preferential formation of the calix[6]arenes.[20,21] This ready availability of the calixarenes is quite amazing, since during this reaction either 8, or 12, or 16 covalent bonds are newly formed in a defined manner.
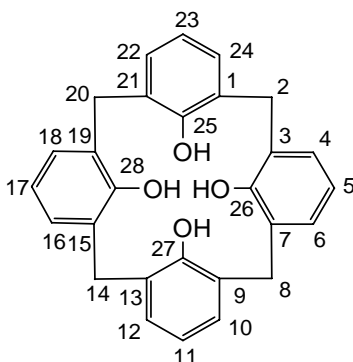
Figure 9. Systematic numbering of the calix[4]arene skeleton.

1.2.2   Conformations of Calix[4]arenes

One of the most fascinating aspects of calixarenes lies in the variety of conformations which they can adopt owing to the unhindered rotation of the phenolic rings around the σ-bonds of the methylene bridges. In the case of calix[4]arenes the hydroxyl group can pass through the annulus, and considering the position of the phenolic OH groups with respect to the "reference" plane (crossing the four methylene bridges), four main conformations can be defined: *cone*, *partial cone*, *1,2-alternate*, and *1,3-alternate* (see Figure 10).[20] Due to the mobility of the phenolic units these conformations can interconvert into each other by flipping of the aromatic rings. In solution, tetrahydroxy-*tert*-butylcalix[4]arenes are exclusively found in the *cone* conformation owing to a stabilizing intramolecular array of hydrogen bonds, in which all hydroxyl groups are orientated in the same direction (see schematic representation in Figure 11A). However, upon increasing temperature ring inversion processes in which the OH groups pass through the interior of the macrocycle are observed with a rapid exchange between the two opposed (but identical) *cone* conformations (see schematic representation in Figure 11A and 11B).

$$\text{cone} \qquad \text{partial cone} \qquad \text{1,2-alternate} \qquad \text{1,3-alternate}$$

$$C_{4V} \qquad\qquad C_{s} \qquad\qquad C_{2h} \qquad\qquad D_{2d}$$
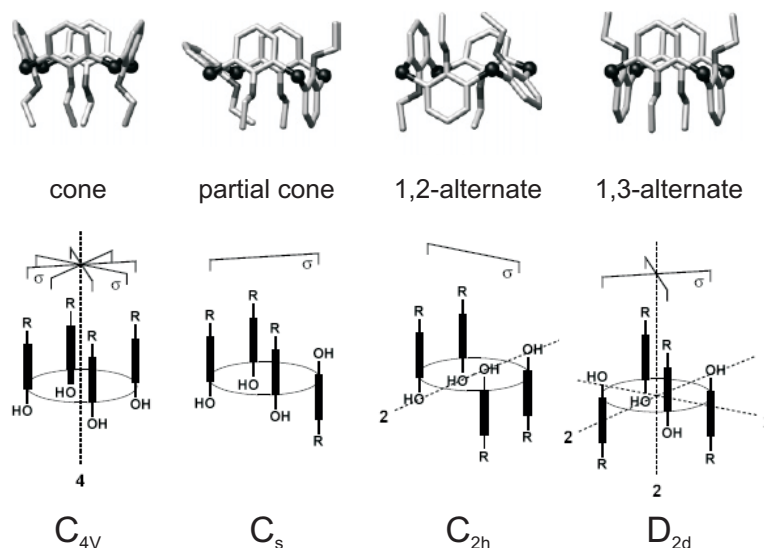
Figure 10. The four basic conformations of calix[4]arene derivatives and their symmetry classes.[20] Figure reprinted with permission from *J. Phys. Chem. A* **2006**, *110*, 861–867. © 2007 American Chemical Society.

The conformational mobility of calix[4]arenes can be restricted upon the incorporation of O-alkyl or O-acyl residues larger than the ethyl moiety.[22,23] Since larger substituents cannot pass through the macrocycle, it is possible to fix all the conformations shown in Figure 10 and to isolate them as stable conformers. Template effects by metal cations (from the applied base) have been especially used to control the formation of a certain conformer. Usually, the *cone* isomer is formed in the presence of Na$^+$ cations.[23,24] Larger cations such as K$^+$ and Cs$^+$ favor the formation of the *1,3-alternate* and *partial cone* conformations, whereas the *1,2-alternate* isomer is seldom formed and usually occurs only as a by-product.
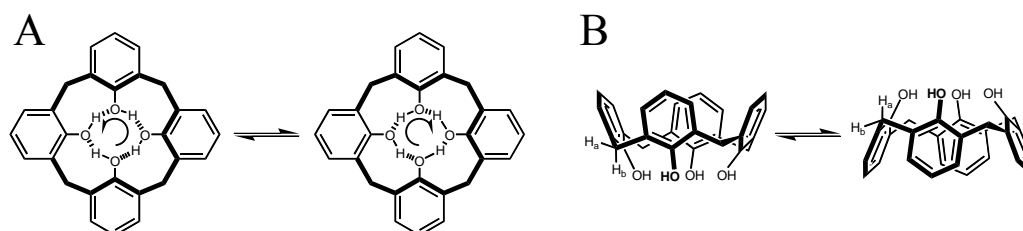
Figure 11. Schematic representation of stabilizing intramolecular hydrogen bonding (**A**) and ring interconversion equilibrium (**B**) in tetrahydroxycalix[4]arenes.[20b]

The structure of any tetra-O-alkylated calix[4]arene fixed in one of the above mentioned conformations can be easily distinguished from its ^{1}H NMR spectrum, where for each conformer the protons of the methylene bridge show distinct patterns owing to symmetry reasons.[20] Accordingly, in the ^{1}H NMR spectra of calix[4]arenes in the *cone* conformation one pair of doublets for the Ar-CH$_2$-Ar signals is observed which is characteristic for geminal protons showing coupling constants of 12-14 Hz with the protons being not magnetically equivalent as the system shows C$_{4V}$ symmetry (see Figure 10). From the two protons at the methylene bridges the doublet at higher field is assigned to the equatorial positioned proton, whereas the doublet at lower field corresponds to the axial proton which is in closer contact to the O-alkyl-residues of the calix[4]arene. In contrast, for a calix[4]arene possessing the *1,3-alternate* conformation only one singlet is observed for the signals of the methylene bridge protons as these are now magnetically equivalent due to symmetry reasons as the system shows D$_{2d}$ symmetry (see Figure 10). A representation of the ^{1}H NMR signals of the Ar-CH$_2$-Ar protons in the various conformations is shown in
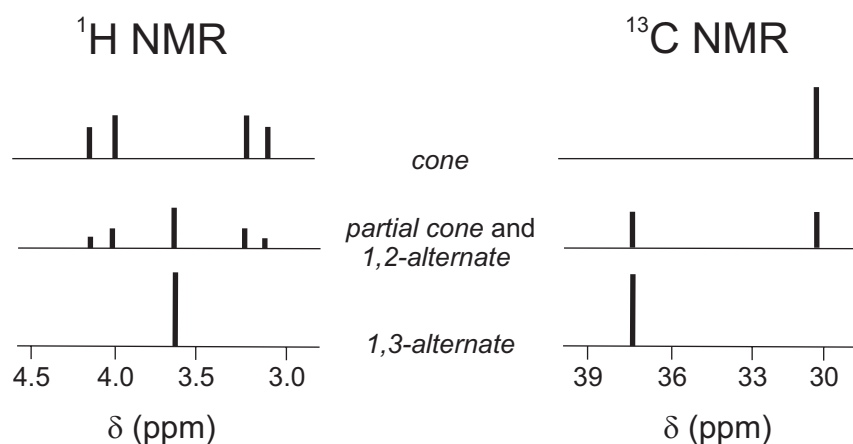
Figure 12. Characteristic signals of the Ar-C*H*$_2$-Ar protons and Ar-C*H*$_2$-Ar carbon atoms in the variate conformations of calix[4]arenes in ^{1}H NMR (left) and ^{13}C NMR spectroscopy (right). Calix[4]arene conformations are as indicated above.[20b]

Figure 12. Furthermore, a distinction of the variate conformers is also possible via ^{13}C NMR. The signals of the methylene bridges of *cone* calix[4]arenes, for example, are found around 31 ppm, whereas those of the *1,3-alternate* calix[4]arenes are observed at 37 ppm (see Figure 12).[25]

As discussed above, the *cone* isomer of calix[4]arenes can be conformationally fixed in solution, but interestingly, the thus rigidified skeleton reveals still some remaining flexibility. Hence, *cone* isomers of calix[4]arenes are known to undergo geometric changes that vary the distance between two opposite phenol rings.[26] Accordingly, the averaged C$_{4V}$ symmetry found for calix[4]arenes in the *cone* conformation can be interpreted in terms of a rapid interconversion between two equivalent and relatively stable so-called *pinched cone* isomers possessing lower C$_{2V}$ symmetry, *e.g.* showing a geometric arrangement in which the two opposite aromatic rings are almost parallel, while the other two aromatic rings are almost orthogonal positioned to each other (for a schematic representation of the two *pinched cone* conformers see Figure 13). Thus, the structure with C$_{4V}$ symmetry represents rather a transition state of the above-mentioned interconversion for alkylated phenolic units, while both C$_{2V}$ conformers are the minima on the potential energy hypersurface. Upon substitution in the *para*-positions of the phenolic units the two *pinched cone* conformations are not equivalent any more, and as a consequence a shift of the equilibrium towards one favorable isomer can be observed, depending on the nature of the substituent and also on interactions between the substituting units (see Figure 13).[27]

23

$$C_{2V} \qquad C_{4V} \qquad C_{2V}$$
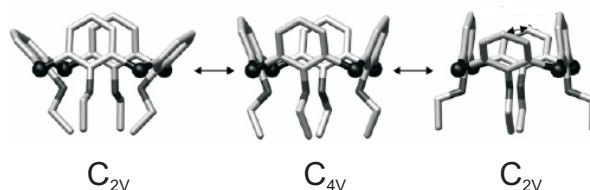
Figure 13. Graphic representation of the *pinched cone-pinched cone* interconversion.[27d] Figure reprinted with permission from *J. Phys. Chem. A* **2006**, *110*, 861–867. © 2007 American Chemical Society.

1.2.3   Functionalization on the *Wide Rim* of Calix[4]arenes

Calix[4]arenes afforded from phenol derivatives can mainly undergo modification either by the introduction of functional groups at the phenolic hydroxy groups (modification at the so-called *narrow rim*) or by (electrophilic) substitution in the *para*-position with respect to the phenolic hydroxy or alkoxy group (modification at the so-called *wide rim*), subsequent to the elimination of the *tert*-butyl group originally present in the parent compound. In general, all reactions characteristic for phenol derivatives may also be applied to calix[4]arenes. Once a calix[4]arene is fixed in a certain conformation it can be used as skeleton for further attachment of various groups either at the *narrow rim* or at the *wide rim* or at both sides.

Since the one-pot synthesis of calixarenes works best with the *p-tert*-butylphenol, often the *p-tert*-butylcalix[4]arenes are used as starting materials for other derivatives. Therefore, one of the most important exhaustive modifications at the *wide rim* is the transalkylation reaction with AlCl$_3$ in toluene, converting *p-tert*-butylcalix[4]arenes into their respective unsubstituted counterparts. As a consequence, the *para*-positions are now available for a variety of electrophilic substitution reactions, such as sulphonation, nitration, bromination or iodination, bromomethylation, aminomethylation, formylation, acylation and coupling with diazonium salts among many others.[20,28-30]

One of the most important building blocks utilized in this thesis is the 5-monoBoc-17-monoamino functionalized calix[4]arene shown in Scheme 1. Based on the synthesis of the latter derivative some important functionalization methods on both the *wide rim* and the *narrow rim* will be discussed exemplarily in the following (see Scheme 1). First, the calix[4]arene skeleton is afforded by one-pot reaction of *p-tert*-butylphenol with formaldehyde in the presence of NaOH,[21a] followed by transalkylation with AlCl$_3$ in

toluene, leading to the respective unsubstituted tetrahydroxy-calix[4]arene.[31] The latter is fully O-alkylated upon reaction with propyl iodide in the presence of NaH in DMF.[32] Subsequently, the *para*-positions of the phenolic rings are nitrated in the 5 and 17 positions to obtain the respective 5,17-dinitro-derivative.[33] The latter is further reduced to the related 5,17-diamino-compound,[33b,34] which is finally converted into the monoBoc-functionalized calix[4]arene precursor shown as final compound in Scheme 1.[35]

Scheme 1. Synthetic routes towards calix[4]arene precursor compounds utilized in this thesis.
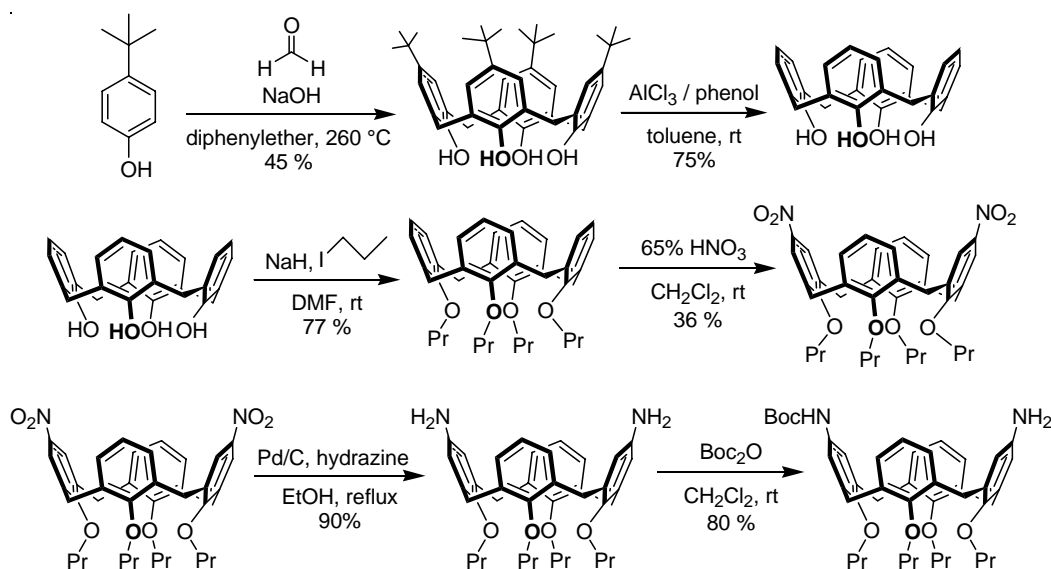
1.3   Basic Concepts of Photoinduced Processes in Dye Arrays

1.3.1   Energy Transfer

Photoinduced energy transfer processes are widely observed within both natural and artificial light-harvesting systems. They occur when the excitation energy from a donor dye is transferred to an acceptor dye, typically resulting in the generation of an excited state acceptor. Depending on the spatial arrangement of the chromophores and hence the coupling between the dye units, these electronic energy transfer processes are described either by the mechanism according to Dexter ("exchange")[36] or to Förster ("coulombic", "dipole-dipole" or "resonance").[37] These mechanisms are also addressed as a through-bond (Dexter) or through-space (Förster) energy transfer in the literature, for a schematic representation of both mechanisms see Figure 14. Within aggregated assemblies with distances between donor and acceptor units of 10 Å and less, the stronger Dexter-type coupling is likely, whereas between spatially separated subunits long-range Förster-type energy transfer is considered to be the relevant mechanism (distances of donor and acceptor units ranging from 10 to 80 Å).[38,39]
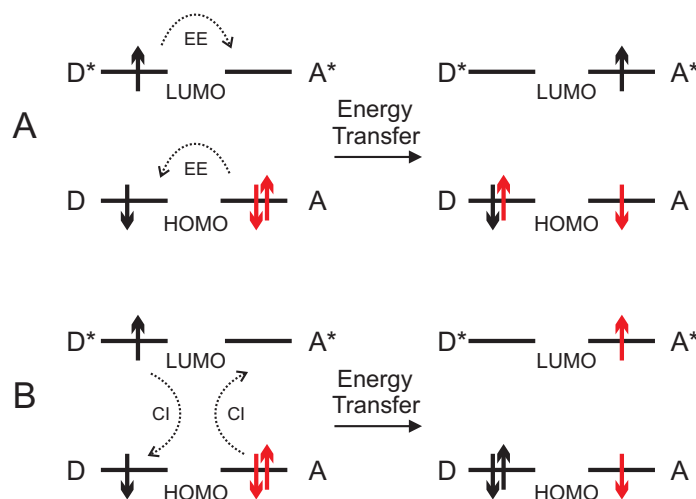
Figure 14. Schematic representation of exchange (Dexter) (A) and coulombic (Förster) (B) mechanisms of excitation energy transfer. EE denotes electron exchange and CI coulombic interactions.[38]

Hence, in the Dexter energy transfer mechanism, the bridging ligand, its electronic nature, geometry and rigidity are the most important parameters that determine the electronic coupling between the donor and acceptor moieties, and thereby the energy transfer rate. In contrast, in the Förster-type energy transfer the intrinsic properties of the chromophores

themselves (transition dipole moment and spectral overlap of donor emission and acceptor absorption spectra) as well as the interchromophore distance and orientation do substantially influence the transfer rate. For the present thesis perylene bisimide chromophores are used to construct light-harvesting arrays showing efficient energy transfer processes between the individual dye units. For this purpose, calix[4]arene spacers are attached at the imide nitrogens of the chromophore. This causes an efficient electronic decoupling of the individual chromophoric subunits because nodes in the HOMO and LUMO at the imide nitrogen reduce the coupling between the perylene bisimide units and the calix[4]arene substituents to a minimum.[40] Therefore, the through-bond coupling between two perylene bisimide units along the calix[4]arene framework is negligible. Accordingly, in the absence of π–π-stacking the Förster-type energy transfer through space should be preferred instead of the Dexter-type energy transfer through bond for the systems studied in this thesis (see Chapter 4). This is further corroborated by the fact that a center-to-center distance between the chromophoric subunits of around 20 Å is found, again suggesting an energy-transfer mechanism of Förster-type (see Chapter 4).

1.3.1.1   Dexter Energy Transfer

The Dexter energy transfer mechanism is schematically illustrated in Figure 14A and can be briefly described as follows. Upon interaction between the excited donor unit and the non-excited acceptor unit, formally a double electron transfer takes place in which the electron that was excited to the lowest unoccupied molecular orbital (LUMO) of the donor (D*) is transferred to the LUMO of the acceptor (A), and simultaneously, an electron from the highest occupied molecular orbital (HOMO) of A is transferred to the HOMO of D. This electron exchange requires a strong D-A orbital overlap and is therefore of short range nature (< 10 Å) and diminishes exponentially with distance.[41,42] The transfer rate can be obtained as follows:

$$k_{ET} = \frac{1}{\hbar^2 c} \beta^2 J(\lambda) \qquad\qquad (1)$$

where J(λ) denotes the spectral overlap integral (quantifying the degree of spectral overlap between the donor fluorescence emission and the acceptor UV/vis absorption spectra), and

β is the electronic coupling matrix element which is expressed for the case of the Dexter transfer mechanism according to equation 2:

$$\beta^2{}_{Dexter} \propto \exp\left(-\frac{2R_{DA}}{L}\right) \qquad (2)$$

where R_{DA} denotes the distance between donor and acceptor unit, and L the van der Waals radius of the donor-acceptor pair (e.g. the sum of the individual van der Waals radii). Furthermore, the spectral overlap integral is defined according to equation 3:

$$J(\lambda) = \frac{\int_0^\infty I_D(\lambda)\varepsilon_A(\lambda)\lambda^4 d\lambda}{\int_0^\infty I_D(\lambda) d\lambda} \qquad (3)$$

where $I_D(\lambda)$ is the corrected fluorescence intensity in the wavelengths range λ to $\lambda+\Delta\lambda$, with the total intensity (area under the curve) normalized to unity and $\varepsilon_A(\lambda)$ is the extinction coefficient of the acceptor at λ.

1.3.1.2   Förster Energy Transfer

Fluorescence resonance energy transfer (FRET) following the Förster mechanism is driven by the through-space dipole–dipole interaction of donor and acceptor (for a schematic representation see Figure 14B).[37-39] For this transfer mechanism donor-acceptor orbital overlap is not necessary but instead spectral overlap is required, allowing the chromophores to be spatially separated by relatively large distances (10 to 80 Å).[38] The Förster energy transfer rate constant is described by the following equation:

$$k_{ET} = \frac{1}{\tau_D}\left(\frac{R_0}{r}\right)^6 \qquad (4)$$

where r denotes the center-to-center distance of the donor and acceptor transition dipole, τ_D the fluorescence lifetime of the donor in the absence of the acceptor and R_0 the Förster distance (the distance at which the energy transfer efficiency is 50%). The Förster distance R_0 can be calculated according to the simplified equation:

$$R_0 = 0.211\left[\kappa^2 n^{-4}\Phi_D J(\lambda)\right]^{1/6} \qquad (5)$$

with κ^2 being the orientation factor, n the refractive index of the medium, Φ_D the quantum yield of the donor in the absence of the acceptor, and $J(\lambda)$ the overlap integral of the donor fluorescence emission and the acceptor UV/vis absorption spectra (see equation 3). The orientation factor κ^2 between the donor and acceptor dipole moments is given by:

$$\kappa^2 = \left(\cos\Theta_T - 3\cos\Theta_D \cos\Theta_A\right)^2$$
$$\kappa^2 = \left(\sin\Theta_D \sin\Theta_A \cos\phi - 2\cos\Theta_D \cos\Theta_A\right)^2 \qquad (6)$$

with Θ_T being the angle between the emission transition dipole of the donor and the absorption transition dipole of the acceptor, and Θ_D and Θ_A being the angles between these dipoles and the vector joining the donor and the acceptor and ϕ being the angle between the planes (for a schematic representation see Figure 15). Depending on the relative orientation of donor and acceptor transition dipoles the values for κ^2 range from zero to four. Accordingly, for collinear and parallel orientation of the transition dipoles κ^2 equals 4, and for parallel orientation κ^2 equals 1, whereas for a perpendicular arrangement of the transition dipoles κ^2 vanishes to zero (see Figure 15). For a randomized arrangement of donors and acceptors due to rotational diffusion prior to energy transfer, κ^2 is generally assumed to be 2/3, given that a variety of static donor-acceptor orientations are present and that these orientations do not change during the lifetime of the excited state. Notably, the Förster energy transfer rate can thus be expressed as a function depending only on the center-to-center distance r, when the refractive index of the solvent and the fluorescence and absorption spectra of donor and acceptor, respectively, are known (see equation 4). Therefore, one of the most common applications of the Förster energy transfer is the (time-resolved) determination of distances between donor and acceptor units in, for example, macromolecules of less defined geometry or protein folding processes.[39] However, one has to keep in mind that for donor-acceptor pairs that are connected by a (rigid) spacer unit at close distances significant ambiguities arise due to, first, conformational effects (different κ^2 values for different orientations), and second, the limitations of the point-dipole approximation of the Förster-theory as the coulombic coupling is not described properly at center-to-center distances of less than 10 Å.
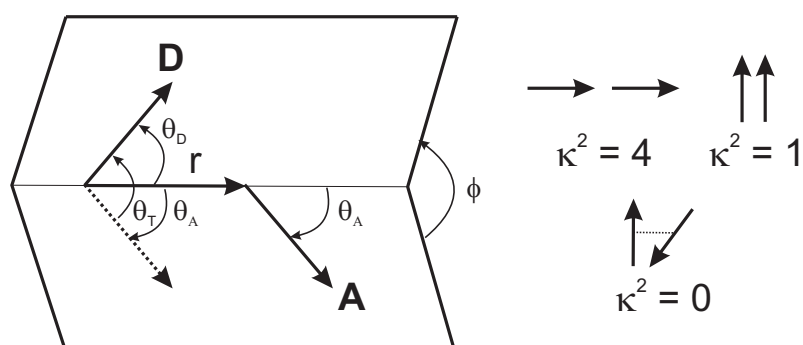
Figure 15. Dependence of the orientation factor κ^2 on the directions of the emission dipole of the donor and the absorption dipole of the acceptor.[39]

1.3.2   Electron Transfer

Photoinduced electron transfer is of crucial importance in many processes in biological systems, such as molecular signaling, conversion of solar energy in artificial systems and photosensitized catalysis.[43] In a system consisting of an electron donating moiety (D) and an electron accepting group (A), upon photoexcitation, an electron transfer can occur from the donor to the acceptor moiety, resulting in the creation of a charge-separated (CS) state (consisting of the corresponding radical cation and anion), from which charge recombination can take place to bring the system back to the ground state.

A theoretical description of the energetics and rates of the electron transfer process is formulated in a Marcus-Weller type analysis. An estimate of the driving force for photoinduced charge separation $-\Delta G_{CS}$ in a solvent with a dielectric constant ε_s can be made using the standard Weller-type approach according to the following equation:[44]

$$\Delta G_{CS} = e\left[E_{ox}(D) - E_{red}(A)\right] - E_{00} - \frac{e^2}{4\pi\varepsilon_0\varepsilon_S R_{CC}} - \frac{e^2}{8\pi\varepsilon_0}\left(\frac{1}{r^+} + \frac{1}{r^-}\right)\left(\frac{1}{\varepsilon_{ref}} - \frac{1}{\varepsilon_S}\right) \qquad (7)$$

"polar driving force term"   "coulombic term"   "solvation term"

This requires, in addition to the donor and acceptor redox potentials $E_{ox}(D)$ and $E_{red}(A)$ (determined in a solvent with dielectric constant ε_{ref}) knowledge about the singlet excited state energy E_{00}, the center-to-center distance R_{CC} and the effective ionic radii of the donor radical cation r^+ and the acceptor radical anion r^-, respectively. Values for R_{cc} can be estimated from molecular modeling, and r^+ and r^- values can either be calculated from the

apparent molar volumes or alternatively obtained from crystal structure data. In equation 7 the first term is often referred to as the so-called "polar driving force", whereas in the second term the coulombic interaction between two ions is taken into account, and the last term of the equation represents the so-called "solvation term". The latter accounts for the smaller ability of low polarity solvents to stabilize charge separated states compared to higher polarity solvents (see equation 7).

Values for the barrier for the charge separation $\Delta G_{CS}{}^{\#}$ and the rate constant of electron transfer k can be estimated via the classical Marcus equation[43f,g,45] and can be described as follows

$$k = A\exp\left[\frac{-\Delta G_{CS}{}^{\neq}}{k_B T}\right] \qquad (8)$$

and

$$\Delta G_{CS}{}^{\neq} = \frac{\lambda}{4}\left(1 + \frac{\Delta G_{CS}}{\lambda}\right)^2 \qquad (9)$$

where k_B is the Boltzmann constant and λ is the nuclear reorganization energy. The relation between these quantities and the representation of the potential energy curve (resulting from the harmonic approximation made in the theory) are shown in Figure 16.
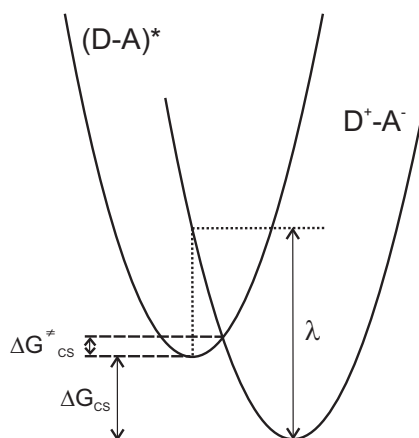
Figure 16. Representation of the potential energy curve description used in electron transfer theory. The barrier for the charge separation ($\Delta G^{\neq}_{CS}$), the overall Gibbs free energy change (ΔG_{CS}) and total reorganization energy (λ) are indicated.

As can be seen from Figure 16 the reorganization energy λ is defined as the potential energy change occurring during the nuclear reorganization in response to the electronic changes when going from the reactant to the product potential energy curve. It consists of two contributions since the reorganization will occur both within the molecule (internal reorganization, λ_i, *i.e.* changes in bond lengths and angles) and also in the surrounding medium (solvent reorganization, λ_s). Thus, λ can be described as follows:[43f]

$$\lambda = \lambda_i + \lambda_s \qquad\qquad (10)$$

where λ_S is the solvent reorganization energy which can be estimated from:[43f]

$$\lambda_S = \frac{e^2}{4\pi\varepsilon_0}\left(\frac{1}{r} - \frac{1}{R_{CC}}\right)\left(\frac{1}{n^2} - \frac{1}{\varepsilon_S}\right) \qquad (11)$$

and the expression for the vibrational term λ_i is given by equation (12), where Q_j^r and Q_j^p are equilibrium values for the jth normal mode coordinate Q, and k_j is a reduced force constant. The superscripts r and p refer to reactants and products.[43f]

$$\lambda_i = \frac{1}{2}\sum_j k_j \left(Q_j^r - Q_j^p\right)^2 \qquad\qquad (12)$$

The Marcus theory implies that barrier-less electron transfer ($\Delta G^{\neq}_{CS} = 0$) can occur if λ equals $-\Delta G_{CS}$ (referred to as the optimal region). If λ is larger than $-\Delta G_{CS}$ the electron transfer rate increases with larger driving force (normal region). However, in the so-called Marcus inverted region, with λ being smaller than $-\Delta G_{CS}$, the rate counter-intuitively *decreases* with larger driving force. In Figure 17, all these conditions are schematically shown.

normal   optimal   inverted

Figure 17. Illustration of the harmonic potential energy curves of (D-A)* (left curves) and (D$^+$-A$^-$) (right curves) for photoinduced charge separation in the Marcus normal (left), optimal (middle) and inverted region (right).[43e]

1.3.3   Optical Properties of Dye Aggregates

Owing to electronic interactions between the π-systems and/or structural changes of the chromophores, the formation of dye assemblies is usually accompanied by pronounced spectral changes in the UV/vis absorption bands an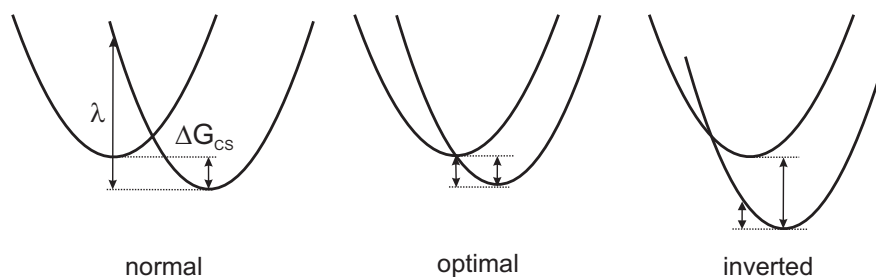d significant alterations of the fluorescence spectra and quantum yields. The optical properties of aggregated dyes with a typical distance of three to four Å between the dye molecules can be explained in a semi-quantitative way by the molecular exciton theory in the point-dipole approximation: For chromophores in close contact, the electronic transitions of the chromophores cannot be treated individually, and as a result a splitting in the excited state energy levels is observed as shown in Figure 17 for the dimer case.[46] In the sandwich geometry, the higher dimer excited state exhibits an in-phase relation of the transition dipoles, and the lower dimer excited state an out-of-phase relation. For this situation, the transition from the ground to the lower dimer excited state is forbidden. Thus, the dimer absorption band results from a transition to the higher state and is therefore blue-shifted with respect to the monomer. Furthermore, for this arrangement of the chromophores, usually no fluorescence is observed. In contrast, for a head-tail arrangement of the transition dipole moments, the transition from the ground to the lower dimer excited state is allowed, and the resulting dimer absorption band is red-shifted, accordingly. Dye aggregates with chromophores positioned in this geometry are often fluorescent.

The angle θ is defined as the angle between the coplanar transition dipoles and the axis which connects the dipole centers. For continuous variation of θ from 0° (head-tail arrangement of the dipoles) to 90° (parallel or sandwich geometry of the dipoles), the forbidden exciton state (dotted line) interchanges position with the allowed exciton state (solid line) as a function of the dimer geometry (see Figure 17). For θ = 54.7° the exciton splitting ΔE is zero, meaning that the dipole-dipole interaction is zero for this orientation of transition dipole moments.

These observations lead directly to the most common model for H- and J-aggregates[47,48] where the flat elongated dye molecules are stacked on top of each other in a parallel fashion. The angle between the long molecular axis and the aggregation direction corresponds to θ and decides over the prevalence of a J- or H-aggregate formation.
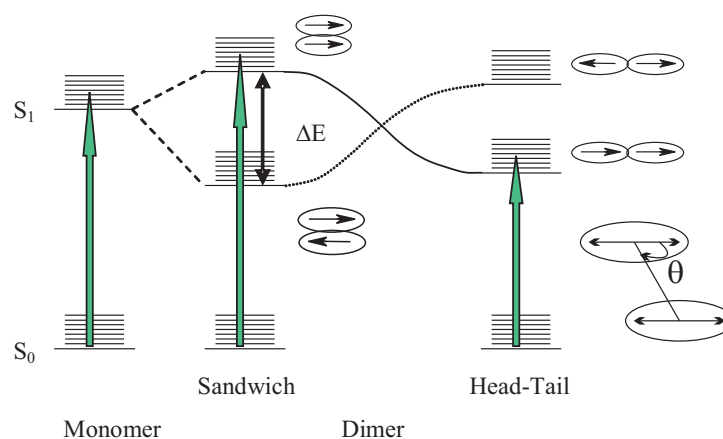
Figure 17. Schematic energy level diagram for the excitonic coupling in dimer aggregates with coplanar transition dipoles tilted towards the interconnecting axis by the angle θ. Shown are the allowed states for $S_0 \rightarrow S_1$ excitation for a parallel (sandwich) and a head-tail geometric arrangement. The solid line represents the allowed state, the dotted line the forbidden state.

For $0° < θ < 54.7°$, a J-aggregate (longer wavelength absorption band, fluorescence) and for $54.7° < θ < 90°$, an H-aggregate (shorter wavelength absorption band, no fluorescence because the transition to the lowest state is forbidden) is formed.

1.4   References

(1)   (a) *Supramolecular Photochemistry*; Balzani, V., Scandola, F., Eds.; Horwood: Chichester, UK, 1991. (b) *Comprehensive Supramolecular Chemistry*, *Vol. 1– 11*; Lehn, J.-M., Atwood, J. L., Davies, J. E. D., MacNicol, D. D., Vögtle, F., Eds.; Pergamon: Oxford, 1996. (c) Balzani, V.; Ceroni, P.; Maestri, M.; Vicinelli, V. *Curr. Opin. Chem. Biol.* **2003**, *7*, 657–665. (d) Holzwarth, A. R. In *Series on Photoconversion of Solar Energy*; Archer, M. D., Barber, J., Eds.; Imperial College Press: London, UK, 2002. (e) Katz, J. J. *Photosynth. Res.* **1990**, *26*, 143–160. (f) Wasielewski, M. R. *Chem. Rev.* **1992**, *92*, 435–461. (g) Wasielewski, M. R. *J. Org. Chem.* **2006**, *71*, 5051–5066. (h) Scandola, F. Chiorboli, C.; Prodi, A.; Iengo, E.; Alessio, E. *Coord. Chem. Rev.* **2006**, *250*, 1471–1496.

(2)   (a) Grondelle, R.; Dekker, J. P.; Gillbro, T.; Sundström, V. *Biochim. Biophys. Acta* **1994**, *1187*, 1–65. (b) McDermott, G.; Prince, S. M.; Freer, A. A.; Hawthornthwaite-Lawless, A. M.; Papiz, M. Z.; Cogdell, R. J.; Isaacs, N. W. *Nature* **1995**, *374*, 517–21. (c) Kühlbrandt, W. *Nature* **1995**, *374*, 497–498. (d) Ritz, T.; Park, S.; Schulten, K. *J. Phys. Chem. B* **2001**, *105*, 8259–8267. (e) Papiz, M. Z.; Prince, S. M.; Howard, T.; Cogdell, R. J.; Isaacs, N. W. *J. Mol. Biol.* **2003**, *326*, 1523–1538. (f) Huber, R. *Angew. Chem. Int. Ed.* **1989**, *28*, 848–869.

(3)   Pullerits, T.; Sundström, V. *Acc. Chem. Res.* **1996**, *29*, 381–389.

(4)   Ritz, T.; Damjanović, A.; Schulten, K. *ChemPhysChem* **2002**, *3*, 243–248.

(5)   Gvishi, R.; Reisfeld, R.; Burshtein, Z. *Chem. Phys. Lett.* **1993**, *213*, 338– 344.

(6)   Langhals, H. *Heterocycles*, **1995**, *40*, 477–500.

(7)   Würthner, F. *Chem. Commun.* **2004**, 1564–1579.

(8)   Tang, C. W. *App. Phys. Lett.* **1986**, *48*, 183–185.

(9)   Sadrai, M.; Hadel, L.; Sauers, R. R.; Husain, S.; Krogh-Jespersen, K.; Westbro, J. D.; Bird, G. R. *J. Phys. Chem.* **1992**, *96*, 7988–7996.

(10)   Suzuki, H.; Hoshino, S. *J. Appl. Phys.* **1996**, *79*, 8816–8822.

(11)   Horowitz, G.; Kouki, F.; Spearman, P.; Fichou, D.; Nogues, C.; Pan, X.; Garnier, F. *Adv. Mater.* **1996**, *8*, 242–245.

(12)   Law, K.-Y. *Chem. Rev.* **1993**, *93*, 449–486.

(13)   Roncali, J.; Garnier, F. *Appl. Opt.* **1984**, *23*, 2809–2817.

(14)   (a) You, C.-C.; Dobrawa, R.; Saha-Möller, C. R.; Würthner, F. *Top. Curr. Chem.* **2005**, *258*, 39–82. (b) *Supramolecular Dye Chemistry*; Würthner, F., Ed.; Topics in Current Chemistry 258, Springer-Verlag: Berlin, 2005.

(15)   For examples containing perylene bisimides, see: (a) O'Neil, M. P.; Niemczyk, M. P.; Svec, W. A.; Gosztola, D.; Gaines, G. L.; Wasielewski, M. R. *Science* **1992**, *257*, 63–65. (b) Prathapan, S.; Yang, S. I.; Seth, J.; Miller, M. A.; Bocian, D. F.; Holten, D.; Lindsey, J. S. *J. Phys. Chem. B* **2001,** *105,* 8237–8248. (c) Rybtchinski, B.; Sinks, L. E.; Wasielewski, M. R. *J. Am. Chem. Soc.* **2004**, *126*, 12268–12269. (d) Langhals, H.; Saulich, S. *Chem. − Eur. J.* **2002**, *8*, 5630–5643. (e) Ego, C.; Marsitzky, D.; Becker, S.; Zhang, J.; Grimsdale, A. C.; Müllen, K.; MacKenzie, J. D.; Silva, C.; Friend, R. H. *J. Am. Chem. Soc.* **2003**, *125*, 437–443. (f) Loewe, R. S.; Tomizaki, K.-Y.; Youngblood, W. J.; Bo, Z.; Lindsey, J. S. *J. Mat. Chem.* **2002**, *12*, 3438–3451. (g) Schlichting, P.; Duchscherer, B.; Seisenberger, G.; Basché, T.; Bräuchle, C.; Müllen, K. *Chem. − Eur. J.* **1999**, *5*, 2388–2395. (h) Metivier, R.; Nolde, F.; Müllen, K.; Basché, T. *Phys. Rev. Lett.* **2007**, *98*, 047802/1–047802/4. (i) Hinze, G.; Haase, M.; Nolde, F.; Müllen, K.; Basché, T. *J. Phys. Chem. A* **2005**, *109*, 6725–6729.

(16)   For general examples of linear light-harvesting arrays, see: (a) Ziessel, R.; Hissler, M.; El-ghayoury, A.; Harriman, A. *Coord. Chem. Rev.* **1998**, *178-180,* 1251–1298. (b) Aratani, N.; Osuka, A.; Cho, H. S.; Kim, D. *J. Photochem. Photobiol. C* **2002,** *3*, 25–52. (c) Bossart, O.; De Cola, L.; Welter, S.; Calzaferri, G. *Chem. − Eur. J.* **2004**, *10*, 5771–5775. (d) Berglund Baudin, H.; Davidsson, J.; Serroni, S.; Juris, A.; Balzani, V.; Campagna, S.; Hammarström, L. *J. Phys. Chem. A* **2002,** *106*, 4312–4319. (e) Chiorboli, C.; Indelli, M. T.; Scandola, F. *Top. Curr. Chem.* **2005**, *257*, 63–102. (f) Harriman, A.; Ziessel, R. *Coord. Chem. Rev.* **1998**, *171,* 331–339. (g) Yang, S. I.; Seth, J.; Balasubramanian, T. Kim, D. Lindsey, J. S.; Holten, D.; Bocian, D. F. *J. Am. Chem. Soc.* **1999**, *121*, 4008–4018.

(17)   (a) Fujita, M. *Chem. Soc. Rev.* **1998**, *27*, 417–425. (b) Stang, P. J.; Olenyuk, B. *Acc. Chem. Res.* **1997**, *30*, 502–518. (c) Würthner, F.; You, C.-C.; Saha-Möller, C. R. *Chem. Soc. Rev.* **2004**, *33*, 133–146. (d) Sautter, A.; Kaletas, B. K.; Schmid, D. G.; Dobrawa, R.; Zimine, M.; Jung, G.; Van Stokkum, I. H. M.; De Cola, L.; Williams, R. M.; Würthner, F. *J. Am. Chem. Soc.* **2005**, *127*, 6719–6729. (e) You, C.-C.; Hippius, C.; Grüne, M.; Würthner, F. *Chem. – Eur. J.* **2006**, *12*, 7510–7519. (f) Slone, R. V.; Benkstein, K. D.; Bélanger, S.; Hupp, J. T.; Guzei, I. A.; Rheingold, A. L. *Coord. Chem. Rev.* **1998**, *171*, 221–243. (g) Amijs, C. H. M.; van Klink, G. P. M.; van Koten, G. *Dalton Trans.*, **2006**, 308–327. (h) Seidel, S. R.; Stang, P. J. *Acc. Chem. Res.* **2002**, *35*, 972–983. (i) Drain, C. M.; Lehn, J.-M. *J. Chem. Soc., Chem. Commun.*, **1994**, 2313–2315. (j) Chi, X.; Guerin, A. J.; Haycock, R. A.; Hunter, C. A.; Sarson, L. D. *J. Chem. Soc., Chem. Commun.*, **1995**, 2567–2569. (k) Tsuda, A.; Nakamura, T.; Sakamoto, S.; Yamaguchi, K. Osuka, A. *Angew. Chem., Int. Ed. Engl.* **2002**, *41*, 2817–2821. (l) Vollmer, M. S.; Würthner, F.; Effenberger, F.; Emele, P.; Meyer, D. U.; Stümpfig, T.; Port, H.; Wolf, H. C. *Chem. – Eur. J.* **1998**, *4*, 260–269.

(18)   For light-harvesting dendrimers containing perylene bisimides, see: (a) De Schryver, F. C.; Vosch, T.; Cotlet, M.; Van der Auweraer, M.; Müllen, K.; Hofkens, J. *Acc. Chem. Res.* **2005**, *38*, 514–522. (b) Gronheid, R.; Stefan, A.; Cotlet, M.; Hofkens, J.; Qu, J.; Müllen, K.; Van der Auweraer, M.; Verhoeven, J. W.; De Schryver, F. C. *Angew. Chem., Int. Ed. Engl.* **2003**, *42*, 4209–4214. (c) Weil, T.; Reuther, E.; Müllen, K. *Angew. Chem., Int. Ed. Engl.* **2002**, *41*, 1900–1904. (d) Gronheid, R.; Hofkens, J.; Köhn, F.; Weil, T.; Reuther, E.; Müllen, K.; De Schryver, F. C. *J. Am. Chem. Soc.* **2002**, *124*, 2418–2419. (e) Jordens, S.; De Belder, G.; Lor, M.; Schweitzer, G.; Van der Auweraer, M.; Weil, T.; Reuther, E.; Müllen, K.; De Schryver, F. C. *Photochem. Photobiol. Sc.* **2003**, *2*, 177–186. (f) Schweitzer, D.; Gronheid, R.; Jordens, S.; Lor, M.; De Belder, G.; Weil, T.; Reuther, E.; Müllen, K.; De Schryver, F. C. *J. Phys. Chem. A* **2003**, *107*, 3199–3207. (g) Serin, J. M.; Brousmiche, D. W.; Fréchet, J. M. J. *Chem. Commun.* **2002**, 2605–2607. (h) Serin, J. M.; Brousmiche, D. W.; Fréchet, J. M. J. *J. Am. Chem. Soc.* **2002**, *124*, 11848–11849.

(19)   For general examples on light-harvesting dendrimers, see: (a) Dirksen, A.; De Cola, L. *C. R. Chimie* **2003**, *6*, 873–882. (b) *Dendritic Molecules: Concepts, Syntheses, Perspectives*; Newkome, G. R.; Moorefield, C. N.; Vögtle, F., Eds.; VCH: New York,

1996. (c) Balzani, V.; Ceroni, P.; Maestri, M.; Saudan, C.; Vicinelli, V. *Top. Curr. Chem.* **2003**, *228*, 159–191. (d) Venturi, M; Serroni, S.; Juris, A.; Campagna, S.; Balzani, V. *Top. Curr. Chem.* **1998**, *197*, 193–228. (e) Hahn, U.; Gorka, M.; Vögtle, F.; Vicinelli, V.; Ceroni, P.; Maestri, M.; Balzani, V. *Angew. Chem., Int. Ed. Engl.* **2002**, *41*, 3595–3598. (f) Balzani, V.; Ceroni, P.; Maestri, M.; Vicinelli, V. *Curr. Opin. Chem. Biol.* **2003**, *7*, 657–665. (g) Balzani, V.; Campagna, S.; Denti, G.; Juris, A.; Serroni, S.; Venturi, M. *Acc. Chem. Res.* **1998**, *31*, 26–34.

(20)   (a) *Calixarenes 2001*; Asfari, Z., Böhmer, V., Harrowfield, J., Eds.; Kluwer Academic Publishers: Dordrecht, 2001. (b) *Calixarenes*; Gutsche, C. D.; The Royal Society of Chemistry: Cambridge, 1993. (c) *Calixarenes Revisited*; Gutsche, C. D.; The Royal Society of Chemistry: Letchworth, 1998. (d) Böhmer, V.; *Angew. Chem., Int. Ed. Engl.* **1995**, *34*, 713–745.

(21)   (a) Gutsche, C. D.; Iqbal, M. *Org. Synth.* **1990**, *68*, 234–237. (b) Gutsche, C. D.; Dhawan, B.; Leonis, M.; Steward, D. *Org. Synth.* **1990**, *68*, 238–242. (c) Munch, J. H.; Gutsche, C. D. *Org. Synth.* **1990**, *68*, 243–246. (d) Stewart, D.; Gutsche, C. D. *Org. Prep. Proc. Int*. **1993**, *25,* 137–139. (e) Iwamoto, K.; Araki, K.; Shinkai, S. *Bull. Chem. Soc. Jpn.* **1994**, *67*, 1499–1502.

(22)   Iwamoto, K.; Araki, K.; Shinkai, S. *Tetrahedron* **1991**, *47*, 4325–4342.

(23)   Iwamoto, K.; Shinkai, S. *J. Org. Chem.* **1992**, *57*, 7066–7073.

(24)   Groenen, L. C.; Ruel, B. H. M.; Casnati, A.; Timmerman, P.; Verboom, W.; Harkema, S.; Reinhoudt, D. N. *Tetrahedron Lett.* **1991**, *32*, 2675–2678.

(25)   Jaime, C.; de Mendoza, J.; Prados, P.; Nieto, P. M.; Sanchez, C. *J. Org. Chem.* **1991**, *56*, 3372–3376.

(26)   (a) Conner, M.; Janout, V.; Regen, S. L. *J. Am. Chem. Soc.* **1991**, *113*, 9670–9671. (b) Scheerder, J.; Vreekamp, R. H.; Engbersen, J. F. J.; Verboom, W.; van Duynhoven, J. P. M.; Reinhoudt, D. N. *J. Org. Chem.* **1996**, *61*, 3476–3481. (c) Grootenhuis, P. D. J.; Kollman, P. A.; Groenen, L. C.; Reinhoudt, D. N.; van Hummel, G. J.; Ugozzoli, F.; Andreetti, G. D. *J. Am. Chem. Soc.* **1990**, *112*, 4165–4176. (d) Harada, T.; Rudzinski, J. M.; Osawa, E.; Shinkai, S. *Tetrahedron Lett.* **1993**, *49*, 5941–5954.

(27)   (a) Arduini, A.; Fabbi, M.; Mirone, L.; Pochini, A.; Secchi, A.; Ungaro, R. *J. Org. Chem.* **1995**, *69*, 1454–1457. (b) Ikeda, A.; Tsuzuki, K.; Shinkai, S. *J. Chem. Soc., Perkin Trans. 2* **1994**, 2073–2080. (c) Timmerman, P.; Nierop, K. G. A.; Brinks, E. A.; Verboom, W.; van Veggel, F. C. J. M.; van Hoorn, W. P.; Reinhoudt, D. N. *Chem.–Eur. J.* **1995**, *1*, 132–143. (d) Matoušek, J.; Kulhánek, P.; Čajan, M.; Koča, J. *J. Phys. Chem. A* **2006**, *110*, 861–867.

(28)   Morita, Y.; Agawa, T.; Nomura, E.; Taniguchi, H. *J. Org. Chem.* **1992**, *57*, 3658–3662.

(29)   Shinkai, S.; Araki, K.; Shibata, J.; Tsugawa, D.; Manabe, O. *J. Chem. Soc., Perkin Trans. 1* **1990**, *4*, 3333–3337.

(30)   Kelderman, E.; Derhaeg, L.; Verboom, W.; Engbersen, J. F. J.; Harkema, S.; Persoons, A.; Reinhoudt, D. N. *Supramol. Chem.* **1993**, *2*, 183–190.

(31)   Gutsche, C. D.; Lin, L.-G. *Tetrahedron* **1986**, *42*, 1633–40.

(32)   Timmerman, P.; Vreekamp, R. H.; Hulst, R.; Verboom, W.; Reinhoudt, D. N.; Rissanen, K.; Udachin, K. A.; Ripmeester, J. *Chem.–Eur. J.* **1997**, *3*, 1823–1832.

(33)   (a) Kelderman, E.; Derhaeg, L.; Heesink, G. J. T.; Verboom, W.; Engbersen, J. F. J.; Van Hulst, N. F.; Persoons, A.; Reinhoudt, D. N. *Angew. Chem., Int. Ed. Engl.* **1992**, *31*, 1075–1077. (b) Vreekamp, R. H.; Verboom, W.; Reinhoudt, D. N. *Rec. Trav. Chim. Pays-Bas* **1996**, *115*, 363–370.

(34)   (a) Rudkevich, D. M.; Verboom, W.; Reinhoudt, D. N. *J. Org. Chem.* **1994**, *59*, 3683–3686. (b) Van Wageningen, A. M. A.; Snip, E.; Verboom, W.; Reinhoudt, D. N.; Boerrigter, H. *Liebigs Annalen/Recueil* **1997**, *11*, 2235–2245.

(35)   (a) Saadioui, M.; Shinvanyuk, A.; Böhmer, V.; Vogt, W. *J. Org. Chem.* **1999**, *64*, 3774–3777. (b) Prins, L. J.; Jollife, K. A.; Hulst, R.; Timmerman, P.; Reinhoudt, D. N. *J. Am. Chem. Soc.* **2000**, *122*, 3617–3627.

(36)   Dexter, D. L. *J. Chem. Phys.* **1953**, *21*, 836–850.

(37)   (a) Förster, T. *Ann. Phys.* **1948**, *2*, 55–75. (b) Förster, T. *Z. Naturforsch. A* **1949**, *4a*, 321–327.

(38)   *Molecular Fluorescence*; Valeur, B.; Wiley-VCH: Weinheim 2002; pp 247–272.

(39)   *Principles of Fluorescence Spectroscopy*; Lakowicz, J. R., Ed.; Kluwer Academic Press: New York 1999; Chapters 13 and 14.

(40)   Langhals, H.; Demmig, S.; Huber, H. *Spectrochim. Acta* **1988**, *44A*, 1189–1193.

(41)   *Modern Molecular Photochemistry*; Turro, N. J., Ed.; University Science Books: Sausalito, CA, 1991.

(42)   *Essentials of Molecular Photochemistry;* Gilbert, A., Baggott, J., Eds.; Blackwell Science Ltd.: Oxford, 1991.

(43)   (a) *Electron Transfer in Chemistry*; Balzani, V., Ed.; Wiley-VCH: Weinheim, 2001; Vol. 1-5. (b) Closs, G. L.; Miller, J. R. *Science* **1988**, *240*, 440–447. (c) *Photoinduced Electron Transfer*; Fox, M. A.; Chanon, M., Eds.; Elsevier Science: Amsterdam, 1988. (d) *Fundamentals of Photoinduced Electron Transfer*; Kavarnos, G. J., Ed.; VCH Publishers Inc: New York, 1993. (e) *Charge and Energy Transfer Dynamics in Molecular Systems;* May, V., Kühn, O., Eds.; Wiley-VCH: Weinheim, 2005. (f) Marcus, R. A. *Angew. Chem. Int. Ed. Engl.* **1993**, *32*, 1111–1121. (g) Marcus, R. A.; Sutin, N. *Biochim. Biophys. Acta* **1985**, *811*, 265–322.

(44)   (a) Weller, A. Z. *Phys. Chem., Neue Folge* **1982**, *133*, 93–98. (b) Kroon, J.; Verhoeven, J. W.; Paddon-Row, M. N.; Oliver, A. M. *Angew. Chem., Int. Ed.* **1991**, *30*, 1358–1361. (b) Oevering, H.; Paddon-Row, M. N.; Heppener, M.; Oliver, A. M.; Cotsaris, E.; Verhoeven, J. W.; Hush, N. S. *J. Am. Chem. Soc.* **1987**, *109*, 3258–3269.

(45)   (a) Marcus, R. A. *J. Chem. Phys.* **1956**, *24*, 966–978. (b) Marcus, R. A. *J. Chem. Phys.* **1965**, *43*, 2654–2657.

(46)   (a) *Theory of Molecular Excitons;* Davydov, A. S.; Plenum Press: New York, 1971. (b) Kasha, M.; Rawls, H. R.; Ashraf-El Bayoumi, M. *Pure Appl. Chem.* **1965**, *11*, 371–392.

(47)   (a) Emerson, E. S.; Conlin, M. A.; Rosenoff, A. E.; Norland, K. S.; Rodriguez, H.; Bird, G. R. *J. Phys. Chem.* **1967**, *71*, 2396–2403. (b) Czikkely, V.;

Försterling, H. D.; Kuhn, H. *Chem. Phys. Lett.* **1970**, *6*, 11–14. (c) Daltrozzo, E.; Scheibe, G.; Gschwind, K.; Haimerl, F. *Photogr. Sci. Eng.* **1974**, *18*, 441–450. (d) Wolthaus, L.; Schaper, A.; Möbius, D. *Chem. Phys. Lett.* **1994**, *225*, 322–326. (e) Czikkely, V.; Försterling, H. D.; Kuhn, H. *Chem. Phys. Lett.* **1970**, *6*, 207–210.

(48)   (a) Bohn, P. W. *Annu. Rev. Phys. Chem.* **1993**, *44*, 37–60. (b) *J-Aggregates;* Kobayashi, T., Ed.; World Scientific: Singapore, **1996**.

2

Instrumentation and Experimental Methods

Abstract: In this thesis, several spectroscopic techniques have been applied to study the photophysical properties of the synthesized compounds in their ground and excited state (inspected by light or electric current). In this Chapter, the methods used are briefly described and the experimental set-ups used are specified. A short description of the spectrotemporal parameterization method is given. Conditions for common techniques (NMR, UV/vis absorption and steady state fluorescence measurements) are given in the following chapters.[i]

---

[i] Femtosecond transient absorption and time-resolved fluorescence data were measured at the Universiteit van Amsterdam, The Netherlands, under the guidance of Dr. R. Williams. Global and target analysis was performed by Dr. I. van Stokkum at the Vrije Universiteit van Amsterdam, The Netherlands. Spectro-electrochemical data were measured in the group of Prof. Dr. Ch. Lambert under the guidance of D. Nowak at the University of Würzburg, Germany. Cyclic voltammetry was performed by A.-M. Krause at the University of Würzburg, Germany.

2.1   Time-Resolved Spectroscopy Measurements

2.1.1   Femtosecond transient absorption measurements

Femtosecond transient absorption experiments were performed with a Spectra-Physics Hurricane Titanium:Sapphire regenerative amplifier system[1] using the setup installed at the Universiteit van Amsterdam. For a schematic representation of the setup see Figure 1. The optical bench assembly of the Hurricane includes a seeding laser (Mai Tai), a pulse stretcher, a Titanium:Sapphire regenerative amplifier, a Q-switched pump laser (Evolution) and a pulse compressor. The full spectrum setup was based on an optical parametric amplifier (Spectra-Physics OPA 800) as the pump. The residual fundamental light from the pump OPA was used for white light generation, which was detected with a CCD spectrograph (Ocean Optics). The polarization of the pump light was controlled by a Berek Polarization Compensator (New Focus). The Berek-Polarizer was always included in the setup to provide the Magic-Angle conditions. The probe light was passed over a delay line (Physik Instrumente, M-531DD) that provides an experimental time window of 1.0 ns with a maximal resolution of 0.6 fs/step. The OPA was used to generate excitation pulses at 530 nm and 640 nm, respectively. The laser output was typically 5 mJ pulse^{-1} (130 fs FWHM) with a repetition rate of 1 kHz. The samples were placed into cells of 2 mm path length (Hellma) and were stirred with a stir bar. Samples were prepared to have an optical density of *ca.* $0.3 - 0.6$ at the excitation wavelength and were degassed for 15 minutes with argon gas prior to the measurements. The UV/vis absorption spectra of the samples were measured before and after the laser experiments, and the spectra were virtually identical, thus possible degradation or chemical change of the samples could be ruled out. All photophysical data reported here have a 5-10% error limit, unless indicated otherwise. The experiments were performed at room temperature. The power dependence was determined and it was found that the spectral and kinetic behavior was independent of the laser power used. Four different laser powers were applied by modulating the maximum laser power of the pump beam with a neutral density filter wheel.
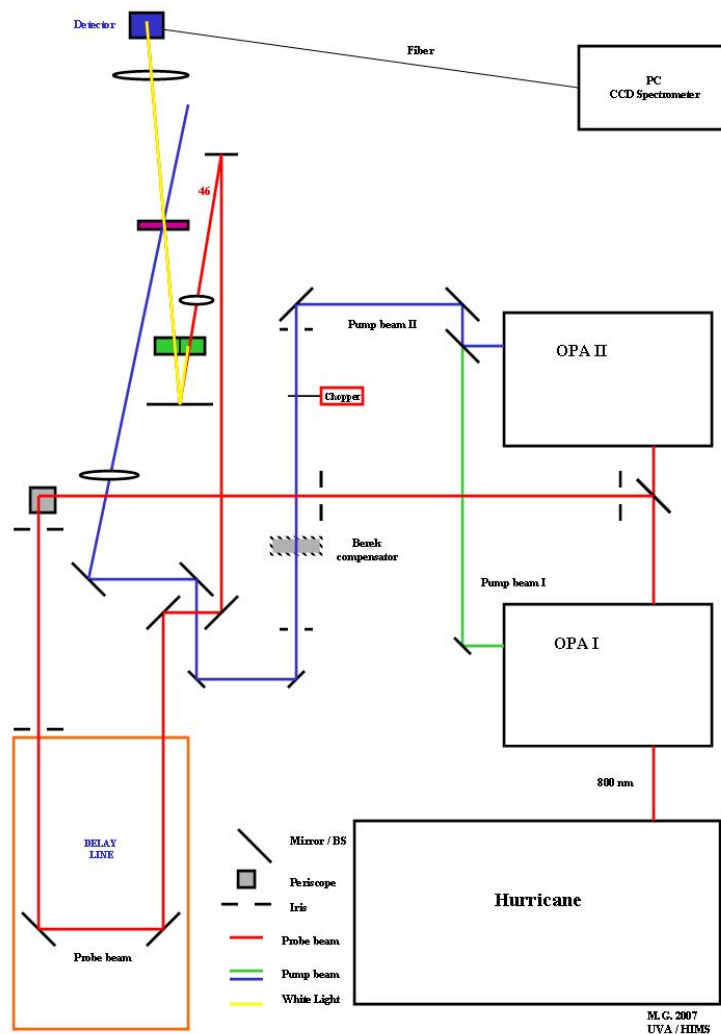
Figure 1. Schematic representation of the femtosecond transient absorption setup used.

2.1.2   Time-Resolved Fluorescence Measurements

Time-resolved fluorescence data were measured with a streak camera system, a schematic representation of the experimental setup is shown in Figure 2. Accordingly, the photocathode converts light into electrons that are accelerated by a positive electrode. When the electrons reach the area of the sweep electrodes a voltage ramped linearly in time is applied to sweep the electrons downwards. The voltage ramp can be varied in such a way to obtain time windows from 1 ns to 10 ms. Then the spectrally and time-separated electrons reach a micro channel plate intensifier to be multiplied 10^4 times, depending on the MCP gain voltage applied and successively hit a phosphor screen. The light-emitting

from the phosphor is then recorded by a lens coupled digital CCD camera. Further details of the method are described in the literature.[2] As excitation source a Spectra-Physics Hurricane Titanium:Sapphire regenerative amplifier system was used.[1] The excitation wavelengths of 530 and 640 nm, respectively, were generated with an optical parametric amplifier (Spectra-Physics OPA 800). The excitation light was imaged onto the cell with a mirror and the emission light was collected with a fiber coupled to the spectrograph of the streak setup. To get the best temporal resolution at short times, the streak camera was run in "dump mode". In this mode, the sync signal from the hurricane setup is combined with the trigger signal form a triggering diode to gain optimal resolution yielding a system response of approximately 150 ps. Typical laser output was 5 mJ per pulse (130 fs FWHM) with a repetition rate of 1 kHz. The samples were placed into 10 mm quartz cells and were degassed for 15 minutes with argon gas prior to the measurements. Samples were prepared to have an optical density of *ca.* 0.3 − 0.6 at the excitation wavelength. Steady state absorbance measurements were performed before and after the laser experiments to rule out possible degradation of the sample.
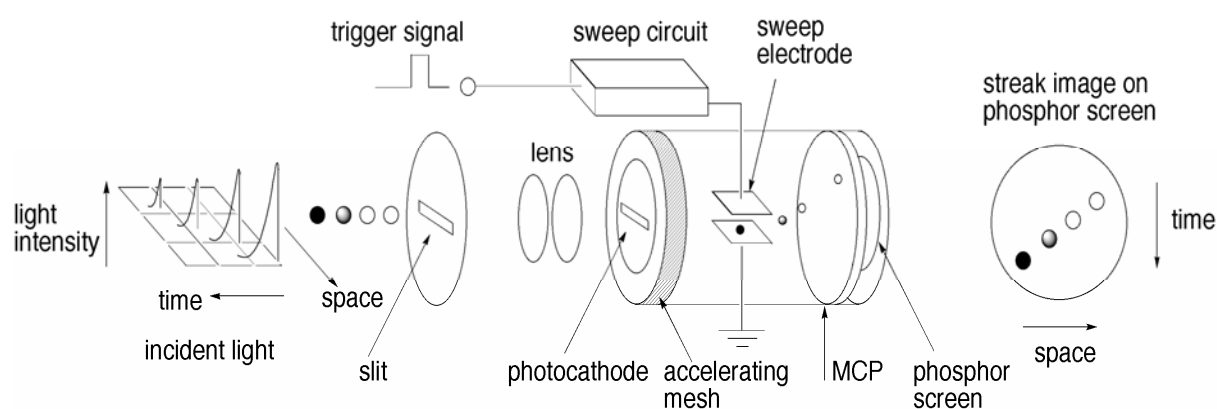

Figure 2. Schematic representation of the streak camera setup.

2.2   Global and Target Analysis

The kinetic profiles of the observed photoinduced processes are difficult to analyze by single wavelength fitting because usually several processes take place concomitantly after photoexcitation. For this reason, the femtosecond transient absorption data-matrices as well as the streak camera data were analyzed with spectrotemporal parameterization, an advanced global and target analysis method that has been developed in particular to elucidate photoinduced processes in complex biological systems such as photosystems.[3] Here *global* refers to a simultaneous analysis of all measurements, whereas *target* refers to the applicability of a particular target model (see below). Because the time information at all wavelengths is analyzed, this analysis gives a more in-depth view of the occurring photoinduced processes. For this purpose, all time-gated spectra are collected in a matrix, which was globally fitted applying a *sequential* kinetic scheme with increasing lifetimes. This procedure yields the evolution-associated difference spectra (EADS) – the steady state spectra of the individual excited state species – together with their respective rate constants. The EADS thus represent the spectral evolution of the excited state species.[ii] The instrument response function (IRF) is described by a Gaussian shape, and the white light dispersion over the spectral range is modeled by a third order polynomial. With increasing lifetimes, and thus decreasing rates, the first EADS decays with the first lifetime and corresponds to the difference spectrum at time zero with an ideal infinitely small IRF. The second EADS is formed with the first lifetime and decays with the second lifetime, etc. The final EADS represents the difference spectrum of the longest living species. The error in the lifetimes obtained from the fitting procedure does not exceed 10%. However, in the EADS the time constants of the processes may correspond to the *lifetimes* of the transient species, but the spectral profiles do not necessarily need to represent the pure excited-state *spectra* of the molecules: given the fact, that the applied sequential scheme with increasing lifetimes represents the correct physicochemical picture, the EADS indeed correspond to the true spectra of the individual excited state species characterizing the intermediate states. These "true spectra" are also referred to as Species Associated

---

[ii] Note for comparison: DADS = decay associated difference spectra, are interpreted as loss or gain of a certain property, *e.g.* absorption, with a certain lifetime.

Difference Spectra (SADS) and will in this case be identical to the EADS. EADS are thus interpreted as a weighted sum (with only positive contributions) of species-associated difference spectra (SADS). The quality of the fit was judged by inspection of the singular vectors of the matrix of residuals, which had to be structureless. However, for more complex systems following *non-sequential* kinetical schemes (see above) the EADS will *not* truly reproduce the spectra of the individual excited species; and EADS and SADS will differ substantially. To obtain the *correct* SADS (= the correct difference spectra of the individual species) a target analysis needs to be applied. Thus, one needs to take into account additional (e.g. experimentally based) parameters that are summarized into a specific photophysical or photochemical model utilized for the fitting procedure. Accordingly, in the target analysis a kinetic scheme is used in combination with spectral assumptions to estimate microscopic rate constants and SADS. As a further refinement, to deal with fluctuations in the pump-probe overlap, we used the estimated SADS to fit the original data matrices, with the help of a spectral model. Finally, the thus estimated concentration profiles were again fitted with the kinetic scheme. A full description of the method has been given in the literature.[3]

2.3   Spectroelectrochemistry

Spectroelectrochemical experiments were performed in a specially designed sample compartment consisting of a cylindrical quartz cell, a platinum disc electrode ($\varnothing$ 6 mm), a gold-covered metal (V2A) plate as the auxiliary electrode and a Ag/AgCl pseudo-reference electrode. All spectra were recorded in reflection mode and the optical path length was varied by adjusting the vertical position of the working electrode with a micrometer screw. The potential applied was varied in steps of 10-100mV and a UV/vis/NIR absorption spectrum was recorded ca. 1 minute after increasing the potential. All compounds were checked for reversibility of the spectra.

2.4   Cyclic voltammetry

Cyclic voltammetry (CV) was performed with a BAS Cell Stand C3 electrochemical analyzer in a three electrode single-component cell under argon. Dichloromethane (HPLC grade, VWR International, stabilized with 0.1% ethanol) was used as solvent that was dried over calcium hydride and degassed prior to measurement. The supporting electrolyte tetrabutylammoniumhexafluorophosphate (TBAHFP) was recrystallized from ethanol/water and dried in high vacuum. The measurements were carried out at a concentration of 10^{-4} M with ferrocene as internal standard for the calibration of potential. Working electrode: Pt disc; reference electrode: Ag/AgCl; auxiliary electrode: Pt wire.

2.5   References

(1)   Vergeer, F. W.; Kleverlaan, C. J.; Stufkens, D. J. *Inorg. Chim. Acta* **2002**, *327*, 126–133.

(2)   Lauteslager, X. Y.; Van Stokkum, I. H. M.; Van Ramesdonk, H. J.; Brouwer, A. M.; Verhoeven, J. W. *J. Phys. Chem. A*, **1999**, *103*, 653–659.

(3)   (a) Van Stokkum, I. H. M.; Larsen, D. S.; Van Grondelle, R. *Biochim. Biophys. Acta* **2004**, *1657*, 82–104. (b) Van Stokkum, I. H. M.; Lozier, R. H. *J. Phys. Chem. B* **2002**, *106*, 3477–3485.

50

3

Excited State Interactions in Calix[4]arene–Perylene Bisimide Dye Conjugates

Abstract: The syntheses and photophysical properties of a series of perylene bisimide–calix[4]arene conjugates, consisting of three different types of perylene bisimide (PBI) chromophores (orange, red and green) either substituted with one or two calix[4]arene moieties in the N-imide position, are described. A complete picture of the processes taking place after photoexcitation in toluene, CH_2Cl_2 and benzonitrile was obtained by means of UV/vis absorption, steady state and time-resolved emission, as well as femtosecond transient absorption spectroscopy. It has been found that the fluorescence quantum yields of the orange compounds **oc** and **oc2** are almost completely quenched compared to the highly emissive reference compound **oref** due to fast electron transfer processes from the calix[4]arene moieties to the perylene bisimide chromophore (k_{CS} = 3 x 10^{10} s^{-1} for compound **oc** and k_{CS} = 9 x 10^{10} s^{-1} for compound **oc2** in CH_2Cl_2, respectively) leading to a short-lived charge-separated state consisting of the reduced perylene bisimide unit and the oxidized calix[4]arene moiety. No such effects are observed for the red and green conjugates **rc**, **r2c**, **gc**, and **g2c**, respectively, which is rationalized by the more electron-rich perylene bisimide cores of these compounds.

3.1   Introduction

The proper spatial organization of functional dye building blocks in nanoscopically ordered supramolecular structures enhances both efficiency and output of specific processes, such as energy and electron transfer for light-harvesting purposes and conversion or storage of photochemical energy.[1] Calixarenes[2] are readily available supramolecular building blocks which represent next to the crown ethers[3] and the cyclodextrins[4] the third generation of supramolecular host molecules. They consist of aromatic (*arene)* units (separated by methylene groups) that make up the walls of the chalice *(calix)*[2] and are thus an ideal scaffold on which to assemble various desired functionalities such as nonlinear optical dyes,[5] electrophores,[6] and fluorophores.[7] Their applications range from the use as highly specific ligands for analytical chemistry and sensor techniques to applications in medical diagnostics. Accordingly, a variety of receptors for cations, anions, and neutral guests made from calix[4]arenes have been reported.[8]

Perylene bisimides (PBIs) represent important photo- and electro-active building blocks in supramolecular dye chemistry.[9,10] Apart from their excellent emissive properties[11] also their high absorption coefficients, their exceptional photochemical stability and the fact that they are suitable for single-molecule spectroscopy[12] make them highly promising candidates for photoactive supramolecular constructs. Furthermore, the perylene bisimide chromophore can be easily fine-tuned by proper substitution in the so-called *bay*-positions to exhibit quite divers electronic and optical properties.[9] As such, the classes of phenoxy-(red)[13] and pyrrolidino-(green)[14] *bay*-substituted perylene bisimides as well as the core-unsubstituted PBIs (orange)[15] are available.

Towards the goal of designing new photofunctional supramolecular architectures, the covalent combination of perylene bisimide dyes with calix[4]arene moieties has been reported recently, using the latter as a versatile scaffold to organize the dye units.[16-18] However, if the design of the new building block involves the incorporation of photo- or redoxactive components, it is possible that both ground- and excited state properties of the dyes change upon formation of the conjugated system and thus can give rise to novel properties, *e.g.* the system might, for example, exhibit luminescence properties different from those of the parent chromophores.[19] As such, it has been observed for calix[4]arene-

perylene bisimide conjugates containing an orange PBI unit that both lifetimes and quantum yields of the attached perylene bisimide chromophores dramatically changed upon substitution with the calix[4]arene unit due to a fluorescence quenching process[16] whereas the respective unsubstituted perylene bisimide moiety shows a fluorescence quantum yield of about unity.[9,11a] However, only basic studies of the observed photoinduced processes have been conducted so far. Furthermore, these preliminary results did not provide detailed insight into the exact processes following photoexcitation.

In the present Chapter a series of PBI-calix[4]arene derivatives has been synthesized, consisting of three different types of perylene bisimide chromophores (orange, red and green) either substituted with one or two calix[4]arene moieties in the N-imide position. Their photophysical properties as well as those of the related reference PBI chromophores without calix[4]arene functionalization are investigated. The photoinduced processes are studied with time-resolved emission and femtosecond transient absorption spectroscopy. A quantitative analysis of the photophysical processes as well as their rates have been obtained by using UV/vis absorption, steady state and time-resolved emission, and femtosecond transient absorption spectroscopy, and furthermore, a spectrotemporal analysis of the energetics of the processes was carried out. The compounds studied as well as their syntheses and the structures of the related reference systems are shown in Scheme 1. Three types of perylene bisimide dyes are used: orange (**o**), red (**r**) and green (**g**). Thus, three compounds containing one calix[4]arene unit (**oc**, **rc** and **gc**), three compounds containing two calix[4]arene units (**oc2**, **rc2**, and **gc2**) and the reference systems containing no calix[4]arene units (**oref**, **rref**, and **gref**) are studied.

Scheme 1. Synthetic routes and chemical structures of PBI–calix[4]arene conjugates and reference compounds studied.[a]
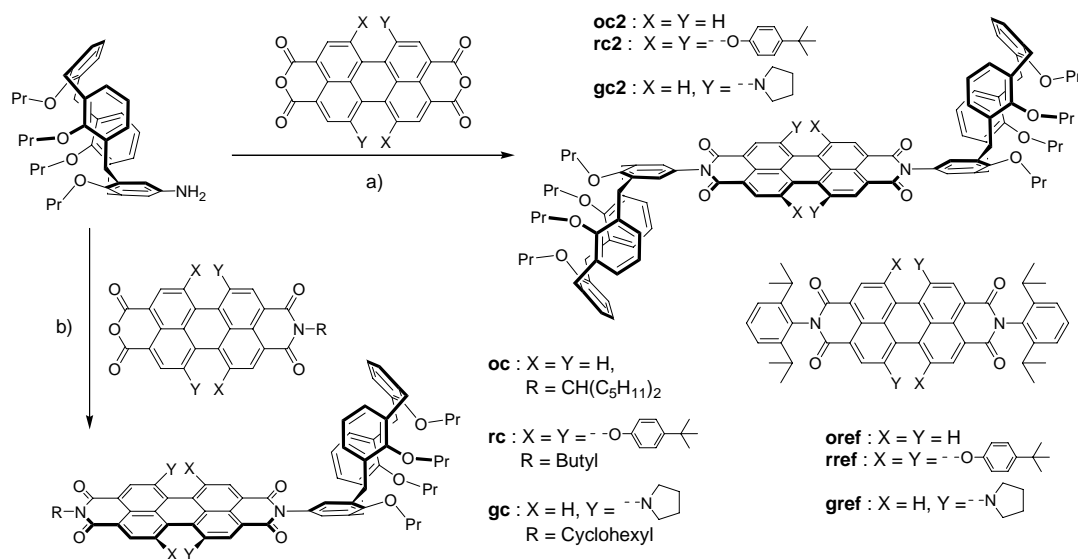
[a] Reagents and conditions: a) **oc2**: Zn(OAc)$_2$, quinoline, 160 °C, yield 28%; **rc2**: Et$_3$N, toluene, 90 °C, yield 47%; **gc2**: Zn(OAc)$_2$, quinoline, 150 °C, yield 43%. b) Zn(OAc)$_2$, quinoline, 165 °C for both compounds **oc** (yield 85%) and **rc** (yield 40%), respectively; for **gc**: Zn(OAc)$_2$, quinoline, 140 °C, yield 38%.

3.2   Synthesis and Structural Characterization

The studied perylene bisimide–calix[4]arene arrays were synthesized according to Scheme 1. For this purpose, two equivalents of 5-monoamino-25,26,27,28-tetrakis(propyloxy)-calix[4]arene were reacted with three different types (orange, red and green) of perylene bisanhydrides (PBA) to yield the biscalix[4]arene-substituted perylene bisimide (PBI) compounds **oc2**, **rc2** and **gc2.** The imidization was carried out either in toluene/Et$_3$N at 90 °C (for compound **rc2**) or in quinoline (at 150 °C or 160°C), using Zn(OAc)$_2$ as a catalyst (for the syntheses of compounds **g2c** and **o2c**, respectively). Upon reaction of only one equivalent of 5-monoamino-25,26,27,28-tetrakis(propyloxy)-calix[4]arene with the respective perylene monoanhydride monoimide, the monocalix[4]arene-substituted PBI-compounds **oc**, **rc**, and **gc** were obtained under similar reaction conditions (for details see Scheme 1). All products were purified by column chromatography (SiO$_2$) and were characterized by ^{1}H NMR spectroscopy and high resolution mass spectrometry.

Single crystals of compound **oc2** suitable for an X-ray analysis could be obtained by slow crystallization from chloroform/methanol at room temperature. Figure 1 shows the molecular structure and a view of the crystal packing of **oc2**, revealing a herringbone arrangement of the molecules. The crystal packing does not show any π–π-stacking of the perylene units and no lattice solvent molecules are included in the crystal. The molecule
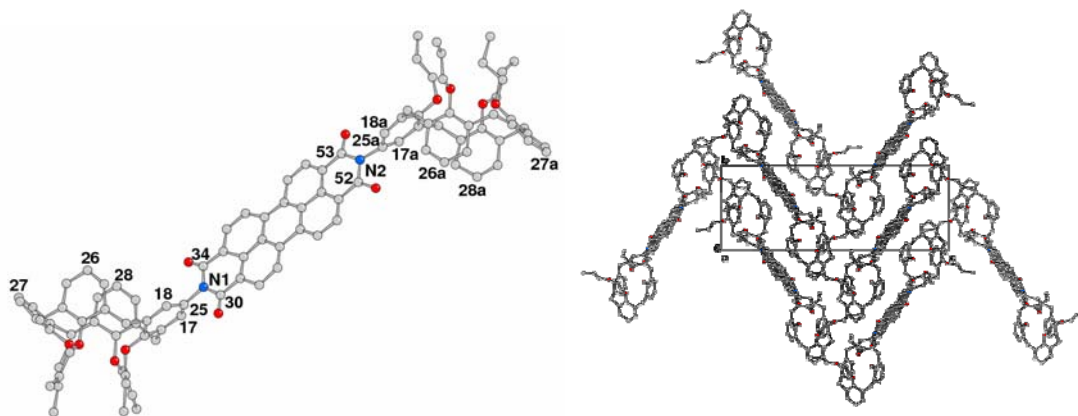

Figure 1. Molecular structure of **oc2** in the crystalline state (left, H atoms omitted for clarity, only number of relevant C atoms indicated) and view of the packing of **oc2** in the crystal (right).

has a pseudo 2/m symmetry with the twofold axis passing almost normally to the perylene moiety. Two calix[4]arene residues at the imide-N are oriented almost orthogonal on opposite sides of the plane dissecting the perylene chromophore. The PBI exhibits a flat π-system, being ±0.10 Å the maximum deviation of atoms from their mean plane. The calix[4]arene units are found in a *pinched cone* conformation. The dihedral angles formed by the C26/C28 and C25/C27 rings are of 11.8° and 80.3° (mean values), and correspondingly the C26-C28 and C25-C27 distances are 4.52(3) Å and 9.77(4) Å, respectively. The dihedral angles between the calix[4]arene phenyl rings of the calix[4]arene and a "reference plane" passing through the four CH_2-methylene bridges of the calix[4]arene are 40.8(6)° for the phenyl ring containing the carbon atom C25 (phenyl rings are indicated by C label, see Figure 1), 89.5(4)°, 39.1(6)° and 78.0(4)° for the phenyl unit containing the carbon atom C26, C27, and C28, respectively. The corresponding values measured in the other calix[4]arene moiety are 43.4(7), 82.1(4), 37.5(6), and 86.8(4)° for ring 25a, 26a, 27a and 28a, respectively. The conformation of the calix[4]arene units with respect to the perylene bisimide moiety is provided by the torsion angles around the N1-C25 and N2-C25a bonds. The calculated values are -111.7(19)°

(C30-N1-C25-C17), 74.9(19)° (C30-N1-C25-C18), 65(2)° (C34-N1-C25-C17) and -108.9(18)° (C34-N1-C25-C18). The analogous data in the other unit are 107(2)°, -58(4)° and 118(3)°, -77(3)°.

3.3   Optical Properties

All compounds were studied by UV/vis absorption and steady state fluorescence emission spectroscopy in CH_2Cl_2. Their photophysical properties are summarized in Table 1, and the UV/vis absorption and fluorescence emission spectra of compounds **oc**, **rc**, and **gc** in CH_2Cl_2 are exemplarily depicted in Figure 2. The absorption spectra in CH_2Cl_2 show the characteristic maxima of the respective perylene bisimide (PBI) chromophores: for compound **oc** maxima at 526 and 490 nm (orange PBI), for compound **rc** at 578 nm (red PBI), and for compound **gc** at 701 nm (green PBI) are observed. The biscalix[4]arene-substituted compounds **oc2**, **rc2** and **gc2** exhibit similar absorption profiles, but the absorption maxima are slightly shifted for compound **rc2** to 579 nm and for compound **gc2** to 704 nm.

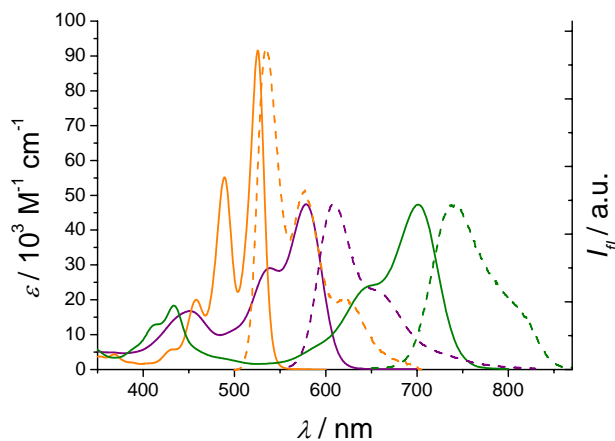

Figure 2. UV/vis absorption (orange, solid line) and fluorescence emission spectra (orange, dashed line) of compound **oc**; UV/vis absorption (violet, solid line) and fluorescence emission spectra (violet, dashed line) of compound **rc**; UV/vis absorption (green, solid line) and fluorescence emission spectra (green, dashed line) of compound **gc**. All spectra are taken in CH_2Cl_2.

For the green compounds **gc** and **gc2** the values for the fluorescence quantum yield range from 0.17 in the more polar solvent benzonitrile up to 0.29 in the less polar solvent toluene (see Table 1). This is in good agreement with the values obtained for the green reference compound **gref** in the variate solvents. In general, for less polar solvents higher values for the fluorescence quantum yield are observed for all compounds **gref**, **gc**, and **gc2**, respectively. The fluorescence emission data thus indicate that the fluorescence properties of the green systems remain almost unchanged upon attachment of one or two calix[4]arene substituents in the imide positions, respectively, and that the latter are apparently independent of the solvent polarity.

Table 1. Optical properties in toluene (Tol), CH_2Cl_2, and benzonitrile (PhCN).[a]

Cmpd	UV/vis absorption		Fluorescence emission						
	λ_{max} (nm) CH_2Cl_2	ε ($M^{-1}cm^{-1}$) CH_2Cl_2	λ_{max} (nm) CH_2Cl_2	Φ_{fl} Tol	Φ_{fl} CH_2Cl_2	Φ_{fl} PhCN	τ (ns) Tol	τ (ns) CH_2Cl_2	τ (ns) PhCN
oref	527	93600	534	~1.00[b]	0.99	~1.00[b]	4.0	4.9	3.9
oc	526	91600	535	0.02	0.03	0.02	---[c]	---[c]	---[c]
oc2	526	97200	532	<0.01	<0.01	<0.01	---[c]	---[c]	---[c]
gref[d]	709	43000	747	0.24	0.19	0.18	4.3	3.1	2.5
gc[d]	701	47300	742	0.29	0.19	0.17	4.4	3.3	2.7
gc2[d]	704	51200	741	0.25	0.18	0.19	4.4	3.3	2.8
rref	582	49700	615	0.97	0.99	0.95	6.1	6.9	6.3
rc	578	47400	608	~1.00[b]	0.80	0.81	6.3	5.6	4.7
rc2	579	54000	610	0.98	0.71	0.70	5.5	4.6	4.1

[a] All spectra were recorded at room temperature. [b] $\Phi_{Fl} \pm 0.02$. [c] Values could not be determined as the signal falls into the time response of the instrument of ca. 150 ps. [d] Note, that for all lifetimes determined for compounds **gref, gc** and **gc2** biexponential decays were observed. Accordingly, additional small components are found which are considered to be inherent to the green PBI chromophore itself (values given in ns with the respective amplitudes in brackets): For compound **gref**: 0.7 (5%) in toluene, 0.4 (8%) in CH_2Cl_2, 0.3 (30%) in benzonitrile, respectively. For compound **gc**: 0.5 (20%) in toluene, 0.4 (15%) in CH_2Cl_2, 0.2 (30%) in benzonitrile, respectively. For compound **gc2**: 0.9 (15%) in toluene, 1.0 (15%) in CH_2Cl_2, 1.0 (12%) in benzonitrile, respectively.

In contrast, solutions of the two calix[4]arene substituted orange compounds **oc** and **oc2** exhibit almost no fluorescence ($\Phi_{fl} = 0.03$ for **oc** and $\Phi_{fl} < 0.01$ for **oc2**, respectively), whereas without calix[4]arene substituents the orange perylene bisimide reference compound **oref** belongs to one of the most efficient fluorophores with a fluorescence quantum yield of about unity.[9,11a,15] This behavior is also observed for the values for the

fluorescence quantum yields in the less polar solvent toluene (Φ_{fl} = 0.02 for **oc** and Φ_{fl} = <0.01 for **oc2**) and the more polar solvent benzonitrile (Φ_{fl} = 0.02 for **oc** and Φ_{fl} = <0.01 for **oc2**), whereas the values for the fluorescence quantum yields for the orange reference compound **oref** remain of about unity independent of solvent polarity (see Table 1). The fluorescence emission data thus indicate an additional process taking place for both compounds **oc** and **oc2** that strongly reduces the perylene bisimide fluorescence intensity upon attachment of the calix[4]arene moiety in the variate solvents. Thus, the electron-rich calix[4]arene acts as a fluorescence quencher for the electron-poor PBI chromophore.

This quenching effect is also present to a slight extent in the red systems **rc** and **rc2**. The latter are, however, still highly fluorescent as they show fluorescence quantum yields of 0.80 for compound **rc** and 0.71 for compound **rc2** in CH_2Cl_2, respectively, compared to the reference compound **rref** without calix[4]arene substitution for which a quantum yield of Φ_{fl} = 0.99 is observed. Likewise, slightly reduced values for the fluorescence quantum yields for arrays **rc** and **rc2** (Φ_{fl} = 0.81 for **rc** and Φ_{fl} = 0.70 for **rc2**, respectively) compared to the value for the red reference compound **rref** (Φ_{fl} = 0.95) are also found for the more polar solvent benzonitrile. In contrast, in the less polar solvent toluene no fluorescence quenching effect is observed, and a good agreement of the values for the fluorescence quantum yields of the calix[4]arene-substituted arrays **rc** and **rc2** with those obtained for the non calix[4]arene-substituted red reference compound **rref** is found (quantum yields of about unity for **rc**, **rc2**, and **rref**, respectively). The fluorescence emission data thus indicate that the fluorescence properties of the red calix[4]arene-functionalized systems **rc** and **rc2** are slightly disturbed upon attachment of one or two calix[4]arene substituents in the imide positions, respectively, and that a slight fluorescence quenching is observed for increasing solvent polarity. However, considering the overall performance of the red systems **rc** and **rc2,** both arrays are still highly luminescent despite calix[4]arene substitution.

Furthermore, the fluorescence lifetimes of all compounds have been determined in toluene, CH_2Cl_2, and benzonitrile, respectively; and the obtained values are summarized in Table 1. For the green reference compound **gref** fluorescence lifetime values of 2.5 ns in benzonitrile, of 3.1 ns in CH_2Cl_2, and of 4.3 ns in toluene are found, respectively (see Table 1), that are in good agreement with literature data for a related derivative.[9] The

fluorescence lifetime values for compounds **gc** and **gc2** are found to be similar to those of compound **gref** in the respective solvent (see Table 1). Apparently, the fluorescence lifetime of the green systems remains almost unchanged upon attachment of one or two calix[4]arene substituents in the imide positions.[i]

For the orange reference compound **oref** fluorescence lifetime values of 3.9 ns in benzonitrile, 4.9 ns in CH_2Cl_2, and of 4.0 ns in toluene, respectively, have been determined, being in reasonable agreement with literature data for this compound[10] and also for related derivatives.[9,11a] In contrast, for the orange calix[4]arene substituted PBI compounds **oc** and **oc2** drastically shortened fluorescence lifetimes values of less than the system response time of approximately 150 ps are found in all three solvents. Apparently, the lifetime of the orange systems is strongly reduced upon attachment of one or two calix[4]arene substituents.

For the red reference compound **rref** fluorescence lifetime values of 6.3 ns, of 6.9 ns, and of 6.1 ns are found in benzonitrile, CH_2Cl_2, and toluene, respectively, being in good agreement with literature data for this compound.[10,11b] The fluorescence lifetimes of both the red calix[4]arene substituted compounds **rc** and **rc2** are in reasonable agreement with those obtained for the reference compound **rref** (see Table 1). Accordingly, the lifetime values in toluene do not change significantly for compounds **rc** and **rc2**, respectively, compared to the reference compound **rref** (see Table 1), and also for the more polar solvents CH_2Cl_2 and benzonitrile only a slight decrease is observed (reduction of the lifetime values in CH_2Cl_2 to 80% for **rc** of the value obtained for **rref**, and to 67% for **rc2**, respectively; and in benzonitrile to 75% for **rc** and to 65% for **rc2**; see Table 1). These observations indicate a solvent dependent quenching process of minor importance for the red calix[4]arene compounds.

Accordingly, the changes in the fluorescence lifetimes upon attachment of one or two calix[4]arene units to the respective orange, red and green PBI chromophore depending on

---

[i] Note, that for all lifetimes determined for compounds **gref, gc**, and **gc2** biexponential decays are observed. Accordingly, additional small components of ca. 0.5 ns are found for each compound independent of the solvent polarity and of the calix[4]arene substitution of the chromophore. The latter components are thus considered to be independent of the calix[4]arene substitution of the dye unit and are assumed to be inherent to the green PBI chromophore itself (for details refer to Table 1.)

the solvent polarity thus relate to the general trends already observed by steady state fluorescence spectroscopy: a strong quenching is observed for the orange chromophoric unit in both compounds **oc** and **oc2**, whereas the properties of the red systems **rc**, **rc2** are only slightly, and those of the green systems **gc**, **gc2** are not substantially influenced by the calix[4]arene substituent.

3.4   Electrochemistry and Spectroelectrochemistry

Compounds **oc**, **rc** and **gc** were investigated by cyclic voltammetry in CH_2Cl_2 (vs. Fc/Fc$^+$), and the obtained cyclic voltammograms (CVs) are shown in Figure 3, and the respective data are summarized in Table 2. For the orange compound **oc** two reversible reduction bands at –1.01 V and –1.32 V (vs. Fc/Fc$^+$ couple) are observed that can be attributed to the radical monoanion and dianion formation of the perylene bisimide chromophore.[10] In the anodic cycle an irreversible oxidation wave is found at around +1.10 V. This process can not be attributed to the perylene bisimide unit whose oxidation is known to occur at higher voltage.[10] When examining the CV of the plain tetrapropyloxy-calix[4]arene bearing no PBI-substituents, a similar irreversible feature above +1.15 V is observed (see Figure 3, bottom right, and Figure 16 in the Appendix of this Chapter). For methoxybenzene, which serves as a reference compound for the attached calix[4]arene moiety, an oxidation potential of +1.24 V (recalculated from +1.76 V vs. SCE, value in acetonitrile)[20] is reported in the literature. The irreversible oxidation features observed in the CV of compound **oc** are thus attributed to the oxidation of the calix[4]arene moiety (further on referred to as E_{ox}(Calix)). The reduction potentials found for the perylene bisimide moiety (further on referred to as E_{red}(PBI)) closely resemble the values reported in the literature for the non-calix[4]arene substituted reference compound **oref** (see Table 2).[9,10]

The red compound **rc** shows two reversible waves in the reductive cycle at –1.20 V and –1.35 V due to the formation of the red PBI radical monoanion and dianion, and one reversible wave in the oxidative cycle at +0.81 V (formation of the radical monocation of the red PBI unit),[10] accompanied by an irreversible oxidation process above +1.12 V, which was assigned to the oxidation of the calix[4]arene moiety (see above). Again, a close match of the observed redox potentials with literature data is found.[9,10]
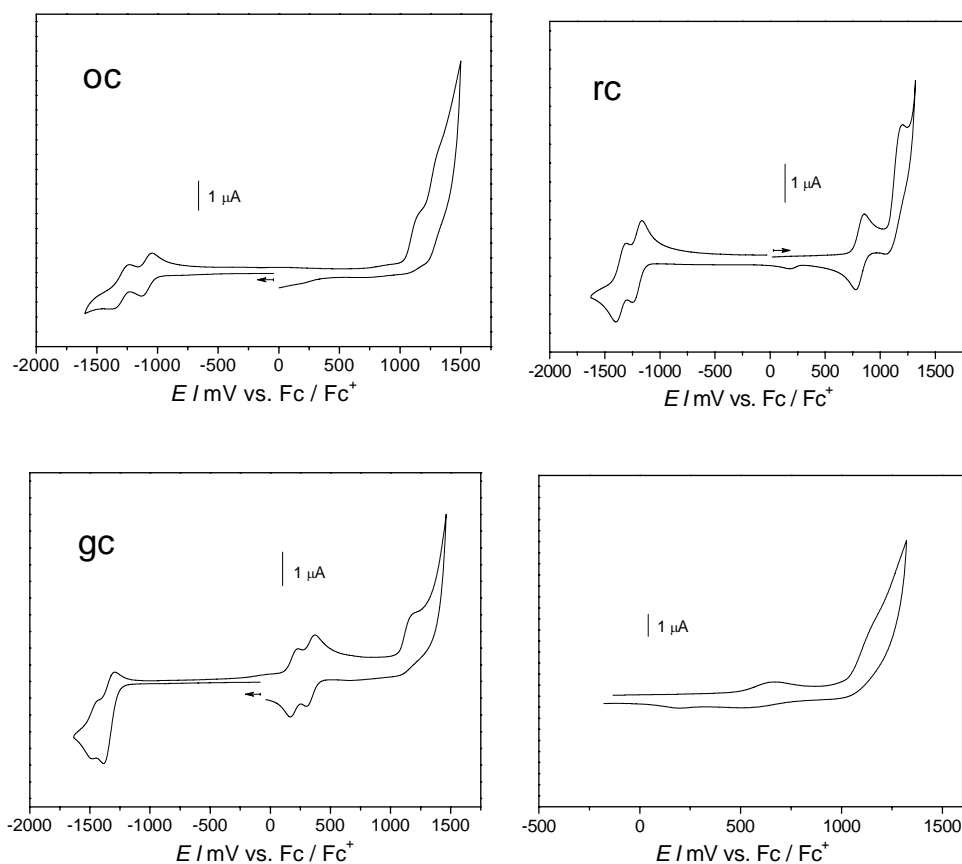
Figure 3. Cyclic voltammograms in CH_2Cl_2 of compound **oc** (top left, concentration = 1.0 x 10^{-4} M), of compound **rc** (top right, concentration = 1.8 x 10^{-4} M), of compound **gc** (bottom left, concentration = 1.0 x 10^{-4} M), and of tetrapropyloxy-calix[4]arene (bottom right, concentration = 1.60 x 10^{-3} M, scan rate 250 mV s^{-1}, see also Figure 16 in the Appendix). Scan rate 100 mV s^{-1} if not indicated otherwise. Working electrode: Pt disc, $\varnothing$ 1 mm; auxiliary electrode: Pt wire; reference electrode: Ag/AgCl; supporting electrolyte TBAHFP (0.1 M).

Table 2. Redox properties in CH_2Cl_2 (in V *vs.* Fc/Fc$^+$). Values of reference compounds are given for comparison.

	E_{red} (PBI$^-$/PBI^{2-})	E_{red} (PBI/PBI$^-$)	E_{ox} (PBI/PBI$^+$)	E_{ox} (PBI$^+$/PBI^{2+})	Onset of irrev. oxidation
oc	−1.32	−1.01	n. det.[b]		+1.10
oref[a]	−1.24	−1.01	+1.29		
rc	−1.35	−1.20	+0.81		+1.12
rref[a]	−1.35	−1.15	+0.86		
gc	−1.48	−1.36	+0.18	+0.32	+1.15
gref	−1.47	−1.33	+0.23	+0.36	

[a] See ref. 10. [b] Value could not be determined owing to the irreversible oxidation process of the calix[4]arene moiety.

For the green compound **gc** potential values of −1.36 V and −1.48 V upon reduction (formation of radical anion and dianion, respectively) and of +0.18 V and +0.32 V upon oxidation (formation of radical cation and dication, respectively) are examined together with an irreversible oxidation wave above +1.15 V, assigned to the oxidation of the calix[4]arene moiety. These values closely relate to the redox potentials observed for compound **gref**. All values are in good agreement with literature data of a related green PBI derivative.[9]

The reduced states of all three reference compounds **oref**, **rref**, and **gref**, respectively, were characterized by spectroelectrochemistry in CH_2Cl_2. All electron transfer products show absorption bands in the visible or near infrared region, their spectroelectrograms are depicted in Figure 4. For the orange compound **oref** an absorption band with a maximum of 713 nm is observed for the mono-reduced chromophore together with smaller bands at 800 nm and 955 nm, being in good agreement with literature data.[21] Upon formation of the radical dianion state an absorption maximum at 575 nm is observed. For the red compound **rref** the absorption band upon mono-reduction is centered around a maximum of 790 nm, together with smaller bands at 980 nm and 1085 nm, being in good agreement with the literature data.[22] For the radical dianionic species a band at 690 nm is found. For the green compound **gref** a band at 820 nm is observed together with a smaller maximum at 505 nm for the mono-reduced state, whereas upon the formation of the radical dianion a band with a maximum at 615 nm is present.
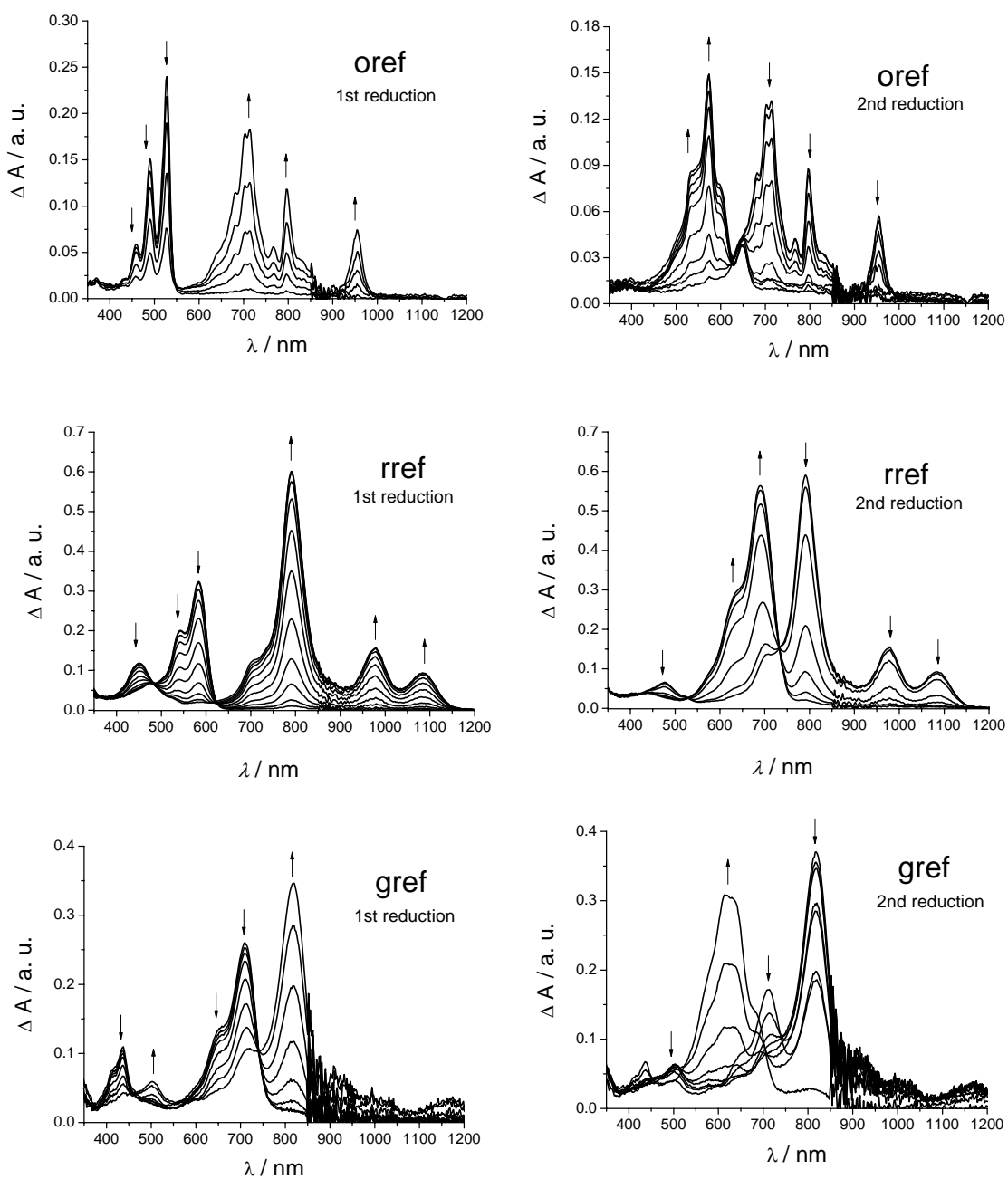
Figure 4. Spectroelectrograms of compounds **oref** (top), **rref** (middle) and **gref** (bottom) in CH$_2$Cl$_2$ with TBAHFP (0.1 M) as supporting electrolyte. Working electrode: Pt disc, $\varnothing$ 6 mm; auxiliary electrode: gold covered metal (V2A) plate; reference electrode: Ag/AgCl. Arrows indicate the spectral changes upon stepwise decrease of the applied potential leading to formation of the respective radical monoanionic (left) and dianionic perylene bisimide species (right).

3.5   Gibbs Energy of Photoinduced Electron Transfer

As discussed above, in the cyclic voltammograms of all three compounds **oc**, **rc**, and **gc**, respectively, an irreversible wave between +1.10 V and +1.15 V was observed, that was attributed to the oxidation of the calix[4]arene moiety. To examine the feasibility of a photoinduced charge separation involving a calix[4]arene radical cationic species it is instructive to consider the thermodynamics of such a process. Therefore, the Gibbs free energy of an intramolecular charge-separated state (ΔG_{CS}) in a covalently bonded donor−acceptor system was calculated for compounds **oc**, **rc** and **gc** using equation (1) where E_{ox}(Calix) represents the value for the first oxidation potential of the calix[4]arene moiety, E_{red}(PBI) denotes the first reduction potential of the respective PBI-acceptor chromophore, E_{00} is the energy of the $S_1 \rightarrow S_n$ excited state, R_{CC} refers to the distance between the centers of the donor and acceptor segments, r^+ and r^- represent the effective ionic radii of the donor radical cation and the acceptor radical anion, respectively, whereas ε_{ref} denotes the reference dielectric constant of the solvent used in electrochemistry and ε_S is the dielectric constant of the actual solvent used:[23]

$$\Delta G_{CS} = e\left[E_{ox}(Calix) - E_{red}(PBI)\right] - E_{00} - \frac{e^2}{4\pi\varepsilon_0\varepsilon_S R_{CC}} - \frac{e^2}{8\pi\varepsilon_0}\left(\frac{1}{r^+} + \frac{1}{r^-}\right)\left(\frac{1}{\varepsilon_{ref}} - \frac{1}{\varepsilon_S}\right) \qquad (1)$$

To calculate ΔG_{CS} according to equation 1, the first reduction potential E_{red}(PBI) (being the first reduction potential of compounds **oc, rc** and **gc**, respectively) in CH_2Cl_2 ($\varepsilon_S = 8.93$), and the onset of irreversible oxidation of the plain tetrapropyloxy-calix[4]arene (+1.10 V for compound **oc**, +1.12 V for compound **rc** and +1.15 V for compound **gc**, respectively) in CH_2Cl_2 were used (for values see Table 3). The distance between the centers of the donor and acceptor segments R_{cc} was estimated from an energy minimized structure (see Figure 5) as $R_{cc} = 8.60$ Å for compound **oc**, $R_{cc} = 8.61$ Å for compound **rc**, and $R_{cc} = 8.62$ Å for compound **gc**, respectively. All electrochemical values were obtained in CH_2Cl_2, and therefore ε_{ref} equals ε_s, and thus the last, solvent related term in equation (1) vanishes.

Table 3. Selected values for the calculation of thermodynamic feasibility of a photoinduced electron transfer process in CH_2Cl_2.

Cmpd	R_{cc} (Å)	E_{00}[a] (nm)	E_{00}[a] (eV)	E_{ox} (V)	E_{red} (V)	ΔG_{CS} (eV)
oc	8.60[b]	529	2.34	+1.10	−1.01	−0.419
rc	8.61[b]	599	2.07	+1.12	−1.20	+0.063
gc	8.62[b]	720	1.72	+1.15	−1.36	+0.603

[a] Calculated from the intersection of the normalized absorption and fluorescence spectra. [b] Values derived from an energy minimized structure obtained from forcefield calculations (Macromodel 8.0, potential MMFF).

The values summarized in Table 3 show that the energy of the intramolecular charge-separated state in CH_2Cl_2 is lower than the energy of the respective singlet excited state for compound **oc** (E_{00} = 2.34 eV), but slightly higher for compounds **rc** (E_{00} = 2.07 eV) and significantly higher for **gc** (E_{00} = 1.72 eV). The thus estimated values for ΔG_{CS} reveal that only for compound **oc** the electron transfer is an exergonic reaction in CH_2Cl_2, whereas for compound **gc** the electron transfer from the calix[4]arene substituent to the perylene bisimide moiety is an endergonic process. Therefore, it can be concluded that the creation of a charge separated state consisting of the radical cation of the calix[4]arene moiety and the radical anion of the perylene bisimide unit is energetically feasible for compound **oc** as the calculation of ΔG_{CS} reveals a negative value of ΔG_{CS} = −0.419 eV. Thus, the strongly decreased fluorescence quantum yields and lifetimes for the orange systems **oc** and **oc2** upon attachment of one or two calix[4]arene moieties compared to the orange reference compound **oref** can be most likely attributed to a rapid photoinduced electron transfer process. For the green system **gc** it can be concluded that the creation of a charge separated state consisting of the radical cation of the calix[4]arene moiety and the radical anion of the perylene bisimide unit is energetically not feasible as the calculation of ΔG_{CS} reveals a positive value of ΔG_{CS} = +0.603 eV. This finding relates to the observations made for the fluorescence quantum yields and lifetimes for both green compounds **gc** and **gc2**, where no changes of the values are found upon attachment of one or two calix[4]arene substituents, respectively, compared to the plain green reference compound **gref**. In contrast, for the red systems **rc** and **rc2** the situation is less conclusive and might be highly dependent on the solvent polarity. The thermodynamic feasibility of the electron transfer is furthermore not
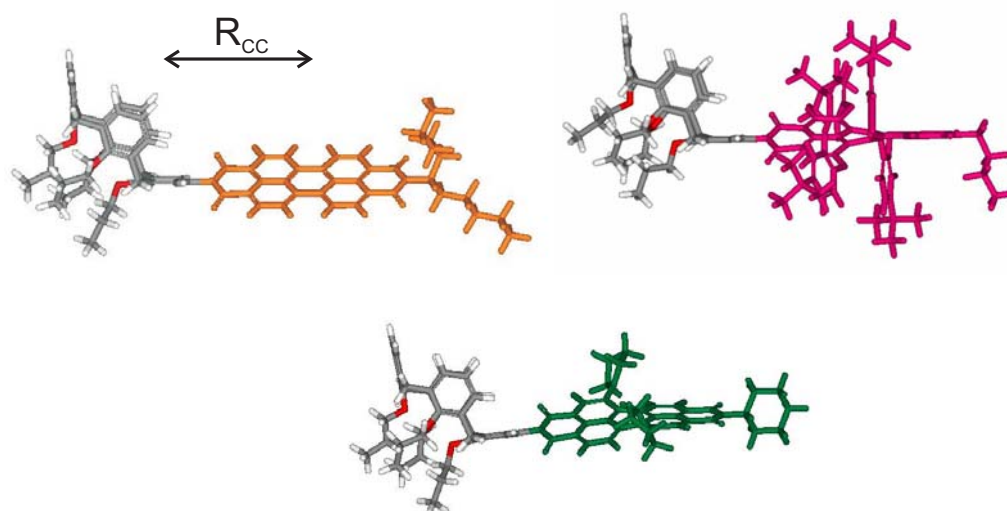
Figure 5. Energy minimized structures of compound **oc** (top left), compound **rc** (top right), and compound **gc** (bottom) obtained from forcefield calculations (Macromodel 8.0, potential MMFF). PBI units are colored for clarity.

easy to predict, because the R_{CC} values as well as the E_{00} energies and the calix[4]arene oxidation potential are only based on estimations.

3.6 Femtosecond Transient Absorption Spectroscopy

As mentioned before, a strong fluorescence quenching, together with a drastically reduced fluorescence lifetime is observed for the orange compounds **oc** and **oc2**. To shed more light on this quenching process, the orange compounds **oc** and **oc2**, as well as the red and green systems **rc**, **rc2**, **gc** and **gc2**, respectively, were investigated with femtosecond transient absorption spectroscopy in toluene, CH_2Cl_2, and benzonitrile. The spectral data obtained in toluene for compounds **oc**, **oref**, **rc**, **rref** and **gc**, **gref** are shown in Figure 6, 7, and 8, respectively (for the spectra in the other solvents and those for compounds **oc2**, **rc2**, and **gc2** see Figures 19, 20 and 21 in the Appendix of this Chapter). For both orange compounds **oc** and **oc2** upon photoexcitation an intense bleaching due to the depopulation of the ground state molecules in the probe area is observed at both 530 nm and 490 nm. These bands are related to the $S_0 \rightarrow S_1$ transitions of the orange PBI chromophore (see Figure 6, left, and Figure 19 in the Appendix of this Chapter). Furthermore, an intense

negative signal is present in both the spectra of **oc** and **oc2** at around 530 and 580 nm which can be assigned to the stimulated emission of the orange PBI chromophore (see Figure 6, left, and Figure 19). These features are accompanied by a strong positive absorption band with a maximum centered at 700 nm for both compounds. The latter is assigned to a higher excited state $S_1 \rightarrow S_n$ absorption band of the orange perylene bisimide chromophore by comparison with the femtosecond transient absorption data of compound **oref** (see Figure 6, right) and with literature data.[21] It is noteworthy, however, that the radical anion of **oref** also absorbs at 700 nm (for spectra of the latter see Figure 4, top). When changing to the more polar solvents CH_2Cl_2 and benzonitrile, for all three compounds **oref**, **oc**, and **oc2** only slight changes in the overall spectral features are observed. However, the maximum of the strong positive absorption band is shifted to 715 nm in CH_2Cl_2 and to 735 nm in benzonitrile (for spectra see Figures 22 and 25 in the Appendix of this Chapter).
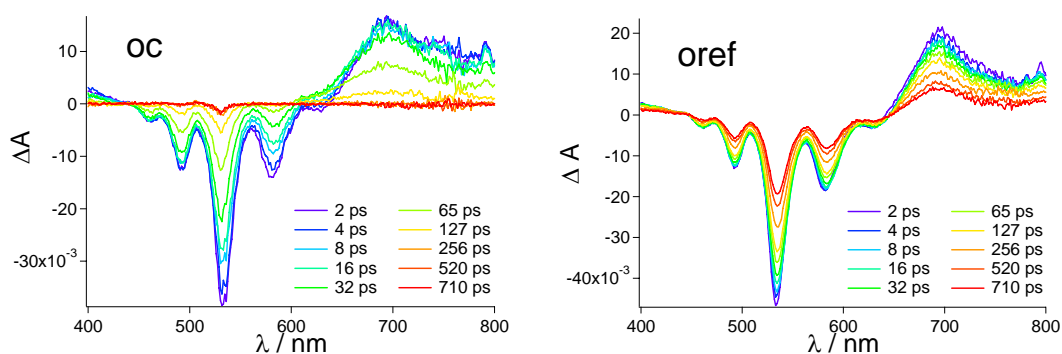

Figure 6. Femtosecond transient absorption spectra and corresponding time delays in toluene of compounds **oc** (left) and **oref** (right). Shown are processes after photoexcitation at 530 nm.

The femtosecond transient absorption spectra of the red compounds **rc** and **rc2** in toluene following photoexcitation at 530 nm both display a broad absorption band centered at 700–740 nm due to $S_1 \rightarrow S_n$ singlet excited state absorption, a strong bleach of the ground state below 590 nm, and a band centered at 610 nm due to the stimulated emission from the lowest excited singlet state of the perylene unit (see spectra in Figure 7, left, and in Figure 20 in the Appendix of this Chapter). These bands are in very good agreement with the photoexcited state properties of the red reference compound **rref** in toluene (see Figure 7, right) and with those reported in the literature.[24] When examining the spectra of compounds **rref**, **rc,** and **rc2** in more detail, a shift of the maximum of the broad negative

signal at 590 nm (λ_{max} after 2 ps) to 610 nm (λ_{max} after 710 ps) is observed which might be attributed to conformational changes of the red perylene bisimide dye.[ii] Femtosecond transient absorption data obtained in solvents of increasing polarity such as CH_2Cl_2 and benzonitrile reveal similar features as observed for toluene. For the spectra in benzonitrile again a solvent-related bathochromic shift of several nanometers for the band maximum is found (see Figures 23 and 26 in the Appendix of this Chapter).
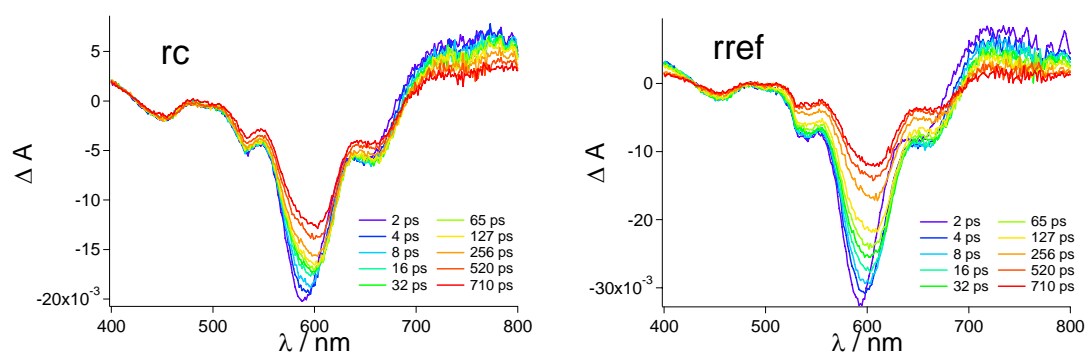

Figure 7. Femtosecond transient absorption spectra and corresponding time delays in toluene of compounds **rc** (left) and **rref** (right). Shown are processes after photoexcitation at 530 nm.

Photoexcitation of the green compounds **gc** and **gc2** in toluene at 640 nm leads to ground state bleaching below 715 nm and to the stimulated fluorescence emission between 715–740 nm for both compounds, observed as a combined negative signal. Furthermore, the spectra of both compounds show a small broad, positive absorption feature that extends from 470 to 570 nm, and a higher energy transition centered at 430 nm (bleach), which is attributed to the higher excited state transition of the perylene unit (spectrum in Figure 8, left). The transient absorption spectrum of the green reference compound **gref** reveals similar features and is in good agreement with spectral data in the literature (see Figure 8, right, and Figure 21 in the Appendix of this Chapter).[26] Upon photoexcitation of all three green compounds **gref**, **gc**, and **gc2**, respectively, in CH_2Cl_2 very similar features are observed. However, the maximum of the strong negative signal is shifted bathochromically

---

[ii] Similar behavior is also known from single molecule spectroscopy for the red perylene bisimides bearing phenoxy substituents at the *bay* positions that were immobilized in a polymer matrix. It is known that local reorganizations in the vicinity of the molecule have an impact on the orientation of the phenoxy substituents for these red PBIs. For details, see ref. 25a. For a recent study dealing with processes in solution, see ref. 25b.
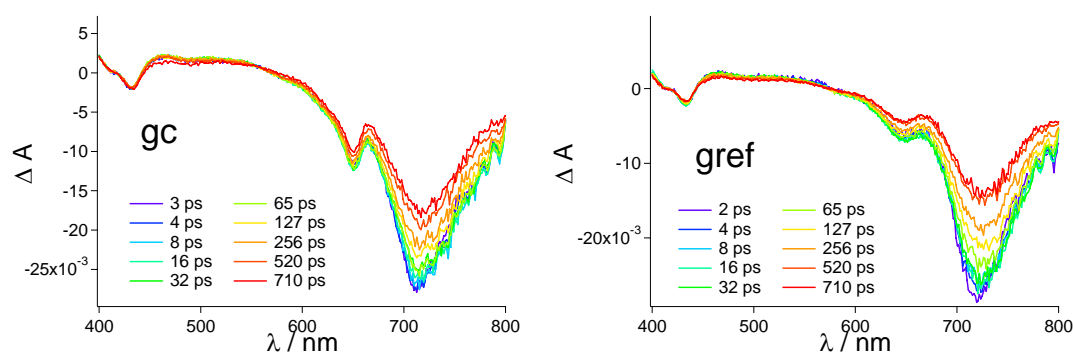
Figure 8. Femtosecond transient absorption spectra and corresponding time delays in toluene of compounds **gc** (left) and **gref** (right). Shown are processes after photoexcitation at 640 nm.

to 735 nm and the maximum of the small bleach signal is shifted to 435 nm, respectively. When changing to the even more polar solvent benzonitrile, similar band positions as in CH_2Cl_2 are observed for all three compounds (see Figure 24 and 27 in the Appendix of this Chapter).

3.7   Global and Target Analysis[iii]

The kinetic profiles of the observed photoinduced processes are difficult to analyze by single wavelength fitting because several processes take place concomitantly after photo-excitation. For this reason, the femtosecond transient absorption data-matrices in toluene, CH_2Cl_2 and benzonitrile were analyzed with spectrotemporal parameterization, an advanced global and target analysis method that has been developed in particular to elucidate photoinduced processes in complex biological systems such as photosystems.[27] Here *global* refers to a simultaneous analysis of all measurements, whereas *target* refers to the applicability of a particular target model (see below). Because the time information at all wavelengths is analyzed, this analysis gives a more in-depth view of the occurring photoinduced processes. For this purpose, all time-gated spectra are collected in a matrix, which was globally fitted applying a *sequential* kinetic scheme with increasing lifetimes.

[iii] The femtosecond transient absorption data analysis by spectrotemporal parameterization was accomplished by Dr. I. H. M. van Stokkum at the Vrije Universiteit van Amsterdam, The Netherlands.

This procedure yields the evolution-associated difference spectra (EADS) – the spectra of the individual excited state species – together with their respective rate constants. The EADS thus represent the spectral evolution of the excited state species. However, in the EADS the time constants of the processes may correspond to the *lifetimes* of the transient species, but the spectral profiles do not necessarily need to represent the pure excited-state *spectra* of the molecules: given the fact, that the applied *sequential* scheme with increasing lifetimes represents the correct physicochemical picture, the EADS indeed correspond to the true spectra of the individual excited state species characterizing the intermediate states. These "true spectra" are also referred to as Species Associated Difference Spectra (SADS) and will in this case be identical to the EADS. However, for more complex systems following *non-sequential* kinetic schemes the EADS will *not* truly reproduce the spectra of the individual excited species; and EADS and SADS will differ substantially. To obtain the *correct* SADS (= the correct difference spectra of the individual species) a target analysis needs to be applied. Thus, one needs to take into account additional (*e.g.* experimentally based) parameters that are summarized into a specific photophysical or photochemical model utilized for the fitting procedure.

In case of compound **oc** the EADS resulting from the global fit of the data obtained in toluene are presented in Figure 9A. Three decay components of 1.8 ps, 22 ps and 50 ps are observed. The very first lifetime we assume to be due to fast solvent reorganization processes.[28] The EADS corresponding to this component is shown as a green line in Figure 9A; it closely resembles the features typical for the transient absorption spectrum of the orange PBI chromophore (for comparison see spectra of compound **oref** in Figure 6). With a representative time of 1.8 ps this spectrum is converted into an EADS with a lifetime of 22 ps (black line in Figure 9A) showing a loss of amplitude in the negative bands at 530 nm and 580 nm, whereas the amplitude remains almost unchanged at the ground-state bleaching band of 490 nm and the absorption band of ca. 700 nm, characteristic of the solvation effect. The spectrum of the third component (red line in Figure 9A) is obtained during further evolution of the system, this EADS decays with 50 ps. The spectrum suggests very strongly the formation of a different excited state as a strongly reduced signal of the stimulated emission at 580 nm is observed, together with a broadening and apparent blue shift of the positive transient absorption band around 700 nm.
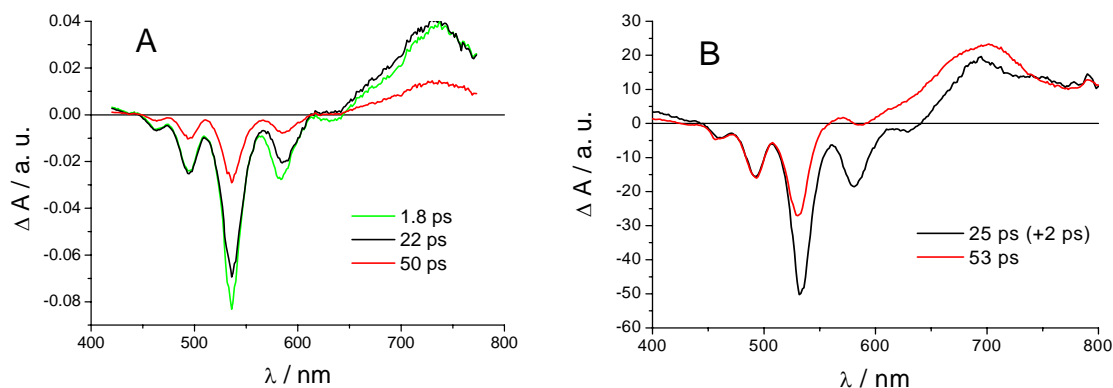
Figure 9. Compound **oc** in toluene. (**A**): Evolution-associated difference spectra (EADS) resulting from the global fitting analysis of femtosecond transient absorption spectral data. Features due to Raman scattering were omitted for clarity. (**B**): Species-associated difference spectra (SADS) resulting from the simultaneous target analysis of femtosecond transient absorption spectral data of compounds **oc** and **oc2** using the kinetic scheme depicted in Figure 10. The black SADS represents the excited state of **oc**, and the red SADS belongs to the charge transfer state of **oc**. Shown are processes after photoexcitation at 530 nm.

Although the sequential model used above for fitting of the data provides important information on the time evolution of the system, it can not truly reproduce the spectra of the individual excited species that are involved into the processes occurring in compound **oc** upon photoexcitation. Therefore, a target analysis with a specific model of the excited state processes was applied: according to the calculations of the Gibbs energy of electron transfer as well as the observed trends in the fluorescence lifetimes and quantum yields (see above), the formation of the PBI radical anion of the orange PBI chromophore is expected after photoexcitation of compound **oc** as a result of a photoinduced electron transfer. Accordingly, an additional charge transfer (CT) state was integrated into the model. The respective energy level diagram is depicted in Figure 10. The resulting species-associated difference spectra (SADS), now representing the true spectra of the individual excited species, are shown in Figure 9B.[iv] The SADS of the excited state (black line in

---

[iv] To quantify the differences between the rates of charge separation (k_{CS}) and charge recombination (k_{CR}) a *simultaneous* target analysis of compounds **oc** and **oc2** was performed. The kinetic model used consists of a biexponential decay of the excited state to a charge separated state, which in turn decays with k_{CR}. In order to limit the number of free parameters, the SADS of the excited state were assumed to be identical in **oc** and **oc2**, and also the fractions of slow and fast charge separation (see also remark v). For the charge separated

Figure 9B) shows again the transient absorption features of the orange PBI chromophore and decays with 25 ps (80%) and with 2 ps (20%),[v] respectively, to the following state (red line). The SADS of the latter shows a lifetime of 53 ps and exactly reveals the spectral features of a charge transfer state as the stimulated emission at 580 nm is not observed any longer and the band at around 700 nm is significantly broadened. From this clear spectral evidence the formation of a charge separated state involving the formation of the orange PBI monoanion can be concluded.
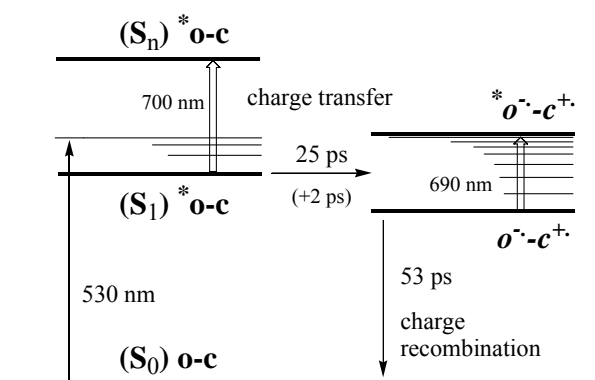

Figure 10. Energy level diagram of compound **oc** in toluene showing the electron transfer pathway obtained with global and target analysis, together with the respective decay times corresponding to the states.[iv,v]

The formation of the CT state is furthermore illustrated by the kinetic traces presented in Figure 11A and 11B: a clear difference is found when comparing the decay of the ground state bleaching (probed at 485 nm) and that of the stimulated emission (probed at 580 nm), respectively (see red and black line in Figure 11A, respectively). It can be seen clearly, that the signal of the stimulated emission (black line in Figure 11A) vanishes much faster than that of the ground state bleaching (red line in Figure 11A). Thus, the ground state is still bleached when no emission occurs any more from the excited singlet state by stimulated emission. Accordingly, an additional, non-emissive state (*e.g.* a CT state) is populated

state both the SADS and k_{CR} were assumed to be identical in **oc** and **oc2**. Thus the difference between **oc** and **oc2** is quantified by the rates of slow (the dominant fraction) and fast charge separation (the minor fraction).

[v] A second minor deactivation pathway with 20% amplitude of the singlet excited state of compound **oc** is observed in toluene which is most probably related to the decay of a second possible *pinched cone* conformation of the calix[4]arene moiety. As we are dealing here with merely conformational isomers, the additionally assumed species of this second pathway has identical spectral features and an indistinguishable depopulation pathway to the ground state (see also remark iv).

during the photoexcitation process. Furthermore, the kinetic profile measured at 635 nm (red line in Figure 11B) shows a clear rise time. At this very wavelength the charge transfer state absorbs almost exclusively (refer also to the spectrum of the CT state, red line in Figure 9B), as the $S_1 \rightarrow S_n$ absorbance of the excited state equals zero, and the time-resolved trace at this wavelengths thus exclusively resembles the time course of the CT state concentration. In comparison, the kinetic profile probed at 700 nm (black line in Figure 11B) shows no such clearly pronounced rise time, as both the decay of the $S_1 \rightarrow S_n$ absorption and the rise and decay of the CT state, respectively, are concomitantly observed at this wavelength. Detailed analysis of the late time gated spectra furthermore reveals that a very small amount ($< 2\%$) of triplet is created.
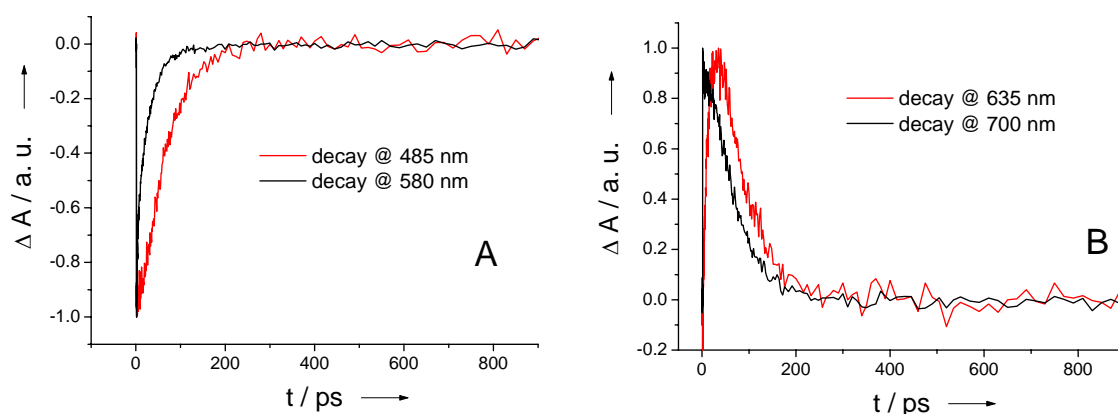

Figure 11. Kinetic profiles of the transient absorption of compound **oc** in toluene. (**A**): the decay of the ground state bleaching probed at 485 nm (red line), and the decay of the stimulated emission at 580 nm (black line). (**B**): the rise and decay time of the CT state probed at 635 nm (red line), and the concomitant decay of CT state and singlet excited state at 700 nm (black line).

Similar processes are observed in the spectrum of **oc2** in toluene and also in the spectra of compounds **oc** and **oc2** in the other two solvents CH_2Cl_2 and benzonitrile; the respective SADS are depicted in Figure 28 in the Appendix of this Chapter. However, the charge transfer character of the charge separated states of both compounds is less pronounced in these solvents compared to toluene because of the much faster decay of the CT state. To further analyze this phenomenon, for all femtosecond transient absorption data obtained in all three solvents for both compounds **oc** and **oc2**, respectively, a target analysis has been applied. The obtained values for the rates of charge separation and charge recombination in

the various solvents are collated in Table 4. The values for charge separation reveal for compound **oc** values of 25 ps (in toluene), 32 ps (in CH_2Cl_2), and 64 ps (in benzonitrile).[vi] The charge recombination after photoinduced charge separation within the system **oc** occurs with 53 ps in toluene.[v,vi] This value lowers to 10 ps when changing to the more polar solvent CH_2Cl_2, and also shows a reduced value of 15 ps in benzonitrile.[v,vi] Similar trends in the rate constants are observed for the biscalix[4]arene-substituted compound **oc2** (see Table 4).[vi] Accordingly, values for the charge separation for compound **oc2** of 11 ps (in toluene), 11 ps (in CH_2Cl_2), and 24 ps (in benzonitrile) are obtained, respectively,[vi] and charge recombination values of 53 ps in toluene, of 10 ps in the more polar CH_2Cl_2 and of 15 ps in benzonitrile were determined, respectively. Hence, the rate for charge separation decreases with increasing solvent polarity for both compounds **oc** and **oc2** whilst the rates of charge recombination increase with increasing solvent polarity. Furthermore, the formation of the charge separated state occurs about twice as fast for compound **oc2** compared to compound **oc** in the respective solvent which is apparently a result of the presence of two electron transfer channels for deactivation in compound **oc2** due to bis-calix[4]arene substitution of the PBI chromophore.

Table 4. Lifetimes for charge separation (τ_{CS}) and charge recombination (τ_{CR}) obtained from the target analysis of compounds **oc** and **oc2** in various solvents.

Cmpd	Solvent	τ_{CS}[a] (ps)	τ_{CR} (ps)
oc	toluene	25	53
	CH_2Cl_2	32	10
	benzonitrile	64	15
oc2	toluene	11	53
	CH_2Cl_2	11	10
	benzonitrile	24	15

[a] See also remarks v and vi.

[vi] Likewise, as discussed in remark iv for the solvent toluene, faster components are also observed for the data of compound **oc** in the solvents CH_2Cl_2 (7.7 ps, 32%) and benzonitrile (8.3 ps, 33%). These are again attributable to the decay of the second *pinched cone* conformation of the calix[4]arene moiety. Likewise, for compound **oc2** in all three solvents a fast component showing a lifetime of <1 ps (20%) in toluene, 3.6 ps (32%) in CH_2Cl_2 and of 3.8 ps (33%) in benzonitrile is observed. Note that, the lifetimes of compound **oc2** reduce by half compared to those obtained for compound **oc** for the respective solvents owing to the availability of a second electron transfer deactivation channel in compound **oc2**.

The solvent dependence of the charge separation and charge recombination rates can not be unambiguously explained. A thermodynamic analysis according to equation 1 in variate solvents reveals that the formation of the charge-separated state in toluene is a slightly exergonic process (values are summarized in Table 5) and accordingly, no electron transfer quenching should be observed in this solvent which is not in accordance with the findings discussed above. However, it has to be noted, that toluene as a solvent shows a quadrupole moment revealing microscopic values of ε_S comparable to those of $CHCl_3$.[29] For the latter solvent the calculated values are also given in Table 5 for comparison, leading to a negative value of the driving force of the charge separation. Hence, the observed findings are interpreted as an effect of the quadrupole moment of toluene, accordingly.[29] In the more polar solvents CH_2Cl_2 and benzonitrile the charge-separated state will be lower in energy and therefore thermodynamically more stabilized. An increase in solvent polarity results thus in an increase of the driving force for photoinduced charge separation. Consequently, the driving force for charge recombination becomes smaller. According to the data presented in Table 4, this leads to faster recombination rates which may be attributed to the energy-gap law[30] or to increased overlap of vibrational wavefunctions in the Marcus inverted region. Due to the fact that charge recombination is normally in the Marcus inverted region, the process becomes faster with the increase of the polarity of the solvent and hence a decrease of the driving force. Similar behavior has also been observed previously in other electron donor-acceptor systems.[31]

Table 5. Selected values for the calculation of thermodynamic feasibility of a photoinduced electron transfer process for compound **oc** in variate solvents.[a]

Solvent	ε_S	R_{cc}[b]	E_{00}[c]	E_{ox}	E_{red}	"coulomb energy"[d]	"solvation energy"[e]	ΔG_{CS}
		(Å)	(eV)	(V)	(V)	(eV)	(eV)	(eV)
Toluene	2.38	8.6	2.34	+1.10	−1.01	0.704	-1.108	+0.175
$CHCl_3$	4.70	8.6	2.34	+1.10	−1.01	0.356	-0.361	−0.225
CH_2Cl_2	8.93	8.6	2.34	+1.10	−1.01	0.188	0.000	−0.418
PhCN	25.30	8.6	2.34	+1.10	−1.01	0.066	0.262	−0.558

[a] Calculations according to equation (1) employing an average ion radius of 4.0 Å according to ref. 32. [b] Values derived from an energy minimized structure obtained from forcefield calculations (Macromodel 8.0, potential MMFF). [c] Calculated from the intersection of the normalized UV/vis absorption and fluorescence emission spectra. [d] Refer to the second term of equation (7) in Chapter 1. [e] Refer to the third term of equation (7) in Chapter 1.

The data analysis for both orange calix[4]arene–perylene bisimide conjugates **oc** and **oc2** clearly reveals the formation of a charge-separated state, involving the formation of the radical anion of the orange perylene bisimide chromophore. Owing to this process the excited state lifetime is strongly reduced from approximately 4 ns to around 65 ps and less in both compounds. The charge transfer state is clearly characterized by the absence of stimulated emission and the broadened absorption features in the 600–750 nm spectral region attributable to the radical anion of the perylene bisimide unit. Concomitantly, the radical cation of the calix[4]arene moiety (*i.e.* dimethyl substituted methoxybenzene) should be formed. This radical cationic species, however, is expected to absorb mainly in the UV and with a very small extinction coefficient and thus could not be observed in the spectra.

The femtosecond transient absorption spectra obtained for the red and green compounds **rc**, **rref**, **gc**, and **gref** in toluene are shown in Figures 7 and 8, for the spectra in CH_2Cl_2 and benzonitrile as well as all spectra of compounds **rc2** and **gc2** refer to the Appendix of this Chapter. Notably, within the femtosecond transient absorption spectra obtained for the red compounds in all three solvents the negative band at 590 nm slightly shifts the position of its maximum to 610 nm during the time frame of the experiment (see below). The obtained data were also fitted by means of global analysis, the respective rate constants are summarized in Tables 6 and 7. For all spectral data in all three solvents of the red and green compounds no formation of an additional competitive deactivation pathway via a charge-transfer state was observed, thus closely mirroring the findings from the fluorescence quantum yields and steady state and time-resolved emission spectroscopy. A typical dataset obtained from the global analysis for all red conjugates consists of four rate constants: i) a short component of several hundred femtoseconds due to fast solvent organization processes;[28] ii) a component of between 5 to 15 ps picoseconds; iii) a component of several hundred picoseconds; and iv) a long-lived component of several nanoseconds (exceeding the instruments time frame of ca. 1 ns) which was assigned to the lifetime of the relaxed S_1 state of the reference chromophore. The latter values are prone to large errors due to the timeframe of the instrument and are therefore differing from the fluorescence lifetime values obtained from the streak experiments, but however reveal the correct order of magnitude of the values found for the reference chromophores. The above-

mentioned components ii) and iii) correlate with the shift in the band maximum observed for all three red systems and might be attributed to conformational changes of the red perylene bisimide dye. Similar behavior is also known from single molecule spectroscopy for the red perylene bisimides bearing phenoxy substituents at the bay positions that were immobilized in a polymer matrix. It is known that local reorganizations in the vicinity of the molecule have an impact on the orientation of the phenoxy substituents for these red PBIs.[25a] Furthermore, a recent study describes similar effects for conformationally fixed red perylene bisimide derivatives in solution.[25b]

Table 6. Rate constants obtained from global fitting of the experimental data of compounds **rref**, **rc**, and **rc2**.

Cmpd	rate constants in Toluene (ps)	rate constants in CH$_2$Cl$_2$ (ps)	rate constants in PhCN (ps)
rref	0.5	0.4	0.9
	9.2	4.8	15.6
	229	117	282
	4600	1200	9000
rc	0.3	0.4	0.2
	7.5	4.7	6.8
	354	389	45
	2000	3000	1900
rc2	0.5	0.2	0.1
	2.9	4.3	9.4
	68	331	112
	1000	4300	1300

For the green systems a typical dataset obtained from the global analysis consists of three rate constants: of i) a component of between 1 to 8 ps picoseconds attributed to fast solvent reorganization processes;[28] ii) a component of several hundred picoseconds; and iii) a long-lived component of several nanoseconds (exceeding the instruments time frame of ca. 1 ns) which was assigned to the lifetime of the relaxed S$_1$ state of the reference chromophore. The latter values are prone to large errors due to the timeframe of the instrument and are therefore differing from the fluorescence lifetime values obtained from the streak experiments, but however reveal the correct order of magnitude of the values found for the reference chromophores. The fast component of several hundred picoseconds relates to the biexponential fluorescence lifetime values obtained already from the streak experiments (see Table 1), and is assumed to be inherent to the green chromophore itself.

Table 7. Rate constants obtained from global fitting of the experimental data of compounds **gref**, **gc**, and **gc2**.

Cmpd	rate constants in Toluene (ps)	rate constants in CH$_2$Cl$_2$ (ps)	rate constants in PhCN (ps)
gref	2.4	1.4	6.0
	282	235	304
	4500	2400	2200
gc	3.3	1.4	7.1
	229	442	292
	2700	3800	1300
gc2	8.3	2.2	3.8
	767	610	540
	3000	2800	1400

3.8   Conclusions

In this Chapter the basic photophysical properties of calix[4]arene–perylene bisimide conjugates have been elucidated. It has been shown that calix[4]arene functionalization does not influence the photophysical properties of the red PBI (1,6,7,12-tert-butylphenoxy perylene bisimide) and the green PBI (1,7-dipyrrolidino perylene bisimide), whereas calix[4]arene functionalization does substantially change the properties of the orange fluorophore. For this most electron-poor chromophore, a charge-separated state is formed, consisting of the reduced perylene bisimide unit and the oxidized calix[4]arene moiety. As a consequence, the excited state lifetime is strongly reduced from around 4 ns to 65 ps and less. The resulting charge transfer state is characterized by ground state bleaching, the absence of stimulated emission and absorption features in the 600–750 nm region attributable to the radical anion of the perylene bisimide. It is assumed, that the closest substituted methoxybenzene of the calix[4]arene acts as the donor, and thus the radical cation of (dimethyl substituted) methoxybenzene should be formed. Furthermore, global and target analysis is exemplified as a strong tool to elucidate competing processes involving excited state species with similar absorption properties. Thus, spectrotemporal parameterization is the tool of choice for the investigation of complex multichromophoric supramolecular and biological assemblies.

3.9   Experimental Section

Materials and Methods

Reference compounds **oref** and **rref**,[13] perylene bisanhydrides 1,6,7,12-tetra(4-*tert*-butylphenoxy)perylene-3,4:9,10-tetra-carboxylic acid bisanhydride,[33] 1,7-dipyrrolidinylperylene-3,4:9,10-tetracarboxylic acid bisanhydride,[34] and perylene monoimide monoanhydrides *N*-(1-pentylhexyl)-perylene-3,4:9,10-tetracarboxylic acid monoanhydride monoimide,[35] *N*-butyl-1,6,7,12-tetra(4-*tert*-butylphenoxy)perylene-3,4:9,10-tetracarboxylic acid monoanhydride monoimide,[36] *N*-cyclohexyl-1,7-dipyrrolidinyl-perylene-3,4:9,10-tetracarboxylic acid monoimide monoanhydride[34,37] and 5-monoamino-25,26,27,28-tetrakis(propyloxy)-calix[4]arene[38] were synthesized according to literature procedures. All compounds were characterized by ^{1}H NMR spectroscopy and high resolution mass spectrometry. Solvents were purified and dried according to standard procedures. Column chromatography was performed with silica gel 60 (0.035–0.070 mm); preparative TLC on 20 x 20 cm plates, height 1 mm, silica gel 60 (0.035–0.070 mm). High performance liquid chromatography (HPLC) was performed on SiO_2 columns, normal phase (NP), with p.a. grade purified solvents. NMR spectra were recorded on a Bruker 400 MHz spectrometer. Mass Spectra were performed on a Finnigan MAT MS 8200 or on a Bruker microTOF$_{LC}$. For UV/vis absorption and fluorescence experiments spectroscopy grade solvents were used.

UV/vis absorption spectra were measured on a Perkin-Elmer Lambda 40P UV/vis absorption spectrophotometer.

Steady state fluorescence emission spectra were recorded on a PTI QM4-2003 fluorescence spectrometer and are corrected against photomultiplier and lamp intensity. A long wavelength range emission corrected photomultiplier R928 was used. Fluorescence quantum yields were determined in CH_2Cl_2 vs. *N,N'*-(2,6-diisopropylphenyl)-1,6,7,12-tetraphenoxyperylene-3,4:9,10-tetracarboxylic acid bisimide (Φ_{fl} = 0.96 in $CHCl_3$) or Fluorescein (Φ_{fl} = 0.92 in 0.1N NaOH) as reference.[11b,39] The given quantum yields are averaged from values measured at three different excitation wavelengths with OD 0.02–0.05 in the absorption maximum (standard deviation σ = 1–3 %).

Fluorescence lifetimes were measured with a streak camera system at the Universiteit van Amsterdam, The Netherlands, under the guidance of Dr. R. Williams. Details are described in Chapter 2 and in the literature.[40]

Femtosecond transient absorption data were measured at the Universiteit van Amsterdam, The Netherlands, under the guidance of Dr. R. Williams. Experimental details are described in Chapter 2 and in the literature.[41]

Global and target analysis was performed by Dr. I. H. M. van Stokkum at the Vrije Universiteit van Amsterdam, The Netherlands. For details of the method refer to Chapter 2 and to the literature.[27]

Data collections for the **Crystal Structure** determination were carried out at the X-ray diffraction beam line of the Elettra Synchrotron, Trieste (Italy), using the rotating crystal method with the monochromatic wavelength of 1.000 Å. Data were collected on a CCD MAR detector. Measurements were performed at 100 K using a nitrogen stream cryo-cooler. Cell refinement, indexing and scaling of the data sets were carried out using Denzo[42] and Scalepack.[42] The structure was solved by Prof. Dr. E. Zangrando at the University of Trieste, Italy, by direct methods using SHELXS[43] and refined by the full-matrix least-squares method based on F^2 with all observed reflections.[43] The hydrogen atoms were placed at geometrically calculated positions. All the calculations were performed using the WinGX System, Version 1.70.01.[44] Crystal data for compound **oc2**: $C_{104}H_{102}N_2O_{12}$, M = 1571.88, monoclinic; space group $P\,2_1$, a = 10.707(4), b = 11.962(4), c = 32.120(5) Å, β = 91.17(2) V = 4113(2) Å^3, Z = 2, ρ_{calcd} = 1.269 g/cm^3, F(000) = 1672. Final R = 0.1226, $wR2$ = 0.3304, S = 1.173 for 943 parameters and 21133 reflections, 6648 unique [R(int) = 0.0420], of which 5193 with I > 2σ(I).

Spectroelectrochemical experiments were data were measured in the group of Prof. Dr. Ch. Lambert under the guidance of D. Nowak at the University of Würzburg, Germany. For experimental details refer to Chapter 2.

Cyclic voltammetry (CV) was performed by A.-M. Krause at the University of Würzburg, Germany, experimental details are described in Chapter 2.

**Synthesis and Chemical Characterization**

Compound oc
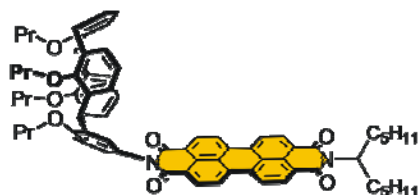
A suspension of 100 mg (1.65 x 10^{-4} mol, 1 equiv.) of 5-monoamino-25,26,27,28-tetrakis(propyloxy)-calix[4]-arene, 135 mg (2.48 x 10^{-4} mol, 1.5 equiv.) of *N*-(1-pentyl-hexyl)-perylene-3,4:9,10-tetracarboxylic acid monoanhydride monoimide and 61 mg (3.30 x 10^{-4} mol, 2 equiv.) of $Zn(OAc)_2$ (H_2O-free) was heated in 0.7 mL distilled quinoline at 165°C for 11 h under an argon atmosphere. The cooled reaction mixture was poured into 2N HCl and stirred for 30 minutes at 40 °C. To the solution 50 mL of CH_2Cl_2 were added and the resulting organic phase was washed with water and brine and dried over $MgSO_4$. The crude product was purified by column chromatography with CH_2Cl_2/ethylacetate 99:1 and precipitated from CH_2Cl_2/methanol. Compound **oc** was obtained as a light red powder (160 mg, 1.41 x 10^{-4} mol, yield 85 %). $C_{75}H_{78}N_2O_8$ (1135.43). Mp = 208–220°C. TLC CH_2Cl_2/ethyl acetate 99:1; R_f = 0.56. **^{1}H NMR** (400 MHz, $CDCl_3$, 25 °C): δ (ppm) = 8.77 – 8.63 (m, 8H; Per-*H*); 7.11 and 7.08 (d and s, 4H, ^3J = 7.5 Hz; Ar-*H*); 6.92 (t, 1H, ^3J = 7.5 Hz; Ar-*H*); 6.35 and 6.30 (t and dd, 4H, ^3J = 7.5 Hz and ^3J = 7.5 Hz / ^4J = 1.8 Hz; Ar-*H*); 6.16 (dd, 2H, ^3J = 7.3 Hz / ^4J = 1.6 Hz; Ar-*H*); 5.24 – 5.16 (m, 1H; N-C*H*) 4.53 and 3.20 (AX, 4H, ^2J = 13.4 bzw. 13.5 Hz; Ar-C*H₂*-Ar); 4.48 and 3.17 (AX, 4H, ^2J = 13.4 and 13.5 Hz; Ar-C*H₂*-Ar); 4.11 and 4.03 (each t, 4H, ^3J = 8.2 bzw. 8.1 Hz; O-C*H₂*); 3.72 – 3.66 (m, 4H; O-C*H₂*); 2.30 – 2.22 (m, 2H; Alkyl-*H*); 2.06 – 1.84 (m, 10H; Propyl-*H* and Alkyl-*H*); 1.37 – 1.24 (m, 12H; Alkyl-*H*); 1.10 (t, 6H, ^3J = 7.4 Hz; Propyl-*H*); 0.94 and 0.91 (each t, 6H, each ^3J = 7.5 Hz; Propyl-*H*); 0.84 (t, 6H, ^3J = 7.3 Hz; Propyl-*H*). **HR-MS** (ESI in $CHCl_3$/acetonitrile): calcd for $C_{75}H_{78}N_2O_8Na$ (m/z) 1157.5656 [M+Na]$^+$; found 1157.5650. **Analysis**: calcd (%) for $C_{75}H_{78}N_2O_8$ (1135.43): C 79.34; H 6.92; N 2.47; found: C 79.25; H 7.04; N 2.52. **UV/vis** (CH_2Cl_2): λ (nm) [ε ($M^{-1}cm^{-1}$)] = 526 [91600], 489 [55200], 458 [20000]. **Fluorescence** (CH_2Cl_2): $λ_{max}$ (nm) = 535; $Φ_{Fl}$ = 0.03.
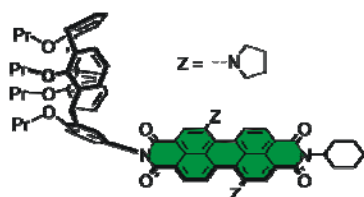
Compound oc2
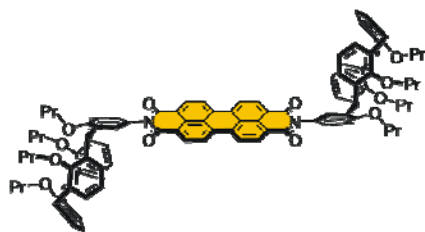
A suspension of 30 mg (4.93 x 10^{-2} mmol, 2 equiv.) of 5-Monoamino-25,26,27,28-   tetrakis(propyloxy)-calix[4]arene, 10 mg (2.46 x 10^{-2} mmol, 1 equiv.) of perylene-3,4:9,10-tetracarboxylic acid bisanhydride and 18 mg (9.87 x 10^{-2} mmol, 4 equiv.) Zn(Oac)$_2$ (H$_2$O-free) was heated in quinoline (0.4 mL) at 160 °C for 5 h under an argon atmosphere. The cooled reaction mixture was poured into 35 mL of 2N HCl and stirred for 30 minutes. The resulting precipitate was filtered, washed with water, dried and heated to 100 °C together with 15 mL NaOH (0.5 M) for 30 minutes. The remaining precipitate was filtered, dissolved in CH$_2$Cl$_2$, and the solution was washed with water to pH neutral and dried over MgSO$_4$. The crude product was purified by column chromatography with CH$_2$Cl$_2$ and precipitated from CH$_2$Cl$_2$/methanol to yield compound **oc2** as a light red powder (11 mg, 7.00 x 10^{-3} mmol, yield 28%). C$_{104}$H$_{102}$N$_2$O$_{12}$ (1571.93). Mp = 314–315 °C. TLC: CH$_2$Cl$_2$; R$_f$ = 0.23. **^{1}H NMR** (400 MHz, CDCl$_3$, 25 °C): δ (ppm) = 8.80 and 8.71 (each d, 8H, ^{3}J = 7.8 Hz; Per-*H*); 7.09 (d, 4H, ^{3}J = 7.7 Hz; Ar-*H*); 7.08 (s, 4H; Ar-*H*); 6.92 (t, 2H, ^{3}J = 7.5 Hz; Ar-*H*); 6.73 – 6.30 (m, 8H; Ar-*H*); 6.16 (dd, 4H, ^{3}J = 7.3 Hz, ^{4}J = 1.6 Hz; Ar-*H*); 4.53 and 3.19 (AX, 8H, ^{2}J = 13.4 Hz; Ar-C*H*$_2$-Ar); 4.47 and 3.17 (AX, 8H, ^{2}J = 13.5 Hz; Ar-C*H*$_2$-Ar); 4.11 and 4.03 (each t, 8H, ^{3}J = 8.2 Hz and 8.1 Hz; O-C*H*$_2$); 3.74 – 3.68 (m, 8H; O-C*H*$_2$); 2.06 – 1.84 (m, 16H; Propyl-*H*); 1.10 (t, 12H, ^{3}J = 7.4 Hz; Propyl-*H*); 0.94 and 0.91 (each t, 12H, each ^{3}J = 7.4 Hz; Propyl-*H*). **MS** (MALDI in DCTB): calcd for C$_{104}$H$_{102}$N$_2$O$_{12}$ (m/z) 1570.74 [M]$^+$; found 1570.77. **HR-MS** (ESI in CHCl$_3$/Acetonitrile): calcd for C$_{104}$H$_{102}$N$_2$NaO$_{12}$ [M+Na]$^+$ m/z = 1593.7329; found 1593.7325. **UV/vis** (CH$_2$Cl$_2$): λ (nm) [ε (M^{-1}cm^{-1})] = 526 [97200], 490 [60700], 458 [22300]. **Fluorescence** (CH$_2$Cl$_2$): Φ$_{Fl}$ < 0.001.

*Compound **rc***
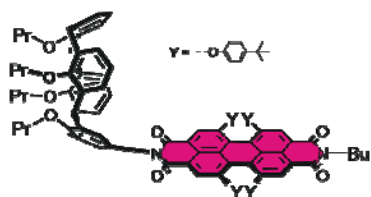
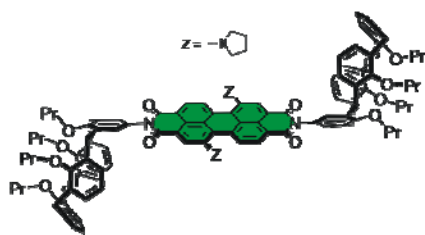A suspension of 20 mg (3.24×10^{-5} mol, 1 equiv.) of 5-monoamino-25,26,27,28-tetrakis(propyloxy)-calix[4]-arene, 38 mg (3.89×10^{-5} mol, 1.2 equiv.) of *N*-(butyl)-1,6,7,12-tetra(4-*tert*-butylphenoxy)-perylene-3,4:9,10-tetracarboxylic acid imide anhydride and 61 mg (3.30×10^{-4} mol, 2 equiv.)

of $Zn(OAc)_2$ (H_2O-free) was heated in 0.3 mL distilled quinoline at 165°C for 10 h under an argon atmosphere. The cooled reaction mixture was poured into 2N HCl and stirred for 30 minutes at 40 °C. To the solution 50 mL of CH_2Cl_2 were added and the resulting organic phase was washed with water and brine and dried over $MgSO_4$. The crude product was purified by column chromatography with CH_2Cl_2/hexane 60:40 and 50:50 and successively by precipitation from CH_2Cl_2/methanol. Compound **rc** was obtained as a red powder (21 mg, 1.29×10^{-5} mol, yield 40%). $C_{108}H_{112}N_2O_{12}$ (1630.05). Mp = 377–379 °C. TLC: CH_2Cl_2/hexane 60:40; R_f = 0.38. **^{1}H NMR** (400 MHz, $CDCl_3$, 25 °C): δ (ppm) = 8.28 and 8.25 (bs and s, 4H; Per-*H*); 7.26 – 7.20 (m, 4H; Phen-*H*); 7.09 (d, 2H, ^3J = 7.5 Hz; Ar-*H*); 6.99 (s, 2H; Ar-*H*); 6.91 and 6.88 – 6.88 (t and m, 9H, ^3J = 7.4 Hz; Phen-*H* and Ar-*H*); 6.24 (t, 2H, ^3J = 7.6 Hz; Ar-*H*); 6.16 (dd, 2H, ^3J = 7.5 Hz / ^4J = 1.0 Hz; Ar-*H*); 6.07 (dd, 2H, ^3J = 7.5 Hz / ^4J = 1.0 Hz; Ar-*H*); 4.46 and 3.14 (AX, 4H, ^2J = 13.4 and 13.6 Hz; Ar-C*H*$_2$-Ar); 4.44 and 3.12 (AX, 4H, ^2J = 13.2 and 13.5 Hz; Ar-C*H*$_2$-Ar); 4.13 and 4.06 and 4.01 (each t, 6H, ^3J = 7.5 and 8.3 and 8.2 Hz; N-C*H*$_2$ and O-C*H*$_2$); 3.69 – 3.60 (m, 8H; O-C*H*$_2$); 1.99 – 1.80 (m, 8H; Propyl-*H*); 1.71 – 1.63 (m, 2H; Butyl-*H*); 1.45 – 1.38 (m, 2H; Butyl-*H*); 1.30 and 1.28 (each s, 36H, *tert*-Butyl-Phen-*H*); 1.08 (t, 6H, ^3J = 7.5 Hz; Propyl-*H*); 0.94 (t, 3H, ^3J = 7.5 Hz; Propyl-*H*); 0.87 and 0.86 (each t, 6H, each ^3J = 7.5 Hz; Propyl-*H*). **MS** (ESI in $CHCl_3$/acetonitrile): calcd for $C_{108}H_{112}N_2O_{12}$ (m/z) 1628.82 $[M]^+$ and $C_{108}H_{116}N_3O_{12}$ (m/z) 1646.86 $[M+NH_4]^+$ and $C_{108}H_{112}N_2O_{12}Na$ (m/z) 1651.81 $[M+Na]^+$ and $C_{108}H_{112}N_2O_{12}K$ (m/z) 1667.79 $[M+K]^+$; found 1628.82 and 1646.86 and 1651.81 and 1667.79. **HR-MS** (ESI in $CHCl_3$/acetonitrile): calcd for $C_{108}H_{112}N_2O_{12}$ (m/z) 1628.8215 $[M]^+$ and $C_{108}H_{116}N_3O_{12}$ (m/z) 1646.8558 $[M+NH_4]^+$ and $C_{108}H_{112}N_2O_{12}Na$ (m/z) 1651.8113 $[M+Na]^+$; found 1628.8210 and 1646.8554 and 1651.8108. **Analysis**: calcd (%) for $C_{112}H_{116}N_4O_{12}$ (1710.14): C 78.66; H 6.84; N 3.28; found: C 78.58; H 6.91; N 3.34. **UV/vis** (CH_2Cl_2): λ (nm) [ε ($M^{-1}cm^{-1}$)] = 578 [47400]. **Fluorescence** (CH_2Cl_2): λ_{max} (nm) = 608; Φ_{Fl} = 0.80.

*Compound **rc2***
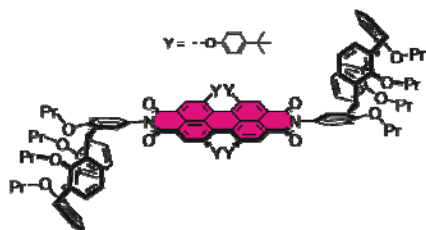
Under an argon atmosphere 50 mg (8.22×10^{-2} mmol, 2 equiv.) of 5-Monoamino- 25,26,27,28-tetrakis(propyloxy)-calix[4]arene were heated to 90 °C for 14 h together with 41 mg (4.11×10^{-2} mmol, 1 equiv.) of 1,6,7,12-tetra(4-*tert*-butylphenoxy)-perylene-3,4:9,10-tetracarboxylic acid bisanhydride and 2-3 drops of triethylamine in toluene (0.6 mL). The solvent was evaporated, the remaining crude product purified by column chromatography with CH_2Cl_2/hexane 50:50 and precipitated from CH_2Cl_2/methanol. Compound **rc2** was obtained as a red powder (42 mg, 1.94×10^{-2} mmol, yield 47%). $C_{144}H_{150}N_2O_{16}$ (2164.74). Mp = 392–393 °C. TLC: CH_2Cl_2/hexane 80:20; $R_f = 0.87$. **^{1}H NMR** (400 MHz, CDCl$_3$, 25 °C): δ (ppm) = 8.31 (bs, 4H; Per-*H*); 7.24 (d, 8H; ^3J = 8.6 Hz; Phen-*H*); 7.10 (bd, 4H; ^3J = 7.1 Hz; Ar-*H*); 7.00 (s, 4H; Ar-*H*); 6.93 – 6.87 (m, 10H; Phen-*H* and Ar-*H*); 6.25 (bt, 4H; ^3J = 7.1 Hz; Ar-*H*); 6.17 (bd, 4H; ^3J = 6.3 Hz; Ar-*H*); 6.07 (bd, 4H; ^3J = 7.0 Hz; Ar-*H*); 4.47 and 3.14 (AX, 8H, ^2J = 13.2 Hz; Ar-C*H$_2$*-Ar); 4.44 and 3.13 (AX, 8H, ^2J = 13.3 Hz; Ar-C*H$_2$*-Ar); 4.07 and 4.01 (two bt, 8H; each ^3J = 7.9 Hz; O-C*H$_2$*); 3.69 – 3.61 (m, 8H; O-C*H$_2$*); 2.00 – 1.81 (m, 16H; Propyl-*H*); 1.29 (s, 36H, *tert*-Butyl-Phen); 1.09 (t, 12H, ^3J = 7.3 Hz; Propyl-*H*); 0.88 and 0.87 (two bt, 12H, each ^3J = 7.2 Hz; Propyl-*H*). **MS** (MALDI in DCTB): calcd for $C_{144}H_{150}N_2O_{16}$ (m/z) 2163.10 [M]$^+$; found 2163.07. **HR-MS** (ESI in CHCl$_3$/acetonitrile): calcd for $C_{144}H_{150}N_2NaO_{16}$ [M+Na]$^+$ (m/z) 2186.0881; found 2186.0877. **UV/vis** (CH_2Cl_2): λ (nm) [ε ($M^{-1}cm^{-1}$)] = 579 [54000]. **Fluorescence** (CH_2Cl_2): λ_{max} (nm) = 610; Φ_{Fl} = 0.71.

*Compound **gc***

A suspension of 25 mg (4.11 x 10^{-2} mmol, 1 equiv.) of 5-Monoamino-25,26,27,28- tetrakis(propyloxy)-calix[4]arene, 38 mg (6.16 x 10^{-2} mmol, 1.5 equiv.) of compound 1,7-dipyrrolidinylperylene-3,4:9,10-tetracarboxylic acid bisanhydride and 15 mg (8.22 x 10^{-2} mmol, 2 equiv.) Zn(OAc)$_2$ (H$_2$O-free) was heated in quinoline (0.5 mL) at 140 °C for 5.5 h under an argon atmosphere. The cooled reaction mixture was poured into 30 mL of 1N HCl and stirred for 60 minutes. The resulting precipitate was filtered, washed with water, dissolved in CH$_2$Cl$_2$, and the obtained solution was washed with water to pH neutral and dried over MgSO$_4$. The crude product was purified by column chromatography with CH$_2$Cl$_2$ and precipitated from CH$_2$Cl$_2$/methanol. Compound **gc** was obtained as a green powder (19 mg, 1.94 x 10^{-2} mmol, yield 38%). C$_{78}$H$_{80}$N$_4$O$_8$ (1201.49). Mp > 450 °C (340 °C phase transition). TLC: CH$_2$Cl$_2$/ethyl acetate 98:2; R$_f$ = 0.70. **^{1}H NMR** (400 MHz, CDCl$_3$, 25 °C): δ (ppm) = 8.56 (bs, 1H; Per-*H*); 8.47 and 8.45 (d and s, 2H; Per-*H*); 8.38 (d, 1H, ^3J = 7.8 Hz; Per-*H*); 7.72 and 7.69 (each bd, 2H, each ^3J = 7.8 Hz; Per-*H*); 7.11 (d, 2H; ^3J = 7.5 Hz; Ar-*H*); 7.08 (s, 2H; Ar-*H*); 6.93 (t, 1H, ^3J = 7.5 Hz; Ar-*H*); 6.35 – 6.29 (m, 4H; Ar-*H*); 6.12 (dd, 2H, ^3J = 7.1 Hz, ^4J = 1.9 Hz; Ar-*H*); 5.08 (tt, 1H; $^3J_1$ = 12.1 Hz, $^3J_1$ = 3.4 Hz, Cy-*H*); 4.52 and 3.19 (AX, 4H, ^2J = 13.5 Hz; Ar-C*H*$_2$-Ar); 4.47 and 3.17 (AX, 4H, ^2J = 13.5 Hz; Ar-C*H*$_2$-Ar); 4.12 (t, 2H, ^3J = 8.2 Hz; O-C*H*$_2$); 4.04 (t, 2H, ^3J = 8.1 Hz; O-C*H*$_2$); 3.75 and 3.69 (bs and t, 8H, ^3J = 6.8 Hz; Pyrr-*H* and O-C*H*$_2$); 2.85 (bs, 4H; Pyrr-*H*); 2.66 – 2.57 (m, 2H; Cy-*H*); 2.08 – 1.84 (m, 18H; Pyrr-*H*, Propyl-*H*, Cy-*H*); 1.79 – 1.73 (m, 3H; Cy-*H*); 1.53 – 1.34 (m, 3H; Cy-*H*); 1.11 (t, 6H, ^3J = 7.5 Hz; Propyl-*H*); 0.93 and 0.90 (two t, 6H, each ^3J = 7.5 Hz; Propyl-*H*). **MS** (MALDI in DCTB): calcd for C$_{78}$H$_{80}$N$_4$O$_8$ (m/z) 1200.60 [M]$^+$; found 1200.59. **HR-MS** (ESI in THF/acetonitrile): calcd for C$_{78}$H$_{80}$N$_4$O$_8$ [M]$^+$ (m/z) 1200.5976; found 1200.5971. **UV/vis** (CH$_2$Cl$_2$): λ (nm) [ε (M^{-1}cm^{-1})] = 701 [47300]. **Fluorescence** (CH$_2$Cl$_2$): λ$_{max}$ (nm) = 742; Φ$_{Fl}$ = 0.19.

85

*Compound **gc2***

A suspension of 126 mg (2.07×10^{-4} mol, 2.2 equiv.) of 5-monoamino-25,26,27,28-tetrakis(propyloxy)-calix[4]-arene, 50 mg (9.42×10^{-5} mol, 1 equiv.) of 1,7-di(pyrrolidinyl)perylene-3,4:9,10-tetracarboxylic acid bisanhydride and 69 mg (3.77×10^{-4} mol, 4 equiv.) of $Zn(OAc)_2$ (H_2O-free) was heated in 0.7 mL distilled quinoline at 150 °C for 18.5 h under an argon atmosphere. The cooled reaction mixture was poured into 2N HCl and stirred for 30 minutes at 40 °C. The mixture was adjusted to pH > 9 with NH_3 solution (25%). To the solution 50 mL of CH_2Cl_2 were added and the resulting organic phase was washed with water and brine and dried over $MgSO_4$. The crude product was purified by column chromatography with CH_2Cl_2/ethylacetate 99:1 and successively by precipitation from CH_2Cl_2/methanol. Compound **gc2** was obtained as a dark green powder (69 mg, 4.04×10^{-5} mol, yield 43%). $C_{112}H_{116}N_4O_{12}$ (1710.14). Mp>400 °C. TLC CH_2Cl_2/ethylacetate 99:1; R_f = 0.58. **^{1}H NMR** (400 MHz, $CDCl_3$, 25 °C): δ (ppm) = 8.61 (s, 2H; Per-*H*); 8.54 (d, 2H, ^3J = 8.1 Hz; Per-*H*); 7.82 (d, 2H, each ^3J = 8.1 Hz; Per-*H*); 7.12 and 7.09 (d and s, 8H, ^3J = 7.5 Hz; Ar-*H*); 6.93 (t, 2H, ^3J = 7.5 Hz; Ar-*H*); 6.33 and 6.30 (t and dd, 8H, ^3J = 7.4 Hz and ^3J = 7.5 Hz / ^4J = 1.9 Hz; Ar-*H*); 6.12 (dd, 4H, ^3J = 7.2 Hz / ^4J = 1.9 Hz; Ar-*H*); 4.52 and 3.19 (AX, 8H, ^2J = 13.4 and 13.6 Hz; Ar-C*H$_2$*-Ar); 4.48 and 3.17 (AX, 8H, ^2J = 13.4 and 13.6 Hz; Ar-C*H$_2$*-Ar); 4.12 and 4.04 (each t, 8H, each ^3J = 8.2Hz; O-C*H$_2$*); 3.80 and 3.69 (bs and t, 12H, ^3J = 6.8 Hz; Pyrr-*H* and O-C*H$_2$*); 2.91 (bs, 4H; Pyrr-*H*); 2.10 – 1.84 (m, 24H; Propyl-*H* and Pyrr-*H*); 1.11 (t, 12H, ^3J = 7.5 Hz; Propyl-*H*); 0.93 and 0.90 (each t, 12H, each ^3J = 7.5 Hz; Propyl-*H*). **HR-MS** (ESI in $CHCl_3$/acetonitrile): calcd $C_{112}H_{116}N_4O_{12}$ (m/z) 1731.8488 [M+Na]$^+$; found 1731.8482. **Analysis**: calcd (%) for $C_{112}H_{116}N_4O_{12}$ (1710.14): C 78.66; H 6.84; N 3.28; found: C 78.58; H 6.91; N 3.34. **UV/vis** (CH_2Cl_2): λ (nm) [ε ($M^{-1}cm^{-1}$)] = 704 [51200]. **Fluorescence** (CH_2Cl_2): $λ_{max}$ (nm) = 741; $Φ_{Fl}$ = 0.18.

*Compound **gref***

A solution of 60 mg (6.91 x 10^{-5} mol, 1 equiv.) of isomerically pure 1,7-dibromo-*N,N'*-2,6-diisopropylphenyl-perylene-3,4:9,10-tetracarboxylic acid bisimide[45] in 3.5 mL pyrrolidine (42 mmol, 608 equiv.) was heated at 50°C for 17 h under an argon atmosphere. The cooled reaction mixture was poured into 40 mL 1N HCl and was stirred for 90 minutes at 50 °C. To the solution 50 mL of CH_2Cl_2 were added and the resulting organic phase was washed with water and brine and dried over Na_2SO_4. The crude product was purified by column chromatography with CH_2Cl_2 and successively by preparative HPLC with $CHCl_3$/acetone/hexane 12:1.5:9 (SiO_2, normal phase) and by subsequent precipitation from CH_2Cl_2/methanol. Compound **gref** was obtained as a dark green powder (10 mg, 1.18 x 10^{-2} mmol, yield 17%). $C_{56}H_{56}N_4O_4$ (849.07). Mp=286 °C (decomp.). TLC: $CHCl_3$/acetone/hexane 12:1.5:9; R_f = 0.65. **^{1}H NMR** (400 MHz, $CDCl_3$, 25 °C): δ (ppm) = 8.58 (s, 2H; Per-*H*); 8.51 (d, 2H, ^3J = 8.0 Hz; Per-*H*); 7.79 (d, 2H, ^3J = 8.1 Hz; Per-*H*); 7.49 (t, 2H, ^3J = 7.7 Hz; Ar-*H*); 7.34 (d, 4H, ^3J = 7.7 Hz; Ar-*H*); 3.83 (bs, 4H, ^3J = 6.8 Hz; Pyrr-*H*); 2.93 and 2.83 − 2.76 (bs and m, 8H; Pyrr-*H* and *i*-Propyl-*H*); 2.10 and 2.03 (each bs, 8H; Pyrr-*H*); 1.18 (dd, 24H, ^3J = 6.8 Hz and ^4J = 1.5 Hz; *i*-Propyl-*H*). **HR-MS** (ESI in $CHCl_3$/acetonitrile): calcd $C_{56}H_{56}N_4O_4$ (m/z) 848.4302 $[M]^+$; found 848.4296. **UV/vis** (CH_2Cl_2): λ (nm) [ε ($M^{-1}cm^{-1}$)] = 709 [43000]. **Fluorescence** (CH_2Cl_2): λ_{max} (nm) = 747; Φ_{Fl} = 0.18.

3.10   Appendix

Cyclovoltammetry on Tetrapropyloxy-calix[4]arene
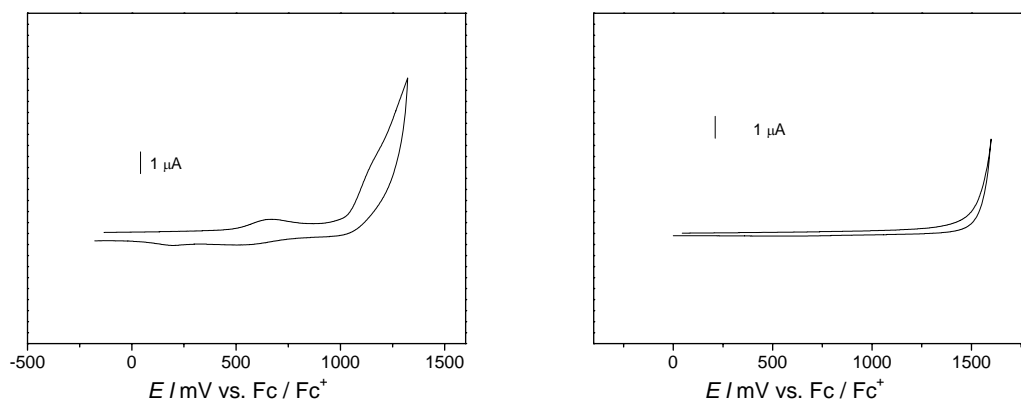
Figure 12. Cyclic voltammograms in CH_2Cl_2 of tetrapropyloxy-calix[4]arene (left, concentration = 1.60 x 10^{-3} M, scan rate 250 mV s^{-1}) and pure solvent (right, scan rate 100 mV s^{-1}). Working electrode: Pt disc, $\varnothing$ 1 mm; auxiliary electrode: Pt wire; reference electrode: Ag/AgCl; supporting electrolyte TBAHFP (0.1 M).

Femtosecond Transient Absorption Spectra in Toluene

Figure 19. Femtosecond transient absorption spectra and corresponding time delays in toluene after photoexcitation at 530 nm of compound **oc** (left), compound **oc2** (middle), and compound **oref** (right). For compound **oc2** the scattered laser pulse is observed.

Figure 20. Femtosecond transient absorption spectra and corresponding time delays in toluene after photoexcitation at 530 nm of compound **rc** (left), compound **rc2** (middle), and compound **rref** (right). For compounds **rc** and **rc2** the scattered laser pulse is observed.
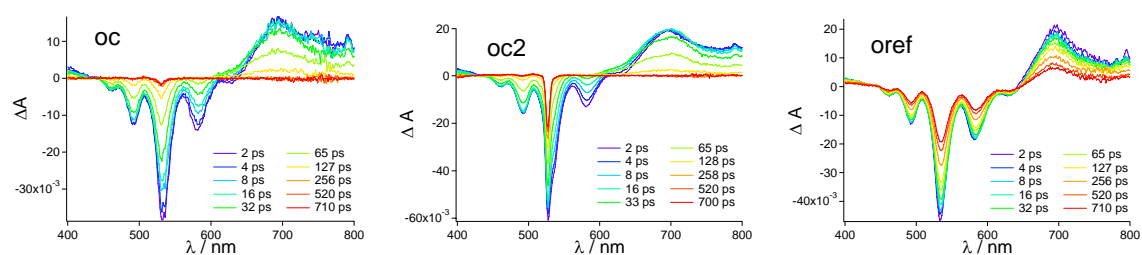

Figure 21. Femtosecond transient absorption spectra and corresponding time delays in toluene after photoexcitation at 640 nm of compound **gc** (left), compound **gc2** (middle), and compound **gref** (right). For compound **gc** the scattered laser pulse is observed.

Femtosecond Transient Absorption Spectra in CH$_2$Cl$_2$
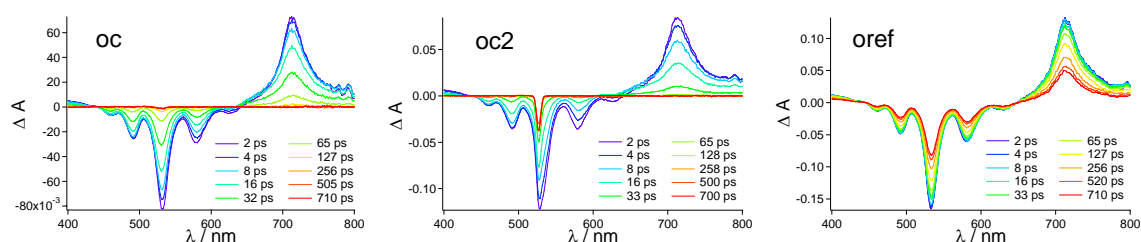
Figure 22. Femtosecond transient absorption spectra and corresponding time delays in CH$_2$Cl$_2$ after photoexcitation at 530 nm of compound **oc** (left), compound **oc2** (middle), and compound **oref** (right). For compound **oc2** the scattered laser pulse is observed.
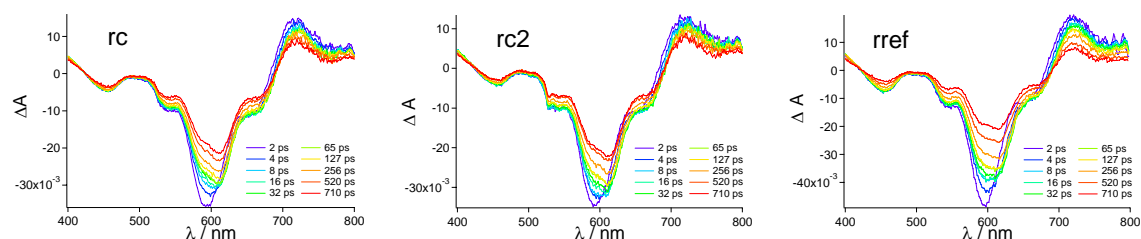
Figure 23. Femtosecond transient absorption spectra and corresponding time delays in CH$_2$Cl$_2$ after photoexcitation at 530 nm compound **rc** (left), compound **rc2** (middle), and compound **rref** (right). For compound **rc2** the scattered laser pulse is observed.
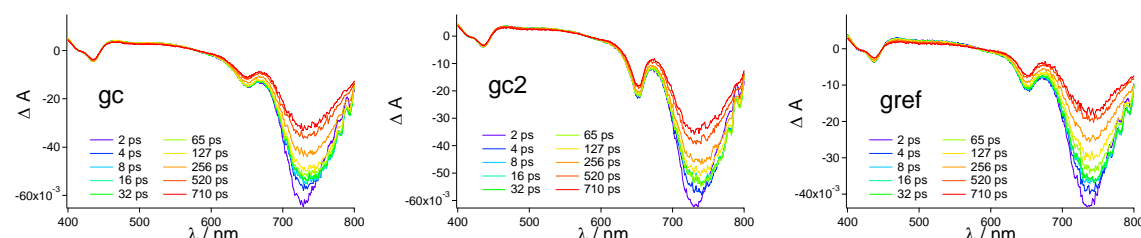
Figure 24. Femtosecond transient absorption spectra and corresponding time delays in CH$_2$Cl$_2$ after photoexcitation at 640 nm of compound **gc** (left), compound **gc2** (middle), and compound **gref** (right). For compound **gc2** the scattered laser pulse is observed.
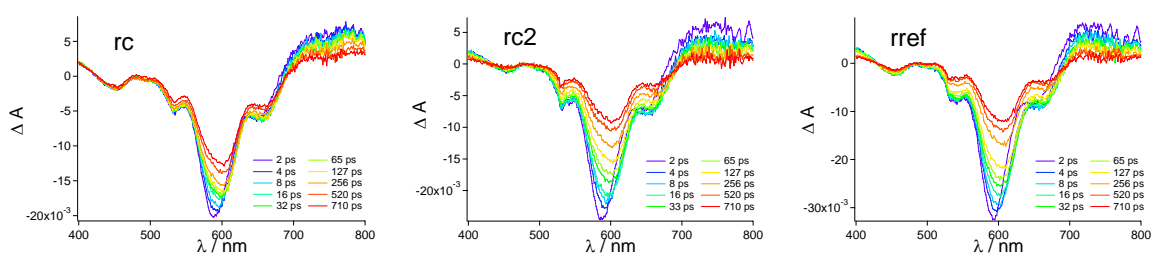
Femtosecond Transient Absorption Spectra in Benzonitrile
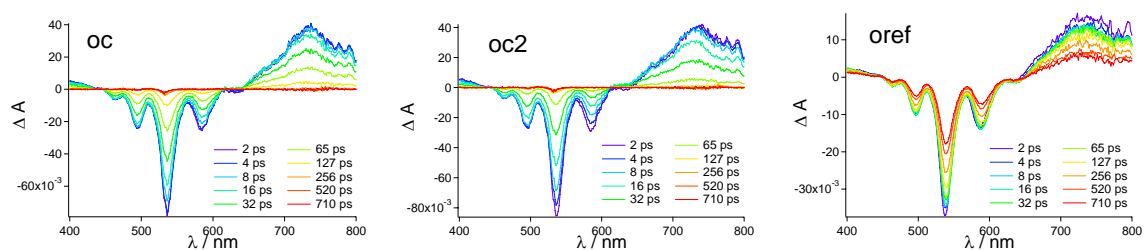
Figure 25. Femtosecond transient absorption spectra and corresponding time delays in benzonitrile after photoexcitation at 530 nm of compound **oc** (left), compound **oc2** (middle), and compound **oref** (right).
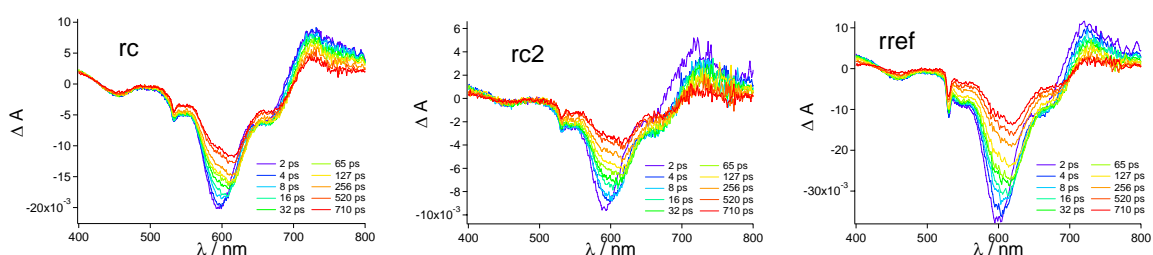
Figure 26. Femtosecond transient absorption spectra and corresponding time delays in benzonitrile after photoexcitation at 530 nm of compound **rc** (left), compound **rc2** (middle), and compound **rref** (right). For all three compounds the scattered laser pulse is observed.
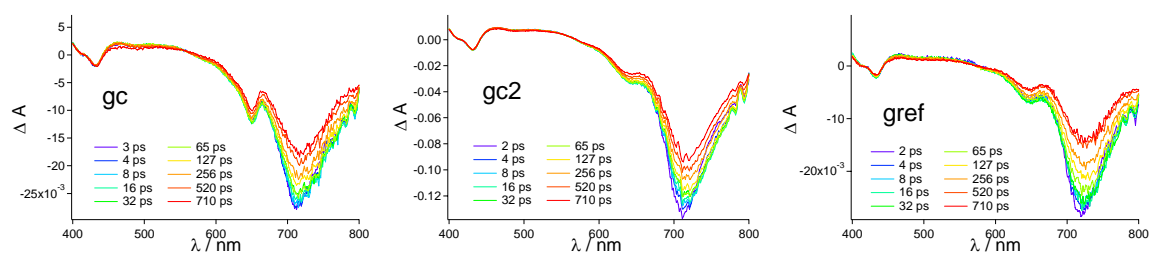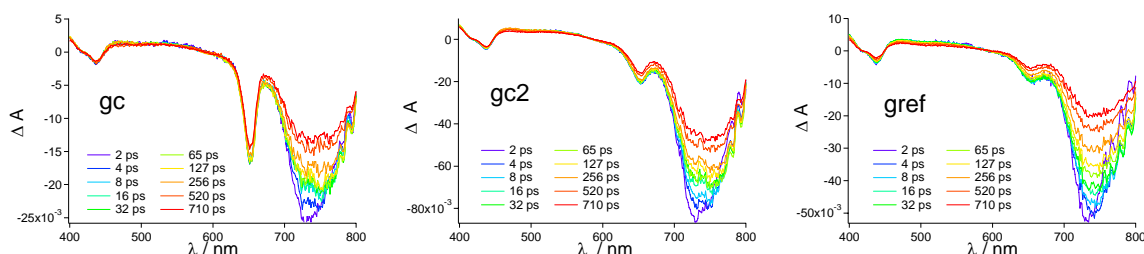

Figure 27. Femtosecond transient absorption spectra and corresponding time delays in benzonitrile after photoexcitation at 640 nm of compound **gc** (left), compound **gc2** (middle), and compound **gref** (right). For compound **gc** the scattered laser pulse is observed.

SADS
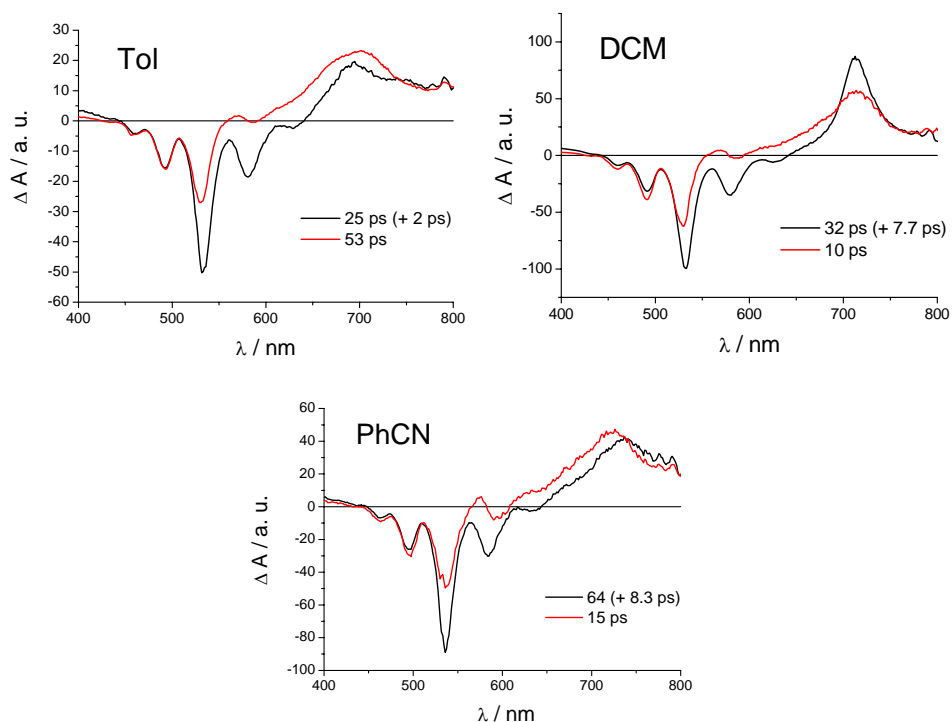
Figure 28. Species-associated difference spectra (SADS) obtained from the simultaneous target analysis of femtosecond transient absorption data of compounds **oc** and **oc2** with the related lifetimes given exemplarily for compound **oc** in toluene (Tol, top left), in CH_2Cl_2 (DCM, top right), and in benzonitrile (PhCN, bottom). SADS in toluene are repeated from Figure 9B for comparison. Shown are processes after photoexcitation at 530 nm. Features due to Raman scattering were omitted for clarity. The black SADS represents the biexponentially decaying excited state of **oc**, and the red SADS belongs to the CT state of **oc**.

3.11 References

(1)   (a) *Supramolecular Photochemistry*; Balzani, V., Scandola, F., Eds.; Horwood: Chichester, UK, 1991. (b) *Comprehensive Supramolecular Chemistry*, *Vol. 1– 11*; Lehn, J.-M., Atwood, J. L., Davies, J. E. D., MacNicol, D. D., Vögtle, F., Eds.; Pergamon: Oxford, 1996. (c) *Series on Photoconversion of Solar Energy*; Archer, M. D., Barber, J., Eds.; Imperial College Press: London, UK, 2002. (d) *Essentials of Molecular Photochemistry*; Gilbert, A.; Baggott, J., Eds.; Blackwell Science Ltd.: Oxford, 1991. (e) *Electron Transfer in Chemistry*; Balzani, V., Ed.; Wiley-VCH: Weinheim, 2001; Vol. 1–5.

(2)   (a) *Calixarenes 2001*; Asfari, Z., Böhmer, V., Harrowfield, J., Eds.; Kluwer Academic Publishers: Dordrecht, 2001. (b) *Calixarenes*; Gutsche, C. D.; The Royal Society of Chemistry: Cambridge, 1993. (c) *Calixarenes Revisited*; Gutsche, C. D.; The Royal Society of Chemistry: Letchworth, 1998. (d) Böhmer, V.; *Angew. Chem., Int. Ed. Engl.* **1995**, *34*, 713–745.

(3)   Pedersen, C. J. *J. Am. Chem. Soc.* **1967**, *89*, 7017–7036.

(4)   *Cyclodextrin Chemistry*; Bender, M. L., Komiyama, M., Eds.; Springer: Berlin, 1978.

(5)   Kenis, P. J. A.; Noordman, O. F. J.; Houbrechts, S.; van Hummel, G. J.; Harkema, S.; van Veggel, F. C. J. M.; Clays, K.; Engbersen, J. F. J.; Persoons, A.; van Hulst, N. F.; Reinhoudt, D. N. *J. Am. Chem. Soc.* **1998,** *120,* 7875–7883.

(6)   (a) Zhao, B.-T.; Blesa, M.-J.; Mercier, N.; Le Derf, F.; Sallé, M. *J. Org. Chem.* **2005**, *70*, 6254–6257. (b) Yu, H.-h.; Xu, B.; Swager, T. M. *J. Am. Chem. Soc.* **2003**, *125*, 1142–1143. (c) Scherlis, D. A.; Marzari, N. *J. Am. Chem. Soc.* **2005,** *127,* 3207–3212. (d) Yu, H.-h.; Pullen, A. E.; Büschel, M. G.; Swager, T. M. *Angew. Chem., Int. Ed. Engl.* **2004**, *43*, 3700–3703.

(7)   (a) Schazmann, B.; Alhashimy, N.; Diamond, D. *J. Am. Chem. Soc.* **2006**, *128*, 8607–8614. (b) Souchon, V.; Leray, I.; Valeur, B. *Chem. Commun*. **2006**, 4224–4226. (c) Lee, S. H.; Kim, S. H.; Kim, S. K.; Jung, J. H.; Kim, J. S. *J. Org. Chem.* **2005**, *70*, 9288–9295. (d) Kim, S. K.; Bok, J. H.; Bartsch, R. A.; Lee, J. Y.; Kim, J. S. *Org. Lett.* **2005**, *7*, 4839–4842. (e) Kim, S. K.; Lee, S. H.; Lee, J. Y.; Bartsch, R. A.; Kim, J. S. *J. Am.*

Chem. Soc. **2004**, *126*, 16499–16506. (f) Leray, I.; Lefevre, J.-P.; Delouis, J.-F.; Delaire, J.; Valeur, B. *Chem.–Eur. J.* **2001**, *7*, 4590–4598. (g) van der Veen, N.; Flink, S.; Deij, M. A.; Egberink, R. J. M.; van Veggel, F. C. J. M.; Reinhoudt, D. N. *J. Am. Chem. Soc.* **2000**, *122*, 6112–6113. (h) Ji, H.-F.; Dabestani, R.; Brown, G. M.; Sachleben, R. A. *Chem. Commun*. **2000**, 833–834. (i) Ji, H.-F.; Brown, G. M.; Dabestani, R. *Chem. Commun.* **1999**, 609–610. (j) Jin, T.; *Chem. Commun.* **1999**, 2491–2492. (k) Larey, I.; O'Reilly, F.; Habib Jiwan, J.-L.; Soumillion, J.-Ph.; Valeur, B. *Chem. Commun.* **1999**, 795–796. (l) Beer, P. D.; Timoshenko, V.; Maestri, M.; Passaniti, P.; Balzani, V. *Chem. Commun.* **1999**, 1755–1756. (m) Unob, F.; Asfari, Z.; Vicens, J. *Tetrahedron Lett.* **1998**, *39*, 2951–2954. (n) Jin, T.; Monde, K. *Chem. Commun.* **1998**, 1357–1358. (o) Ikeda, A.; Yoshimura, M.; Lhotak, P.; Shinkai, S. *J. Chem. Soc., Perkin Trans. 1*, **1996**, 1945–1950. (p) Grigg, R.; Holmes, J. M.; Jones, S. K.; Norbert, W. D. J. A. *J. Chem. Soc., Chem. Comm.* **1994**, 185–187. (q) Aoki, I.; Sakaki, T.; Shinkai, S. *J. Chem. Soc., Chem. Comm.* **1992**, 730–732. (r) Jin, T.; Ichikawa, K.; Koyama, T. *J. Chem. Soc., Chem. Comm.* **1992**, *25*, 499–501.

(8)   (a) *Calixarenes in Action*; Mandolini, L., Ungaro, R., Eds.; Imperial College Press: London, 2000. (b) Schazmann, B.; O'Malley, S.; Nolan, K.; Diamond, D. *Supramol. Chem.* **2006**, *18*, 515–522. (c) Lemli, B.; Peles, J.; Kollár, L.; Nagy, G.; Kunsági-Máté, S. *Supramol. Chem.* **2006**, *18*, 251–256. (d) Rozhenko, A. B.; Schoeller, W. W.; Letzel, M. C.; Decker, B.; Agena, C.; Mattay, J. *Chem. – Eur. J.* **2006**, *12*, 8995–9000. (e) Eckel, R.; Ros, R.; Decker, B.; Mattay, J.; Anselmetti, D. *Angew. Chem., Int. Ed. Engl.* **2005**, *44*, 484–488. (f) Ji, H.-F.; Dabestani, R.; Brown, G. M. *J. Am. Chem. Soc*. **2000**, *122*, 9306–9307. (g) Kim, J. S.; Shon, O. J.; Ko, J. W.; Cho, M. H.; Yu, I. Y.; Vicens, J. *J. Org. Chem.* **2000**, *65*, 2386–2392. (h) Ikeda, A.; Shinkai, S. *Chem. Rev*. **1997**, *97*, 1713–1734. (i) Diamond, D.; McKervey, M. A. *Chem. Soc. Rev.* **1996**, 15–24.

(9)   Würthner, F. *Chem. Comm.* **2004**, 1564–1579.

(10)   You, C.-C.; Dobrawa, R.; Saha-Möller, C. R.; Würthner, F. *Top. Curr. Chem.* **2005**, *258*, 39–82.

(11)   (a) Ford, W. E.; Kamat, P. V. *J. Phys. Chem.* **1987**, *91*, 6373–6380. (b) Gvishi, R.; Reisfeld, R.; Burshtein, Z. *Chem. Phys. Lett.* **1993**, *213*, 338–344.

(12)   (a) De Schryver, F. C.; Vosch, T.; Cotlet, M.; Van der Auweraer, M.; Müllen, K.; Hofkens, J. *Acc. Chem. Res.* **2005**, *38*, 514–522. (b) Zang, L.; Liu, R.; Holman, M. W.; Nguyen, K. T.; Adams, D. M. *J. Am. Chem. Soc.* **2002**, *124*, 10640–10641. (c) Sauer, M. *Angew. Chem. Int. Ed.* **2003**, 42, 1790 – 1793. (d) Han, J. J.; Wang, W.; Li, A. D. Q. *J. Am. Chem. Soc.* **2006**, *128*, 672–673.

(13)   Seybold, G.; Stange, A. (BASF AG), *Ger. Pat.* DE 35 45 004, 1987 (*Chem. Abstr.*, 1988, **108**, 77134c).

(14)   Zhao, Y.; Wasielewski, M. R. *Tetrahedron Lett.* **1999**, *40*, 7047–7050.

(15)   Langhals, H. *Heterocycles*, **1995**, *40*, 477–500.

(16)   Vysotsky, M. O.; Böhmer, V.; Würthner, F.; You, C.-C.; Rissanen, K. *Org. Lett.* **2002**, *4*, 2901–2904.

(17)   Van der Boom, T.; Evmenenko, G.; Dutta, P.; Wasielewski, M. R. *Chem. Mater.* **2003**, *15*, 4068–4074.

(18)   Hippius, C.; Schlosser, F.; Vysotsky, M. O.; Böhmer, V.; Würthner, F. *J. Am. Chem. Soc.* **2006**, *128*, 3870–3871.

(19)   *Supramolecular Chemistry*; Lehn, J.-M. Ed., VCH: Weinheim, 1995.

(20)   Zweig, A.; Hodgson, W. G.; Jura, W. H. *J. Am. Chem. Soc.* **1964**, *86*, 4124–4129.

(21)   Ford, W. E.; Hiratsuka, H.; Kamat, P. V. *J. Phys. Chem.* **1989**, *93*, 6692–6696.

(22)   Würthner, F.; Sautter, A. *Chem. Commun.* **2000**, 445–446.

(23)   Weller, A. *Z. Phys. Chem.* **1982**, *133*, 93–98.

(24)   Prodi, A.; Chiorboli, C.; Scandola, F.; Iengo, E.; Alessio, E.; Dobrawa, R.; Würthner, F. *J. Am. Chem. Soc.* **2005**, *127*, 1454–1462.

(25)   (a) Hofkens, J.; Vosch, T.; Maus, M.; Köhn, F.; Cotlet, M.; Weil, T.; Herrmann, A.; Müllen, K.; De Schryver, F. C. *Chem. Phys. Lett.* **2001**, *333*, 255–263. (b) Osswald, P.; Leusser, D.; Stalke, D.; Würthner, F. *Angew. Chem., Int. Ed. Engl.* **2005**, *44*, 250–253.

(26)   (a) Lukas, A. S.; Zhao, Y.; Miller, S. E.; Wasielewski, M. R. *J. Phys. Chem. B,* **2002**, *106*, 1299–1306. (b) Shibano, Y.; Umeyama, T.; Matano, Y.; Tkachenko, N. V.; Lemmetyinen, H.; Imahori, H. *Org. Lett*. **2006**, *8*, 4425–4428.

(27)   (a) van Stokkum, I. H. M.; Larsen, D. S.; van Grondelle, R. *Biochim. Biophys. Acta* **2004**, *1657*, 82–104. (b) van Stokkum, I. H. M.; Lozier, R. H. *J. Phys. Chem. B* **2002**, *106*, 3477–3485. (c) Mullen, K. M.; van Stokkum, I. H. M. *J. Statistical Software* **2007,** 18 (3). URL http://www.jstatsoft.org/v18/i03/ (d) Global and target analysis can be performed with e.g., the R package TIMP, see http://cran.r-project.org/doc/packages/TIMP.pdf

(28)   (a) Schweitzer, G.; Gronheid, R.; Jordens, S.; Lor, M.; De Belder, G.; Weil, T.; Reuther, E.; Müllen, K.; De Schryver, F. C. *J. Phys. Chem. A* **2003,** *107,* 3199–3207. (b) De Belder, G.; Jordens, S.; Lor, M.; Schweitzer, G.; De, R.; Weil, T.; Herrmann, A.; Wiesler, U. K.; Müllen, K.; De Schryver, F. C. *J. Photochem. Photobiol. A* **2001**, *145*, 61–70.

(29)   (a) Price, S. L.; Stone, A. J. *J. Chem. Phys.* **1987**, *86*, 2859–2868. (b) Perez-Casas, S.; Hernandez-Trujillo, J.; Costas, M. *J. Phys. Chem. B* **2003**, *107*, 4167–4174. (c) Suppan, P. *J. Photochem. Photobiol. A*, **1990**, *50*, 293–330.

(30)   *Modern Molecular Photochemistry*; Turro, N. J., Ed.; University Science Books: Sausalito, California 1991.

(31)   (a) Asahi, T.; Ohkohchi, M.; Matsusaka, R.; Mataga, N., Zhang, R. P.; Osuka, A; Maruyamat, K. *J. Am. Chem. Soc.* **1993**, *115,* 5665–5614. (b) Imahori, H.; Hagiwara, K.; Aoki, M.; Akiyama, T.; Taniguchi, S.; Okada, T.; Shirakawa, M.; Sakata, Y. *J. Am. Chem. Soc.* **1996,** *118,* 11771–11782. (c) Tan, Q.; Kuciauskas, D.; Lin, S.; Stone, S.; Moore, A. L.; Moore, T. A.; Gust, D. *J. Phys. Chem. B* **1997,** *101,* 5214–5223. (d) Armaroli, N.; Accorsi, G.; Song, F.; Palkar, A.; Echegoyen, L.; Bonifazi, D.; Diederich, F. *ChemPhysChem* **2005**, *6*, 732–743.

(32)   Beckers, E. H. A.; Meskers, S. C. J.; Schenning, A. P. H. J.; Chen, Z.; Würthner, F.; Janssen, R. A. J. *J. Phys. Chem A* **2004**, *108*, 6933–6937.

(33)   (a) Würthner, F.; Sautter, A.; Schilling, J. *J. Org. Chem.* **2002**, *67*, 3037–3044. (b) Würthner, F.; Thalacker, C.; Sautter, A.; Schärtl, W.; Ibach, W.; Hollricher, O. *Chem. Eur. J.* **2000**, *6*, 3871–3886.

(34)   (a) Würthner, F.; Stepanenko, V.; Chen, Z.; Saha-Möller, C. R.; Kocher, N.; Stalke, D. *J. Org. Chem.*, **2004**, *69*, 7933–7939. (b) Fuller, M. J.; Sinks, L. E.; Rybtchinski, B.; Giaimo, J. M.; Li, X.; Wasielewski, M. R. *J. Phys. Chem. A* **2005**, *109,* 970–975.

(35)   (a) Kaiser, H.; Lindner, J.; Langhals, H. *Chem. Ber.* **1991**, *124*, 529–535. (b) Nagao, Y.; Naito, T.; Abe, Y.; Misono, T. *Dyes Pigm.* **1996**, *32*, 71–83.

(36)   Würthner, F.; Sautter, A.; Schmid, D.; Weber, P. J. A. *Chem. Eur. J.* **2001**, *7*, 894–902.

(37)   Lukas, A. S.; Zhao, Y.; Miller, S. E.; Wasielewski, M. R. *J. Phys. Chem. B* **2002**, *106*, 1299–1306.

(38)   Van Wageningen, A. M. A.; Snip, E.; Verboom, W.; Reinhoudt, D. N.; Boerrigter, H. *Liebigs Annalen/Recueil* **1997**, *11*, 2235–2245.

(39)   Demas, J. N.; Grosby, G. A. *J. Phys. Chem.* **1971**, *75*, 991–1024.

(40)   Lauteslager, X. Y.; van Stokkum, I. H. M.; van Ramesdonk, H. J.; Brouwer, A. M.; Verhoeven, J. W. *J. Phys. Chem. A*, **1999**, *103*, 653–659.

(41)   Vergeer, F. W.; Kleverlaan, C. J.; Stufkens, D. J. *Inorg. Chim. Acta* **2002**, *327*, 126–133.

(42)   Collaborative Computational Project, Number 4. *Acta Crystallogr.* **1994**, *Sect. D 50*, 760–763.

(43)   SHELX97 Programs for Crystal Structure Analysis (Release 97–2). Sheldrick, G. M. University of Göttingen, Germany, **1998**.

(44)   Farrugia, L. J. *J. Appl. Crystallogr.* **1999**, *32*, 837–838.

(45)   Würthner, F.; Osswald, P.; Schmidt, R.; Kaiser, T. E.; Mansikkamäki, H.; Könemann, M. *Org. Lett.* **2006**, *8*, 3765–3768.

4

Sequential FRET Processes in Calix[4]arene-Linked Orange-Red-Green Perylene Bisimide Dye Arrays

Abstract: Perylene bisimide–calix[4]arene arrays composed of up to three different types of perylene bisimide chromophores (*orange*, *red* and *green* PBIs) have been synthesized. A quantitative analysis of the photophysical processes after photoexcitation as well as their rates have been obtained by using UV/vis absorption, steady state and time-resolved emission, femtosecond transient absorption spectroscopy and spectrotemporal analysis of the femtosecond transient absorption data. According to these studies, very efficient energy transfer processes do occur from the *orange* perylene bisimide chromophoric unit to the *red* chromophoric unit ($k_{ET} = 6.4 \times 10^{11}$ s^{-1} for compound **or**), from the *red* PBI moiety to the *green* dye unit ($k_{ET} = 4.0 \times 10^{11}$s^{-1} for compound **rg**), and slightly less efficient from the *orange* to the *green* PBI chromophore ($k_{ET} = 1.5 \times 10^{11}$s^{-1} for compound **og**) within these systems. The experimentally obtained rate constants are in very good agreement with those calculated according to the Förster theory as $k_{ET} = 5.9 \times 10^{11}$ s^{-1} (for compound **or**, with $R_0 = 70.8$ Å), $k_{ET} = 4.0 \times 10^{11}$ s^{-1} (for compound **rg**, with $R_0 = 74.5$ Å), and $k_{ET} = 1.9 \times 10^{11}$ s^{-1} (for compound **og**, with $R_0 = 58.7$ Å), respectively.

4.1   Introduction

Photosynthesis in plants and bacteria represents one of the most important biological processes responsible for the development and sustenance of life on earth. Among the different classes of photosynthetic organisms, many different types of light-harvesting systems are used.[1] It has been demonstrated that, for example, in purple bacteria the primary steps of photosynthesis involve the absorption of photons by light-harvesting multichromophoric antenna complexes and subsequent directional transport of the energy through excited-state energy transfer to the photosynthetic reaction centers. The high efficiency of natural photosynthesis is thus an outcome of proper organization of a multitude of chromophores in space that exhibit distinct absorption, emission, and redox properties. Inspired by these biofunctional systems many organic chemists aim at artificial structures containing multiple chromophores that provide sequential energy transfer, and functional dye assemblies possessing energy and charge transport properties for mimicking the basic processes of photosynthesis have thus attracted considerable attention in materials as well as in biological sciences in the past years.[2,3]

Accordingly, the synthetic approach towards *artificial* structures based on organized functional dye systems aims at the defined spatial arrangement of multiple chromophores, thus, ensuring efficient sequential energy transfer processes between the individual dye units.[4] Numerous classes of functional dyes have been employed to design multichromophoric architectures among which, particularly, perylene bisimides (PBIs) have been proven useful to investigate the basic light-harvesting energy transfer processes.[5-7] Perylene bisimides are especially suitable for this purpose due to their bright photoluminescence with quantum yields up to unity,[8] chemical inertness, and exceptional photostability.[9,10] Accordingly, perylene bisimides (among other classes of functional dyes) have been successfully applied to afford a variety of covalently constructed and self-assembled light-harvesting architectures such as *rigid linear arrays* of chromophores linked by spacer units,[5,11] *molecular squares*[7a,b,12] as well as *dendrimers* (in general, with energy transfer from peripheral dyes to the core dye).[6,13] For a schematic representation of the respective dye architectures and of the spatial orientation of the chromophoric units therein see Figure 1. Furthermore, numerous examples of $\pi-\pi$-stacked supramolecular dye aggregates[3,14,15] exist as well. In contrast, only few examples of *covalently stacked*

arrangements of dyes (Figure 1) are known from the literature which are typically limited to bichromophoric systems, as in most cases, only dimeric units,[16,17] or systems of less defined geometry have been realized.[18] This might be due to two reasons: first, there are few well-defined rigid scaffolds that provide good solubility as required for obtaining longer oligomers; second, such architectures require a set of dyes with tunable absorption and emission properties without extension of the molecular lengths or the variation of the direction of the transition dipole moment upon tuning of the optical properties.
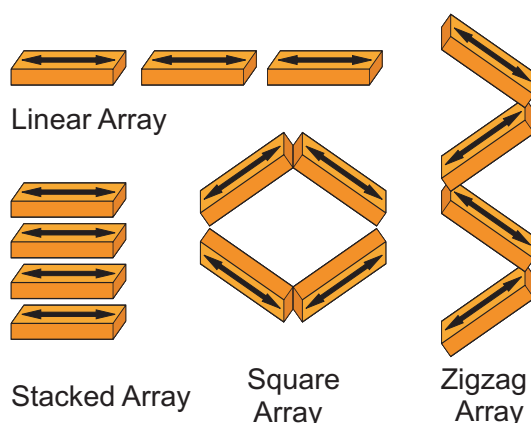
Figure 1. Schematic representation of different types of spatial arrangements of chromophoric units employed for supramolecular dye architectures.

In this Chapter, a new design principle for an artificial light-harvesting architecture has been employed aiming at the structural organization of perylene bisimide dyes along a supramolecular scaffold in a zigzag chain (Figure 1, right) thus providing a favorable situation for highly efficient sequential fluorescence energy transfer (FRET). For this purpose, calix[4]arenes[19] were chosen as the supramolecular spacer unit which offer an ideal scaffold that has been utilized for the organization of nonlinear optical dyes,[20] electrophores,[21] and fluorophores[22] before. Furthermore, calix[4]arenes have been used for the construction of larger species through self-assembly by, e.g., hydrogen bonding,[23] or metal-ion-coordination.[24]

An ideal chromophore type toward zigzag architectures with well-defined orientation of the respective transition dipole moments (see arrows in Figure 1) is given with perylene bisimide dyes (PBIs).[9] The perylene bisimide chromophore can be easily fine-tuned by proper substituents in the so-called *bay* positions to exhibit quite divers electronic and optical properties.[9] As such, the classes of phenoxy-(*red*),[25] and pyrrolidino-(*green*)[26] *bay*-

substituted perylene bisimides as well as the core-unsubstituted perylene bisimides (*orange*)[8b] are available, and thus a large part of the visible spectrum can be utilized for light harvesting purposes. The first examples for perylene bisimide dyes connected to calix[4]arene moieties, using the latter as a versatile scaffold to organize the functional dye units have been described in Chapter 3 and in the literature.[27,28] In this Chapter a detailed study of an extensive series of multichromophoric PBI–calix[4]arene conjugates is discussed towards the applicability of the latter conjugates as light-harvesting systems, and their photophysical properties are elucidated by means of femtosecond transient absorption spectroscopy.

Towards this goal, a variety of perylene bisimide–calix[4]arene arrays composed of up to three different types of perylene bisimide chromophores (*orange*, *red*, and *green* PBIs) connected to each other by calix[4]arene spacers has been synthesized. The compounds studied here are shown in Scheme 1. Three types of perylene bisimide dyes are used: *orange* (**o**) (with UV/vis absorption maxima at 526 and 490 nm), *red* (**r**) (with an UV/vis absorption maximum at 578 nm), and *green* (**g**) (with an UV/vis absorption maximum at 701 nm), that are linked by calix[4]arene spacers (**c**) via the N-imide bond of the perylene bisimide. Thus, three different types of arrays were synthesized: the first type is composed of two chromophoric units, *i.e.*, one compound containing an *orange* and a *red* PBI chromophore connected by one calix[4]arene unit (named accordingly as compound **or**), a second derivative constructed from a *red* and a *green* moiety unit linked by a calix[4]arene scaffold (compound **rg**) and a third array obtained by combining an *orange* and a *green* PBI chromophore through a calix[4]arene spacer (compound **og**) have been obtained. The second type of arrays contains each three chromophoric PBI units, and four compounds of this type were prepared accordingly: the compound constructed from *two outer orange* PBI units and *one inner red* PBI unit linked via two calix[4]arene spacers is denoted as **oro** (for structures see Scheme 1). Likewise, the compounds obtained from the respective other combinations of three PBI dye units linked by two calix[4]arene scaffolds have been obtained and are referred to as **ror**, **rgr**, and **grg**. The compound containing an *orange*, a *red* and a *green* PBI unit linked by two calix[4]arene units was also synthesized and is named as **org**, accordingly. Finally, an array composed of five chromophores, *i.e.*, one *orange*, two *red* and two *green* PBI units was synthesized that is denoted as **grorg** (for structures see Scheme 1). The monochromophoric reference systems containing only one

PBI dye unit linked to a calix[4]arene moiety **oc**, **rc** and **gc**, respectively, are given for comparison (see also Chapter 3).

4.2   Synthesis and Structural Characterization

The chemical structures and syntheses of the investigated perylene bisimide–calix[4]arene arrays are depicted in Scheme 1. The syntheses of these arrays follows a general strategy outlined here in detail for compound **org** (see Scheme 1). First, a monoBoc-protected calix[4]arene precursor **pcA** was reacted with the red perylene bisanhydride **rPBA** in refluxing toluene/Et_3N to afford the respective Boc-protected compound **pcB**. The latter was used as a key intermediate also for the syntheses of the arrays **grorg**, **oro**, and **grg**. Deprotection and partial imidization with the green perylene monoimide **gPMI** in quinoline (catalyst $Zn(OAc)_2$, 150 °C) yielded the NH_2-functionalized precursor **pcC** which was further reacted with the orange perylene monoimide **oPMI** (quinoline/$Zn(OAc)_2$, 165 °C) to afford the desired array **org** containing three different perylene bisimide chromophores in 49% yield. Compound **org** was purified by column chromatography (SiO_2) and preparative HPLC (SiO_2, normal phase). All other arrays shown in Scheme 1 were obtained likewise by subsequent imidization of the calix[4]arene precursor **pcA**, successively employing the respective desired orange, red, or green perylene monoimide anhydrides or perylene bisanhydrides by following very similar synthetic protocols (details are given in the Experimental Section). All the present perylene bisimide–calix[4]arene arrays were purified by column chromatography (SiO_2) and preparative HPLC (SiO_2, normal phase), and were characterized by ^{1}H NMR spectroscopy and high resolution mass spectrometry. For the synthesis of the monochomophoric reference compounds **oc**, **rc**, and **gc**, respectively, refer to Chapter 3.

Scheme 1. Synthetic routes and chemical structures of PBI–calix[4]arene arrays studied.[a]
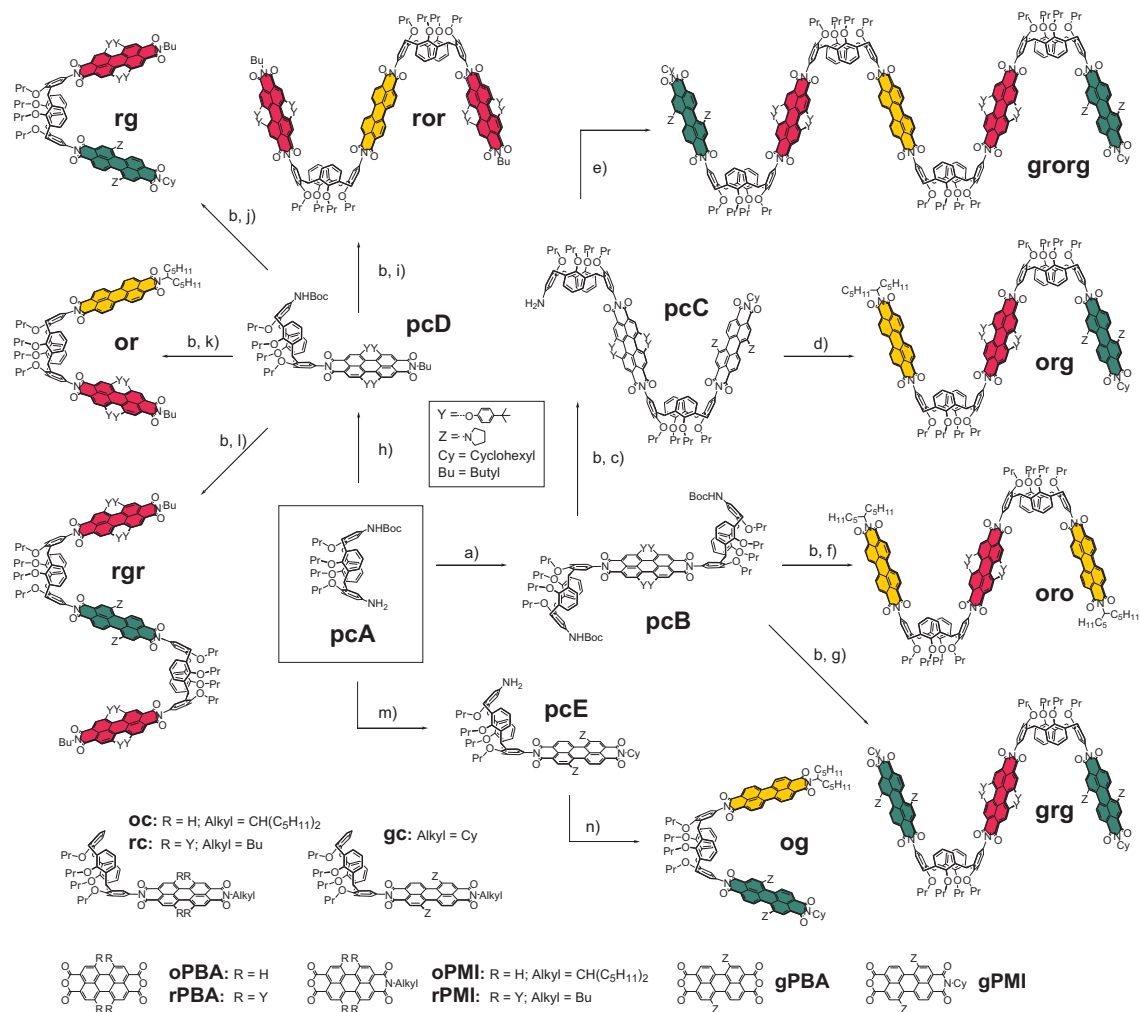
[a] Reagents and conditions: a) **rPBA**, Et$_3$N, toluene, reflux, yield 10%; b) CF$_3$COOH, CH$_2$Cl$_2$, rt; c) **gPMI**, Zn(OAc)$_2$, quinoline, 150 °C, yield 17% over two steps; d) **oPMI**, Zn(OAc)$_2$, quinoline, 165 °C, yield 49%; e) **oPBA**, Zn(OAc)$_2$, quinoline, 165 °C, yield 18%; f) **oPMI**, Zn(OAc)$_2$, quinoline, 175 °C, yield 38% over two steps; g) **gPMI**, Zn(OAc)$_2$, quinoline, 140 °C, yield 18% over two steps; h) **rPMI**, Et$_3$N, toluene, reflux, yield 23%; i) **oPBA**, Zn(OAc)$_2$, quinoline, 160 °C, yield 35% over two steps; j) **gPMI**, Zn(OAc)$_2$, quinoline, 160 °C, yield 28% over two steps; k) **oPMI**, Zn(OAc)$_2$, quinoline, 170 °C, yield 23% over two steps; l) **gPBA**, Zn(OAc)$_2$, quinoline, 160 °C, yield 30% over two steps; m) **gPMI**, Zn(OAc)$_2$, quinoline, 130 °C, yield 14%; n) **oPMI**, Zn(OAc)$_2$, quinoline, 155 °C, yield 23%.

104

4.3   Molecular Structure

In order to get an insight into the 3D structure and the most likely arrangement of the chromophores within the obtained PBI arrays, molecular modeling of the three bichromophoric compounds **or**, **rg**, and **og** was performed (force field calculations using Macromodel 8.0, potential MMFF). The energetically most favorable structures are shown in Figure 2. All three molecules are found in a *pinched cone* conformation with outward-oriented perylene bisimide residues pointing away from each other. These calculated structures are in good agreement with the structural features of recently investigated naphthalene imide functionalized calix[4]arenes.[27] Thus, cofacial orientation of the perylene bisimide chromophores is not preferred for calix[4]arenes bearing different types of core-substituted PBI units. The obtained molecular structure for compound **or** reveals a center-to-center distance between the orange and the red chromophoric unit of r = 19.9 Å. The angles of the transition dipole moments of the S_0-S_1 transitions (along the N-N-axis of the PBI chromophore) have been determined; with Θ_D denoting the angle between the emission transition dipole moment of the *donor* dye unit and the vector joining donor and acceptor unit, and with Θ_A denoting the angle between the emission transition dipole moment of the *acceptor* dye unit and the vector joining donor and acceptor unit. Accordingly, for compound **or** values of $\Theta_D = 44.1°$ (for the *orange* chromophore, here being the energy *donor*) and $\Theta_A = 43.1°$ (for the *red* chromophore, here being the energy *acceptor*) are obtained. The other two compounds **rg** and **og** show very similar structural features. For compound **rg**, values of r = 20.1 Å, $\Theta_D = 43.0°$ (for the *red* chromophore, here being the energy *donor*) and $\Theta_A = 40.9°$ (for the *green* chromophore, here being the energy *acceptor*) are obtained. Compound **og** reveals values of r = 20.0 Å, $\Theta_D = 44.0°$ (for the *orange* chromophore, here being the energy *donor*) and $\Theta_A = 40.3°$ (for the *green* chromophore, here being the energy *acceptor*). The respective data are summarized together with photophysical properties of these compounds in Table 3 (see below).
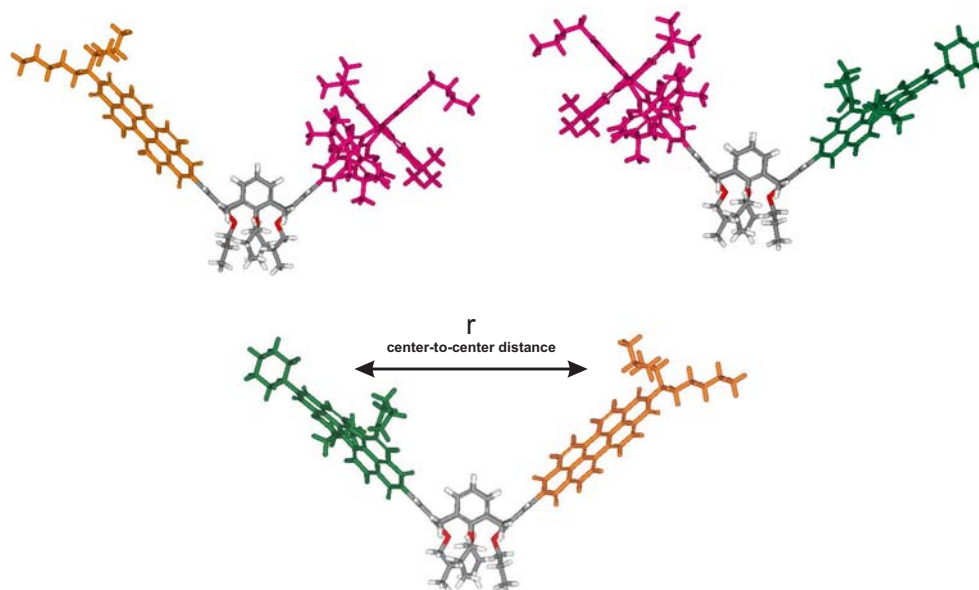
Figure 2. Side views of molecular structures obtained from force field calculations (Macromodel 8.0, potential MMFF) of PBI–calix[4]arene arrays. Top Left: compound **or**. Top Right: compound **rg**. Bottom: compound **og**. Color of the respective PBI chromophores (orange, red, and green, respectively) is applied for clarity.

Obviously, the obtained values for the center-to-center distance r between the respective chromophoric units and the angles Θ_D and Θ_A do not substantially change upon variation of the three different PBI building blocks. Hence, within these arrays the individual building blocks can be easily replaced by each other without influencing the overall geometric arrangement of the supramolecular system, a design principle which is reminiscent of the construction of several natural and synthetic biomacromolecules.[29] The energy gradients within the array are controlled by the optical properties of the respective PBI units by means of core substituents with electron donating character, leading to bathochromic shifts of the UV/vis absorption maxima. Similar fine-tuning of optical properties had also been found for the related chromophore class of naphthalene bisimide dyes.[30] In contrast to the fine-tuning of the optical properties in the present array, commonly a varied absorption and emission behavior is achieved by the extension of the chromophoric π-system, leading, for example, in the case of perylene bisimides to the higher homologues terrylene and quaterrylene dyes.[31] Building blocks obtained in this manners (here the terrylene and quaterrylene dyes), however, differ substantially in length

and would therefore not maintain the overall geometry of the supramolecular array owing to the varied dimensions of the individual chromophoric units.

4.4   Temperature-dependent ^{1}H NMR Studies

The modeling studies (see above) reveal a favorable molecular structure showing a *pinched cone* conformation of the calix[4]arene unit with outward-oriented perylene bisimide residues. As these results were obtained from computational studies, further verification with respect to the actual molecular conformation preferred in solution is of interest. Therefore, variable temperature ^{1}H NMR measurements were conducted for all three compounds **or**, **rg**, and **og** in the temperature range from 271 K to 213 K. A section of the obtained spectra showing the signals of the Ar-CH$_2$-Ar protons of the respective calix[4]arene moiety is depicted in Figure 3. In the ^{1}H NMR spectra at room temperature (400 MHz, in CDCl$_3$) for all three dimers only *one* set of signals for the Ar-CH$_2$-Ar protons of the calix[4]arene moiety is observed (for comparison see also ^{1}H NMR spectra in the Experimental Section), although in principle, two *pinched cone* conformations of the calix[4]arene unit are possible, the first conformation with the PBI residues pointing away from each other (zigzag-conformation) and the second one with the PBI units bent towards each other (stacked conformation). Slow interconversion of these two populated conformations would lead to two sets of signals. The fact that only one set of signals, and thus a single conformation is detected in the ^{1}H NMR spectra of compounds **or**, **rg**, and **og**, respectively, may be rationalized in terms of the following explanation: Either the mutual interconversion between the two possible *pinched cone* conformations is fast on the NMR time scale, so that the observed spectra correspond to the weighted average of the signals, or the mutual interconversion is slow on the NMR time scale, with the population of one of the two possible *pinched cone* conformations being too low in concentration to be detected by NMR spectroscopy. Lowering the temperature to around 215 K did not result in any significant change in the ^{1}H NMR spectra of all three compounds **or**, **rg**, and **og**, respectively, suggesting that the observed spectra correspond to the prevalence of a single *pinched cone* conformation within the whole temperature range applied (see Figure 3). Apparently, in all cases the population of the second *pinched cone* conformer is too low to

allow its detection by ^{1}H NMR spectroscopy. Taking into account that the chemical shift values for all protons of the perylene bisimide subunits experience negligible shifts (as one would in contrast expect by aromatic ring currents in a stacked geometry) compared to those of the reference systems **oc**, **rc**, and **gc**, and in corroboration with the results from molecular modeling, it is concluded that also in solution the *pinched cone* conformation with the outward-oriented perylene bisimide residues prevails. This is further supported by the fact, that an excellent agreement of the experimentally obtained energy transfer rate constants with those calculated according to the Förster theory is observed (for details see below), with the rate of energy transfer being strongly dependent on the center-to-center distance r of the donor and acceptor transition dipoles.
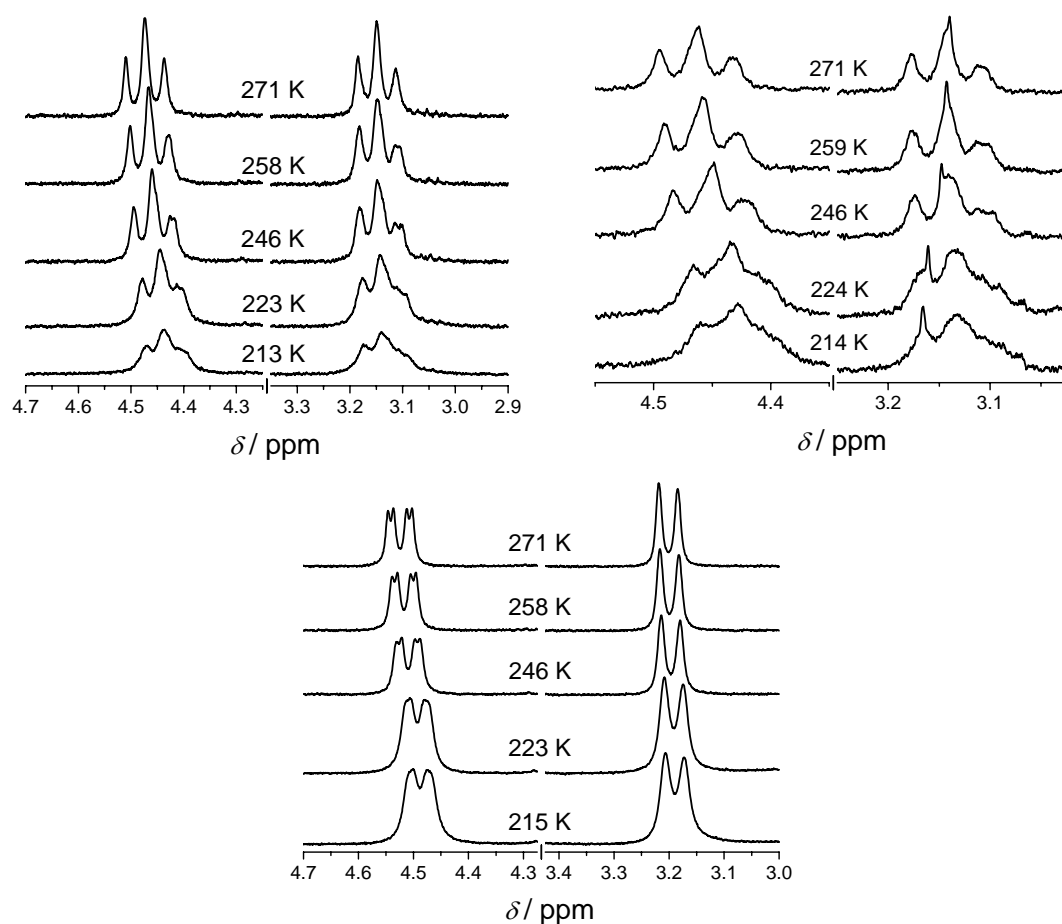

Figure 3. Sections of variable temperature ^{1}H NMR spectra (400 MHz, in CDCl$_3$) of compounds **or** (top left), **rg** (top right), and **og** (bottom) showing the Ar-CH$_2$-Ar protons of the respective calix[4]arene moiety. Temperatures are as indicated above in the individual spectra.

4.5   Optical Properties

The optical properties of the synthesized PBI–calix[4]arene arrays were investigated by UV/vis absorption and steady state fluorescence emission spectroscopy at room temperature. The spectra of the array **org** are shown in Figure 4A and the spectra of the monochromophoric reference compounds **oc**, **rc**, and **gc** are depicted in Figure 4B for comparison (see also Chapter 3). The optical spectra of all other arrays are given in Figures 5–8. The optical data of all compounds are summarized in Table 1. For all the investigated arrays neither additional absorption nor emission bands emerged, indicating no significant ground state interaction between the chromophores. For comparison, the corresponding calculated UV/vis absorption spectra (obtained by summation of UV/vis absorption spectra of the related reference compounds) are also given in the respective Figures, and they closely resemble the absorption patterns of the respective measured spectra for all conjugates studied. For instance, the UV/vis absorption spectrum of array **org** in Figure 4A shows the characteristic maxima of all three perylene bisimide (PBI) chromophores: the spectrum is composed of absorption bands of one orange PBI chromophoric unit (maxima at 527 and 489 nm), one red PBI chromophoric unit (at 580 nm) and one green PBI chromophoric unit (at 701 nm). Likewise, for compound **or** absorption bands of one orange (maxima at 526 nm and 489 nm) and one red PBI chromophoric unit (maximum at 579 nm) (see Figure 5B), for the system **rg** absorption bands of one red (maximum at 580 nm) and one green PBI dye unit (maximum at 701 nm) (see Figure 8A) and for the array **og** absorption bands of one orange (maxima at 525 nm and 489 nm) and one green PBI chromophore (maximum at 700 nm) are found, respectively (see Figure 5A). For all other compounds, similar UV/vis absorption features are observed, and thus, the absorption properties of all investigated arrays are determined by the individual absorption patterns of the parent chromophoric units.

Upon photoexcitation of compound **org** at $\lambda_{ex} = 490$ nm (almost exclusive absorption of the orange dye unit) fluorescence emission of the green PBI chromophore at 737 nm is observed, indicating efficient energy transfer between the chromophoric units. The spectrum in Figure 4A (inset) also shows very weak concomitant fluorescence emission from the red PBI unit at 610 nm. Similar behavior is also observed for arrays **rg**, **rgr**, and

grg, where upon excitation in the red PBI unit at 560 nm almost exclusive fluorescence emission at 738, 739, and 738 nm, respectively, is detected, again along with a very weak concomitant fluorescence emission from the red PBI unit at around 610 nm (see Figures 7 and 8). Upon photoexcitation of the arrays **or**, **oro**, and **ror** at 490 nm (almost exclusively in the orange PBI chromophore) solely fluorescence emission of the red PBI chromophore at 608, 611, and 608 nm, respectively, is observed. For these arrays no concomitant emission from the orange PBI chromophore could be observed (see Figures 5 and 6). Furthermore, fluorescence excitation spectra of compounds **or**, **oro** and **ror** were recorded (λ_{det} = 700 nm; thus exclusive detection in the emission of the red PBI chromophore) within which all UV/vis absorption bands, also including those of the orange chromophoric unit (here being the energy donor), are reproduced. Accordingly, photons absorbed by both the red and the orange perylene bisimide units contribute to the emission from the S_1 state of the red PBI chromophore for all three compounds (for spectra see Figures 5 and 6). Thus, the fluorescence emission of these compounds originates from the lowest energy S_1 state of the red PBI.[i] This implies that independent of the excitation energy, the lowest excited state located on the red perylene acceptor unit is populated, and thus efficient energy transfer from the orange to the red chromophoric units takes place. The comparison of the fluorescence excitation spectra of compounds **or**, **oro** and **ror** with the respective UV/vis absorption spectra reveals an almost perfect overlap, and thus an almost quantitative energy transfer process can be assumed.

The fluorescence quantum yields of the arrays were measured for different excitation wavelengths (for compounds **or**, **oro**, and **ror** at λ_{ex} = 450 and 560 nm; for compound **og** at λ_{ex} = 450 and 615 nm; for all other compounds at λ_{ex} = 450, 560 and 615 nm), and the obtained data are collected in Table 1. Quantum yields of 0.72 and 0.74 for compound **or**, values of 0.19, 0.18 and 0.21 for compound **rg**, and values of 0.16, 0.18 and 0.18 for com-

---

[i] It is to note, that for detection at wavelengths of the exclusive green chromophore emission, wavelengths of above 850 nm are required. However, the used fluorescence spectrophotometer shows insufficient wavelength correction for excitation spectra above 800 nm. Accordingly, for all compounds containing the green chromophore no excitation spectra were recorded.
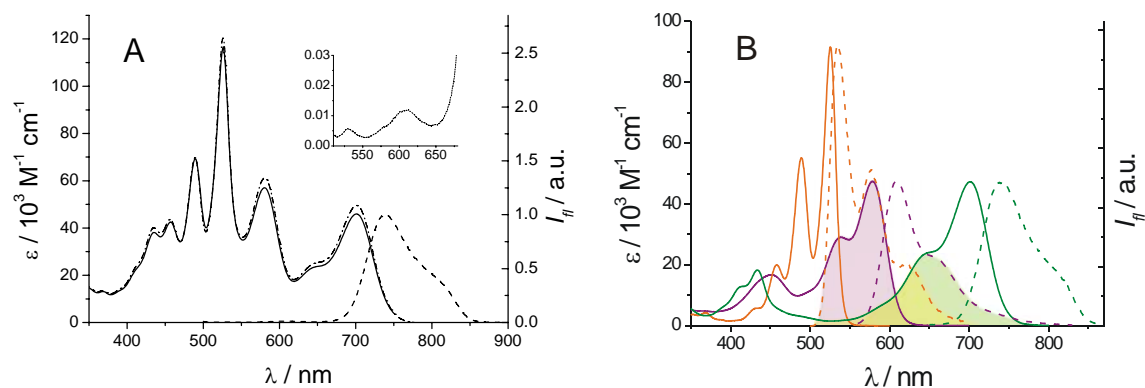
Figure 4. (A): UV/vis absorption (black, solid line), calculated UV/vis absorption (black, dash-dotted line; from $\varepsilon(\mathbf{oc}) + \varepsilon(\mathbf{rc}) + \varepsilon(\mathbf{gc})$) and fluorescence emission spectra (black, dashed line; $\lambda_{ex} = 490$ nm) of compound **org** in CH_2Cl_2. Inset: Magnification of fluorescence emission spectrum in the range of 510 nm to 680 nm. (B): UV/vis absorption (orange, solid line) and fluorescence emission spectra (orange, dashed line) of compound **oc**; UV/vis absorption (violet, solid line) and fluorescence emission spectra (violet, dashed line) of compound **rc**; UV/vis absorption (green, solid line) and fluorescence emission spectra (green, dashed line) of compound **gc**. For comparison, the overlap integrals for the respective dye units are highlighted by shading: violet area for the donor-acceptor pair orange-red, yellow-green area for the donor-acceptor pair red-green and yellow area for the donor-acceptor pair orange-green. All spectra are taken in CH_2Cl_2.

pound **org**, were determined. Thus, within the error range of ± 0.03 the quantum yields of these arrays are independent of the excitation wavelength. All other systems, except compound **og**, show similar behavior owing to reasons discussed below. For all arrays studied, the fluorescence quantum yields are in reasonable agreement with those observed for the respective monochromophoric reference compounds. Accordingly, arrays **or**, **oro**, and **ror** with a fluorescence emission maximum attributed to the red PBI chromophore (with $\lambda_{ex} = 450$ nm) show quantum yields of 0.72, 0.72, and 0.73, respectively. These values are comparable to the quantum yield obtained for the red reference compound **rc** ($\Phi_{fl} = 0.80$). Likewise, the arrays **rg**, **rgr**, **grg**, **org**, and **grorg** with a fluorescence emission maximum attributed to the green PBI chromophore (with $\lambda_{ex} = 560$ nm) exhibit quantum yields of 0.18, 0.21, 0.18, 0.18, and 0.14, respectively, that are comparable to the value obtained for the green reference compound **gc** ($\Phi_{fl} = 0.20$). However, for the array **og** fluorescence quantum yields of $\Phi_{fl} = 0.12$ (for $\lambda_{ex} = 450$ nm) and of 0.25 (for $\lambda_{ex} = 615$ nm) were determined, showing that the quantum yields are in this case, in contrast to the other systems, dependent on the excitation wavelength. The latter value for excitation at

λ_{ex} = 615 nm in the green chromophore is in reasonable agreement with the value obtained for the green reference compound **gc** (Φ_{fl} = 0.20). However, when the array **og** was excited at 450 nm exclusively in the orange PBI chromophore a significantly reduced value of 0.12 was obtained. This indicates that, apart from the energy transfer from the excited orange to the green perylene bisimide chromophore, again concomitant electron transfer from the attached calix[4]arene unit to the orange PBI moiety takes place, which reduces the emission intensity of the green PBI upon excitation at 450 nm (see Chapter 3).

Table 1. Optical Properties of PBI-calix[4]arene arrays in CH_2Cl_2.[a]

| Cmpd | UV/vis Absorption | | | | | | Fluorescence Emission | | | |
| | orange PBI | | red PBI | | green PBI | | | | | |
	λ_{max} (nm)	ε ($M^{-1}cm^{-1}$)	λ_{max} (nm)	ε ($M^{-1}cm^{-1}$)	λ_{max} (nm)	ε ($M^{-1}cm^{-1}$)	λ_{max} (nm)	Φ_{fl}[b]	Φ_{fl}[c]	Φ_{fl}[d]
oc[e]	526	91600					535	0.03		
rc[e]			578	47400			608		0.80[f]	
gc[e]					701	47300	742	0.20		
or	526	107900	579	46200			608[g]	0.72	0.74	
oro	526	194900	580	50300			611[g]	0.72	0.70	
ror	527	135000	578	91600			608[g]	0.73	0.71	
rg			580	50800	701	44600	738[h]	0.19	0.18	0.21
rgr			579	93700	703	43700	739[h]	0.19	0.21	0.22
grg			580	61300	701	84800	738[h]	0.19	0.18	0.17
og	525	89600			700	45200	741[g]	0.12		0.25
org	527	116800	580	57100	701	46000	737[g]	0.16	0.18	0.18
grorg	527	127900	581	97600	701	77100	739[g]	0.17	0.14	0.15

[a] All spectra were recorded at room temperature. [b] λ_{ex} = 450 nm. [c] λ_{ex} = 560 nm. [d] λ_{ex} = 615 nm. [e] See Chapter 3, values are given for comparison. [f] λ_{ex} = 550 nm. [g] λ_{ex} = 490 nm. [h] λ_{ex} = 560 nm.

The above-mentioned results unequivocally confirm efficient energy transfer between the *orange* (here: energy donor) and *red* (here: energy acceptor) chromophoric units in the arrays **or**, **oro**, **ror** and **org**, **grorg**, as well as between the *red* (here: energy donor) and *green* (here: energy acceptor) chromophoric units in the case of arrays **rg**, **rgr**, **grg** and **org**, **grorg**, and also, but to a lesser extend, for compound **og** between the *orange* (here: energy donor) and the *green* (here: energy acceptor) chromophoric unit. The significant emission of all compounds containing the *orange* PBI dye upon excitation at λ_{ex} = 490 nm (excitation almost exclusively in the orange chromophore) is particularly impressive because the respective reference compound **oc** is almost non-fluorescent. According to the

findings discussed in Chapter 3, the fluorescence quenching mechanism is attributed to a photoinduced electron transfer (PET) from the electron-rich calix[4]arene substituents to the electron-poor orange PBI unit with a rate constant of about 3×10^{10} s^{-1} in CH_2Cl_2 for compound **oc**. Thus, the energy transfer process from the orange PBI unit to the adjacent red chromophoric unit in compound **org**, and in all other arrays containing orange and red chromophoric units, has to be significantly faster than the fluorescence quenching by PET processes from the neighboring calix[4]arene unit.

Figure 5. (A) UV/vis absorption (black, solid line), calculated UV/vis absorption (black, dash-dotted line; from ε(**oc**) + ε(**gc**)) and fluorescence emission spectra (black, dashed line; λ$_{ex}$ = 490 nm) of compound **og** in CH_2Cl_2. (B) UV/vis absorption (black, solid line), calculated UV/vis absorption (black, dash-dotted line; from ε(**oc**) + ε(**rc**)), fluorescence emission (black, dashed line; λ$_{ex}$ = 490 nm) and fluorescence excitation spectra (red, solid line; λ$_{det}$ = 700 nm) of compound **or** in CH_2Cl_2.

Figure 6. (A) UV/vis absorption (black, solid line), calculated UV/vis absorption (black, dash-dotted line; from $\varepsilon(\mathbf{oc}) + 2x\ \varepsilon(\mathbf{rc})$), fluorescence emission (black, dashed line; $\lambda_{ex} = 490$ nm) and fluorescence excitation spectra (red, solid line; $\lambda_{det} = 700$ nm) of compound **ror** in CH$_2$Cl$_2$. (B) UV/vis absorption (black, solid line), calculated UV/vis absorption (black, dash-dotted line; from $\varepsilon(\mathbf{rc}) + 2x\ \varepsilon(\mathbf{oc})$), fluorescence emission (black, dashed line; $\lambda_{ex} = 490$ nm) and fluorescence excitation spectra (red, solid line; $\lambda_{det} = 700$ nm) of compound **oro** in CH$_2$Cl$_2$.
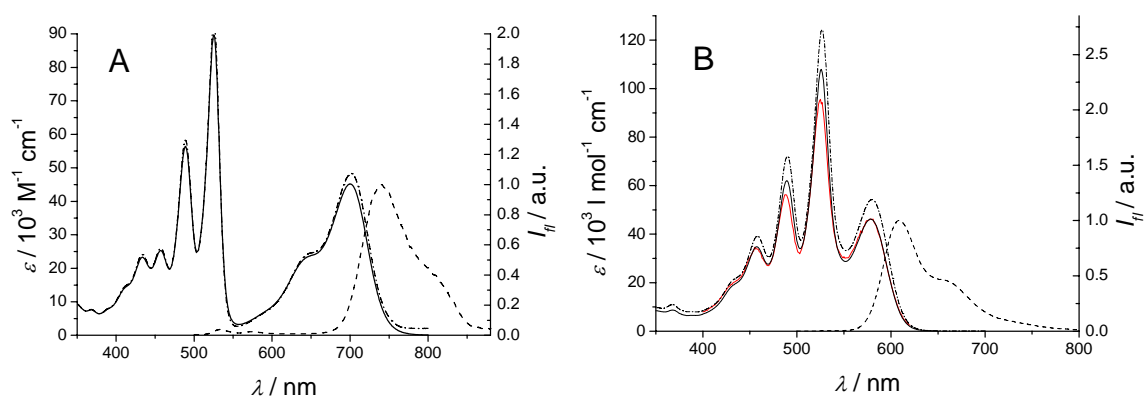

Figure 7. (A) UV/vis absorption (black, solid line), calculated UV/vis absorption (black, dash-dotted line; from $\varepsilon(\mathbf{rc}) + 2x\ \varepsilon(\mathbf{gc})$) and fluorescence emission spectra (black, dashed line; $\lambda_{ex} = 560$ nm) of compound **grg** in CH$_2$Cl$_2$. Inset: Magnification of fluorescence emission spectrum in the range of 560 nm to 670 nm. (B) UV/vis absorption (black, solid line), calculated UV/vis absorption (black, dash-dotted line; from $\varepsilon(\mathbf{gc}) + 2x\ \varepsilon(\mathbf{rc})$) and fluorescence emission spectra (black, dashed line; $\lambda_{ex} = 560$ nm) of compound **rgr** in CH$_2$Cl$_2$. Inset: Magnification of fluorescence emission spectrum in the range of 550 nm to 680 nm.
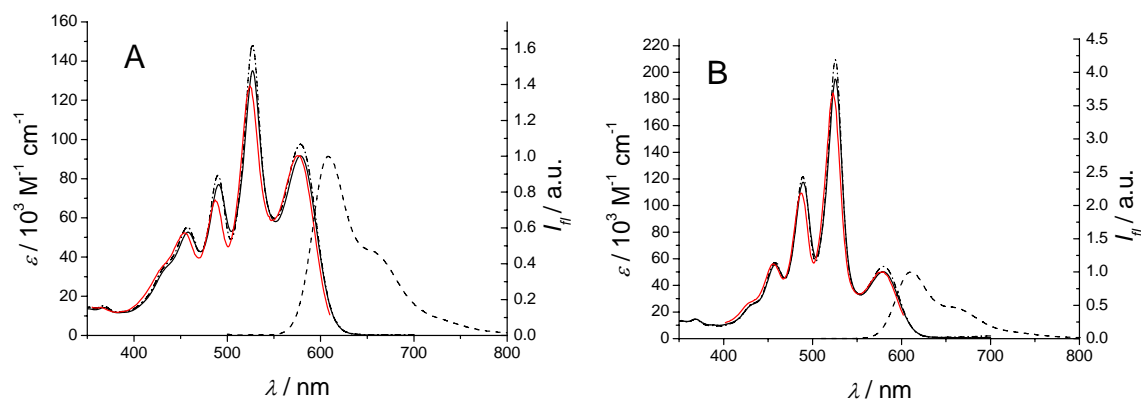
114

Figure 8. (A) UV/vis absorption (black, solid line), calculated UV/vis absorption (black, dash-dotted line, from $\varepsilon(\mathbf{rc}) + \varepsilon(\mathbf{gc})$) and fluorescence emission spectra (black, dashed line; $\lambda_{ex} = 490$ nm) of compound **rg** in CH$_2$Cl$_2$. Inset: Magnification of fluore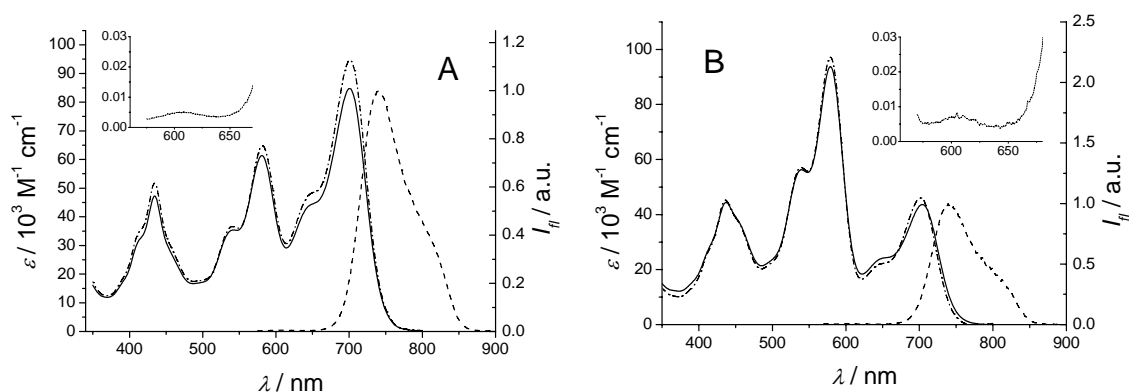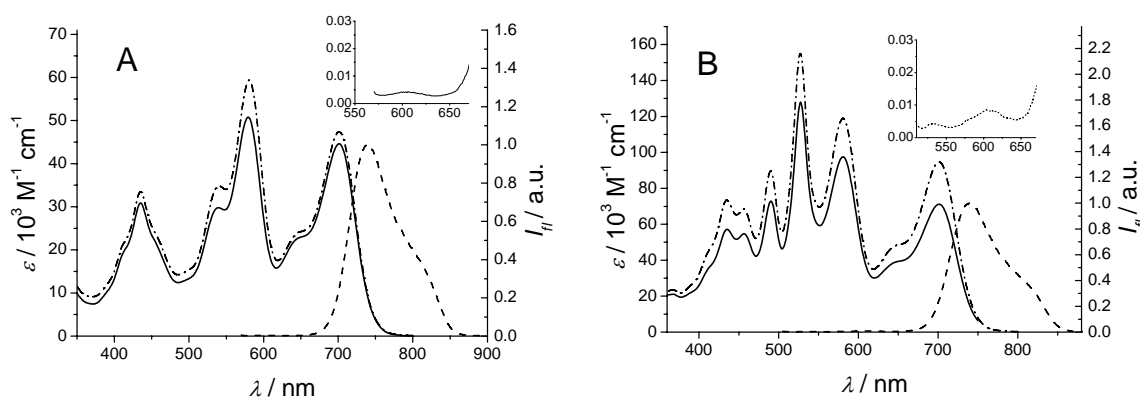scence emission spectrum in the range of 550 nm to 680 nm. (B) UV/vis absorption (black, solid line), calculated UV/vis absorption (black, dash-dotted line; from $\varepsilon(\mathbf{oc}) + 2x$ $\varepsilon(\mathbf{rc}) + 2x \varepsilon(\mathbf{gc})$) and fluorescence emission spectra (black, dashed line; $\lambda_{ex} = 560$ nm) of compound **grorg** in CH$_2$Cl$_2$. Inset: Magnification of fluorescence emission spectrum in the range of 560 nm to 670 nm.

4.6   Femtosecond Transient Absorption Spectroscopy

As mentioned in the previous section, the steady state spectroscopy data reveal efficient energy transfer processes between the variate PBI chromophoric units within the present calix[4]arene–PBI arrays. More detailed information about the excited state properties of these systems has been acquired by using femtosecond transient absorption spectroscopy. The transient absorption spectra of compounds **or**, **rg**, **og**, **org**, and **grorg**, are depicted in Figure 9 and those of compounds **oro, ror, rgr**, and **grg**, respectively, are shown in Figure 10.

Upon photoexcitation of compound **or** the instantaneous development of strong negative signals at 490, 530 and 580 nm is observed together with a broad positive absorption band centered at 715 nm. The latter features are typical for excited state transitions of the *orange* perylene bisimide chromophore, whilst the bands at 490 nm and 530 nm indicate ground state bleaching and stimulated emission (at 580 nm).[32] The amplitudes of the negative signals decrease and shift toward a negative signal at 590 nm which was assigned to the ground state bleaching of the *red* PBI chromophore.[7d] Within the time frame of the

experiment, the negative band at 590 nm slightly shifts the position of its maximum to 610 nm which might be attributed to conformational changes of the red perylene bisimide dye.[ii] Furthermore, the sharp positive band at 715 nm (excited state absorption of the orange PBI) decreases with a similar rate and converts to a broader feature of low intensity that is attributed to the absorption of the excited state of the red perylene bisimide. No recovery of the ground state was observed within the instrument's time frame of 1 ns, which is plausible because the excited-state lifetime of the red PBI chromophore is in the nanosecond time regime. These findings indicate the depopulation of the singlet excited state of the orange perylene bisimide unit and, therefore, provide evidence for the energy transfer from the *orange* (here: energy donor) to the *red* (here: energy acceptor) PBI unit as already observed by steady state emission spectroscopy. Similar band shapes and positions as well as an identical spectral evolution are also present in the femtosecond transient absorption spectra obtained for compounds **oro** and **ror** (see Figure 10).

The photoexcitation of compound **rg** (see Figure 9) leads to the immediate formation of transient absorption signals at 435 and 588 nm (negative) as well as at 715 nm (positive). These spectral features are inherent to the singlet excited state absorption of the *red* perylene bisimide unit[7d] which decays very rapidly to form a long-lived bleach band centered at 730 nm, together with a small negative absorption pattern at 435 nm. A weak broad positive absorption between 450 and 600 nm is also present. These spectral patterns are typical for the optically excited *green* perylene bisimide chromophore.[34] Such bands clearly confirm the fast energy transfer from the *red* (here: energy donor) to the *green* perylene bisimide (here: energy acceptor) chromophoric units. Similar band shape and position as well as an identical spectral evolution are also present in the femtosecond transient absorption spectra obtained for compounds **rgr** and **grg** (see Figure 10). For all three compounds no conformational effect of the red PBI is observed, probably due to its very fast decay (see above).

[ii] Similar behavior is also known from single molecule spectroscopy for the red perylene bisimides bearing phenoxy substituents at the bay positions that were immobilized in a polymer matrix. It is known that local reorganizations in the vicinity of the molecule have an impact on the orientation of the phenoxy substituents for these red PBIs. For details, see ref. 33a. For a recent study dealing with processes in solution, see ref. 33b.

Intense negative signals are present in the femtosecond transient absorption spectra of compound **og** (Figure 9) at 490, 530 and 580 nm which can be assigned to the combined signals of ground state bleaching and stimulated emission of the *orange* PBI chromophore.[32] These features are accompanied by a strong positive absorption band with a maximum centered at 715 nm that is indicative for the singlet excited state absorption of the *orange* PBI chromophore. These spectral patterns decay very rapidly but concomitantly give rise to a long-lived negative signal at around 730 nm together with a negative feature at 435 nm of very weak intensity. The latter can be attributed to the formation of the excited singlet state of the *green* PBI unit,[34] and thus provide convincing evidence for the energy transfer between the *orange* (here: energy donor) and the *green* (here energy acceptor) chromophoric units. However, the amplitude for the bleaching of the green PBI chromophore at 730 nm remains rather small (compared with that of compound **rg**) due to the formation of radical anions of the orange PBI unit (that absorbs at about 700 nm) by the competing PET process from the electron-rich calix[4]arene to the electron-poor orange PBI (see Chapter 3).

Figure 9. Femtosecond transient absorption spectra and corresponding time delays in CH_2Cl_2 after photoexcitation at 530 nm. Top: compound **or** (left), and compound **rg** (right); Middle: compound **og** (left), and compound **org** (right); Bottom: compound **grorg** (middle). The scattered laser pulse is observed for compounds **rg** and **grorg**.

The femtosecond transient absorption data of compound **org**, containing an *orange*, a *red* and a *green* chromophoric unit, are also shown in Figure 9. Upon photoexcitation, the immediate formation of strong negative signals at 460, 490, 531, and 585 nm are observed (that are assigned to the combined ground state bleaching and stimulated emission signals from the red and the orange chromophore),[7d,32] together with a strong positive band centered at 715 nm due to the overlapping excited singlet state absorptions of the orange and red perylene units at that wavelength. These spectral characteristics change very rapidly during further temporal evolution of the spectra to finally result in the concomitant

rise of the broad negative band centered at 730 nm (together with a small bleach signal at 435 nm) attributed to the spectral features of the *green* chromophore.[34] No recovery of the ground state was observed within the instrument's time frame as the excited-state lifetime of the green PBI chromophore is in the nanosecond time regime. These results clearly reveal the depopulation of the singlet excited state of the *orange* as well as the *red* perylene bisimide unit and provide unambiguous evidence for the very efficient energy transfer process to the *green* chromophore expressed by the population of the singlet excited state of the green PBI unit. Similar band shapes and positions as well as an identical spectral evolution are also observed in the femtosecond transient absorption spectra of the array **grorg**, as the respective spectra in Figure 9 show.

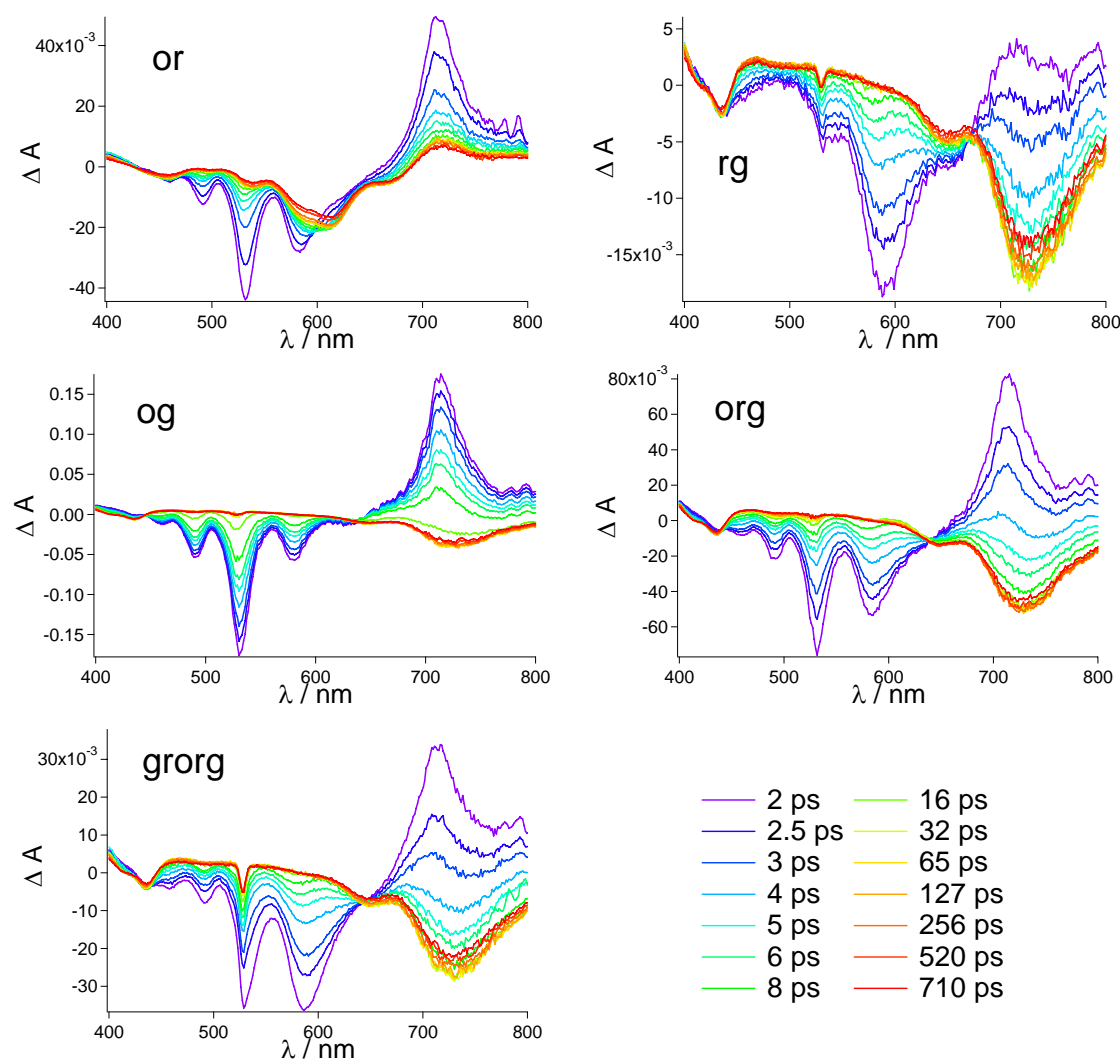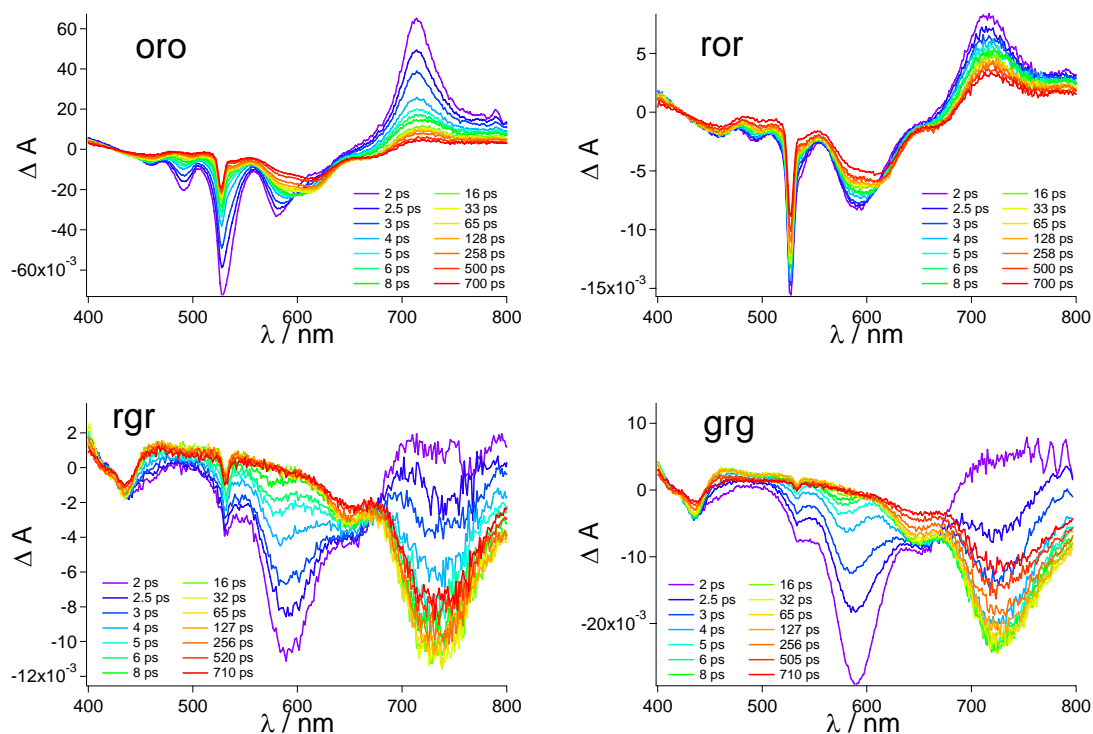**Figure 10.** Femtosecond transient absorption spectra and corresponding time delays in CH_2Cl_2 after photoexcitation at 530 nm. **Top:** compound **oro** (left) and compound **ror** (right). **Bottom**: compound **rgr** (left) and compound **grg** (right). The scattered laser pulse is observed for all four compounds, respectively.

The energy transfer processes are further analyzed in Figures 11 and 12. As can clearly be noted from the kinetic profiles shown for compound **or** (Figure 11, left), the *rise time* of 1.3 ps (trace at 715 nm, red line) observed for the *red* perylene bisimide emission (here: the acceptor dye) is almost identical to the *decay time* of 1.2 ps (trace at 580 nm, black line) of

the *quenched orange* perylene bisimide emission (here: the donor dye). For compound **rg** (Figure 11, middle), the *rise time* of 2.1 ps (trace at 726 nm, red line) was observed for the *green* perylene bisimide emission (here: the acceptor dye) which exactly reflects the *decay time* of 2.0 ps (trace at 590 nm, black line) of the *quenched red* perylene bisimide emission (here: the donor dye). Likewise, compound **og** (Figure 11, right) shows a *rise time* of 3.3 ps (trace at 715 nm, red line) observed for the *green* perylene bisimide emission (here: the acceptor dye) and a complementary *decay time* of 3.9 ps (trace at 580 nm, black line) for the *quenched orange* perylene bisimide emission (here: the donor dye). All these lifetime values were obtained with single line fitting. Also for the arrays **oro**, **ror**, **rgr**, and **grg** (for kinetic profiles see Figure 12) similar complementary decay and rise profiles were found. The evaluation of the single line kinetics, especially for the arrays **org** and **grorg**, turned out to be more complex, as a variety of different processes takes place after photoexcitation. Therefore, the kinetic profiles of all arrays were further investigated in detail by means of global and target analysis which is discussed in the following section.
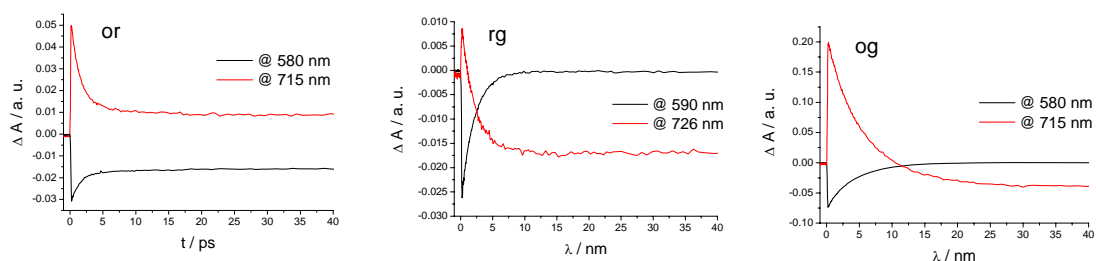

Figure 11. Kinetic profiles of the transient absorption in CH$_2$Cl$_2$. Left: compound **or**, measured at 580 nm (black line) and 715 nm (red line); Middle: compound **rg**, measured at 590 nm (black line) and 726 nm (red line); Right: compound **og**, measured at 580 nm (black line) and 715 nm (red line).
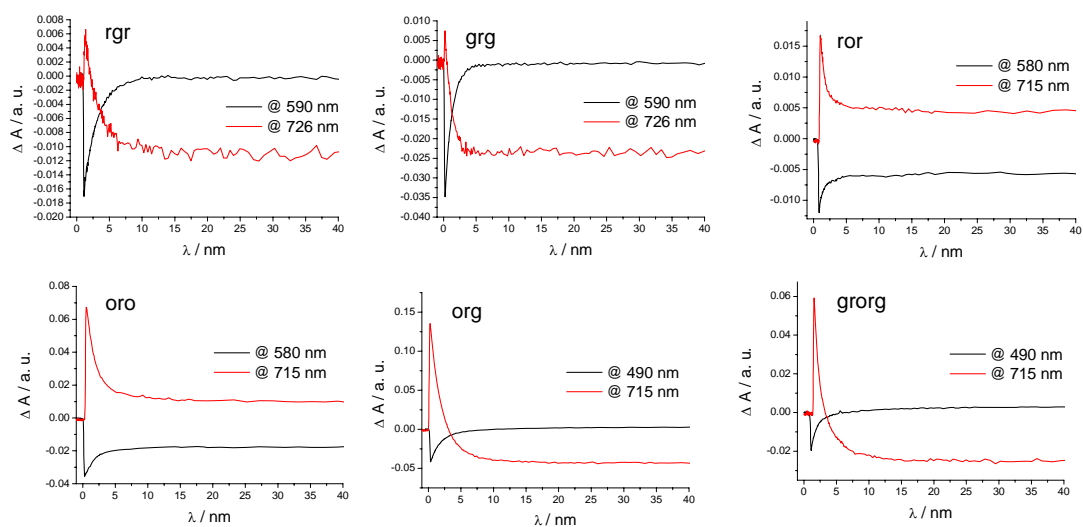
Figure 12. Kinetic profiles of the transient absorption in CH_2Cl_2. **Top** (left): compound **rgr**, measured at 590 nm (black line) and 726 nm (red line). **Top** (middle): compound **grg**, measured at 590 nm (black line) and 726 nm (red line). **Top** (right): compound **ror**, measured at 580 nm (black line) and 715 nm (red line). **Bottom** (left): compound **oro**, measured at 580 nm (black line) and 715 nm (red line). **Bottom** (middle): compound **org**, measured at 490 nm (black line) and 715 nm (red line). **Bottom** (right): compound **grorg**, measured at 490 nm (black line) and 715 nm (red line).

4.7   Global and Target Analysis.[iii]

The femtosecond transient absorption data-matrices were analyzed with spectrotemporal parameterization, an advanced global and target analysis method that has been developed in particular to elucidate photoinduced processes in complex biological systems such as photosystems.[35] Because the time information at all wavelengths is analyzed, this analysis gives a more in-depth view of the occurring photoinduced processes. As a final result, the so-called Species Associated Difference Spectra (SADS) are obtained, which are revealing the lifetimes and also the true spectra of the individual excited state species. For further details of the method refer to Chapters 2 and 3. It has to be noted that the analysis of the single line kinetics is in very good agreement with the time constants obtained from the

---

[iii] The femtosecond transient absorption data analysis by spectrotemporal parametrization was accomplished by Dr. I. H. M. van Stokkum at the Vrije Universiteit van Amsterdam, The Netherlands.

global analysis. However, the latter are considered to be more accurate due to the fact that for the global analysis all wavelengths and thus all data are taken into account.

As general examples the SADS of compounds **og** and **org** resulting from the global fit of the data are presented in Figure 13A and 13B, respectively. For this purpose, a specific model of the excited state processes was applied for the fitting procedure according to the energy level diagrams depicted in Figure 14A for compound **og** and in Figure 14B for compound **org**, respectively. Accordingly, a competitive charge transfer (CT) state formed by electron transfer from the calix[4]arene moiety to the orange PBI unit was integrated into the model (see Chapter 3). The lifetime values obtained from the data analysis of the processes after photoexcitation are summarized in Table 2 (for the related rate constants see Table 5 in the Appendix of this Chapter). For compound **og** the initial spectrum in Figure 13A (red line) shows the transient absorption features of the orange PBI chromophore[32] and was accordingly assigned to the excited singlet state of the orange PBI.[iv] This SADS changes within 4.1 ps into *two* following states (represented by black and green line in Figure 13A) as a second deactivation route via the charge transfer state was included into the model (see Chapter 3). Accordingly, the lifetime value of 4.1 ps reveals the "total" lifetime τ_{total} of the excited singlet state of the orange PBI o* (with the respective rate constant k_{total}), which in this case depopulates via two competitive pathways.[v] The major deactivation pathway (62%) which relates to the energy transfer to the green chromophore is represented by the final green SADS in Figure 13A; this state is populated within 6.7 ps. The related rate constant k_{ET} for the energy transfer between the *orange* and the *green* donor-acceptor pair can be afforded from the respective reciprocal value, giving a rate constant of $k_{ET} = 1.5 \times 10^{11}$ s^{-1}. The obtained green SADS decays with a lifetime of 3.8 ns and its spectral features can be clearly assigned to the excited state of the green chromophore, referred to as g*. Thus, an efficient energy transfer from the

---

[iv] Note that in the SADS depicted in Figure 13 processes of 0.2 ps that have been assigned to fast solvent reorganization processes were omitted from the spectra for clarity. For details see also Table 1 and ref. 36.

[v] Note, that $k_{total} = k_{ET} + k_{CT}$ and $k = 1/\tau$. Accordingly, $1/\tau_{total} = 1/\tau_{ET} + 1/\tau_{CT}$ with, for example, for compound **og** $\tau_{total} = 4.1$ ps, $\tau_{ET} = 6.7$ ps and $\tau_{CT} = 10.8$ ps, respectively (see Table 2 and Table 5 in the Appendix of this Chapter). For calculation details please refer also to equations (1) and (2) of this Chapter.

orange to the *green* chromophore is evident. However, it has to be noted that the longest lifetime values are prone to large errors due to the time frame of the instrument of 1 ns and therefore differ from the values obtained from time-resolved emission experiments (for values see Chapter 3). They however reveal the correct order of magnitude of the lifetimes of the reference chromophores and represent their lower limits. The second competitive deactivation pathway (38%) of the excited state of the orange PBI o* (black line in Figure 13A) relates to the formation of the CT state of the calix[4]arene-orange PBI subunit and is represented by the black SADS; this state is populated within 10.8 ps. The related rate constant k_{CT} can be obtained from the reciprocal value of τ_{CT} and is found to be $k_{CT} = 0.92 \times 10^{11}$ s^{-1}. The black curve decays with a lifetime of 8.6 ps and exactly reveals the spectral features of a charge transfer state as the stimulated emission at 580 nm is not observed any longer and the band at around 700 nm is significantly broadened. From this clear spectral evidence the formation of a charge-separated state involving the formation of the orange PBI monoanion can be concluded. A similar competitive pathway via formation of a CT state of the calix[4]arene-PBI subunit was already observed for the orange reference compound **oc** (see Chapter 3).
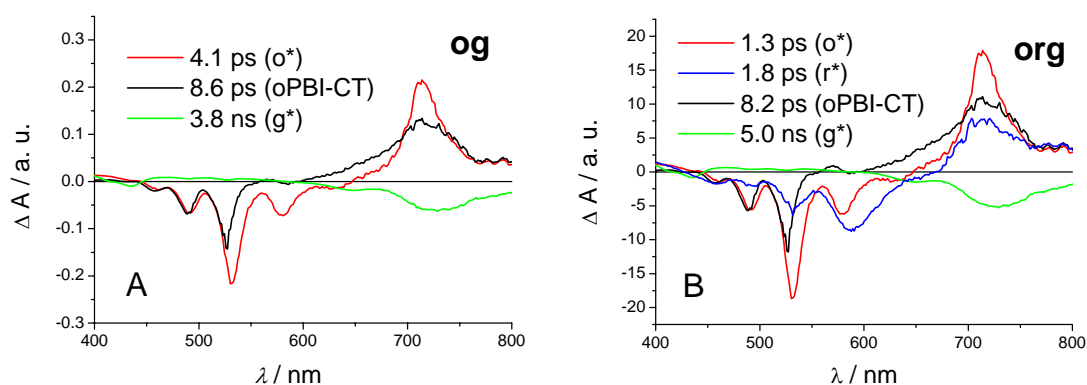
Figure 13. Species-associated difference spectra (SADS) resulting from the simultaneous target analysis of the femtosecond transient absorption data of compounds **og** and **org** employing the kinetic schemes depicted in Figure 14A and 14B, respectively. Shown are processes after photoexcitation at 530 nm. (**A**): Compound **og**, with the species: o* (red line), oPBI-CT (black line), g* (green line). (**B**): Compound **org**, with the species: o* (red line), r* (blue line), oPBI-CT (black line), g* (green line). Features due to Raman scattering and fast solvent reorganization processes were omitted for clarity (see also ref. 36).

The array **org** has also been analyzed in a similar manner, the obtained SADS are shown in Figure 13B, and the respective lifetime values are summarized in Table 2 (for the related rate constants see Table 5 in the Appendix of this Chapter). Accordingly, the first SADS in Figure 13B (red line) was assigned to the excited state of the orange PBI,[32] and this spectrum is decaying with 1.3 ps via *two* deactivation pathways[v] which are due to, first, the energy transfer process from the orange to the red PBI unit (for the formation of the excited state of the red PBI see blue spectrum in Figure 13B) with 89% amplitude, and second, the formation of a CT state of the calix[4]arene-orange PBI subunit with 11% amplitude (see black line in Figure 13B). The latter charge-transfer state recombines with 8.2 ps, whereas the excited state of the red PBI (blue line in Figure 13B) decays further with 1.8 ps to form the final green SADS showing a lifetime of 5.0 ns which was assigned to decay of the excited state of the green PBI unit. The latter value is in reasonable agreement with the lifetime of simple green PBIs reported in literature.[9] These findings provide unambiguous evidence for sequential energy transfer from the orange to the red and from the red to the green PBI moiety in array **org**. Direct excitation energy deactivation from the orange to the green chromophore was not observed, which is most likely owing to the less favorable spectral overlap of these two dye units.

Accordingly, the observed directional sequential energy transfer in array **org** from the orange to the red and from the red to the green PBI unit shows a remarkably high overall efficiency of about 89%. This is especially striking as an additional very fast competitive PET process between the linking calix[4]arene units and the orange perylene bisimide chromophore occurs. However, the energy transfer process turns out to be much more efficient and accordingly, these zigzag-type dye arrays can even harvest the photons absorbed by the orange perylene bisimide dye unit, despite the almost non-fluorescent nature of the energy donor subunit, *i.e.* the parent calix[4]arene–perylene bisimide conjugate **oc** (see Chapter 3). Hence, the present array **org** reveals a much higher overall energy transfer efficiency than observed for many other perylene bisimide based light-harvesting systems known from the literature, where major losses (of 50% and more) of the excitation energy due to undesired competitive PET processes were observed.[7a-c]

Figure 14. Energy level diagrams (A, B) showing energy and electron transfer pathways in CH_2Cl_2 obtained with global and target analysis, together with the main decay times corresponding to the respective states. (A): For compound **og**. (B): For compound **org**. (C): Schematic representation for the processes occurring in array **org** upon photoexcitation of the orange PBI chromophore. Note that lifetimes in the ns time range are less reliable due to the 1ns time frame of the experiment and thus represent lower limits.

Similarly, as discussed for compounds **og** and **org** (see above), all other PBI-calix[4]arene arrays have been analyzed, and the obtained lifetimes are summarized in Table 2 (for the related rate constants see Table 5 in the Appendix of this Chapter). Additional energy level diagrams for compounds **or** and **rg** are shown in Figure 15A and 15B, respectively. For all other PBI-calix[4]arene arrays, very similar lifetimes to those already discussed above are found: a component due to energy transfer from the *orange* to the *red* PBI unit with values ranging from $\tau = 0.6$ ps (for compound **grorg**) to $\tau = 1.6$ ps (for compounds **oro** and **or**), as well as a component due to energy transfer from *red* to *green* with values ranging from $\tau = 1.2$ ps (for compound **grg**) to $\tau = 2.9$ ps (for compound **grorg**). The formation of the CT state of the calix[4]arene-orange PBI subunit is also observed as a competitive side process with values ranging from $\tau = 3.0$ ps (for compound **ror**) to $\tau = 12.0$ ps (for compound **og**).

The latter CT state shows lifetimes with values ranging from τ = 5.7 ps (for compound **ror**) to τ = 9.0 ps (for compound **grorg**). Furthermore, the lifetimes (representing lower limit values due to the timeframe of the experiment) of the final long-living excited acceptor states of the respective PBI unit are also given in Table 2. Notably, for systems containing two acceptor components like in arrays **ror** and **grg**, the decay time of the excited orange (in **ror**) or red (in **grg**) energy donor unit is further reduced by half and the respective rate constant doubles, whereas for arrays containing just one acceptor but two donor units like in compounds **rgr** and **oro** no such effects are observed (see Table 2). Interestingly, a similar behavior is also found for the formation of the CT state of the calix[4]arene-orange PBI subunit. For example, for compound **ror** the lifetime of the CT state formation is about half that observed for compounds **or** and **oro** (see Table 2) which is due to the biscalix[4]arene-substitution of the orange donor unit in compound **ror** (see also for comparison the values obtained for compounds **oc** and **oc2** in Chapter 3).

Table 2. Lifetimes in CH_2Cl_2 obtained from the global and target analysis of the experimental data employing the kinetic models depicted in Figures 14 and 15, respectively.

Cmpd	lifetimes τ (ps)[a]							
	$(o,r)_{solv}$*[b]	ET $o^* \rightarrow r^*$	ET $r^* \rightarrow g^*$	ET $o^* \rightarrow g^*$	CT to $(oPBI)^{\bullet-}$	$(oPBI)^{\bullet-}$	$r^* \rightarrow r$	$g^* \rightarrow g$
or	0.25	1.6			8.2	6.6	5000[c]	
oro	0.25	1.6			7.5	6.6	3400[c]	
ror	0.3	0.8			3.0	5.7	3300[c]	
rg	0.3		2.5					3300
rgr	0.3		2.6					1800
grg	0.2		1.2					900
org	0.2	1.4	1.8		12.0	8.2		5000
grorg	0.2	0.6	2.9		4.5	9.0		2800
og	0.2			6.7	10.8	8.6		3800
oc[d]					32.0	10.0		
oref					0.0	0.0		

[a] Relative precision of the lifetimes is 10%, except for lifetimes in the ns time range which are less reliable due to the 1ns time frame of the experiment and thus represent lower limits. For the related rate constants see Table 5 in the Appendix of this Chapter. [b] See ref. 36. [c] Note, that for the relaxation of r* also minor components of several hundred picoseconds have been observed which can be attributed to conformational changes of the red perylene bisimide dye (see ref. 33). [d] See Chapter 3.

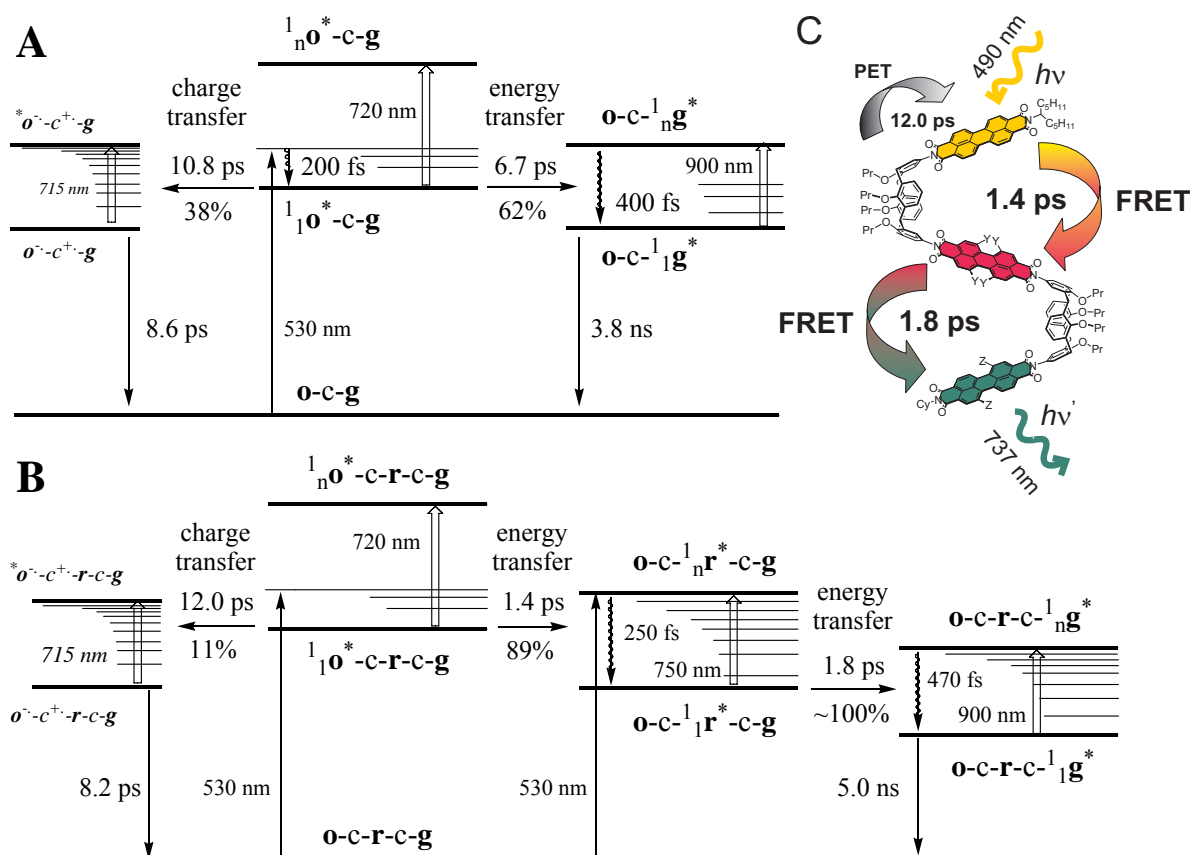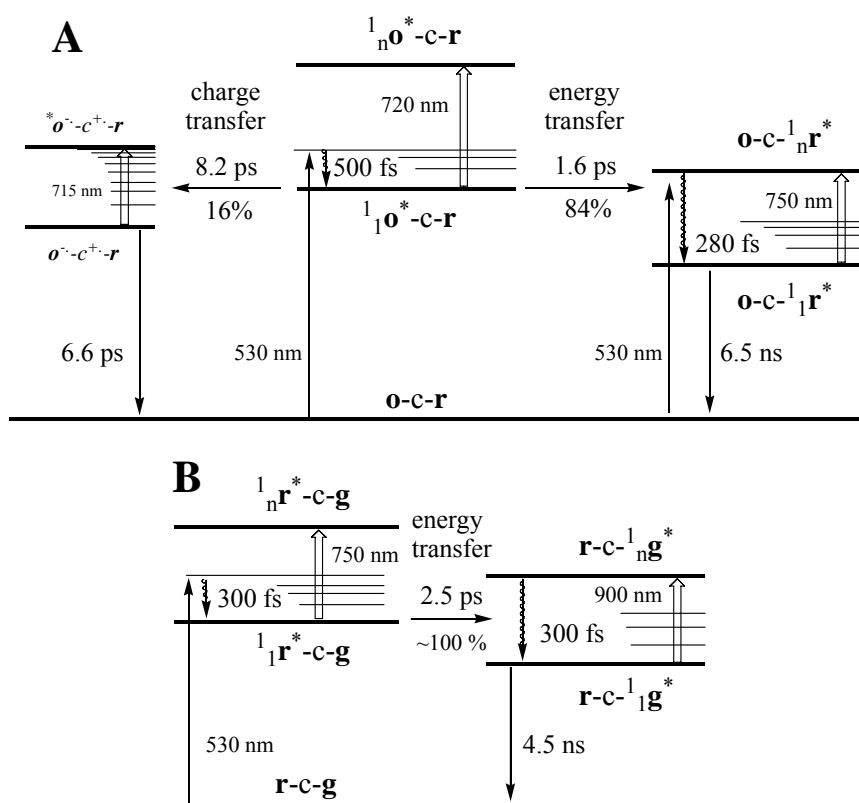**Figure 15.** Energy level diagrams showing energy and electron transfer pathways in CH_2Cl_2 obtained with global and target analysis, together with the main decay times corresponding to the respective states. (A) for compound **or**. (B) for compound **rg**. Note that lifetimes in the ns time range are less reliable due to the 1ns time frame of the experiment and thus represent lower limits.

According to the femtosecond transient absorption results (summarized in Table 2 and in Table 5 in the Appendix of this Chapter), an energy transfer rate of $k_{ET} = 6.4 \times 10^{11}$ s^{-1} for the energy transfer from the *orange* to the *red* PBI unit (for compound **or**), of $k_{ET} = 4.0 \times 10^{11}$ s^{-1} for the energy transfer from the *red* to the *green* PBI moiety (for compound **rg**), and of $k_{ET} = 1.5 \times 10^{11}$ s^{-1} for the energy transfer from the *orange* to the *green* PBI chromophore (for compound **og**) was found. From the obtained rate constants the efficiency of the energy transfer process E_{ET} as well as the efficiency of the competitive charge transfer process E_{CT} can be calculated according to the following equations:

$$E_{ET} = \frac{k_{ET}}{k_{ET} + k_{CT} + k_{fl}} = \frac{\dfrac{1}{\tau_{ET}}}{\dfrac{1}{\tau_{ET}} + \dfrac{1}{\tau_{CT}} + \dfrac{1}{\tau_D}} \qquad (1)$$

$$E_{CT} = \frac{k_{CT}}{k_{ET} + k_{CT} + k_{fl}} = \frac{\dfrac{1}{\tau_{CT}}}{\dfrac{1}{\tau_{ET}} + \dfrac{1}{\tau_{CT}} + \dfrac{1}{\tau_{D}}} \qquad\qquad (2)$$

with k_{ET} being the energy transfer rate (between neighboring PBI units) and k_{CT} the charge transfer rate (from the calix[4]arene moiety to the adjacent PBI chromophore). By employing equations (1) and (2) a value of $E_{ET} = 0.84$ is obtained for the efficiency of the energy transfer process from the orange to the red PBI unit in compound **or**. Likewise, the arrays **oro** ($E_{ET} = 0.82$), **ror** ($E_{ET} = 0.79$), **org** ($E_{ET} = 0.89$), and **grorg** ($E_{ET} = 0.88$) reveal very similar energy transfer efficiencies. Notably, the energy transfer efficiencies for these arrays are a little bit lower than expected from the very fast rate constants in the range of $k_{ET} = 15.8 \times 10^{11}$ s^{-1} (for compound **grorg**) to $k_{ET} = 6.3 \times 10^{11}$ s^{-1} (for compound **oro**). However, due to the competitive charge transfer state formation which is also a pretty fast process (the respective rate constants range from $k_{CT} = 0.92 \times 10^{11}$ s^{-1} for compound **og** to $k_{CT} = 3.3 \times 10^{11}$ s^{-1} for compound **ror**), slightly reduced energy transfer efficiency values are observed. Notably, no formation of a competitive charge transfer state consisting of the *red* PBI monoanion and the cation of the calix[4]arene unit has been observed for the deactivation of the red excited state in arrays **rg**, **rgr**, and **grg**. This is further elaborated by the fact that an estimation of the Gibbs free energy of the photoinduced electron transfer of the PET process from the calix[4]arene substituent to the *red* perylene bisimide moiety in CH$_2$Cl$_2$ reveals this process to be endergonic ($\Delta G_{CS} = +0.063$ eV, for details see also the discussion in Chapter 3). Therefore, it can be concluded that the formation of a charge separated state consisting of the radical cation of the calix[4]arene moiety and the respective radical anion of the *red* perylene unit is energetically *not* favorable (see Chapter 3). In accordance with this thermodynamic analysis, the efficiency of the energy transfer process from the *red* to the *green* PBI unit results in values of E_{ET} of about unity for all the three arrays **rg**, **rgr** and **grg**, respectively.

Finally, the smallest value of $E_{ET} = 0.62$ is obtained for the efficiency of the energy transfer process from the *orange* to the *green* PBI unit in compound **og**. Thus, compared to the orange-red donor acceptor couple ($E_{ET} = 0.84$) with compound **og** the critical limit for efficient energy transfer processes in PBI arrays is elucidated. On the one hand, the charge transfer process from the electron-rich calix[4]arene unit to the electron deficient orange

PBI chromophore is very efficient. On the other hand, for the orange-green donor-acceptor pair the smallest extent of spectral overlap is given (see Figure 4B). As a consequence, the energy transfer between the two chromophoric units is less efficient and the competing charge transfer process becomes more pronounced. All calculated energy transfer and charge transfer efficiency values are summarized in Table 3.

Assuming a fluorescence resonance energy transfer (FRET), the experimentally obtained energy-transfer rates can be compared to the calculated rate constants employing the Förster theory. Accordingly, the transfer rate depends on following factors: the extent of spectral overlap of the emission spectrum of the donor with the absorption spectrum of the acceptor (see Figure 4B), the quantum yield of the donor, the relative orientation of the donor and acceptor transition dipoles, and the distance between the donor and acceptor molecules.[37] The Förster distance R_0 (the distance at which the energy transfer efficiency is 50%) can thus be calculated according to the simplified equation

$$R_0 = 0.211 \left[\kappa^2 n^{-4} \Phi_D J(\lambda) \right]^{1/6} \qquad (3)$$

with κ^2 being the orientation factor, n the refractive index of the medium, Φ_D the fluorescence quantum yield of the donor in the absence of acceptor, and $J(\lambda)$ the overlap integral of the donor emission and the acceptor absorption spectra. By employing this equation, R_0 is calculated for compound **or** as 70.8 Å, with $\kappa^2 = 2.32$ (using the angles of the dipole moments from the respective structure obtained from molecular modeling shown in Figure 2), n (CH_2Cl_2) = 1.4240, $\Phi_D \sim 1.00$[10] and $J(\lambda) = 2.53 \times 10^{15}$ M^{-1} cm^{-1} nm^4. Values of $R_0 = 74.5$ Å for compound **rg** (with $\Phi_D = 0.96$)[8a] and of $R_0 = 58.7$ Å for compound **og** (with $\Phi_D \sim 1.00$)[10], respectively, have been obtained, employing values of $\kappa^2 = 2.41$ and $J(\lambda) = 3.43 \times 10^{15}$ M^{-1} cm^{-1} nm^4 for compound **rg**, and $\kappa^2 = 2.39$ and $J(\lambda) = 8.08 \times 10^{14}$ M^{-1} cm^{-1} nm^4 for compound **og** (see Table 1). Typical values for the Förster distance reported in the literature range from of 10 to 80 Å.[38,39]

Furthermore, the rate of energy transfer from a donor to an acceptor can be calculated using the following equation:

$$k_{ET} = \frac{1}{\tau_D} \left(\frac{R_0}{r} \right)^6 \qquad (4)$$

129

where r denotes the center-to-center distance of the donor and acceptor transition dipole. The latter was derived from the molecular structures obtained with molecular modeling depicted in Figure 2, affording values of r = 19.9 Å for compound **or**, r = 20.1 Å for compound **rg** and r = 20.0 Å for compound **og**. This leads to calculated values for the energy transfer rate of k_{ET} = 5.9 x 10^{11} s^{-1} for compound **or**, of k_{ET} = 4.0 x 10^{11} s^{-1} for compound **rg** and of k_{ET} = 1.9 x 10^{11} s^{-1} for compound **og**. The afforded values excellently resemble the experimentally obtained rate constants of k_{ET} = 6.4 x 10^{11} s^{-1} for compound **or**, of k_{ET} = 4.0 x 10^{11} s^{-1} for compound **rg** and of k_{ET} = 1.5 x 10^{11} s^{-1} for compound **og** (see Table 3). Thus, the molecular structure obtained from molecular modeling provided the correct spatial orientation of the chromophores to explain the energy transfer rates by the Förster theory: according to Equation (4) the rate of energy transfer is inversely proportional to r^6 and thus depends strongly on the center-to-center distance r of the donor and acceptor transition dipoles. Hence, any phenomenon affecting the distance r will also influence the transfer rate to a large extent and accordingly, minor changes in the center-to-center distance would lead to huge differences in the calculated rate constants. When referring to the molecular modeling structures depicted in Figure 2, in principle two *pinched cone* conformations would be possible (see above) with two very different values for the respective center-to-center distances. However, with such an excellent agreement of experimentally observed and theoretically calculated values for the rate constants upon employing the r value related to the zigzag *pinched cone* conformation (*i.e.* the *pinched cone* conformation with the PBI residues pointing away from each other), spectroscopic evidence for the prevalence of the latter conformation is provided. Hence, the time-resolved spectroscopic results corroborate the absence of the stacked *pinched cone* conformation (with cofacial orientation of the dye units), as the center-to-center distance in that case would be substantially less and the values of experimentally and theoretically obtained rate constants would differ to a large extent.

Table 3. Evaluation of time-resolved photophysical properties of calix[4]arene–PBI arrays according to the Förster theory.[a]

Cmpd	k_{ET}(obs)[b] $(10^{11}\,s^{-1})$	E_{ET}[b]	E_{CT}[c]	Θ_D[d]	Θ_A[d]	κ^2	$J(\lambda)$ $(M^{-1}cm^{-1}nm^4)$	R_0 (Å)	r[d] (Å)	k_{ET}(calcd) $(10^{11}\,s^{-1})$
or	6.4	0.84	0.16	44.1°	43.1°	2.32	2.53×10^{15} [e]	70.8	19.9	5.9
oro	6.3	0.82	0.18							
ror	12.6	0.79	0.21							
rg	4.0	~1.00	~0.00	43.0°	40.9°	2.41	3.43×10^{15} [f]	74.5	20.1	4.0
rgr	3.9	~1.00	~0.00							
grg	8.5	~1.00	~0.00							
org	7.1	0.89	0.11							
grorg	15.8	0.88	0.12							
og	1.5	0.62	0.38	44.0°	40.3°	2.39	8.08×10^{14} [g]	58.7	20.0	1.9

[a] All spectra were recorded at room temperature in CH_2Cl_2. [b] Rate constants and efficiency values are given for the energy transfer process from the *orange* to the *red* PBI unit for compounds **or**, **oro**, **ror**, **org**, and **grorg**, and for the energy transfer process from the *red* to the *green* PBI unit for compounds **rg**, **rgr**, and **grg**. [c] Efficiency values are given for the charge transfer process from the calix[4]arene moiety to the *orange* PBI unit for compounds **or**, **oro**, **ror**, **org**, and **grorg**, and for the charge transfer process from the calix[4]arene moiety to the *red* PBI unit for compounds **rg**, **rgr**, and **grg**. [d] Values obtained from force field calculations (Macromodel 8.0, Potential MMFF). [e] Calculated from normalized fluorescence emission spectrum of compound **oc** and UV/vis absorption spectrum of compound **rc**. [f] Calculated from normalized fluorescence emission spectrum of compound **rc** and UV/vis absorption spectrum of compound **gc**. [g] Calculated from normalized fluorescence emission spectrum of compound **oc** and UV/vis absorption spectrum of compound **gc**.

Furthermore, the impact of the solvent polarity on the transient absorption spectra and the energy transfer rates has been studied for the three systems **or**, **rg** and **og**. For this purpose, the less polar solvent toluene ($\varepsilon_r = 2.4$) and the more polar solvent benzonitrile ($\varepsilon_r = 25.9$) were applied. The obtained femtosecond transient absorption spectra (Figures 26-28) as well as representative kinetic traces (Figure 29) are shown in the Appendix of this Chapter, and the respective lifetime values obtained from the global and target analysis are summarized in Table 4. As expected, the energy transfer rates and the kinetic profiles only differ slightly in solvents of different polarity: for the energy transfer rate from the orange to the red PBI unit in compound **or** in both toluene and benzonitrile a rate constant of 1.6 ps was obtained, respectively. Likewise, energy transfer rates from the red to the green PBI unit for compound **rg** in toluene of 2.7 ps and in benzonitrile of 2.9 ps were obtained. Similarly, also for the energy transfer rates from the orange to the green PBI unit for compound **og** rates of 7.4 ps and 8.1 ps were obtained in toluene and benzonitrile,

respectively. This behavior is in agreement with the solvent independence normally observed for Förster-type resonance energy transfer.[40] Remarkably, also the rates of charge separation remain almost constant in these two solvents for compounds **or** and **og**. In contrast, the charge recombination kinetics show a clear solvent dependence: for compound **or** in toluene a value for the recombination of the CT state of the calix[4]arene-PBI subunit of 25 ps is found which is significantly reduced for the more polar solvents CH_2Cl_2 and benzonitrile (see Table 4), and likewise, for compound **og** similar trends for the charge recombination are observed. This behavior can be attributed to Marcus inverted region effects as have already been observed for compound **oc** (see Chapter 3) and for other electron donor-acceptor systems.[41]

Table 4. Selected lifetimes in toluene (Tol), CH_2Cl_2 and benzonitrile (PhCN) obtained from the global and target analysis of the experimental data.

Cmpd		lifetimes τ (ps)[a]						
	solv.[b]	ET o*→r*	ET r*→g*	ET o*→g*	CT to (oPBI)$^{\bullet-}$	(oPBI)$^{\bullet-}$	r*→r	g*→g
or (Tol)	0.3	1.6			11.0	25.0	5000	
or (CH_2Cl_2)	0.2	1.6			8.0	6.7	5000	
or (PhCN)	0.3	1.6			15.0	7.5	5200	
rg (Tol)	0.1		2.7					2000
rg (CH_2Cl_2)	0.3		2.5					3300
rg (PhCN)	0.1		2.9					2400
og (Tol)	0.1			7.4	14.0	35.0		2200
og (CH_2Cl_2)	0.2			6.7	10.8	8.6		3800
og (PhCN)	0.3			8.1	15.0	9.8		1400

[a] Relative precision of the lifetimes and rates is 10%, except for lifetimes in the ns time range which are less reliable due to the 1ns time base of the experiment and thus represent lower limits. [b] See ref. 36.

4.8   Conclusions

Calix[4]arene scaffolds have been applied to organize perylene bisimide chromophores in zigzag-type arrangements providing defined distances and angles between the PBI chromophores. Arrays constructed in such way possess the characteristic feature that the individual chromophoric building blocks can be easily replaced by each other as well as their optical properties can be fine-tuned without influencing the overall geometric arrangement of the supramolecular system. Owing to the excellent spectral overlap of orange and red as well as of red and green perylene bisimide chromophores, the **org** triad displays very fast directional energy transfer leading to the population of the excited green PBI in less than 4 ps and with 89% efficiency. For comparison, in the absence of the red "mediator" chromophore, a slower (7 ps) and less efficient (62%) energy transfer process is observed for the **og** dyad. Therefore, these zigzag type dye arrays can even harvest the photons absorbed by the orange perylene bisimide dye unit, despite the almost non-fluorescent nature of the parent calix[4]arene–perylene bisimide building block **oc**. The zigzag-type arrangement of dyes employed here provide a hitherto unexplored geometry for efficient sequential FRET processes along oligomeric chains. Femtosecond transient absorption spectroscopy provide information on the excited states involved and global analysis revealed intricate details as the three chromophores involved display well separable spectral characteristics. The observed energy transfer processes are in excellent agreement with Förster theory. Stimulated by the fact that such PBI arrays are not only excellent candidates for sequential energy transfer but also enable the formation of long-lived charge separated states,[42] the next logical step would be to combine both features in a sequential energy and electron transfer cascade.

4.9   Experimental Section

Materials and Methods

Perylene bisanhydrides **rPBA**,[43] **gPBA**,[44] perylene monoimide monoanhydrides **oPMI**,[45] **rPMI**,[46] **gPMI**,[44,47] as well as precursor compound **pcA**[48] (for synthetic pathway see also Chapter 1) were synthesized according to literature procedures. Perylene bisanhydride **oPBA** was commercially available. Solvents were purified and dried according to standard procedures. For UV/vis absorption and fluorescence emission experiments spectroscopy grade solvents were used. Column chromatography was performed with silica gel 60 (0.035–0.070 mm) and preparative thin layer chromatography (preparative TLC) on 20 x 20 cm plates, height 1 mm, silica gel 60 (0.035–0.070 mm). High performance liquid chromatography (HPLC) was performed on normal phase (NP) SiO_2 columns, with p.a. grade purified solvents. NMR spectra were recorded on a Bruker 400 MHz spectrometer. Mass spectra were performed on a Finnigan MAT MS 8200 or on a Bruker microTOF$_{LC}$. All compounds were characterized by ^{1}H NMR spectroscopy and high resolution mass spectrometry.

UV/vis absorption spectra were measured on a Perkin-Elmer Lambda 40P UV/vis absorption spectrophotometer.

Steady state fluorescence emission spectra were recorded on a PTI QM4-2003 fluorescence spectrometer and are corrected against photomultiplier and lamp intensity. A long wavelength range emission corrected photomultiplier R928 was used. Fluorescence quantum yields were determined in CH_2Cl_2 vs. *N,N'*-(2,6-diisopropylphenyl)-1,6,7,12-tetraphenoxyperylene-3,4:9,10-tetracarboxylic acid bisimide ($\Phi_{fl} = 0.96$ in $CHCl_3$) or Fluorescein ($\Phi_{fl} = 0.92$ in 0.1N NaOH) as reference.[8b,49] The given quantum yields are averaged from values measured at three different excitation wavelengths with OD 0.02–0.05 in the absorption maximum (standard deviation $\sigma = 1$–3%).

Femtosecond transient absorption spectra were measured at the Universiteit van Amsterdam, The Netherlands, under the guidance of Dr. R. Williams. Experimental details are described in Chapter 2 and in the literature.[50]

Global and target analysis was performed by Dr. I. H. M. van Stokkum at the Vrije Universiteit van Amsterdam, The Netherlands. For details of the method refer to Chapter 2 and to the literature.[35]

Synthesis and chemical characterization

Compound pcB
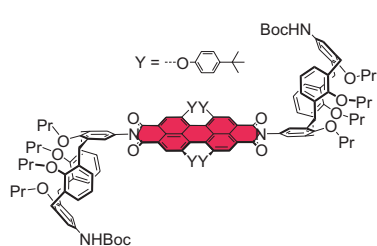
Under an argon atmosphere 90 mg (0.124 mmol, 3 equiv.) of compound **pcA**, 41 mg (0.042 mmol, 1 equiv.) of compound **rPBA** and 2-3 drops of triethylamine in toluene (0.5 mL) were heated to 65 °C for 20 h. The solvent was evaporated, the remaining crude product precipitated from CH$_2$Cl$_2$/methanol and the resulting solid purified by column chromatography with CH$_2$Cl$_2$/hexane 70:30 and precipitated from CH$_2$Cl$_2$/methanol. Compound **pcB** was obtained as a red powder (10 mg, 4.17 x 10^{-3} mmol, yield 10 %). C$_{154}$H$_{168}$N$_4$O$_{20}$ (2395.00). Mp > 400 °C (dec.). TLC CH$_2$Cl$_2$/hexane 80:20; R$_f$ = 0.2. **^{1}H NMR** (400 MHz, CDCl$_3$, 25 °C): δ (ppm) = 8.31 (bs, 4H; Per-*H*); 7.24 (d, ^{3}J = 8.7 Hz, 8H; Phen-*H*); 7.03 (s, 4H; Ar-*H*); 6.96 (s, 4H; Ar-*H*); 6.88 (d, ^{3}J = 8.7 Hz, 8H; Phen-*H*); 6.43 (bs, 2H; Boc-N-*H*); 6.27 (t, 4H, ^{3}J = 7.5 Hz; Ar-*H*); 6.20 (br dd, ^{3}J = 7.6 Hz, 4H; Ar-*H*); 6.18 (br dd, ^{3}J = 7.8 Hz, 4H; Ar-*H*); 4.44 and 3.11 (AX, each 4H, ^{2}J = 13.4 Hz; Ar-C*H$_2$*-Ar); 4.39 and 3.09 (AX, each 4H, ^{2}J = 13.6 Hz; Ar-C*H$_2$*-Ar); 4.03 and 3.93 (each t, 8H, each ^{3}J = 8.2 Hz; O-C*H$_2$*); 3.66 (m, 8H; O-C*H$_2$*); 1.96-1.79 (m, 16H; Propyl-*H*); 1.51 (s, 18H; Boc-*tert*-Butyl); 1.28 (s, 36H, *tert*-Butyl-Phen); 1.06 (t, 12H, ^{3}J = 7.4 Hz; Propyl-*H*); 0.86 and 0.85 (each t, 12H, each ^{3}J = 7.4 Hz; Propyl-*H*). **^{13}C NMR** (150 MHz, CDCl$_3$, 25 °C): δ (ppm) = 163.9, 158.1, 156.3, 155.4, 154.0, 147.5, 137.7, 137.4, 133.3, 133.1, 133.0, 132.1, 128.7 (br), 128.6, 128.5, 128.4 (br), 128.3 (br), 127.7 (br), 127.6 (br), 126.8, 122.7 (br), 122.6 (br), 119.9, 119.6, 119.5 (br), 80.2, 77.4, 77.0, 34.5, 31.6, 31.2 (br), 23.6, 23.0, 10.0, 9.9. **MS** (FAB in Nitrobenzyl alcohol): calcd for C$_{154}$H$_{169}$N$_4$O$_{20}$ (m/z) 2394.23 [M+H]$^+$ and C$_{154}$H$_{168}$N$_4$O$_{20}$Na (m/z) 2417.22 [M+Na]$^+$; found 2394.2; 2417.4. **Analysis:** calcd (%) for C$_{154}$H$_{168}$N$_4$O$_{20}$ (2395.00): C 77.23; H 7.07; N 2.34; found: C 77.22; H 7.07; N 2.34. **UV/vis**

(CH_2Cl_2): λ (nm) [ε ($M^{-1}cm^{-1}$)] = 581 [48500]. **Fluorescence** (CH_2Cl_2): λ_{max} (nm) = 612; Φ_{Fl} = 0.69.
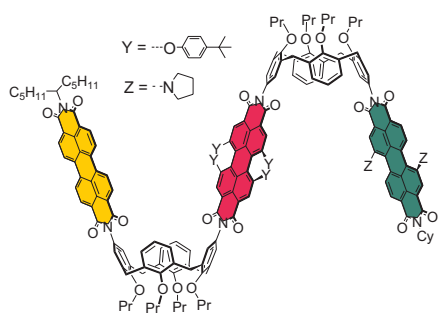
Compound pcC
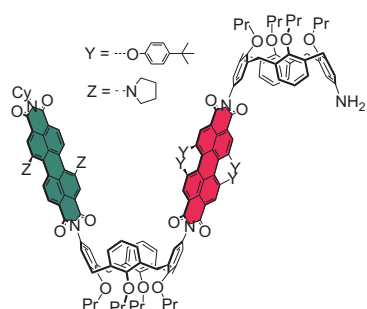
To a solution of 146 mg (6.09 x 10^{-2} mmol) of compound **pcB** in 2 mL dry CH_2Cl_2 were added 3 mL of CF_3COOH under an argon atmosphere. The mixture was stirred for 1 h at room temperature, poured into ice water and adjusted to pH > 9 with NH_3 solution (25%). CH_2Cl_2 (50 mL) was added to the mixture, and the resulting organic phase washed with water and brine and dried over Na_2SO_4. The solvent was evaporated and the resulting crude product dried and used without further purification.

A portion of 100 mg (4.56 x 10^{-2} mmol, 1 equiv.) of the obtained crude product, 24 mg (3.95 x 10^{-2} mmol, 0.9 equiv.) of compound **gPMI** and 16 mg (8.77 x 10^{-2} mmol, 2 equiv.) of $Zn(OAc)_2$ (H_2O-free) were heated in 0.7 mL distilled quinoline at 160 °C for 5 h under an argon atmosphere. The cooled reaction mixture was poured into 10 mL of 2N HCl and stirred for 30 minutes. To the solution 50 mL of CH_2Cl_2 were added and the organic phase was washed with water and brine and dried over $MgSO_4$. The crude product was purified by column chromatography with CH_2Cl_2/ethylacetate 99:1 and by preparative TLC with CH_2Cl_2/ethylacetate 99:1. Compound **pcC** was obtained as a dark-blue powder that shows low stability at air (28 mg, 1.01 x 10^{-2} mmol, yield 17% over two steps). $C_{182}H_{183}N_7O_{20}$ (2788.44). Mp > 400 °C. TLC: CH_2Cl_2/ethylacetate 98:2; R_f = 0.91. **^{1}H NMR** (400 MHz, $CDCl_3$, 25 °C): δ (ppm) = 8.60 (bs, 1H; Per-*H*); 8.53 – 8.50 (m, 2H, Per-*H*); 8.44 (d, 1H, ^3J = 8.2 Hz; Per-*H*); 8.30 (bs, 4H; Per-*H*), 7.78 and 7.76 (two d, 2H, ^3J = 7.5 Hz; Per-*H*); 7.24 – 7.23 (m, 8H; Phen-*H*); 7.10 and 7.05 and 6.98 (each s, 6H; Ar-*H*); 6.89 – 6.87 (m, 8H; Phen-*H*); 6.45 (s, 2H; Ar-*H*); 6.35 (t, 2H, ^3J = 7.6 Hz; Ar-*H*); 6.30 – 6.15 (m, 10H; Ar-*H*); 5.11 – 5.05 (tt, $^3J_1$ = 11.9 Hz, $^3J_1$ = 3.5 Hz, 1H; Cy-*H*); 4.50 and 3.17 (AX, 4H, ^2J = 13.6 Hz; Ar-C*H$_2$*-Ar); 4.48 and 3.14 (AX, 4H, ^2J = 12.6 Hz; Ar-C*H$_2$*-Ar); 4.45 and 3.11 (AX, 4H, ^2J = 12.8 Hz; Ar-C*H$_2$*-Ar); 4.36 and 3.00 (AX, 4H, ^2J = 13.0 Hz; Ar-C*H$_2$*-Ar); 4.13 – 4.02 (m, 6H; O-C*H$_2$*); 3.89 (t, 2H, ^3J = 8.3 Hz; O-C*H$_2$*); 3.79 (bs, 4H; Pyrr-*H*); 3.66 – 3.63 (m, 8H; O-C*H$_2$*); 3.44 (bs, 2H; N*H$_2$*); 2.88 (bs, 4H; Pyrr-*H*); 2.65 – 2.57 (m, 2H; Cy-*H*); 2.11 – 1.76 (m, 29H; Pyrr-*H*, Propyl-*H*, Cy-*H*); 1.47 – 1.37 (m, 3H; Cy-*H*); 1.29 and 1.28

136

(each s, 36H; *tert*-Butyl-Phen); 1.09 and 1.06 (each t, 12H, each ^3J = 7.4 Hz; Propyl-*H*); 0.90 – 0.84 (m, 12H; Propyl-*H*). **MS** (MALDI in Dithranol): calcd for $C_{182}H_{184}N_7O_{20}$ (m/z) 2787.36 $[M+H]^+$ and $C_{182}H_{183}N_7O_{20}Na$ (m/z) 2809.34 $[M+Na]^+$ and $C_{182}H_{183}N_7O_{20}K$ (m/z) 2825.31 $[M+K]^+$; found 2787; 2809; 2825. **UV/vis** (CH_2Cl_2): λ (nm) [ε ($M^{-1}cm^{-1}$)] = 700 [41900], 580 [52000], 435 [29500].
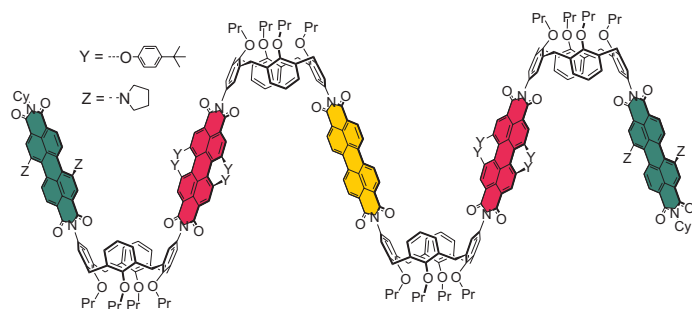

*Compound **org***

Under an argon atmosphere 87 mg (3.12 x 10^{-2} mmol, 1 equiv.) of compound **pcC**, 34 mg (6.24 x 10^{-2} mmol, 2 equiv.) of compound **oPMI** and 12 mg (6.24 x 10^{-2} mmol, 2 equiv.) of $Zn(OAc)_2$ (H_2O-free) were heated in distilled quinoline (0.5 mL) at 165 °C for 15 h. The cooled reaction mixture was poured into 20 mL of 2N HCl and stirred for 30 minutes at 40 °C and adjusted to pH > 9 with NH_3 solution (25%). CH_2Cl_2 (40 mL) was added to the reaction mixture, the resulting two phases were separated, and the organic phase was washed with water and brine and dried over $MgSO_4$. The crude product was purified first by column chromatography with CH_2Cl_2/ethyl acetate 99:1 and successively and successively by preparative HPLC with CH_2Cl_2 (SiO_2, normal phase) and precipitation from CH_2Cl_2/methanol. Compound **org** was obtained as a dark powder (51 mg, 1.54 x 10^{-2} mmol, yield 49%). $C_{217}H_{212}N_8O_{24}$ (3316.04). Mp > 400 °C. TLC: CH_2Cl_2/ethyl acetate 99:1; R_f = 0.49. **^{1}H NMR** (400 MHz, $CDCl_3$, 25 °C): δ (ppm) = 8.79 (bd, 2H, ^3J = 7.6 Hz; Per-*H*); 8.69 – 8.65 (m, 6H; Per-*H*); 8.60 (s, 1H; Per-*H*); 8.53 – 8.50 (m, 2H; Per-*H*); 8.44 (d, 1H, ^3J = 8.0 Hz; Per-*H*); 8.33 (bs, 4H; Per-*H*); 7.80 and 7.78 (each d, 2H, each ^3J = 8.0 Hz; Per-*H*); 7. 26 (bd, 8H; Phen-*H*); 7.12 and 7.11 (each s, 4H; Ar-*H*); 7.05 (s, 4H; Ar-*H*); 6.90 (bd, 8H, ^3J = 8.4 Hz; Phen-*H*); 6.37 and 6.36 (each t, 4H, each ^3J = 7.5 Hz; Ar-*H*); 6.24 and 6.17 (each bd, 8H; Ar-*H*); 5.29 – 5.23 and 5.20 – 5.13 (each m, 2H; N-C*H* and Cy-*H*); 4.53 – 4.47 (m, 8H; Ar-C*H₂*-Ar); 4.11 – 4.05 (m, 8H; O-C*H₂*); 3.78 and 3.65 (bs and t, 12H; Pyrr-*H* and O-C*H₂*); 3.19 – 3.13 (m, 8H; Ar-C*H₂*-Ar); 2.88 (bs, 4H; Pyrr-*H*); 2.66 – 2.57 (m, 2H; Cy-*H*); 2.29 – 2.24 (m, 2H; Alkyl-*H*); 2.09 – 1.76 (m, 31H; Pyrr-*H*, Propyl-*H*, Cy-*H*, Alkyl-*H*); 1.50 – 1.41 (m, 3H; Cy-*H*); 1.30 (bs, 48H; *tert*-Butyl-Phen-*H* und Alkyl-*H*); 1.11 (t, 12H, ^3J = 7.3 Hz; Propyl-*H*); 0.92 – 0.82 (m, 18H; Propyl-*H* and Alkyl-*H*). **HR-MS** (ESI in $CHCl_3$/acetonitrile): calcd for

$C_{217}H_{220}N_{10}O_{24}$ [M+2NH$_4$]$^{2+}$ (m/z) 1674.8151; found 1674.8146. **UV/vis** (CH$_2$Cl$_2$): λ (nm) [ε (M^{-1}cm^{-1})] = 701 [46000], 580 [57100], 527 [116800], 489 [69800], 456 [43700], 435 [38000]. **Fluorescence** (CH$_2$Cl$_2$): λ_{max} (nm) = 737 with λ_{ex} = 490; Φ_{Fl} = 0.16.

*Compound **grorg***

A suspension of 35 mg (1.26 x 10^{-2} mmol, 2 equiv.) of compound **pcC**, 2.5 mg (6.28 x 10^{-3} mmol, 1 equiv.) of compound **oPBA** and 4.5 mg (2.51·x 10^{-2} mmol, 4 equiv.) of Zn(OAc)$_2$ (H$_2$O-free) was heated in 0.3 mL distilled quinoline at 160°C for 7 h under an argon atmosphere. The cooled reaction mixture was poured into 10 mL of 1N HCl and stirred for 30 minutes. The resulting precipitate was filtered and dissolved in CH$_2$Cl$_2$. The solution was washed with water and brine and dried over MgSO$_4$. The crude product was purified first by column chromatography with CH$_2$Cl$_2$/ethylacetate 99:1 and successively by preparative TLC with CH$_2$Cl$_2$/ethylacetate 98:2 and preparative HPLC with CH$_2$Cl$_2$ (SiO$_2$, normal phase). Compound **grorg** was obtained as a dark-brown powder (7 mg, 1.18 x 10^{-3} mmol, 19 %). $C_{388}H_{370}N_{14}O_{44}$ (5933.16). Mp > 450 °C. TLC: CH$_2$Cl$_2$/ethylacetate 98:2; R$_f$ = 0.65. **^{1}H NMR** (400 MHz, CDCl$_3$, 25 °C): δ (ppm) = 8.82 and 8.74 (each bd, 8H, ^{3}J = 7.8 Hz and ^{3}J = 8.0 Hz; Per-*H*); 8.60 (s, 2H; Per-*H*); 8.53 – 8.50 (m, 4H, Per-*H*); 8.44 and 8.34 (d and bs, 10H, ^{3}J = 8.0 Hz; Per-*H*); 7.80 and 7.78 (two d, 4H, ^{3}J = 8.1 Hz; Per-*H*); 7. 26 and 7.24 (two d, ^{3}J = 8.3 Hz; 16H; Phen-*H*); 7.14 and 7.11 (each s, 8H; Ar-*H*); 7.06 and 7.05 (each s, 8H; Ar-*H*); 6.90 (bd, 16H, ^{3}J = 8.3 Hz; Phen-*H*); 6.36 – 6.34 (m, 8H; Ar-*H*); 6.25 – 6.22 and 6.17 – 6.16 (each m, 16H; Ar-*H*); 5.08 (tt, ^{3}J$_1$ = 11.9 Hz, ^{3}J$_1$ = 3.5 Hz, 2H; Cy-*H*); 4.54 – 4.47 (m, 16H; Ar-C*H$_2$*-Ar); 4.13 – 4.10 (m, 16H; O-C*H$_2$*); 3.79 and 3.65 (each bs, 24H; Pyrr-*H* and O-C*H$_2$*); 3.19 – 3.13 (m, 16H; Ar-C*H$_2$*-Ar); 2.88 (bs, 8H; Pyrr-*H*); 2.66 – 2.57 (m, 4H; Cy-*H*); 2.17 – 1.76 (m, 58H; Pyrr-*H*, Propyl-*H*, Cy-*H*); 1.50 – 1.41 (m, 6H; Cy-*H*); 1.30 (bs, 72H; *tert*-Butyl-Phen); 1.11 and 1.10 (each t, 24H, each ^{3}J = 7.4 Hz; Propyl-*H*);

0.92 – 0.83 (m, 24H; Propyl-*H*). **MS** (MALDI in DD/Dithranol 1:10):[vi] calcd for $C_{388}H_{370}N_{14}O_{44}$ (m/z) 5933.30 [M]$^+$ and $C_{388}H_{370}N_{14}O_{44}K$ (m/z) 5972.40 [M+K]$^+$; found 5933.16; 5972.10. **UV/vis** (CH$_2$Cl$_2$): λ (nm) [ε (M^{-1}cm^{-1})]: 701 [77100], 581 [97600], 527 [127900], 435 [57200]. **Fluorescence** (CH$_2$Cl$_2$): λ_{max} (nm) = 739 with λ_{ex}= 490 nm; Φ_{Fl} = 0.17.

*Compound **oro***
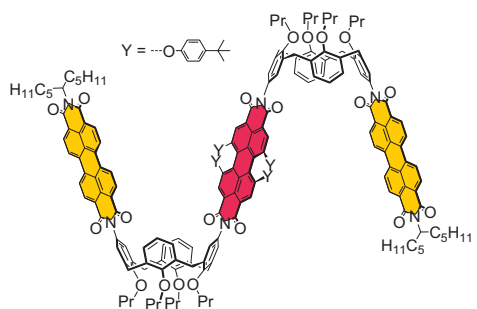
To a solution of 115 mg (4.79 x 10^{-2} mmol) of compound **pcB** in 2 mL dry CH$_2$Cl$_2$ were added 3 mL of CF$_3$COOH under an argon atmosphere. The mixture was stirred for 1 h at room temperature, poured into ice water and adjusted to pH > 9 with NH$_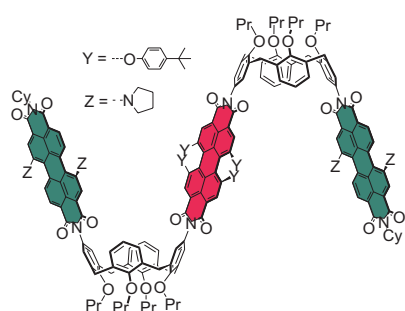3$ solution (25%). CH$_2$Cl$_2$ (50 mL) was added to the mixture, and the resulting organic phase washed with water and brine, and dried over Na$_2$SO$_4$. The solvent was evaporated and the resulting crude product (102 mg; 4.65 x 10^{-2} mmol) dried and used without further purification.

Under an argon atmosphere 102 mg (4.65 x 10^{-2} mmol, 1 equiv.) of the obtained crude product, 101 mg (1.86 x 10^{-2} mmol, 4 equiv.) of **oPMI** and 34 mg (1.86·10^{-5} mol, 4 eq) of Zn(OAc)$_2$ (H$_2$O-free) were heated in quinoline (1.0 mL) at 175 °C for 12.5 h. The cooled reaction mixture was poured into 40 mL of 2N HCl and stirred for 40 minutes at 50 °C. CH$_2$Cl$_2$ (50 mL) was added to the reaction mixture, the resulting two phases were separated, and the organic phase was washed with water and brine and dried over MgSO$_4$. The crude product was purified first by column chromatography with CH$_2$Cl$_2$ and successively by preparative HPLC with CH$_2$Cl$_2$ (SiO$_2$, normal phase) and finally by precipitation from CH$_2$Cl$_2$/methanol. Compound **oro** was obtained as a red powder (59 mg, 1.81 x 10^{-2} mmol, yield 38% over two steps). $C_{214}H_{210}N_6O_{24}$ (3249.98). Mp > 400 °C. TLC: CH$_2$Cl$_2$; R$_f$ = 0.67. **^{1}H NMR** (400 MHz, CDCl$_3$, 25 °C) δ (ppm) = 8.75 and 8.71 – 8.65 (bd and m, 16H; Per-*H*); 8.33 (bs, 4H; Per-*H*); 7.26 (bd, 8H; Phen-*H*, ^3J = 8.7 Hz);

[vi] Due to the resolution of the mass spectrometer only a peak with the **average molecular weight** of the compound can be observed. An additional peak due to oxidation of the sample during the measurement is observed in the spectrum: calcd for $C_{388}H_{370}N_{14}O_{45}K$ m/z = 5988.40 [M+K+O]$^+$, found m/z = 5988.58.

7.14 (s, 4H; Ar-*H*); 7.05 (s, 4H; Ar-*H*); 6.89 (bd, 8H; Phen-*H*, ^3J = 8.3 Hz); 6.37 (t, 4H, ^3J = 7.6 Hz; Ar-*H*); 6.24 and 6.18 (each d, 8H, each ^3J = 7.2 Hz; Ar-*H*); 5.22 – 5.18 (m, 2H, N-C*H*); 4.52 and 3.19 (each AX, each 4H, ^2J = 13.6 Hz and 14.3 Hz; Ar-C*H*$_2$-Ar); 4.49 and 3.16 (each AX, each 4H, ^2J = 13.4 Hz and 14.9 Hz; Ar-C*H*$_2$-Ar); 4.14 – 4.07 (m, 8H; O-C*H*$_2$); 3.66 (t, 8H, ^3J = 6.2 Hz; O-C*H*$_2$); 2.29 – 2.25 (m, 4H; Alkyl-*H*); 2.04 – 1.81 (m, 20H; Alkyl-*H*); 1.36 – 1.24 (m, 60H, Alkyl-*H* und *tert*-Butyl-Phen-*H*); 1.10 (t, 12H, ^3J = 7.4 Hz; Alkyl-*H*); 0.96 – 0.82 (m, 24H; Alkyl-*H*). **HR-MS** (ESI in acetonitrile): calcd for $C_{214}H_{210}N_6Na_2O_{24}$ [M+2Na]$^{2+}$ (m/z) 1646.7596; found 1646.7591. **Analysis**: calcd (%) for $C_{214}H_{210}N_6O_{24}$ x CH_3OH (3282.03): C 78.68; H 6.57; N 2.56; found: C 78.98; H 6.94; N 2.51. **UV/vis** (CH_2Cl_2): λ (nm) [ε ($M^{-1}cm^{-1}$)] = 580 [50300], 526 [194900], 489 [117500] 458 [57100]. **Fluorescence** (CH_2Cl_2): λ_{max} (nm) = 611 with λ_{ex} = 490 nm; Φ_{fl} = 0.72.
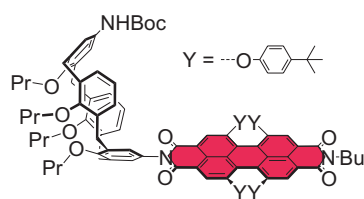
*Compound **grg***

To a solution of 75 mg (3.15 x 10^{-2} mmol) of compound **pcB** in 1.5 mL dry CH_2Cl_2 were added 3 mL of CF_3COOH under an argon atmosphere. The mixture was stirred for 1 h at room temperature, poured into ice water and adjusted to pH > 9 with NH_3 solution (25%). CH_2Cl_2 (50 mL) was added to the mixture, and the resulting organic phase washed with water and brine and dried over Na_2SO_4. The solvent was evaporated and the resulting crude product (65 mg; 2.96 x 10^{-2} mmol) dried and used without further purification.

A solution of 62 mg (2.82 x 10^{-2} mmol, 1equiv.) of the obtained crude product, 26 mg (4.24 x 10^{-2} mmol, 1.5 equiv.) of **gPMI** and 10 mg (5.65 x 10^{-5} mmol, 2 equiv.) of Zn(OAc)$_2$ (H_2O-free) in distilled quinoline (2.5 mL) was heated under an argon atmosphere at 140 °C for 15 h. The cooled reaction mixture was poured into 20 mL of 1N HCl and stirred for 30 minutes at 50 °C. CH_2Cl_2 (20 mL) was added to the reaction mixture, the resulting two phases were separated, and the organic phase was washed with water and brine and dried over MgSO$_4$. The crude product was purified first by column chromatography with CH_2Cl_2/ethyl acetate 99:1 and successively by preparative TLC with CH_2Cl_2/ethyl acetate 99:1 and by preparative HPLC with CH_2Cl_2 (SiO_2, normal phase), and finally by precipitation from CH_2Cl_2/methanol. Compound **grg** was obtained as a dark-

blue powder (20 mg, 5.91 x 10^{-3} mmol, yield 18% over two steps). $C_{220}H_{214}N_{10}O_{24}$ (3382.11). Mp > 500 °C. TLC: CH_2Cl_2/ethyl acetate 98:2; R_f = 0.96. **^{1}H NMR** (400 MHz, CDCl$_3$, TMS, 25 °C): δ (ppm) = 8.59 (bs, 2H; Per-*H*); 8.51 − 8.49 (m, 4H, Per-*H*); 8.42 and 8.33 (d and bs, 6H, ^3J = 8.1 Hz; Per-*H*); 7.78 − 7.76 (m, 4H; Per-*H*); 7. 26 − 7.24 (m, 8H; Phen-*H*); 7.11 and 7.05 (each s, each 4H; Ar-*H*); 6.90 − 6.89 (m, 8H; Phen-*H*); 6.36 (t, 4H, ^3J = 7.5 Hz; Ar-*H*); 6.24 (d, 4H, ^3J = 7.1 Hz; Ar-*H*); 6.17 (d, 4H, ^3J = 7.3 Hz; Ar-*H*); 5.11 − 5.05 (m, 2H; Cy-*H*); 4.51 and 3.18 (each AX, each 4H, ^2J = 13.1 Hz; Ar-C*H*$_2$-Ar); 4.48 and 3.15 (each AX, each 4H, ^2J = 12.6 Hz; Ar-C*H*$_2$-Ar); 4.14 − 4.07 (m, 8H; O-C*H*$_2$); 3.78 and 3.65 (bs and t, 16H, ^3J = 6.3 Hz; Pyrr-*H*, O-C*H*$_2$); 2.87 (bs, 8H; Pyrr-*H*); 2.65 − 2.57 (m, 4H; Cy-*H*); 2.08 − 1.76 (m, 42H; Pyrr-*H*, Propyl-*H*, Cy-*H*); 1.50 − 1.37 (m, 6H; Cy-*H*); 1.30 (s, 36H; *tert*-Butyl-Phen-*H*); 1.01 (t, 12H, ^3J = 7.4 Hz; Propyl-*H*); 0.91 and 0.87 (each t, 12H, each ^3J = 7.4 Hz; Propyl-*H*). **MS** (MALDI in dithranol): calcd for $C_{220}H_{215}N_{10}O_{24}$ (m/z) 3380.6 $[M+H]^+$ and for $C_{220}H_{214}N_{10}O_{24}K$ (m/z) 3418.5 $[M+K]^+$; found 3380 and 3419. **HR-MS** (ESI in CHCl$_3$/acetonitrile): calcd for $C_{220}H_{214}N_{10}O_{24}$ (m/z) 1689.7916 $[M]^{2+}$; found 1689.7911. **UV/vis** (CH_2Cl_2): λ (nm) [ε ($M^{-1}cm^{-1}$)] = 701 [84800], 580 [61300], 435 [47200]. **Fluorescence** (CH_2Cl_2): λ_{max} (nm) = 738 with λ_{ex} = 560; Φ_{Fl} = 0.19.
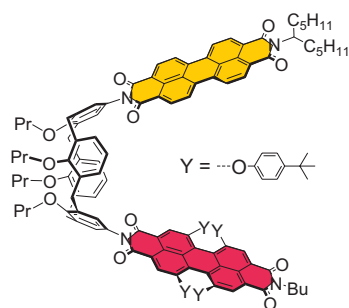
*Compound **pcD***

A solution of 110 mg (1.52 x 10^{-2} mmol, 1 equiv.) of calix[4]arene compound **pcA**, 190 mg (1.83 x 10^{-2} mmol, 1.2 equiv.) of **rPMI** were heated under an argon atmosphere to 110 °C for 23 h together with 5 drops of triethylamine in toluene (1.5 mL). The solvent was evaporated, the remaining crude product purified by column chromatography with CH_2Cl_2/hexane 70:30 and precipitated from CH_2Cl_2/methanol. Compound **pcD** was obtained as a red powder (101 mg, 5.79 x 10^{-3} mmol, yield 38%). $C_{113}H_{121}N_3O_{14}$ (1745.18). Mp = 295 − 296 °C. TLC: CH_2Cl_2/hexane 80:20; R_f = 0.54. **^{1}H NMR** (400 MHz, CDCl$_3$, TMS, 25 °C): δ (ppm) = 8.27 and 8.24 (bs and s, 4H; Per-*H*); 7.25 − 7.20 (m, 8H; Phen-*H*); 7.06 (s, 2H; Ar-*H*); 6.95 (s, 2H; Ar-*H*); 6.87 − 6.82 (m, 8H; Phen-*H*); 6.42 (bs, 1H; Boc-N-*H*); 6.26 (t, 2H, ^3J = 7.5 Hz; Ar-*H*); 6.19 − 6.15 (m, 4H; Ar-*H*); 4.44 and 3.10 (AX, 4H, ^2J = 13.5 Hz; Ar-C*H*$_2$-Ar); 4.39 and 3.09 (AX, 4H, ^2J = 13.6 Hz; Ar-C*H*$_2$-Ar); 4.12 (t, 2H, ^3J = 7.2 Hz; N-C*H*$_2$); 4.05 − 4.01 and

3.95 – 3.91 (each m, 4H; O-CH_2); 3.66 – 3.62 (m, 4H; O-CH_2); 1.79 (m, 8H; Propyl-H); 1.70 – 1.62 (m, 2H, Butyl-H); 1.51 (s, 9H; Boc-*tert*-Butyl-H); 1.44 – 1.35 (m, 2H, Butyl-H); 1.29 and 1.27 (each s, 36H, *tert*-Butyl-Phen-H); 1.06 (t, 6H, ^3J = 7.4 Hz; Propyl-H); 0.94 (t, 3H, ^3J = 7.3 Hz; Butyl-H); 0.86 and 0.85 (each t, 6H, each ^3J = 7.5 Hz; Propyl-H). **^{13}C NMR** (100 MHz, CDCl$_3$, TMS, 25 °C): δ (ppm) = 163.6 (*C*=O), 156.2, 156.1 (br), 155.4, 153.1 (br), 147.5, 137.7, 137.4, 133.2, 133.1, 133.0, 132.1, 128.5, 128.4, 127.7, 127.6, 126.8, 122.7, 122.6, 120.7, 120.1, 119.9, 119.6, 119.5, 77.4 (Boc-*tert*-Butyl-*C*), 76.9, 76.7, 76.6 (O-*C*H$_2$ and N-*C*H$_2$), 34.5 (Phen-*tert*-Butyl-*C*), 31.6 (*C*H$_3$-*tert*-Butyl), 31.2, 30.3 (Ar-*C*H$_2$-Aryl); 23.6, 23.0, 20.5, 13.9, 10.9, 10.0, 9.9. **HR-MS** (ESI in THF/CHCl$_3$): calcd for C$_{113}$H$_{125}$N$_4$O$_{14}$ [M+NH$_4$]$^+$ (m/z) 1761.9192; found 1761.9187. **UV/vis** (CH$_2$Cl$_2$): λ (nm) [ε (M^{-1}cm^{-1})] = 579 [45600]. **Fluorescence** (CH$_2$Cl$_2$): λ$_{max}$ (nm) = 610; Φ$_{Fl}$ = 0.73.
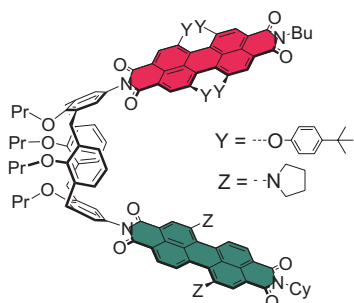
*Compound **or***

A portion of 36 mg (2.05 x 10^{-2} mmol) of compound **pcD** was dissolved in 2 mL dry CH$_2$Cl$_2$ and 3 mL of CF$_3$COOH were added under an argon atmosphere. The mixture was stirred for 1 hour at room temperature, poured into ice water and adjusted to pH > 9 with NH$_3$ solution (25%). CH$_2$Cl$_2$ (50 mL) was added to the reaction mixture, the two phases were separated, and the organic phase was washed with water and brine and dried over Na$_2$SO$_4$. The solvent was removed under vacuum and the resulting crude product (32 mg; 1.95 x 10^{-2} mmol) dried and used without further purification.

Under an argon atmosphere 32 mg (1.95 x 10^{-2} mmol, 1 equiv.) of the obtained crude product, 21 mg (3.89 x 10^{-2} mmol, 2 equiv.) of compound **oPMI** and 7 mg (3.89 x 10^{-2} mmol, 2 equiv.) of Zn(OAc)$_2$ (H$_2$O-free) were heated in quinoline (0.60 mL) at 170 °C for 12.5 h. The cooled reaction mixture was poured into 30 mL of 2N HCl and stirred for 30 minutes at 50 °C. The resulting precipitate was filtered and dissolved in CH$_2$Cl$_2$. The solution was washed with water and brine and dried over MgSO$_4$. The crude product was purified first by column chromatography with CH$_2$Cl$_2$ and successively by preparative HPLC with CH$_2$Cl$_2$ (SiO$_2$, normal phase) and precipitation from CH$_2$Cl$_2$/methanol. Compound **or** was obtained as a red powder (10 mg, 4.60 x 10^{-3} mmol, yield 23% over two

steps). $C_{143}H_{142}N_4O_{16}$ (2172.67). Mp = 370 – 372 °C. TLC: CH_2Cl_2; R_f = 0.10. **^{1}H NMR** (400 MHz, $CDCl_3$, 25 °C): δ (ppm) = 8.78 and 8.69 – 8.52 (d and m, 8H, ^3J = 7.8 Hz; Per-*H*); 8.29 and 8.23 (bs and s, 4H; Per-*H*); 7.25 – 7.22 (m, 8H; Phen-*H*); 7.10 (s, 2H; Ar-*H*); 7.02 (s, 2H; Ar-*H*); 6.88 – 6.84 (m, 8H; Phen-*H*); 6.35 (t, 2H, ^3J = 7.5Hz; Ar-*H*); 6.20 and 6.15 (each d, 4H, ^3J = 7.7 Hz and 7.5 Hz; Ar-*H*); 5.23 – 5.16 (m, 1H, N-C*H*); 4.51 and 3.19 (each AX, 4H, ^2J = 14.0 Hz and 12.8 Hz; Ar-C*H$_2$*-Ar); 4.47 and 3.16 (each AX, 4H, ^2J = 14.3 Hz and 13.0 Hz; Ar-C*H$_2$*-Ar); 4.14 – 4.06 (m, 6H; O-C*H$_2$* and N-C*H$_2$*); 3.64 (t, 4H, ^3J = 6.6 Hz; O-C*H$_2$*); 2.30 – 2.21 (m, 2H; Alkyl-*H*); 2.04 – 1.82 (m, 10H; Alkyl-*H*); 1.67 – 1.62 (m, 2H, Alkyl-*H*); 1.42 – 1.36 (m, 2H, Alkyl-*H*); 1.31 – 1.29 (m and two s, 48H, *tert*-Butyl-Phen-*H* and Alkyl-*H*); 1.09 (t, 6H, ^3J = 7.4 Hz; Alkyl-*H*); 0.96 – 0.82 (m, 15H; Alkyl-*H*). **HR-MS** (ESI in acetonitrile/$CHCl_3$): calcd for $C_{143}H_{142}N_4NaO_{16}$ $[M+Na]^+$ (m/z) 2194.0319; found 2194.0313. **UV/vis** (CH_2Cl_2): λ (nm) [ε ($M^{-1}cm^{-1}$)] = 579 [46200], 526 [107900], 489 [62000], 457 [34900]. **Fluorescence** (CH_2Cl_2): $λ_{max}$ (nm) = 608 with $λ_{ex}$ = 490 nm; $Φ_{Fl}$ = 0.72.
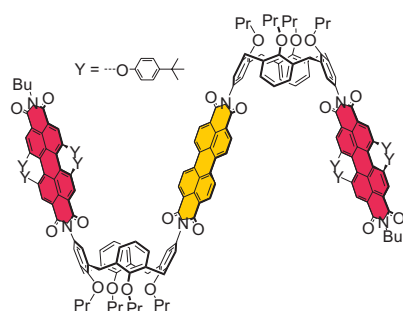
*Compound **rg***

To a solution of 14 mg (8.02 x 10^{-3} mmol) of compound **pcD** in 1.5 mL dry CH_2Cl_2 were added 3 mL of CF_3COOH under an argon atmosphere. The mixture was stirred for 1 hour at room temperature, poured into ice water and adjusted to pH > 9 with NH_3 solution (25%). CH_2Cl_2 (30 mL) was added to the reaction mixture, the two phases were separated, and the

organic phase was washed with water and brine and dried over Na_2SO_4. The solvent was removed and the resulting crude product (9 mg, 5.47 x 10^{-3} mmol) dried and used without further purification.

A portion of 9 mg (5.47 x 10^{-3} mmol, 1 equiv.) of the obtained crude product, 7 mg (1.14 x 10^{-2} mmol, 2 equiv.) of compound **gPMI** and 2 mg (5.47 x 10^{-3} mmol, 2 equiv.) $Zn(OAc)_2$ (H_2O-free) were heated in quinoline (0.75 mL) at 160 °C for 4h under an argon atmosphere. The cooled reaction mixture was poured into 10 mL of 1N HCl and stirred for 30 minutes. The resulting precipitate was filtered and dissolved in CH_2Cl_2. The solution was washed with saturated $NaHCO_3$ solution and water and dried over $MgSO_4$. The crude product was purified first by column chromatography with CH_2Cl_2/hexane 70:30 and

successively by preparative TLC with CH_2Cl_2/hexane 55:45 and preparative HPLC with CH_2Cl_2 (SiO_2, normal phase). Compound **rg** was obtained as a dark-blue powder (5 mg, 2.23 x 10^{-3} mmol, yield 8 % over three steps). $C_{146}H_{144}N_6O_{16}$ (2238.74). Mp > 400 °C. TLC: CH_2Cl_2; R_f = 0.18. **^{1}H NMR** (400 MHz, $CDCl_3$, 25 °C): δ (ppm) = 8.60 (bs, 1H; Per-*H*); 8.53 - 8.50 (m, 2H; Per-*H*); 8.44 (d, 1H, ^3J = 8.1 Hz; Per-*H*); 8.30 and 8.25 (bs and s, 4H; Per-*H*); 7.81 and 7.79 (two d, 2H, ^3J = 7.9 Hz; Per-*H*); 7.24 and 7.23 (two d, 8H, ^3J = 8.7 Hz; Phen-*H*); 7.10 (s, 2H; Ar-*H*); 7.03 (s, 2H; Ar-*H*); 6.86 and 6.85 (two d, 8H, ^3J = 8.7 Hz; Phen-*H*); 6.34 (t, 2H, ^3J =7.6 Hz; Ar-*H*); 6.23 (d, 2H, ^3J = 7.5 Hz; Ar-*H*); 6.14 (d, 2H, ^3J = 6.5 Hz; Ar-*H*); 5.08 (tt, $^3J_1$ = 12.4 Hz, $^3J_1$ = 3.5 Hz, 1H; Cy-*H*); 4.50 and 3.17 (AX, 4H, ^2J = 13.5Hz; Ar-C*H$_2$*-Ar); 4.47 and 3.13 (AX, 4H, ^2J = 13.6 Hz; Ar-C*H$_2$*-Ar); 4.14 – 4.07 (m, 6H; O-C*H$_2$* and N-C*H$_2$*); 3.78 (bs, 4H; Pyrr-*H*); 3.64 (t, 4H, ^3J = 6.6 Hz; O-C*H$_2$*); 2.88 (bs, 4H; Pyrr-*H*); 2.66 – 2.57 (m, 2H; Cy-*H*); 2.09 – 1.63 (m, 23H; Butyl-*H*, Propyl-*H*, Cy-*H*); 1.43 – 1.37 (m, 5H; Butyl-*H*, Cy-*H*); 1.30 and 1.29 (two s, 36H, *tert*-Butyl-Phen-*H*); 1.09 (t, 6H, ^3J = 7.4 Hz; Propyl-*H*); 0.94 and 0.89 and 0.86 (three t, 9H; each ^3J = 7.4 Hz, Butyl-*H*, Propyl-*H*). **MS** (MALDI in Dithranol): calcd for $C_{146}H_{145}N_6O_{16}$ [M+H]$^+$ (m/z) 2238.07; found 2238.0. **HR-MS** (ESI in acetonitrile/$CHCl_3$): calcd for $C_{146}H_{144}N_6O_{16}$ [M]$^+$ (m/z) 2237.0639; found 2237.0633. **UV/vis** (CH_2Cl_2): λ (nm) [ε ($M^{-1}cm^{-1}$)] = 701 [44600], 580 [50800]. **Fluorescence** (CH_2Cl_2): $λ_{max}$ (nm) = 738 with $λ_{ex}$= 560 nm; $Φ_{Fl}$ = 0.18.
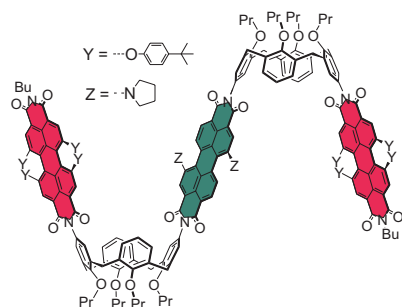
*Compound **ror***

A portion of 73 mg (4.22 x 10^{-2} mmol) of compound **pcD** was dissolved in 2 mL dry CH_2Cl_2 and 3 mL of CF_3COOH were added under an argon atmosphere. The mixture was stirred for 1 hour at room temperature, poured into ice water and adjusted to pH > 9 with NH_3 solution (25%). CH_2Cl_2 (50 mL) was added to the reaction mixture, the two phases were separated, and the organic phase was washed with water and brine and dried over Na_2SO_4. The solvent was removed and the resulting crude product (68 mg; 4.13 x 10^{-2} mmol) dried and used without further purification.

A solution of 68 mg (4.13 x 10^{-2} mmol, 2 equiv.) of the obtained crude product, 8 mg (2.07 x 10^{-2} mmol, 1 equiv.) of **oPBA** and 15 mg (8.27 x 10^{-2} mmol, 4 equiv.) of $Zn(OAc)_2$

(H_2O-free) were heated under an argon atmosphere in quinoline (4.0 mL) at 160 °C for 15.5 h. The cooled reaction mixture was poured into 50 mL of 2N HCl and stirred for 30 minutes at 40 °C. CH_2Cl_2 (50 mL) was added to the reaction mixture, the resulting two phases were separated, and the organic phase was washed with water and brine and dried over $MgSO_4$. The crude product was purified first by column chromatography with CH_2Cl_2/ethyl acetate 99:1 and successively by preparative HPLC with CH_2Cl_2 (SiO_2, normal phase) and precipitation from CH_2Cl_2/methanol. Compound **ror** was obtained as a red powder (27 mg, 7.41 x 10^{-3} mmol, yield 35% over two steps) $C_{240}H_{230}N_6O_{28}$ (3646.42). Mp > 400 °C. TLC: CH_2Cl_2/ethyl acetate 99:1; R_f = 0.20. **^{1}H NMR** (400 MHz, $CDCl_3$, TMS, 25 °C): δ (ppm) = 8.80 and 8.73 (each d, 8H, ^3J = 7.8 and 8.2 Hz; Per-*H*); 8.29 and 8.24 (bs and s, 8H; Per-*H*); 7.24 – 7.22 (m, 16H; Phen-*H*); 7.11 (s, 4H; Ar-*H*); 7.02 (s, 4H; Ar-*H*); 6.87 – 6.84 (m, 16H; Phen-*H*); 6.36 (t, 4H, ^3J = 7.3 Hz; Ar-*H*); 6.23 and 6.17 (each d, 8H, ^3J = 7.5 and 7.2 Hz; Ar-*H*); 4.51 and 3.18 (each AX, each 4H, ^2J = 13.4 Hz and 14.3 Hz; Ar-C*H$_2$*-Ar); 4.47 and 3.14 (each AB, each 4H, ^2J = 13.6 Hz and 14.3 Hz; Ar-C*H$_2$*-Ar); 4.14 – 4.06 (m, 12H; O-C*H$_2$* and N-C*H$_2$*); 3.65 (t, 8H, ^3J = 6.4 Hz; O-C*H$_2$*); 2.03 – 1.80 (m, 16H; Propyl-*H*); 1.70 – 1.63 (m, 4H; Butyl-*H*); 1.45 – 1.37 (m, 4H; Butyl-*H*); 1.30 and 1.29 (each s, 72H, *tert*-Butyl-Phen-*H*); 1.09 (t, 12H, ^3J = 7.4 Hz; Propyl-*H*); 0.94, 0.91, and 0.87 (each t, 18H, ^3J = 7.3 Hz, 7.5 Hz, and 7.5 Hz, respectively; Propyl-*H* und Alkyl-*H*). **HR-MS** (ESI in $CHCl_3$/acetonitrile): calcd for $C_{240}H_{238}N_8O_{28}$ $[M+2NH_4]^{2+}$ (m/z) 1839.8722; found 1839.8717. **Analysis**: calcd (%) for $C_{240}H_{230}N_6O_{28}$ x H_2O (3664.43): C 78.66; H 6.38; N 2.29; found: C 78.49; H 6.69; N 2.32. **UV/vis** (CH_2Cl_2): λ (nm) [ε ($M^{-1}cm^{-1}$)] = 578 [91600]; 527 [135000]; 491 [77000], 457 [51600]. **Fluorescence** (CH_2Cl_2): $λ_{max}$ (nm) = 608 with $λ_{ex}$ = 490 nm; $Φ_{fl}$ = 0.71.
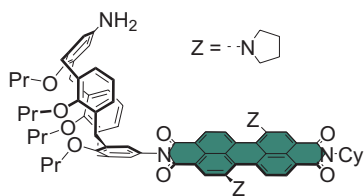
*Compound **rgr***

A portion of 73 mg (4.22 x 10^{-2} mmol, 1 equiv.) of compound **pcD** was dissolved in 2 mL dry CH_2Cl_2 and 3 mL of CF_3COOH were added under an argon atmosphere. The mixture was stirred for 1 hour at room temperature, poured into ice water and adjusted to pH > 9 with NH_3 solution (25%). CH_2Cl_2 (50 mL) was added to the reaction mixture, the two phases were separated, and the organic phase was washed with water and brine and dried over Na_2SO_4. The solvent was removed and the resulting crude product (68 mg; 4.13 x 10^{-2} mmol) dried and used without further purification.

Under an argon atmosphere 68 mg (4.13 x 10^{-2} mmol, 2 equiv.) of the obtained crude product, 11 mg (2.07 x 10^{-2} mmol, 1 equiv.) of **gPBA** and 15 mg (8.27 x 10^{-2} mmol, 4 equiv.) of $Zn(OAc)_2$ (H_2O-free) were heated in distilled quinoline (4.0 mL) at 160 °C for 15.5 h. The cooled reaction mixture was poured into 50 mL of 2N HCl and stirred for 30 minutes at 40 °C. CH_2Cl_2 (50 mL) was added to the reaction mixture, the resulting two phases were separated, and the organic phase was washed with water and brine and dried over $MgSO_4$. The crude product was purified first by column chromatography with CH_2Cl_2/ethyl acetate 99:1 and successively by preparative HPLC with CH_2Cl_2 (SiO_2, normal phase) and finally by precipitation from CH_2Cl_2/methanol. Compound **rgr** was obtained as a dark-violet powder (24 mg, 6.34 x 10^{-3} mmol, yield 30% over two steps). $C_{248}H_{244}N_8O_{28}$ (3784.63). Mp > 400 °C. TLC: CH_2Cl_2/ethyl acetate 99:1; R_f = 0.44. **¹H NMR** (400 MHz, $CDCl_3$, TMS, 25 °C): δ (ppm) = 8.62 (bs, 2H; Per-*H*); 8.55 (bd, 2H, ^3J = 6.6 Hz; Per-*H*); 8.31 and 8.26 (bs and s, 8H; Per-*H*); 7.85 (bd, 2H, ^3J = 7.5 Hz; Per-*H*); 7.26 – 7.22 (m, 16H; Phen-*H*); 7.11 and 7.03 (each s, 8H; Ar-*H*); 6.88 – 6.84 (m, 16H; Phen-*H*); 6.35 (t, 4H, ^3J = 7.5 Hz; Ar-*H*); 6.24 (d, 4H, ^3J = 7.1 Hz; Ar-*H*); 6.15 (d, 4H, ^3J = 6.5 Hz; Ar-*H*); 4.51 and 3.18 (each AX, each 4H, ^2J = 13.1 Hz and 14.7 Hz; Ar-C*H₂*-Ar); 4.48 and 3.14 (each AX, each 4H, ^2J = 13.5 Hz and 14.0 Hz; Ar-C*H₂*-Ar); 4.14 – 4.07 (m, 12H; O-C*H₂* and N-C*H₂*); 3.82 and 3.64 (bs and t, 12H, ^3J = 6.6 Hz; Pyrr-*H*, O-C*H₂*); 2.91 (bs, 4H; Pyrr-*H*); 2.10 – 1.80 (m, 24H; Pyrr-*H*, Propyl-*H*); 1.70 – 1.62 (m, 4H; Alkyl-*H*); 1.45 – 1.36 (m, 4H; Alkyl-*H*); 1.30 and 1.29 (each s, 72H; *tert*-Butyl-Phen-*H*); 1.10 (t, 12H, ^3J = 7.4 Hz; Propyl-*H*); 0.96 – 0.86 (m, 18H; Propyl-*H* and Alkyl-*H*). **HR-MS** (ESI in $CHCl_3$/acetonitrile): calcd for $C_{248}H_{252}N_{10}O_{28}$ $[M+2NH_4]^{2+}$ (m/z) 1908.9301; found

1908.9296. **UV/vis** (CH_2Cl_2): λ (nm) [ε ($M^{-1}cm^{-1}$)] = 703 [43700], 579 [93700], 436 [45300]. **Fluorescence** (CH_2Cl_2): λ_{max} (nm) = 739 with λ_{ex} = 560 nm; Φ_{fl} = 0.19.

Compound pcE

A solution of 100 mg (1.38 x 10^{-2} mmol, 1 equiv.) of calix[4]arene-compound **pcA**, 169 mg (2.76 x 10^{-2} mmol, 2 equiv.) of **gPMI** and 51 mg (2.76 x 10^{-2} mmol, 2 equiv.) of $Zn(OAc)_2$ (H_2O-free) was heated in quinoline (1.5 mL) at 130 °C for 20 h. The cooled reaction mixture was poured into 40 mL of 1N HCl and stirred for 40 minutes at 50 °C. The resulting precipitate was filtered and dissolved in CH_2Cl_2. The solution was washed with water and brine and dried over $MgSO_4$. The crude product was purified by column chromatography with CH_2Cl_2 and subsequent precipitation from CH_2Cl_2/methanol. Compound **pcE** was obtained as a dark-green powder (24 mg, 1.97 x 10^{-3} mmol, yield 14%). It is to note, that these reaction conditions lead to the NH_2-functionalized Calix[4]arene–PBI array **pcE**, and not the expected Boc-functionalized compound, as the Boc-group is cleaved under the applied reaction conditions. $C_{78}H_{81}N_5O_8$ (1216.51). Mp = 356 °C (dec.). TLC: CH_2Cl_2/ethyl acetate 95:5; R_f = 0.20. **^{1}H NMR** (400 MHz, $CDCl_3$, TMS, 25 °C): δ (ppm) = 8.55 (bs, 1H; Per-*H*); 8.47 and 8.45 (d and s, 2H, ^3J = 8.1 Hz; Per-*H*); 8.40 (d, 1H, ^3J = 8.1 Hz; Per-*H*); 7.74 and 7.71 (each d, 2H, ^3J = 8.2 and 8.1 Hz; Per-*H*); 7.02 (s, 2H; Ar-*H*); 6.43 – 6.30 (m, 8H; Ar-*H*); 5.11 – 5.04 (m, 1H; N-C*H*); 4.51 and 3.18 (AX, 4H, ^2J = 13.4 Hz; Ar-C*H*$_2$-Ar); 4.40 and 3.03 (AX, 4H, ^2J = 13.4 Hz; Ar-C*H*$_2$-Ar); 4.07 (t, 2H, ^3J = 8.1 Hz; O-C*H*$_2$); 3.90 and 3.75 and 3.70 (t and bs and t, 10H, ^3J = 8.0 Hz and 6.7Hz; Pyrr-*H* und O-C*H*$_2$); 2.85 (bs, 4H; Pyrr-*H*); 2.65 – 2.57 (m, 2H; Cy-*H*); 2.06 – 1.73 (m, 23H; Pyrr-*H*, Propyl-*H*, Cy-*H*, N*H*$_2$); 1.53 – 1.30 (m, 3H; Cy-*H*); 1.08 (t, 6H, ^3J = 7.5 Hz; Propyl-*H*); 0.93 and 0.91 (each t, 6H, ^3J = 7.6 Hz; Propyl-*H*). **MS** (FAB in NPOE): calcd for $C_{78}H_{81}N_5O_8$ $[M]^+$ (m/z) 1215.6; found 1215.6. **HR-MS** (ESI in acetonitrile/$CHCl_3$): calcd for $C_{78}H_{82}N_5O_8$ $[M+H]^+$ (m/z) 1216.6162; found 1216.6158. **UV/vis** (CH_2Cl_2): λ (nm) [ε ($M^{-1}cm^{-1}$)] = 706 [42700]. **Fluorescence** (CH_2Cl_2): λ_{max} (nm) = 744; Φ_{Fl} = 0.04.

*Compound **og***
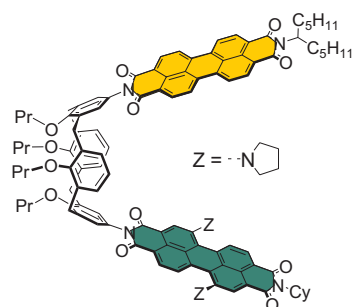
A solution of 21 mg (1.72×10^{-2} mmol, 1 equiv.) of **pcE**, 19 mg (3.45×10^{-2} mmol, 2 equiv.) of **oPMI** and 7 mg (3.45×10^{-2} mmol, 2 equiv.) of $Zn(OAc)_2$ (H_2O-free) was heated in quinoline (0.3 mL) at 155 °C for 15 h. The cooled reaction mixture was poured into 50 mL of 2N HCl and stirred for 30 minutes at 40 °C. CH_2Cl_2 (50 mL) was added to the reaction mixture, the resulting two phases were separated, and the organic phase was washed with water and brine and dried over Na_2SO_4. The crude product was purified first by column chromatography with CH_2Cl_2/ethyl acetate 97:3 and successively by preparative HPLC with CH_2Cl_2 (SiO_2, normal phase) and precipitation from CH_2Cl_2/methanol. Compound **og** was obtained as a light-green powder (7 mg, 4.01×10^{-3} mmol, yield 23%). $C_{113}H_{110}N_6O_{12}$ (1744.12). Mp > 400 °C. TLC: CH_2Cl_2; R_f = 0.07. **^{1}H NMR** (400 MHz, $CDCl_3$, 25 °C) δ (ppm) = 8.79 (bd, 2H, ^3J = 7.9 Hz; Per-*H*); 8.68 – 8.64 (m and s, 7H; Per-*H*); 8.53 – 8.50 (s and bd, 2H, ^3J = 7.8 Hz; Per-*H*); 8.42 (d, 1H, ^3J = 8.0 Hz; Per-*H*); 7.79 and 7.78 (each d, 2H, each ^3J = 8.0 Hz; Per-*H*); 7.14 and 7.13 (each s, 4H; Ar-*H*); 6.44 (t, 2H, ^3J = 7.5 Hz; Ar-*H*); 6.30 and 6.28 (each bd, 4H, ^3J = 8.0 Hz and 7.8 Hz; Ar-*H*); 5.23 – 5.16 and 5.11 – 5.04 (each m, 2H; N-C*H* and Cy-*H*); 4.55 and 3.21 (AX, 4H, ^2J = 13.6 and 13.8 Hz; Ar-C*H$_2$*-Ar); 4.54 und 3.21 (AX, 4H, ^2J = 13.5 und 13.8 Hz; Ar-C*H$_2$*-Ar); 4.17 – 4.12 (m, 4H; O-C*H$_2$*); 3.78 and 3.68 (bs and t, 8H, ^3J = 6.5 Hz; Pyrr-*H* and O-C*H$_2$*); 2.88 and 2.63 – 2.59 (bs and m, 6H; Pyrr-*H*, Cy-*H*); 2.29 – 2.22 (m, 2H; Alkyl-*H*); 2.13 – 1.83 (m, 20H; Pyrr-*H*, Cy-*H*, Alkyl-*H*); 1.79 – 1.73 (m, 3H; Cy-*H*); 1.50 – 1.28 (m, 15H; Cy-*H*, Alkyl-*H*); 1.12 (t, 6H, ^3J = 7.5 Hz; Alkyl-*H*); 0.94 und 0.93 (each t, 6H, each ^3J = 7.5 Hz Alkyl-*H*); 0.84 (t, 6H, ^3J = 7.0 Hz; Alkyl-*H*). **HR-MS** (ESI in acetonitrile/$CHCl_3$): calcd for $C_{113}H_{110}N_6O_{12}$ [M]$^+$ (m/z) 1742.8182; found 1742.8176. **UV/vis** (CH_2Cl_2): λ (nm) [ε ($M^{-1}cm^{-1}$)] = 700 [45200], 525 [89600], 489 [56400]. **Fluorescence** (CH_2Cl_2): λ_{max} (nm) = 741 with λ_{ex} = 490 nm; Φ_{fl} = 0.12.

4.10   Appendix

Femtosecra Transient Absorption Spectra in Toluene and Benzonitrile

Figure 26. Femtosecond transient absorption spectra and corresponding time delays after photoexcitation at 530 nm for compound **or**. Left: in toluene (Tol). **Right**: in benzonitrile (PhCN). The scattered laser pulse is observed for the measurement in benzonitrile.
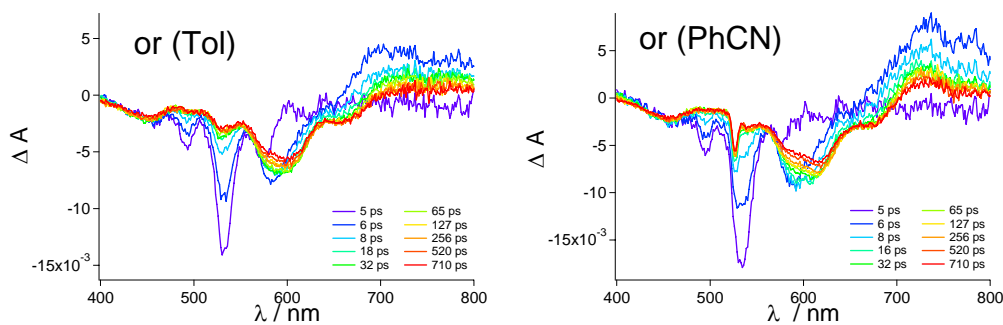

Figure 27. Femtosecond transient absorption spectra and corresponding time delays after photoexcitation at 530 nm for compound **rg**. L**eft**: in toluene (Tol). **Right**: in benzonitrile (PhCN). The scattered laser pulse is observed for the measurement in benzonitrile.
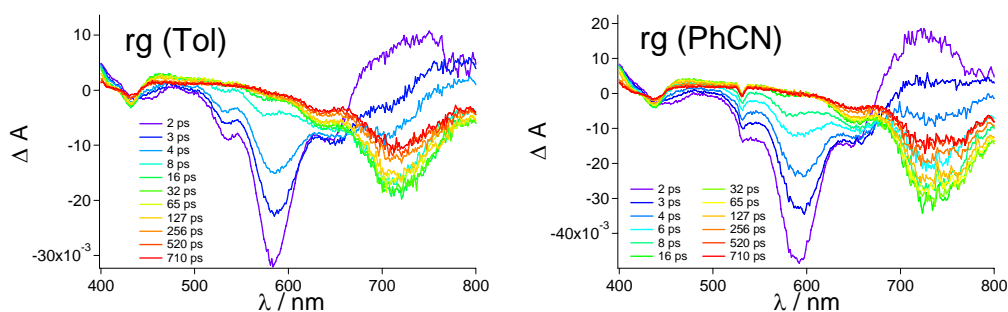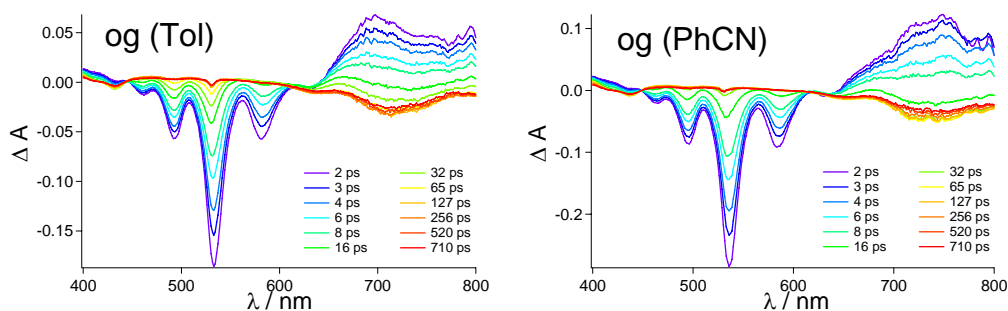

Figure 28. Femtosecond transient absorption spectra and corresponding time delays after photoexcitation at 530 nm for compound **og**. Left: in toluene (Tol). **Right**: in benzonitrile (PhCN).

Representative time-resolved Traces in Toluene and Benzonitrile

Figure 29. Kinetic profiles of the transient absorption in Toluene (Tol) (left) and Benzonitrile (PhCN) (right) of compound **or** (top): measured at 580 nm (black line) and 715 nm (red line); of compound **rg** (middle), measured at 590 nm (black line) and 726 nm (red line); of compound **og** (bottom): measured at 580 nm (black line) and 715 nm (red line).

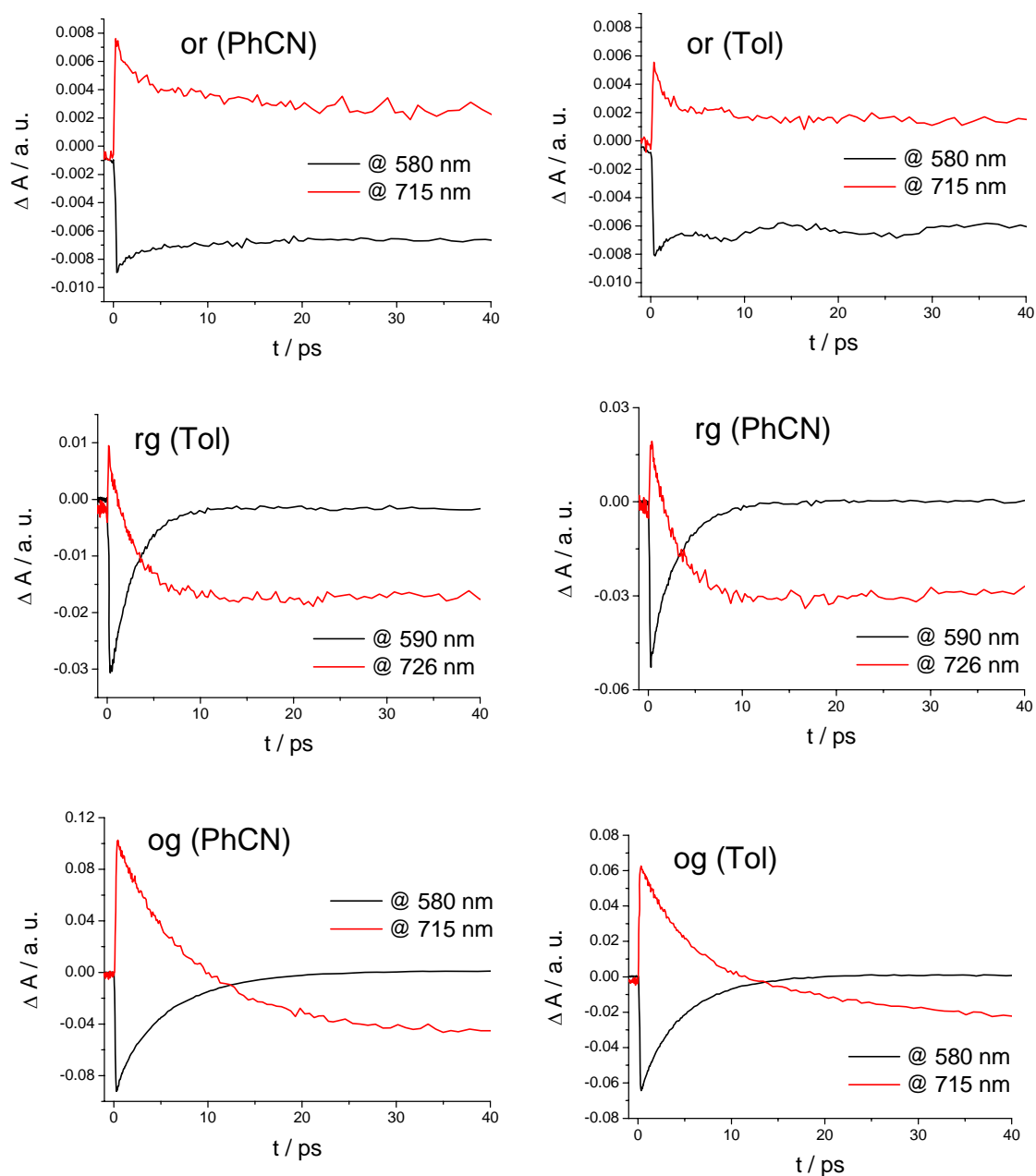## Rate Constants Obtained from Global and Target Analysis

Table 5. Rate constants in CH_2Cl_2 obtained from the global and target analysis of the experimental data employing the model depicted in Figures 14 and 15.

Cmpd	rate constants k (10^{11} s^{-1})				
	ET o*→r*	ET r*→g*	ET o*→g*	CT to (oPBI)$^{\bullet-}$	(oPBI)$^{\bullet-}$
or	6.4			1.2	1.5
oro	6.3			1.34	1.5
ror	12.6			3.3	1.8
rg		4.0			
rgr		3.9			
grg		8.5			
org	7.1	3.9		1.0	0.95
grorg	15.8	3.4		2.2	1.1
og			1.5	0.92	1.2
oc				0.40	1.7
oref				0.00	0.00

[a] Relative precision of the rates is 10%.

4.11   References

(1)   (a) Huber, R. *Angew. Chem., Int. Ed. Engl.* **1989**, *28*, 848–869. (b) Pullerits, T.; Sundström, V. *Acc. Chem. Res.* **1996**, *29*, 381–389. (c) Ritz, T.; Damjanović, A.; Schulten, K. *ChemPhysChem* **2002**, *3*, 243–248. (d) Hu, X.; Ritz, T.; Damjanović, A.; Autenrieth, F.; Schulten, K. *Q. Rev. Biophys.* **2002**, *35*, 1–62. (e) *Molecular Mechanisms of Photosynthesis*; Blankenship, R. E.; Blackwell Science: Oxford, 2002. (f) Cogdell, R. J.; Lindsay, J. G. *New Phytol.* **2000**, *145*, 167–196. (g) Holzwarth, A. R. In *Series on Photoconversion of Solar Energy*; Archer, M. D., Barber, J., Eds.; Imperial College Press: London, UK, 2002; pp 43–115. (h) Katz, J. J. *Photosynth. Res.* **1990**, *26*, 143–160.

(2)   (a) Hoeben, F. J. M.; Jonkheijm, P.; Meijer, E. W.; Schenning, A. P. H. J. *Chem. Rev.* **2005**, *105*, 1491–1546. (b) Wasielewski, M. R. *Chem. Rev.* **1992**, *92*, 435–461. (c) Gust, D.; Moore, T. A.; Moore, A. L. *Acc. Chem. Res.* **2001**, *34*, 40–48. (d) Adronov, A.; Fréchet, J. M. J. *Chem. Commun.* **2000**, 1701–1710. (e) *Comprehensive Supramolecular Chemistry, Vol. 1–11*; Lehn, J.-M., Atwood, J. L., Davies, J. E. D., MacNicol, D. D., Vögtle, F., Eds.; Pergamon: Oxford, 1996. (f) Wasielewski, M. R. *J. Org. Chem.* **2006**, *71*, 5051–5066. (g) Gust, D.; Moore, T. A.; Moore, A. L. *Acc. Chem. Res.* **1993**, *26*, 198–205. (h) Scandola, F.; Indelli, M. T.; Chiorboli, C.; Bignozzi, C. A. *Top. Curr. Chem.* **1990**, *158*, 73–149. (i) Choi, M.-S.; Yamazaki, T.; Yamazaki, I.; Aida, T. *Angew. Chem., Int. Ed. Engl.* **2004**, *43*, 150–158.

(3)   *Supramolecular Dye Chemistry*; Würthner, F., Ed.; Topics in Current Chemistry 258, Springer-Verlag: Berlin, 2005.

(4)   (a) Paddon-Row, M. N. In *Stimulating Concepts in Chemistry*; Vögtle, F., Stoddart, J. F., Shibasaki, M., Eds.; Wiley-VCH: Weinheim, Germany, 2000; pp 267–291. (b) Armaroli, N. *Photochem. & Photobiol. Sci.* **2003**, *2*, 73–87. (c) Barigelletti, F.; Flamigni, L. *Chem. Soc. Rev.* **2000**, *29*, 1–12. (d) Guldi, D. M. *Chem. Soc. Rev.* **2002**, *31*, 22–36. (e) Holten, D.; Bocian, D. F.; Lindsey, J. S. *Acc. Chem. Res.* **2002**, *35*, 57–69. (f) Prodi, A.; Indelli, M. T.; Kleverlaan, C. J.; Alessio, E.; Scandola, F. *Coord. Chem. Rev.* **2002**, *229*, 51–58. (g) Harriman, A.; Sauvage, J.-P. *Chem. Soc. Rev.* **1996**, *25*, 41–48. (h) Nakamura, Y.; Hwang, I.-W.; Aratani, N.; Ahn, T. K.; Ko, D. M.; Takagi, A.; Kawai, T.;

Matsumoto, T.; Kim, D.; Osuka, A. *J. Am. Chem. Soc.* **2005**, *127*, 236–246. (i) Balzani, V.; Juris, A. *Coord. Chem. Rev.* **2001**, *211*, 97–115.

(5)   For light-harvesting linear arrays containing perylene bisimides, see: (a) Prathapan, S.; Yang, S. I.; Seth, J.; Miller, M. A.; Bocian, D. F.; Holten, D.; Lindsey, J. S. *J. Phys. Chem. B* **2001,** *105,* 8237–8248. (b) Rybtchinski, B.; Sinks, L. E.; Wasielewski, M. R. *J. Am. Chem. Soc.* **2004**, *126*, 12268–12269. (c) Langhals, H.; Saulich, S. *Chem. – Eur. J.* **2002**, *8*, 5630–5643. (d) Ego, C.; Marsitzky, D.; Becker, S.; Zhang, J.; Grimsdale, A. C.; Müllen, K.; MacKenzie, J. D.; Silva, C.; Friend, R. H. *J. Am. Chem. Soc.* **2003**, *125*, 437–443. (e) Loewe, R. S.; Tomizaki, K.-Y.; Youngblood, W. J.; Bo, Z.; Lindsey, J. S. *J. Mat. Chem.* **2002**, *12*, 3438–3451. (f) Schlichting, P.; Duchscherer, B.; Seisenberger, G.; Basché, T.; Bräuchle, C.; Müllen, K. *Chem. Eur. J.* **1999**, *5*, 2388–2395. (g) Metivier, R.; Nolde, F.; Müllen, K.; Basché, T. *Phys. Rev. Lett.* **2007**, *98*, 047802/1–047802/4. (h) Hinze, G.; Haase, M.; Nolde, F.; Müllen, K.; Basché, T. *J. Phys. Chem. A* **2005**, *109*, 6725–6729.

(6)   For light-harvesting dendrimers containing perylene bisimides, see: (a) De Schryver, F. C.; Vosch, T.; Cotlet, M.; Van der Auweraer, M.; Müllen, K.; Hofkens, J. *Acc. Chem. Res.* **2005**, *38*, 514–522. (b) Serin, J. M.; Brousmiche, D. W.; Fréchet, J. M. J. *Chem. Commun.* **2002**, 2605–2607. (c) Serin, J. M.; Brousmiche, D. W.; Fréchet, J. M. J. *J. Am. Chem. Soc.* **2002**, *124*, 11848–11849. (d) Gronheid, R.; Stefan, A.; Cotlet, M.; Hofkens, J.; Qu, J.; Müllen, K.; Van der Auweraer, M.; Verhoeven, J. W.; De Schryver, F. C. *Angew. Chem., Int. Ed. Engl.* **2003**, *42*, 4209–4214. (e) Weil, T.; Reuther, E.; Müllen, K. *Angew. Chem., Int. Ed. Engl.* **2002**, *41*, 1900–1904. (f) Gronheid, R.; Hofkens, J.; Köhn, F.; Weil, T.; Reuther, E.; Müllen, K.; De Schryver, F. C. *J. Am. Chem. Soc.* **2002**, *124*, 2418–2419. (g) Jordens, S.; De Belder, G.; Lor, M.; Schweitzer, G.; Van der Auweraer, M.; Weil, T.; Reuther, E.; Müllen, K.; De Schryver, F. C. *Photochem. Photobiol. Sc.* **2003**, *2*, 177–186.

(7)   (a) Sautter, A.; Kaletas, B. K.; Schmid, D. G.; Dobrawa, R.; Zimine, M.; Jung, G.; Van Stokkum, I. H. M.; De Cola, L.; Williams, R. M.; Würthner, F. *J. Am. Chem. Soc.* **2005**, *127*, 6719–6729. (b) You, C.-C.; Hippius, C.; Grüne, M.; Würthner, F. *Chem. Eur. J.* **2006,** *12,* 7510–7519. (c) Flamigni, L.; Ventura, B.; You, C.-C.; Hippius, C.; Würthner, F. *J. Phys. Chem. C* **2007**, *111*, 622–630. (d) Prodi, A.; Chiorboli, C.; Scandola,

F.; Iengo, E.; Alessio, E.; Dobrawa, R.; Würthner, F. *J. Am. Chem. Soc.* **2005**, *127*, 1454–1462. (e) Kaletas, B. K.; Dobrawa, R.; Sautter, A.; Würthner, F.; Zimine, M.; De Cola, L.; Williams, R. M. *J. Phys. Chem. A* **2004**, *108*, 1900–1909.

(8)   (a) Gvishi, R.; Reisfeld, R.; Burshtein, Z. *Chem. Phys. Lett.* **1993**, *213*, 338–344. (b) Langhals, H. *Heterocycles*, **1995**, *40*, 477–500.

(9)   Würthner, F. *Chem. Commun.* **2004**, 1564–1579.

(10)   You, C.-C.; Dobrawa, R.; Saha-Möller, C. R.; Würthner, F. *Top. Curr. Chem.* **2005**, *258*, 39–82.

(11)   For general examples of linear light-harvesting arrays, see: (a) Ziessel, R.; Hissler, M.; El-ghayoury, A.; Harriman, A. *Coord. Chem. Rev.* **1998**, *178-180;* 1251–1298. (b) Aratani, N.; Osuka, A.; Cho, H. S.; Kim, D. *J. Photochem. Photobiol. C* **2002,** *3*, 25–52. (c) Bossart, O.; De Cola, L.; Welter, S.; Calzaferri, G. *Chem. Eur. J.* **2004**, *10*, 5771–5775. (d) Berglund Baudin, H.; Davidsson, J.; Serroni, S.; Juris, A.; Balzani, V.; Campagna, S.; Hammarström, L. *J. Phys. Chem. A* **2002,** *106*, 4312–4319. (e) Chiorboli, C.; Indelli, M. T.; Scandola, F. *Top. Curr. Chem.* **2005**, *257*, 63–102. (f) Harriman, A.; Ziessel, R. *Coord. Chem. Rev.* **1998**, *171,* 331–339. (g) Yang, S. I.; Seth, J.; Balasubramanian, T. Kim, D. Lindsey, J. S.; Holten, D.; Bocian, D. F. *J. Am. Chem. Soc.* **1999**, *121*, 4008–4018.

(12)   (a) Fujita, M. *Chem. Soc. Rev.* **1998**, *27*, 417–425. (b) Stang, P. J.; Olenyuk, B. *Acc. Chem. Res.* **1997**, *30*, 502–518. (c) Würthner, F.; You, C.-C.; Saha-Möller, C. R. *Chem. Soc. Rev.* **2004**, *33*, 133–146. (d) Vollmer, M. S.; Würthner, F.; Effenberger, F.; Emele, P.; Meyer, D. U.; Stümpfig, T.; Port, H.; Wolf, H. C. *Chem. Eur. J.* **1998**, *4*, 260–269. (e) Slone, R. V.; Benkstein, K. D.; Bélanger, S.; Hupp, J. T.; Guzei, I. A.; Rheingold, A. L. *Coord. Chem. Rev.* **1998**, *171*, 221–243. (f) Amijs, C. H. M.; van Klink, G. P. M.; van Koten, G. Dalton Trans., **2006**, 308–327. (g) Seidel, S. R.; Stang, P. J. *Acc. Chem. Res.* **2002**, *35*, 972–983. (h) Drain, C. M.; Lehn, J.-M. *J. Chem. Soc., Chem. Commun.*, **1994**, 2313–2315. (h) Chi, X.; Guerin, A. J.; Haycock, R. A.; Hunter, C. A.; Sarson, L. D. *J. Chem. Soc., Chem. Commun.*, **1995**, 2567–2569. (i) Tsuda, A.; Nakamura, T.; Sakamoto, S.; Yamaguchi, K. Osuka, A. *Angew. Chem. Int. Ed.*, 2002, **41**, 2817–2821. (j) Fan, J.; Whiteford, J. A.; Olenyuk, B.; Levin, M. D.; Stang, P. J.; Fleischer, E. B. *J. Am. Chem.*

Soc. **1999**, *121*, 2741–2752. (k) Slone, R. V.; Hupp, J. T. *Inorg. Chem.* **1997**, *36*, 5422–5423.

(13)   For general examples on light-harvesting dendrimers, see: (a) Dirksen, A.; De Cola, L. *C. R. Chimie* **2003**, *6*, 873–882. (b) *Dendritic Molecules: Concepts, Syntheses, Perspectives*; Newkome, G. R.; Moorefield, C. N.; Vögtle, F., Eds.; VCH: New York, 1996. (c) Balzani, V.; Ceroni, P.; Maestri, M.; Saudan, C.; Vicinelli, V. *Top. Curr. Chem.* **2003**, *228*, 159–191. (d) Venturi, M; Serroni, S.; Juris, A.; Campagna, S.; Balzani, V. *Top. Curr. Chem.* **1998**, 197, 193–228. (e) Hahn, U.; Gorka, M.; Vögtle, F.; Vicinelli, V.; Ceroni, P.; Maestri, M.; Balzani, V. *Angew. Chem., Int. Ed. Engl.* **2002**, *41*, 3595–3598. (f) Balzani, V.; Ceroni, P.; Maestri, M.; Vicinelli, V. *Curr. Opin. Chem. Biol.* **2003**, *7*, 657–665. (g) Balzani, V.; Campagna, S.; Denti, G.; Juris, A.; Serroni, S.; Venturi, M. *Acc. Chem. Res.* **1998**, *31*, 26–34.

(14)   Examples for supramolecular systems containing π–π–stacked perylene bisimides: (a) Würthner, F.; Thalacker, C.; Sautter, A.; Schärtl, W.; Ibach, W.; Hollricher, O. *Chem. Eur. J.* **2000**, *6*, 3871–3886. (b) Peeters, E.; van Hal, P. A.; Meskers, S. C. J.; Janssen, R. A. J.; Meijer, E. W. *Chem. Eur. J.* **2002**, *8*, 4470–4474. (c) Würthner, F.; Chen, Z.; Dehm, V.; Stepanenko, V. *Chem. Commun.* **2006**, 1188–1190. (d) Hernando, J.; De Witte, P. A. J.; Van Dijk, E. M. H. P.; Korterik, J.; Nolte, R. J. M.; Rowan, A. E.; Garcia-Parajó, M. F.; Van Hulst, N. F. *Angew. Chem., Int. Ed. Engl.* **2004**, *43*, 4045–4049. (e) Beckers, E. H. A.; Meskers, S. C. J.; Schenning, A. P. H. J.; Chen, Z.; Würthner, F.; Marsal, P.; Beljonne, D.; Cornil, J.; Janssen, R. A. J. *J. Am. Chem. Soc.* **2006**, *128*, 649–657. (f) Dehm, V.; Chen, Z.; Baumeister, U.; Prins, P.; Siebbeles, L. D. A.; Würthner, F. *Org. Lett.* **2007**, *9*, 1085–1088.

(15)   (a) Talukdar, P.; Bollot, G.; Mareda, J.; Sakai, N.; Matile, S. *J. Am. Chem. Soc.* **2005**, *127*, 6528–6529. (b) Bhosale, S.; Sisson, A. L.; Talukdar, P.; Fürstenberg, A.; Banerji, N.; Vauthey, E.; Bollot, G.; Mareda, J.; Röger, C.; Würthner, F.; Sakai, N.; Matile, S. *Science* **2006**, *313*, 84–86.

(16)   For examples containing perylene bisimides, see: (a) Giaimo, J. M.; Gusev, A. V.; Wasielewski, M. R. *J. Am. Chem. Soc.* **2002**, *124*, 8530–8531. (b) Ahrens, M. J.; Sinks, L. E.; Rybtchinski, B.; Liu, W.; Jones, B. A.; Giaimo, J. M.; Gusev, A. V.; Goshe,

A. J.; Tiede, D. M.; Wasielewski, M. R. *J. Am. Chem. Soc.* **2004**, *126*, 8284–8294. (c) Langhals, H. *Helv. Chim. Acta* **2005**, *88*, 1309–1343. (d) Langhals, H.; Ismael, R. *Eur. J. Org. Chem.* **1998**, 1915–1917. (e) Rybtchinski, B.; Sinks, L. E.; Wasielewski, M. R. *J. Phys. Chem. A* **2004**, *108*, 7497–7505. (f) Van der Boom, T.; Hayes, R. T.; Zhao, Y.; Bushard, P. J.; Weiss, E. A.; Wasielewski, M. R. *J. Am. Chem. Soc.* **2002**, *124*, 9582–9590.

(17)   For other bichromophoric systems, see: (a) Staab, H. A.; Riegler, N.; Diederich, F.; Krieger, C.; Schweitzer, D. *Chem. Ber.* **1984**, *117*, 246–259. (b) Jokic, D.; Asfari, Z.; Weiss, J. *Org. Lett.* **2002**, *4*, 2129–2132. (c) Yu, H.-h.; Pullen, A. E.; Büschel, M. G.; Swager, T. M. *Angew. Chem., Int. Ed. Engl.* **2004**, *43*, 3700–3703. (d) Kadish, K. M.; Frémond, L.; Ou, Z.; Shao, J.; Shi, C.; Anson, F. C.; Burdet, F.; Gros, C. P.; Barbe, J.-M.; Guilard, R. *J. Am. Chem. Soc.* **2005**, *127*, 5625–5631. (e) Chang, C. J.; Loh, Z.-H.; Shi, C.; Anson, F. C.; Nocera, D. G. *J. Am. Chem. Soc.* **2004**, *126*, 10013–10020. (f) Pognon, G.; Boudon, C.; Schenk, K. J.; Bonin, M.; Bach, B.; Weiss, J. *J. Am. Chem. Soc.* **2006**, *128*, 3488–3489. For a trichromophoric example, see: Yagi, S.; Yonekura, I.; Awakura, M.; Ezoe, M.; Takagishi, T. *Chem. Commun.* **2001**, 557–558.

(18)   (a) Neuteboom, E. E.; Meskers, S. C. J.; Meijer, E. W.; Janssen, R. A. J. *Macromol. Chem. Phys.* **2004**, *205*, 217–222. (b) Wang, W.; Wan, W.; Zhou, H.-H.; Niu, S.; Li, A. D. Q. *J. Am. Chem. Soc.* **2003**, *125*, 5248–5249. (c) Wang, W.; Li, L.-S.; Helms, G.; Zhou, H.-H.; Li, A. D. Q. *J. Am. Chem. Soc.* **2003**, *125*, 1120–1121.

(19)   (a) *Calixarenes 2001*; Asfari, Z., Böhmer, V., Harrowfield, J., Eds.; Kluwer Academic Publishers: Dordrecht, 2001. (b) *Calixarenes*; Gutsche, C. D.; The Royal Society of Chemistry: Cambridge, 1993. (c) *Calixarenes Revisited*; Gutsche, C. D.; The Royal Society of Chemistry: Letchworth, 1998. (d) Böhmer, V.; *Angew. Chem., Int. Ed. Engl.* **1995**, *34*, 713–745. (e) *Calixarenes in Action*; Mandolini, L., Ungaro, R., Eds.; Imperial College Press: London, 2000.

(20)   Kenis, P. J. A.; Noordman, O. F. J.; Houbrechts, S.; van Hummel, G. J.; Harkema, S.; van Veggel, F. C. J. M.; Clays, K.; Engbersen, J. F. J.; Persoons, A.; van Hulst, N. F.; Reinhoudt, D. N. *J. Am. Chem. Soc.* **1998,** *120,* 7875–7883.

(21)   See ref. 17c and (a) Zhao, B.-T.; Blesa, M.-J.; Mercier, N.; Le Derf, F.; Sallé, M. *J. Org. Chem.* **2005**, *70*, 6254–6257. (b) Yu, H.-h; Xu, B.; Swager, T. M. *J. Am.*

Chem. Soc. **2003**, *125*, 1142–1143. (c) Scherlis, D. A.; Marzari, N. *J. Am. Chem. Soc.* **2005,** *127,* 3207–3212.

(22)   (a) Schazmann, B.; Alhashimy, N.; Diamond, D. *J. Am. Chem. Soc.* **2006**, *128*, 8607–8614. (b) Souchon, V.; Leray, I.; Valeur, B. *Chem. Commun.* **2006**, 4224–4226. (c) Lee, S. H.; Kim, S. H.; Kim, S. K.; Jung, J. H.; Kim, J. S. *J. Org. Chem.* **2005**, *70*, 9288–9295. (d) Kim, S. K.; Bok, J. H.; Bartsch, R. A.; Lee, J. Y.; Kim, J. S. *Org. Lett.* **2005**, *7*, 4839–4842. (e) Kim, S. K.; Lee, S. H.; Lee, J. Y.; Bartsch, R. A.; Kim, J. S. *J. Am. Chem. Soc.* **2004**, *126*, 16499–16506. (f) Leray, I.; Lefevre, J.-P.; Delouis, J.-F.; Delaire, J.; Valeur, B. *Chem.–Eur. J.* **2001**, *7*, 4590–4598. (g) van der Veen, N.; Flink, S.; Deij, M. A.; Egberink, R. J. M.; van Veggel, F. C. J. M.; Reinhoudt, D. N. *J. Am. Chem. Soc.* **2000**, *122*, 6112–6113. (h) Ji, H.-F.; Dabestani, R.; Brown, G. M.; Sachleben, R. A. *Chem. Commun.* **2000**, 833–834. (i) Ji, H.-F.; Brown, G. M.; Dabestani, R. *Chem. Commun.* **1999**, 609–610. (j) Jin, T.; *Chem. Commun.* **1999**, 2491–2492. (k) Larey, I.; O'Reilly, F.; Habib Jiwan, J.-L.; Soumillion, J.-Ph.; Valeur, B. *Chem. Commun.* **1999**, 795–796. (l) Beer, P. D.; Timoshenko, V.; Maestri, M.; Passaniti, P.; Balzani, V. *Chem. Commun.* **1999**, 1755–1756. (m) Unob, F.; Asfari, Z.; Vicens, J. *Tetrahedron Lett.* **1998**, *39*, 2951–2954. (n) Jin, T.; Monde, K. *Chem. Commun.* **1998**, 1357–1358. (o) Ikeda, A.; Yoshimura, M.; Lhotak, P.; Shinkai, S. *J. Chem. Soc., Perkin Trans. 1*, **1996**, 1945–1950. (p) Grigg, R.; Holmes, J. M.; Jones, S. K.; Norbert, W. D. J. A. *J. Chem. Soc., Chem. Comm.* **1994**, 185–187. (q) Aoki, I.; Sakaki, T.; Shinkai, S. *J. Chem. Soc., Chem. Comm.* **1992**, 730–732. (r) Jin, T.; Ichikawa, K.; Koyama, T. *J. Chem. Soc., Chem. Comm.* **1992**, 499–501.

(23)   (a) Prins, L. J.; Reinhoudt, D. N.; Timmerman, P. *Angew. Chem., Int. Ed.* **2001**, *40*, 2382–2426. (b) Rebek, J., Jr. *Chem. Commun.* **2000**, 637–643. (c) Böhmer, V.; Vysotsky, M. O. *Aust. J. Chem.* **2001**, *54*, 671–677. (d) Conn, M. M.; Rebek, J., Jr. *Chem. Rev.* **1997**, *97*, 1647–1668.

(24)   (a) Steyer, S.; Jeunesse, C.; Armspach, D.; Matt, D.; Harrowfield, J. In *Calixarenes 2001*; Asfari, Z., Böhmer, V., Harrowfield, J., Vicens, J., Eds.; Kluwer: Dordrecht, The Netherlands, 2001; pp 513–535. (b) Fochi, F.; Jacopozzi, P.; Wegelius, E.; Rissanen, K.; Cozzini, P.; Marastoni, E.; Fisicaro, E.; Manini, P.; Fokkens, R.; Dalcanale, E. *J. Am. Chem. Soc.* **2001**, *123*, 7539–7552.

(25)   Seybold, G.; Stange, A. (BASF AG), *Ger. Pat.* DE 35 45 004, 1987 (*Chem. Abstr.*, 1988, **108**, 77134c).

(26)   Zhao, Y.; Wasielewski, M. R. *Tetrahedron Lett.* **1999**, *40*, 7047–7050.

(27)   Vysotsky, M. O.; Böhmer, V.; Würthner, F.; You, C.-C.; Rissanen, K. *Org. Lett*. **2002**, *4*, 2901–2904.

(28)   Van der Boom, T.; Evmenenko, G.; Dutta, P.; Wasielewski, M. R. *Chem. Mater.* **2003**, *15*, 4068–4074.

(29)   (a) Al-Soufi, W.; Reija, B.; Novo, M.; Felekyan, S.; Kühnemuth, R.; Seidel, C. A. M. *J. Am. Chem. Soc.* **2005**, *127*, 8775–8784. (b) Novo, M.; Felekyan, S.; Seidel, C. A. M.; Al-Soufi, W. *J. Phys. Chem. B* **2007**, *111*, 3614–3624.

(30)   Würthner, F.; Ahmed, S.; Thalacker, C.; Debaerdemaeker, T. *Chem. − Eur. J.* **2002**, *20*, 4742–4750.

(31)   (a) Quante, H.; Müllen, K. *Angew. Chem., Int. Ed. Engl.* **1995**, *34*, 1323–1325. (b) Nolde, F.; Pisula, W.; Müller, S.; Kohl, C.; Müllen, K. *Chem. Mat*. **2006**, *18*, 3715–3725. (c) Jung, C.; Müller, B. K.; Lamb, D. C.; Nolde, F.; Müllen, K.; Bräuchle, C. *J. Am. Chem. Soc*. **2006**, *12*8, 5283–5291.

(32)   (a) Ford, W. E.; Kamat, P. V. *J. Phys. Chem.* **1987**, *91*, 6373–6380. (b) Ford, W. E.; Hiratsuka, H.; Kamat, P. V. *J. Phys. Chem.* **1989**, *93*, 6692–6696.

(33)   (a) Hofkens, J.; Vosch, T.; Maus, M.; Köhn, F.; Cotlet, M.; Weil, T.; Herrmann, A.; Müllen, K.; De Schryver, F. C. *Chem. Phys. Lett*. **2001**, *333*, 255–263. (b) Osswald, P.; Leusser, D.; Stalke, D.; Würthner, F. *Angew. Chem., Int. Ed. Engl.* **2005**, *44*, 250–253.

(34)   (a) Lukas, A. S.; Zhao, Y.; Miller, S. E.; Wasielewski, M. R. *J. Phys. Chem. B* **2002**, *106*, 1299–1306. (b) Shibano, Y.; Umeyama, T.; Matano, Y.; Tkachenko, N. V.; Lemmetyinen, H.; Imahori, H. *Org. Lett*. **2006**, *8*, 4425–4428.

(35)   (a) van Stokkum, I. H. M.; Larsen, D. S.; van Grondelle, R. *Biochim. Biophys. Acta* **2004**, *1657*, 82–104. (b) van Stokkum, I. H. M.; Lozier, R. H. *J. Phys. Chem. B* **2002**, *106*, 3477–3485. (c) Mullen, K. M.; van Stokkum, I. H. M. *J. Statistical Software* **2007,** 18. URL http://www.jstatsoft.org/v18/i03/ (d) Global and target analysis

can be performed with e.g., the R package TIMP, see http://cran.r-project.org/doc/packages/TIMP.pdf

(36)   (a) Schweitzer, G.; Gronheid, R.; Jordens, S.; Lor, M.; De Belder, G.; Weil, T.; Reuther, E.; Müllen, K.; De Schryver, F. C. *J. Phys. Chem. A* **2003,** *107,* 3199–3207. (b) De Belder, G.; Jordens, S.; Lor, M.; Schweitzer, G.; De, R.; Weil, T.; Herrmann, A.; Wiesler, U. K.; Müllen, K.; De Schryver, F. C. *J. Photochem. Photobiol. A* **2001**, *145*, 61–70.

(37)   Förster, T. *Ann. Phys.* **1948**, 55–75.

(38)   *Molecular Fluorescence*; Valeur, B.; Wiley-VCH: Weinheim 2002; pp 247–272.

(39)   *Principles of Fluorescence Spectroscopy*; Lakowicz, J. R., Ed.; Kluwer Academic Press: New York 1999; Chapters 13 and 14.

(40)   Pullerits, T.; Heck, S.; Herek, J. L.; Sundström, V. *J. Phys Chem. B* **1997**, *101*, 10560–10567.

(41)   (a) Asahi, T.; Ohkohchi, M.; Matsusaka, R.; Mataga, N., Zhang, R. P.; Osuka, A; Maruyamat, K. *J. Am. Chem. Soc.* **1993,** *115,* 5665–5614. (b) Imahori, H.; Hagiwara, K.; Aoki, M.; Akiyama, T.; Taniguchi, S.; Okada, T.; Shirakawa, M.; Sakata, Y. *J. Am. Chem. Soc.* **1996,** *118,* 11771–11782. (c) Tan, Q.; Kuciauskas, D.; Lin, S.; Stone, S.; Moore, A. L.; Moore, T. A.; Gust, D. *J. Phys. Chem. B* **1997,** *101,* 5214–5223. (d) Armaroli, N.; Accorsi, G.; Song, F.; Palkar, A.; Echegoyen, L.; Bonifazi, D.; Diederich, F. *ChemPhysChem* **2005**, *6*, 732–743.

(42)   Rodríguez-Morgade, M. S.; Torres, T.; Atienza-Castellanos, C.; Guldi, D. M. *J. Am. Chem. Soc.* **2006**, *128*, 15145–15154.

(43)   (a) Würthner, F.; Sautter, A.; Schilling, J. *J. Org. Chem.* **2002**, *67*, 3037–3044. (b) Würthner, F.; Thalacker, C.; Sautter, A.; Schärtl, W.; Ibach, W.; Hollricher, O. *Chem. Eur. J.* **2000**, *6*, 3871–3886.

(44)   (a) Würthner, F.; Stepanenko, V.; Chen, Z.; Saha-Möller, C. R.; Kocher, N.; Stalke, D. *J. Org. Chem.,* **2004**, *69*, 7933–7939. (b) Fuller, M. J.; Sinks, L. E.; Rybtchinski, B.; Giaimo, J. M.; Li, X.; Wasielewski, M. R. *J. Phys. Chem. A* **2005,** *109,* 970–975.

(45)   (a) Kaiser, H.; Lindner, J.; Langhals, H. *Chem. Ber.* **1991**, *124*, 529–535. (b) Nagao, Y.; Naito, T.; Abe, Y.; Misono, T. *Dyes Pigm.* **1996**, *32*, 71–83.

(46)   Würthner, F.; Sautter, A.; Schmid, D.; Weber, P. J. A. *Chem. Eur. J.* **2001**, *7*, 894–902.

(47)   Lukas, A. S.; Zhao, Y.; Miller, S. E.; Wasielewski, M. R. *J. Phys. Chem. B* **2002**, *106*, 1299–1306.

(48)   Prins, L. J.; Jollife, K. A.; Hulst, R.; Timmerman, P.; Reinhoudt, D. N. *J. Am. Chem. Soc.* **2000**, *122*, 3617–3627.

(49)   (a) Demas, J. N.; Grosby, G. A. *J. Phys. Chem.* **1971**, *75*, 991–1024. (b) Sens, R.; Drexhage, K. H. *J. Luminescence* **1981**, *24*, 709–712.

(50)   Vergeer, F. W.; Kleverlaan, C. J.; Stufkens, D. J. *Inorg. Chim. Acta* **2002**, *327,* 126–133.

5

Pinched Cone Equilibria in Calix[4]arenes Bearing Two Identical Perylene Bisimide Dyes

Abstract: A series of bichromophoric compounds **o2c**, **g2c** and **r2c**, respectively, was afforded by the connection of each two identical orange, green or red perylene bisimide (PBI) chromophoric units via a calix[4]arene spacer unit. An equilibrium between the two possible *pinched cone* conformations of the calix[4]arene unit is observed for all three compounds, with one conformation showing a π−stacked sandwich arrangement of the PBI units and the second revealing a non-stacked conformation with the chromophores pointing away from each other. The amount of the π−stacked *pinched cone* calix[4]arene conformation in the equilibrium enhances upon decreasing the sterical demand of the respective PBI unit as well as upon lowering the solvent polarity, in thus increasing the π−π−interactions between the PBI units. Photoexcitation of compound **o2c** in CCl_4 and toluene clearly reveals the spectral features of the π−stacked sandwich conformer. Lifetime values of the excimer-like state have been determined to be 192 ps in CCl_4 and 111 ps in toluene, respectively.

5.1   Introduction

Calix[4]arenes represent one of the most versatile building blocks in supramolecular chemistry.[1] In addition to wide spread applications in molecular recognition[1e] calix[4]arenes have been used as versatile scaffolds to organize functional dye units, such as nonlinear optical dyes,[2] electrophores,[3] and fluorophores.[4] Calix[4]arenes can exist as four conformational isomers in solution, *i.e. cone, partial cone, 1,2-alternate,* and *1,3-alternate* (defined by the orientation of the respective phenolic rings towards each other and the linking methylene bridges). The *cone* isomer of calix[4]arenes can be conformationally fixed in solution,[5] but interestingly, the thus rigidified skeleton still reveals some remaining flexibility. Hence, *cone* isomers of calix[4]arenes are known to undergo geometric changes that vary the distance between two opposite phenol rings.[6] Accordingly, the averaged C_{4V} symmetry found for calix[4]arenes in the *cone* conformation can be interpreted in terms of a rapid interconversion between two equivalent so-called *pinched cone* isomers showing C_{2V} symmetry, *e.g.* showing a geometric arrangement with the two opposite aromatic rings almost parallel, while the other two rings adopt a flattened position. However, upon substitution in the *para*-positions of the phenolic units the two *pinched cone* conformations are not equivalent any more, and as a consequence a shift of the equilibrium towards one favorable isomer is expected, depending on the nature of the substituents and also on the interactions between the substituting units.[7]

Among the available classes of functional π–systems perylene bisimides (PBIs) are outstanding with regards to their fluorescence emission (quantum yields up to unity) and n-type semiconducting properties.[8] They represent important photo- and electroactive building blocks in supramolecular dye chemistry[9-11] with excellent emissive properties[12] and high absorption coefficients and photochemical stability. Different types of intermolecular forces such as hydrogen bonding, π–π stacking and metal–ion interactions have been applied to direct the formation of desirable supramolecular structures of PBIs.[8,11,12] Perylene bisimide dyes and their assemblies find application as functional units in artificial light-harvesting systems,[13] photoinduced electron transfer systems,[14] and organic electronic devices such as organic light emitting diodes (OLED),[15] organic thin-

film transistors (OTFT),[16] and solar cells.[17] The perylene bisimide chromophore can be easily fine-tuned by proper substitution in the so-called *bay*-positions to exhibit quite divers electronic and optical properties. As such, the classes of phenoxy-(*red*),[18] and pyrrolidino-(*green*)[19] *bay*-substituted perylene bisimides as well as the core-unsubstituted (*orange*)[20] PBI dyes are available.

Substitution of two opposing phenolic rings of the calix[4]arene moiety in the *para*-positions with perylene bisimides leads to the formation of bichromophoric systems. Owing to the intrinsic flexibility of the calix[4]arene spacer unit two energetically non-equivalent *pinched cone* species are formed, with one conformer showing π-stacked (PBI residues pointing towards each other) and the other conformer showing non-stacked geometry (PBI residues pointing away from each other). Both species can interconvert into each other, and a schematic representation of this conformational equilibrium is shown in Figure 1. In contrast to this tweezer-type flexible spacer unit, other examples of bichromophoric architectures of dyes are typically limited either to rigid spacer systems without structural flexibility[21,22] or to arrangements of less defined geometry.[23,24] The interconversion process between the two conformational states and hence the position of the equilibrium should be substantially influenced by the impact of the π–π-stacking between the chromophoric planes, that is governed, first, by solvent effects and, second, by the sterical demand of the spacious aromatic systems. As a consequence, proper fine-tuning of all these parameters should enable a controlled adjustment of the conformational equilibrium to afford a switchable bichromophoric system.

Accordingly, in this Chapter the synthesis and photophysical properties of a series of bichromophoric compounds **o2c**, **g2c** and **r2c**, respectively, are elucidated. The latter are afforded by the combination of each two orange, green and red PBI chromophoric units connected by a calix[4]arene spacer unit via the N-imide position of the chromophore. Within this series the three types of PBI substituents used are characterized by their increasing sterical demand depending on the bulkiness of the substituents in the *bay*-positions, ranging from the *orange* chromophore (proton substitution, with UV/vis absorption maxima at 526 and 490 nm in CH_2Cl_2) via the *green* chromophore (pyrrolidino-*bay*-functionalization, showing an UV/vis absorption maximum at 701nm in CH_2Cl_2) to the *red* phenoxy-*bay*-substituted perylene bisimide moiety (with an UV/vis absorption

maximum at 578 nm in CH$_2$Cl$_2$). The sterical demand of the individual chromophore, as well as solvent polarity effects, will strongly affect the interactions between the respective spacious aromatic π-systems and, as a consequence, the position of the equilibrium between π-stacked and non-stacked *pinched cone* conformation of the calix[4]arene unit will substantially be influenced. For a schematic representation of the conformational equilibrium see Figure 1.
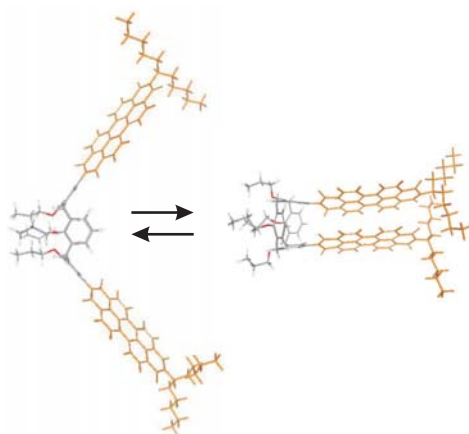

Figure 1. Schematic representation of the equilibrium between non-stacked (left) and π-stacked (right) *pinched cone* conformation of the calix[4]arene unit upon substitution with two orange PBI units (for chemical structure see compound **o2c** in Scheme 1). Molecular structures obtained from force field calculations (Macromodel 8.0, potential MMFF). Color of the PBI chromophore is applied for clarity.

The conformation dependent photophysical properties of these bichromophoric systems are studied by means of UV/vis absorption, steady state and time-resolved emission, and femtosecond transient absorption spectroscopy, and a spectrotemporal analysis of the femtosecond transient absorption data is accomplished. The compounds studied as well as their syntheses and the structures of the related reference systems (without calix[4]arene substitution) are shown in Scheme 1. Thus, three compounds containing *one* perylene bisimide chromophore connected to a calix[4]arene unit (**oc**, **gc** and **rc**), which are further on also referred to as *"monomers"* (for details see Chapter 3); and three compounds containing *two* perylene bisimide moieties linked by one calix[4]arene unit (**o2c**, **g2c** and **r2c**), which are further on also referred to as *"dimers"*; and furthermore the three reference systems containing no calix[4]arene units (**oref**, **gref** and **rref**) are studied.

5.2   Synthesis and Structural Characterization

Scheme 1. Synthetic routes and chemical structures of PBI–calix[4]arene dimers and respective reference compounds studied.[a]
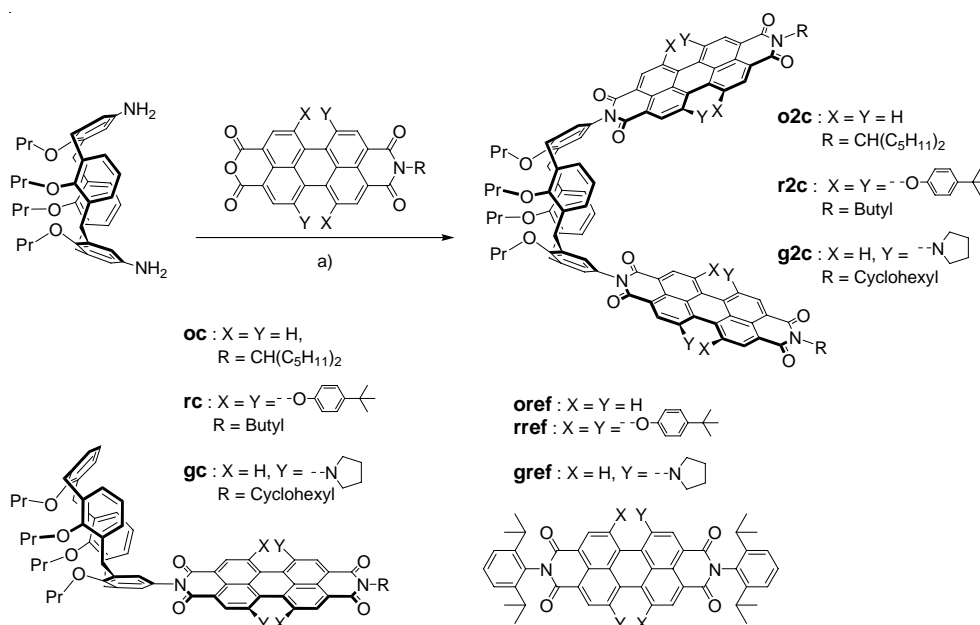
[a] Reagents and conditions: a) for compound **o2c**: Zn(OAc)$_2$, quinoline, 165 °C, yield 55%; for compound **g2c**: Zn(OAc)$_2$, quinoline, 130 °C, yield 32%; for compound **r2c**: Et$_3$N, toluene, 125 °C, yield 82%. For details on compounds **oc**, **gc**, and **rc** see Chapter 3.

The studied perylene bisimide–calix[4]arene arrays were synthesized according to Scheme 1. For this purpose, one equivalent of 5,17-diamino-25,26,27,28-tetrakis(propyloxy)-calix[4]arene was reacted with three different types (orange, green and red) of perylene monoimide monoanhydrides to yield the twofold perylene bisimide-substituted calix[4]arene compounds **o2c**, **g2c** and **r2c.** The imidization was carried out either in refluxing toluene/Et$_3$N (for compound **r2c**) or in quinoline (at 165 °C for compound **o2c** and at 130 °C for compound **g2c**, respectively), using Zn(OAc)$_2$ as a catalyst. The monocalix[4]arene-substituted compounds **oc**, **gc**, and **rc** that are also shown in Scheme 1 were obtained under similar reaction conditions (for details see Chapter 3). All products were purified by column chromatography (SiO$_2$) and were characterized by ^{1}H NMR spectroscopy, high resolution mass spectrometry and elemental analysis.

Single crystals of compound **r2c** suitable for an X-ray analysis were obtained by slow crystallization from chloroform/methanol solution at room temperature. The molecule presents a pseudo twofold symmetry coincident with the calix[4]arene symmetry axis (see Figure 2, left). Two perylene units are oriented away from each other on opposite sides of the calix[4]arene unit which is considerably distorted towards a *pinched cone* conformation. Both the perylene fragments do not exhibit a flat π-system but rather a propeller-like twisted conformation between their respective naphthalene half units, as already observed for other *bay*-substituted perylene bisimides.[8] The measured torsional angle of 29.4° is comparable with the value of 25° measured for other perylene derivative bearing tetraphenoxy-substituents at the *bay*-positions of the PBI core.[25] Noteworthy, the two PBI units are twisted in different directions to afford P and M helical configurations, respectively. Accordingly the whole molecule is found in the *meso* form. This can be seen from the views of the molecular structure depicted in Figure 2, left, and Figure 3, bottom (view of PBI units along the N bound to the calix[4]arene to the N bearing the butyl chain). The dihedral angles formed by the calix[4]arene C26/C28 and C25/C27 phenyl rings are 2.6(5)° and 75.4(2)°, and correspondingly the C26-C28 and C25-C27 distances are 5.22(1) and 9.86(1) Å, respectively. The dihedral angles between the calix[4]arene phenyl rings and a "reference plane" passing through the four CH_2-methylene bridges of the calix[4]arene are 39.0(2)° for the phenyl ring containing the carbon atom C25 atom (phenyl rings are indicated by C label, see Figure 2), 87.3(2), 36.4(2), and 89.9(2)° for the phenyl unit containing the carbon atoms C26, C27, and C28, respectively. The torsion angles around the N1-C25 and N3-C27 bonds are -72.2(8)° (C(17)-C(25)-N(1)-C(34)), 109.4(8)° (C(17)-C(25)-N(1)-C(30)), 105.8(8)° (C(18)-C(25)-N(1)-C(34)), and -72.6(8) (C(18)-C(25)-N(1)-C(30)) for the N1-C25 bond; and the correspondent values about the N3-C27 bond are 68.7(9), -104.3(8), -108.9(8), and 78.1(8)°. Surprisingly, the crystal packing reveals a pair of molecules that is related by an inversion center in such a way that *inter*molecular π–π-stacking of the aromatic perylene systems is enabled at a mean distance of about 4.0 Å (see Figure 2, right and Figure 3 top). Accordingly, no *intra*molecular π–π-interaction has been found within the red dimer system **r2c** in the
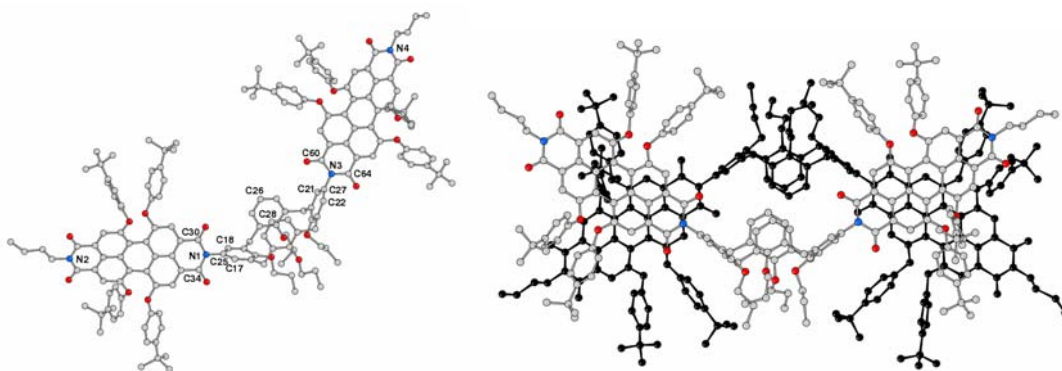
166

Figure 2. Molecular structure of **r2c** with hydrogen atoms omitted for clarity (left) and view of the crystal packing of a pair of molecules related by a center of symmetry (right).
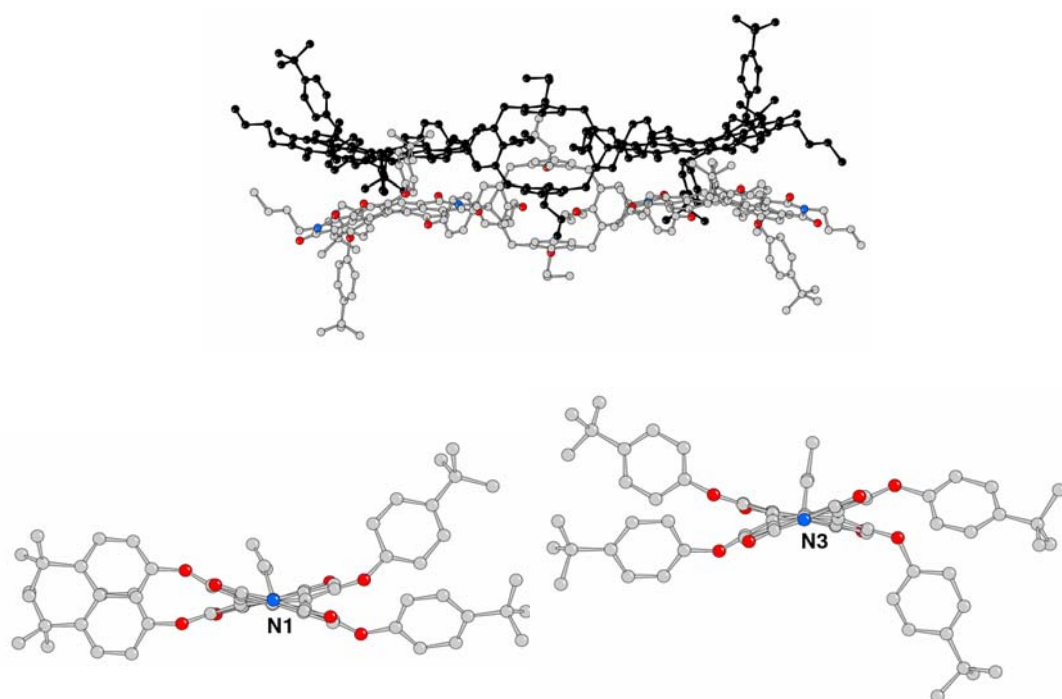

Figure 3. View of the crystal packing of pair of molecules of compound **r2c** related by a center of symmetry (top) and views of perylene bisimide units along the N-N axis showing the twisted backbone (bottom).

solid state. The unit cell has 32.0% of void volume accessible for solvent and a total of six disordered molecules of $CHCl_3$ were found in the asymmetric unit cell.

5.3 ^{1}H NMR Studies

The ^{1}H NMR spectra in CDCl$_3$ of the monomeric compounds **oc**, **gc**, and **rc**, as well as those of the dimeric compounds **o2c**, **g2c**, and **r2c** are sharp at room temperature. A section of the obtained spectra showing the signals of the Ar-CH$_2$-Ar protons of the calix[4]arene moiety is exemplarily depicted in Figure 4. The observed signals correspond to the symmetry expected for the respective substitution pattern of the calix[4]arene moiety. Accordingly, *two* pairs of doublets for the protons of the methylene bridges are observed for the monomeric compounds **oc**, **gc** and **rc** (in agreement with *one* symmetry plane passing through the PBI substituted phenolic ring of the calix[4]arene and through its non-substituted counterpart), whereas for the dimeric compounds **o2c**, **g2c**, and **r2c** *one* pair of doublets for the protons of the methylene bridges is found (in agreement with *two* symmetry planes present in the molecule).

When changing to the less polar solvent CCl$_4$, the signals of the Ar-CH$_2$-Ar protons in the ^{1}H NMR spectra of compound **oc** remain sharp at room temperature (see Figure 4). In contrast, the spectra of compound **o2c** in CCl$_4$ show a pronounced broadening of the doublet at higher field. A similar behavior is also found for the spectra of compounds **g2c** and **r2c** in CCl$_4$ (see Figure 4), and apparently, the Ar-CH$_2$-Ar signals of the calix[4]arene moiety are strongly influenced upon lowering the solvent polarity. As discussed above, an equilibrium between the two possible *pinched cone* conformations of the calix[4]arene unit is expected for the dimeric compounds; with one conformation showing π–stacked arrangement of the PBI units and the second conformation revealing non-stacked geometry as the PBI units point away from each other. Hence, the ^{1}H NMR data should reveal the spectral features of both the π–stacked and the non-stacked *pinched cone* conformations, respectively, being in equilibrium with each other. The fact that only one set of sharp signals is detected in the ^{1}H NMR spectra in CDCl$_3$ may be rationalized either by the fast interconversion between the two possible *pinched cone* conformations on the NMR time scale and that hence the observed spectra correspond to the weighted average of the signals, or by the slow interconversion of the isomers on the NMR time scale, with hence the clear prevalence of one of the two *pinched cone* conformations. Rationalized by the absence of any line broadening effects in the spectra and based on our UV/vis absorption data (see below), however, we may assume the prevalence of the non-stacked *pinched cone*
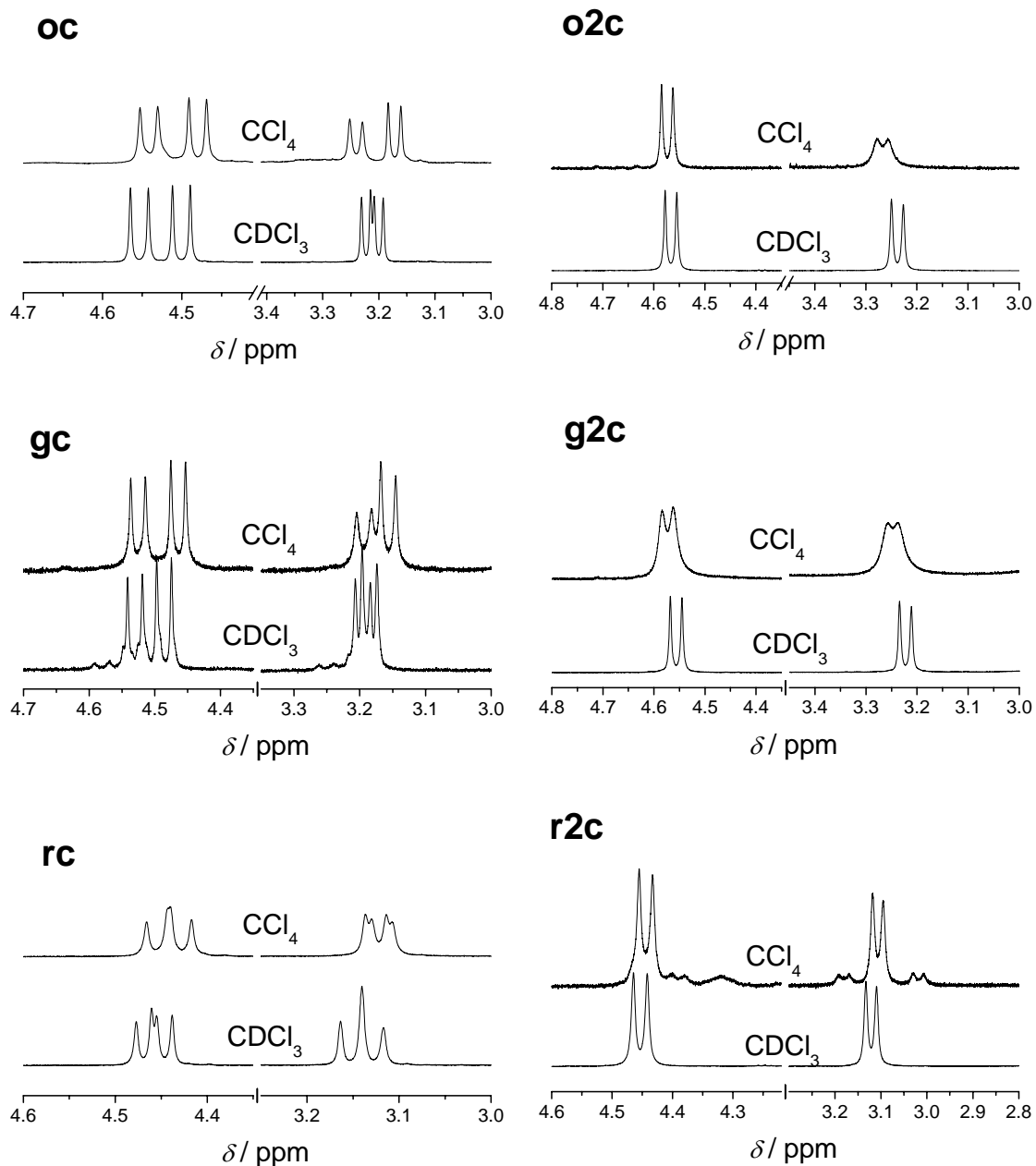
168

Figure 4. Sections of ^{1}H NMR spectra (600 MHz, room temperature) showing the signals of the Ar-CH$_2$-Ar protons of the respective calix[4]arene moiety in CCl$_4$ (top line) and CDCl$_3$ (bottom line) as indicated above in the individual spectra. Top: compound **oc** (left) and compound **o2c** (right). Middle: compound **gc** (left) and compound **g2c** (right). Bottom: compound **rc** (left) and compound **r2c** (right).

conformation. Upon lowering the solvent polarity the $\pi-\pi$-interactions between the PBI units become more pronounced,[8] and accordingly the equilibrium is shifted towards the $\pi-$stacked *pinched cone* conformation, a fact which influences the ^{1}H NMR signals of the Ar-CH$_2$-Ar protons substantially, and as a result, no sharp lines are observed any more. Accordingly, we assume the equilibrium in CCl$_4$ to be substantially shifted towards the $\pi-$stacked *pinched cone* conformation, whereas in the more polar solvent CDCl$_3$ the non-stacked conformation is assumed to be the prevalent one.

To further elucidate this behavior, we conducted variable temperature ^{1}H NMR measurements in CCl$_4$ for all three compounds **o2c**, **g2c**, and **r2c**, respectively, in the range from 273 K to 234 K for compounds **o2c** and **g2c**, and in the range from 273 K to 325 K for compound **r2c**. A section of the obtained spectra showing the signals of the Ar-CH$_2$-Ar protons of the respective calix[4]arene moiety is depicted in Figure 5. Lowering the temperature to around 273 K did result in a more pronounced broadening of the signals in the ^{1}H NMR spectra of compounds **o2c** and **g2c**, respectively. Upon increasing temperature the signals remain broadened up to 315 K suggesting the presence of the $\pi-$stacked conformation also at higher temperatures. In contrast, in the spectra at lower temperatures of compound **r2c** two smaller doublets are observed additionally to the signals present in CDCl$_3$, which vanish upon heating the sample at around 315 K. As expected, for both compounds **o2c** and **g2c**, respectively, the equilibrium between the two *pinched cone* conformations is shifted upon increasing temperature towards the non-stacked conformer resulting in an averaged sharp signal with no spectral differentiation between the two species. In contrast, for compound **r2c** a controversial effect is observed which might be attributed to the dissociation of a dimerized species present at lower temperatures prior to the shift of the equilibrium (compare also structure in the solid state in Figures 2 and 3).
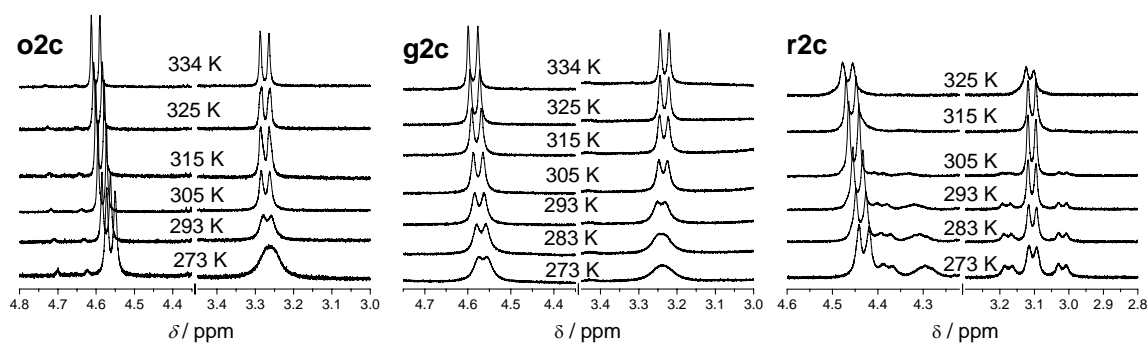
Figure 5. Sections of variable temperature ^{1}H NMR spectra (600 MHz, in CCl$_4$) of compounds **o2c** (left), **g2c** (middle), and **r2c** (right) showing the signals of the Ar-CH$_2$-Ar protons of the respective calix[4]arene moiety. Temperatures are indicated above in the individual spectra.

5.4   UV/vis Absorption Properties

The dimeric compounds **o2c**, **g2c** and **r2c** as well as their respective monomeric compounds **oc**, **gc**, and **rc** and the reference compounds without calix[4]arene substitution **oref**, **gref** and **rref** were characterized by means of UV/vis absorption and steady state fluorescence emission spectroscopy in solvents of varying polarity employing methylcyclohexane (MCH, $\varepsilon_r = 2.0$), tetrachloromethane (CCl$_4$, $\varepsilon_r = 2.2$), toluene ($\varepsilon_r = 2.4$), dichloromethane (CH$_2$Cl$_2$, $\varepsilon_r = 8.9$) and benzonitrile (PhCN, $\varepsilon_r = 25.9$). The related spectroscopic data are summarized in Table 1. The UV/vis absorption spectra of all monomeric and dimeric compounds obtained in various solvents are depicted in Figure 6. The UV/vis absorption curves have been normalized for better comparison of the band shapes varying with changing solvent polarity.

The spectra of the *monomeric orange* compound **oc** show the characteristic vibronic UV/vis absorption pattern of the orange perylene bisimide chromophore in all solvents, thus being in good agreement with the spectral data obtained for the orange reference compound **oref** (for values of band maxima and molar extinction coefficients see Table 1, and for spectra see Figure 6). A modest hypsochromic shift of the band maximum from 530 nm (in benzonitrile) to 517 nm (in MCH) is observed for compound **oc**, which also closely relates to a similar solvent dependent shift found for compound **oref** from 531 nm to 517 nm (see Table 1). Furthermore, the values found for the ratio of the first and second

171

absorption band (here denoted as (0,0)/(0,1)) range between 1.65 and 1.70 for compound **oc** and **oref** in all solvents (see Table 1), which thus indicates the presence of monomeric, non-aggregated PBI dyes.[8]

Table 1. Steady state optical properties in various solvents at room temperature.[a]

Cmpd.		MCH	CCl$_4$	Toluene	CH$_2$Cl$_2$	Benzonitrile
oc	λ_{max} [ε]	517 [96400]	523 [94800]	527 [86400]	526 [91600]	530 [88900]
		480 [56500]	487 [56600]	491 [52500]	489 [55200]	493 [53500]
	λ_{max} [Φ_{Fl}]	520,558 [0.01]	526,566 [0.02]	534,576 [0.02]	535,573 [0.03]	537,579 [0.02]
	(0,0)/(0,1)[b]	1.70	1.68	1.65	1.65	1.66
o2c	λ_{max} [ε]	522 [67100][c]	525 [89700]	527 [114600]	526 [164200]	530 [162000]
		486 [106500]	489 [95800]	490 [90700]	490 [106700]	493 [103400]
	λ_{max} [Φ_{Fl}]	522,562 [<0.01]	527,569 [<0.01]	532,574 [<0.01]	536,577 [0.03]	538,580 [0.03]
	(0,0)/(0,1)[b]	0.63	0.94	1.26	1.54	1.57
oref	λ_{max} [ε]	517 [93700]	523 [96800]	527 [92200]	527 [93600]	531 [91100]
		480 [55200]	487 [57500]	490 [55800]	490 [56000]	494 [54500]
	λ_{max} [Φ_{Fl}]	521,561 [~1.00][d]	527,569 [~1.00][d]	535,579 [~1.00][d]	534,576 [0.99]	540,583 [~1.00][d]
	(0,0)/(0,1)[b]	1.70	1.68	1.65	1.67	1.67
gc	λ_{max} [ε]	664 [44900]	680 [43300]	686 [43100]	701 [47300]	705 [45600]
	λ_{max} [Φ_{Fl}]	685 [0.41]	704 [0.37]	721 [0.29]	742 [0.19]	748 [0.17]
g2c	λ_{max} [ε]	709 [30700][c]	680 [67600]	686 [66500]	706 [92400]	706 [83800]
		657 [33300]				
	λ_{max} [Φ_{Fl}]	684,756 [<0.01]	706 [0.12]	723 [0.27]	744 [0.22]	750 [0.17]
gref	λ_{max} [ε]	669 [44700]	686 [44100]	692 [46100]	709 [43000]	710 [45200]
	λ_{max} [Φ_{Fl}]	691 [0.39]	708 [0.34]	727 [0.24]	748 [0.19]	753 [0.18]
rc	λ_{max} [ε]	564 [45600]	572 [47900]	573 [47300]	578 [47400]	580 [43800]
	λ_{max} [Φ_{Fl}]	588 [~1.00][d]	596 [0.99]	600 [~1.00][d]	608 [0.80]	614 [0.81]
r2c	λ_{max} [ε]	571[72200]	573 [90100]	573 [92800]	580 [92200]	581 [88000]
		534 [49800]				
	λ_{max} [Φ_{Fl}]	588 [0.29]	596 [~1.00][d]	600[~1.00][d]	612 [0.79]	615 [0.82]
rref	λ_{max} [ε]	567 [47400]	578 [50600]	579 [49800]	582 [49700]	586 [46500]
	λ_{max} [Φ_{Fl}]	593 [0.96]	604 [0.96]	608 [0.97]	615 [0.99]	620 [0.95]

[a] Values for ε are given in (M^{-1}cm^{-1}) and values of λ_{max} in (nm). [b] Denoting the ratio of first and second absorption band. [c] Precipitation from solution after ca. 30 minutes. [d] $\Phi_{Fl} \pm 0.02$.

The absorption spectra of the *dimeric orange* compound **o2c** are depicted in Figure 6. The spectrum in the most polar solvent benzonitrile shows the characteristic maxima of the orange perylene bisimide chromophore with bands at 530 and 493 nm very similar to those of the monomeric compound **oc** (see above), but reveals almost doubled values for the molar extinction coefficient of ε(PhCN) = 162000 M^{-1}cm^{-1} for the band at 530 nm. Hence, the absorption spectrum of compound **o2c** in benzonitrile consists of the absorption features of its constitutive two orange PBI units, confirming an insignificant interaction between the chromophores in the ground state in benzonitrile. Neither, additional absorption bands emerged nor did the absorption maxima shift to longer or shorter wavelengths. The band shapes and overall spectral features are very similar to those of
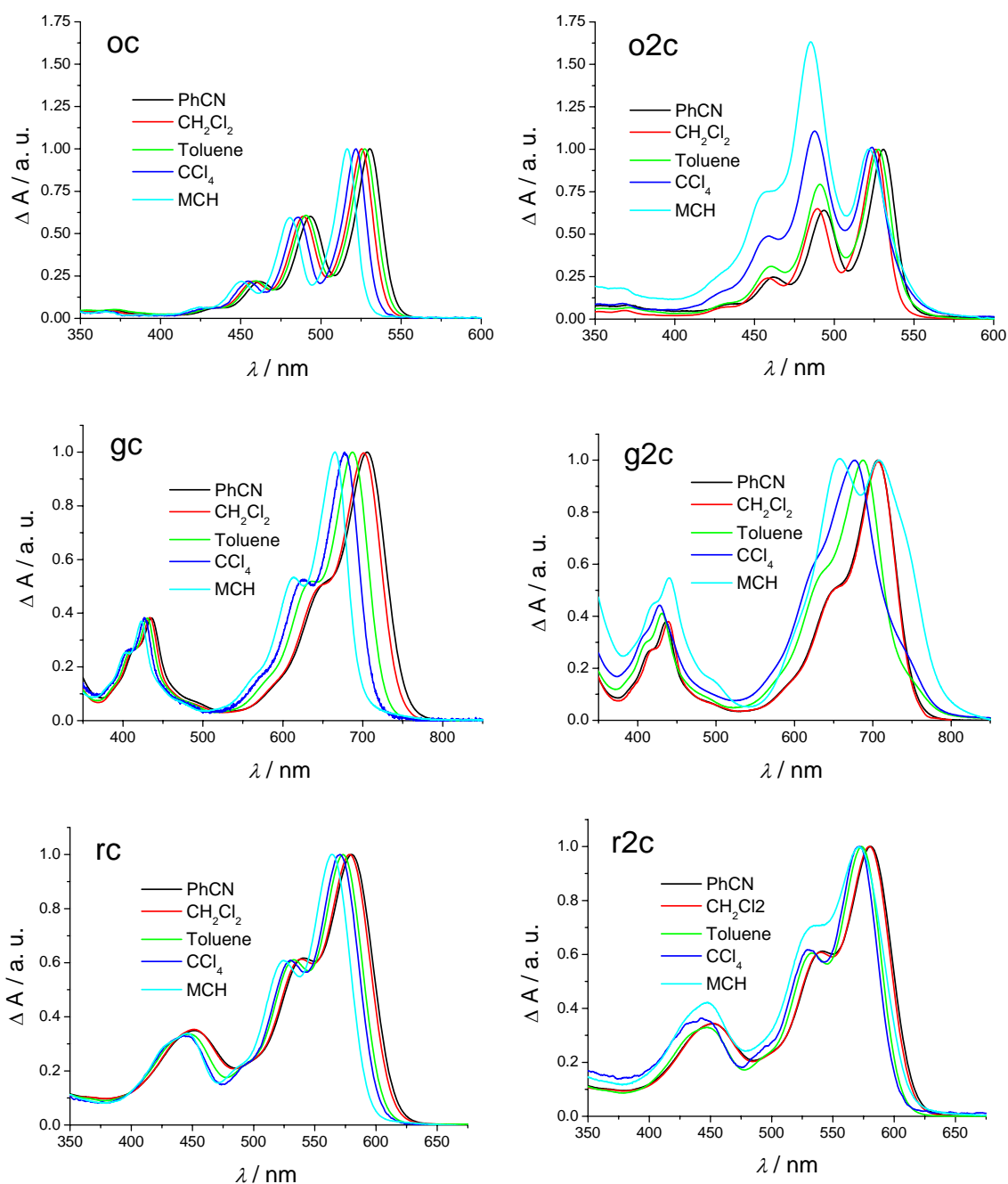
Figure 6. Normalized UV/vis absorption spectra in benzonitrile (PhCN, black line), CH$_2$Cl$_2$ (red line), toluene (green line), CCl$_4$ (blue line) and methylcyclohexane (MCH, cyan line). Top: compound **oc** (left) and compound **o2c** (right). Middle: compound **gc** (left) and compound **g2c** (right). Bottom: compound **rc** (left) and compound **r2c** (right).

compound **oc**, accordingly. Only for the (0,0)/(0,1) ratio a slightly decreased value of 1.57 is observed. In contrast, when changing to solvents of lower polarity the spectral features of the dimeric compound **o2c** differ significantly from those of the monomer **oc**. Thus, the absorbance around 490 nm shows a dramatic increase relative to that around 525 nm for all solvents (for the respective changes in the molar extinction coefficients refer to Table 1). Accordingly, values for the (0,0)/(0,1) ratio are found to be 1.54 in CH_2Cl_2, 1.26 in toluene, 0.94 in CCl_4, and 0.63 in MCH, respectively.

These spectral features are typical for $\pi-\pi$-stacked PBI chromophores in a sandwich-type arrangement, where the transition dipole moments of the dye units are cofacially arranged.[26-28] For such an arrangement, the strong excitonic coupling results in a hypsochromically shifted main absorption band (called H-band) compared to non-aggregated PBI dye units. As illustrated in Figure 1, the two possible *pinched cone* conformations of the calix[4]arene unit are characterized by one conformation showing $\pi-$stacked arrangement of the PBI units and the second conformation revealing non-stacked geometry as the PBI units point away from each other. Hence, the UV/vis absorption curves (shown in Figure 6) reveal the spectral features of both the $\pi-$stacked and the non-stacked *pinched cone* conformations, respectively, which are in equilibrium with each other. For the first conformation, the two PBI chromophores are $\pi-$stacked in a parallel sandwich-type geometry with almost no longitudinal offset. A hypsochromic spectral shift is expected for such H-type aggregates as observed in the low polarity solvents (see Figure 6).[26,27] For the other *pinched cone* conformation with non-stacked arrangement of the PBI chromophores we may expect almost unchanged spectra compared to those of the orange monomers **oc** and **oref** due to the almost orthogonal orientation of the transition dipole moments of the two dye units and the significant distance between the chromophores. Indeed, these spectral features of non-aggregated chromophores are observed for the more polar solvents CH_2Cl_2 and benzonitrile. Accordingly, these solvent dependent spectra reveal a shift of the equilibrium between the two *pinched cone* conformations upon lowering the solvent polarity towards the $\pi-$stacked species. Hence, upon lowering the solvent polarity the spectral features of the $\pi-$stacked *pinched cone* conformation are enhanced, whereas for polar solvents those of the non-stacked conformation clearly dominate the spectra.

Likewise, as observed for the orange compounds **oc** and **oref** also the spectra of the *green monomeric* compounds **gc** and **gref** exhibit the characteristic UV/vis absorption maxima of the green perylene bisimide chromophore in all solvents (see Figure 6), for values of band maxima and molar extinction coefficients refer to Table 1. Thus, no significant changes in the general band shapes are observed upon lowering the solvent polarity. On the other hand, the positive solvatochromism is much more pronounced resulting in a spectral shift from 664 nm in MCH to 705 nm in benzonitrile for compound **gc** and from 669 nm in MCH to 710 nm in benzonitrile for compound **gref** which is in accordance with the pronounced charge transfer character of the $S_0 \rightarrow S_1$ transition for the green chromophore.[29] The related spectra of the *green dimeric* compound **g2c** are also shown in Figure 6. No indication for the formation of a π−stacked *pinched cone* conformation of the calix[4]arene unit in an H-type aggregation arrangement is observed for the spectra in the polar solvents benzonitrile, CH_2Cl_2, and toluene, which closely resemble the spectra of **gc** and **gref** in these solvents. In contrast to the monomeric compound **gc**, however, the spectra of the dimeric derivative **g2c** in CCl_4 reveal a loss of fine-structure and broadening of the band, and in the spectra in MCH a splitted band with two maxima at 657 nm and 709 nm is observed, respectively. These findings again confirm the presence of an equilibrium between the two possible *pinched cone* conformations in compound **g2c**, which is shifted towards the π−stacked species in the low-polarity solvent MCH and also to a smaller extends in CCl_4.

Finally, all spectra of the *red* compounds **rc**, **rref** and **r2c** (see spectra in Figure 6) show the characteristic UV/vis absorption maxima of the red perylene bisimide chromophore, for values of band maxima and molar extinction coefficients see Table 1. No significant changes in the band shapes are observed upon lowering the solvent polarity, and for all three compounds a modest hypsochromic shift of the UV/vis absorption maxima from benzonitrile to MCH is observed. For the *red dimeric* compound **r2c** (see Figure 6) only in MCH a small enhancement of the band at 534 nm is observed that might indicate a small amount of π−stacked *pinched cone* conformation or of a dimerized species present even at this low concentration (also see previous section).

In conclusion, the π−π-interactions between the two PBI units are far more pronounced for the orange dimeric system **o2c** than for the green dimeric derivative **g2c** and for the red

compound **r2c**. This effect very likely originates from the increased sterical hindrance of the dye units due to the more space demanding pyrrolidinyl and *tert*-butylphenoxy substituents in the *bay*-positions of the PBI chromophore, which reduces the chromophoric interaction between the aromatic π–systems accordingly. This increasing sterical hindrance is clearly illustrated by the molecular structures obtained from force field calculations (Macromodel 8.0, potential MMFF) shown in Figure 7. Depicted are the respective non-stacked (Figure 7, top) and π–stacked conformers (Figure 7, middle and bottom). The latter furthermore reveal that for all three π–stacked conformers the inward-oriented parallel PBI substituents are twisted relative to the calix[4]arene core to reach an optimal π–π-stacking of the spacious aromatic systems (see Figure 7, bottom).
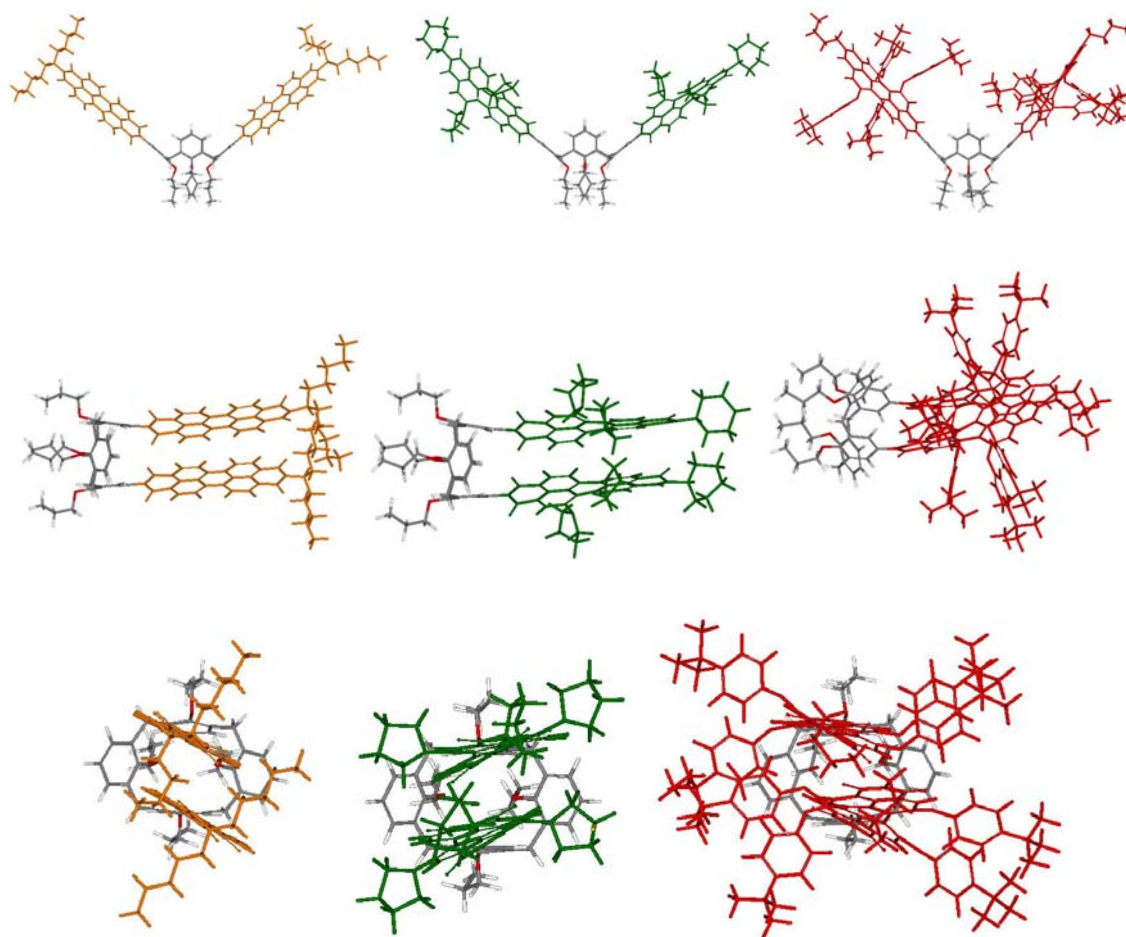
Figure 7. Molecular structures obtained from force field calculations (Macromodel 8.0, potential MMFF) of the non-stacked (top) and the π–stacked (middle and bottom) *pinched cone* conformation of compounds **o2c** (left), **g2c** (middle), and **r2c** (right). Shown is furthermore the view along the N-N axis of the PBI unit (bottom). Color of the respective PBI chromophores is applied for clarity.

5.5   Temperature Dependent UV/vis Absorption Spectra

The UV/vis absorption data depicted in Figure 6 reveal an equilibrium between the two possible *pinched cone* conformations of the calix[4]arene (with one conformation showing π−stacked arrangement of the PBI units and the second conformation revealing non-stacked geometry; see above) for the orange system **o2c** in toluene, CCl_4 and MCH, and also for the green compound **g2c** in MCH and to a small extend in CCl_4; whereas for the red derivative **r2c** almost no spectral changes upon lowering the solvent polarity are observed. These spectral changes have been attributed to an *intra*molecular interaction of the PBI dye units for both the systems **o2c** and **g2c**, respectively (see below and previous section). To exclude the presence of *inter*molecular PBI aggregates at the given concentrations, temperature dependent UV/vis absorption measurements have been carried out that are depicted in Figure 8 and in Figure 9. For entropic reasons *inter*molecular aggregates would dissociate into the respective monomer species at higher temperatures,[30] and the absorption spectra at higher temperatures would thus reveal the spectral features of the monomer species accordingly. In contrast, the interactions within *intra*molecular aggregates would not be changed with respect to the increasing temperature and thus the UV/vis absorption spectra upon heating of the solution would not be influenced substantially. Accordingly, UV/vis absorption spectra of the dimeric compounds **o2c**, **g2c** and **r2c** in CCl_4 as well as those of their related monomers **oc**, **gc**, and **rc** were recorded as a function of the temperature in the range from 20 to 70 °C, with heating steps of 10 °C (see Figure 8).[i] For comparison, the temperature dependent UV/vis absorption spectra of the perylene bisimide reference compounds **oref**, **gref** and **rref** have also been obtained under similar experimental conditions (see Figure 9). For all compounds the spectral changes observed on changing the temperature are fully reversible because the original spectra at 20°C were recovered after cooling the sample from 70 °C. Remarkably, the UV/vis absorption spectra of **o2c** and **g2c** in CCl_4 (see Figure 8) show that both compounds remain π−stacked also at very low concentrations of ca. 5.0 x 10^{-6} M^{-1} (for **g2c**

---

[i] Note, that CCl_4 was chosen as a solvent because precipitation of compounds **o2c** and **g2c** is observed after approximately 30 minutes for the solution of both compounds in MCH, respectively.
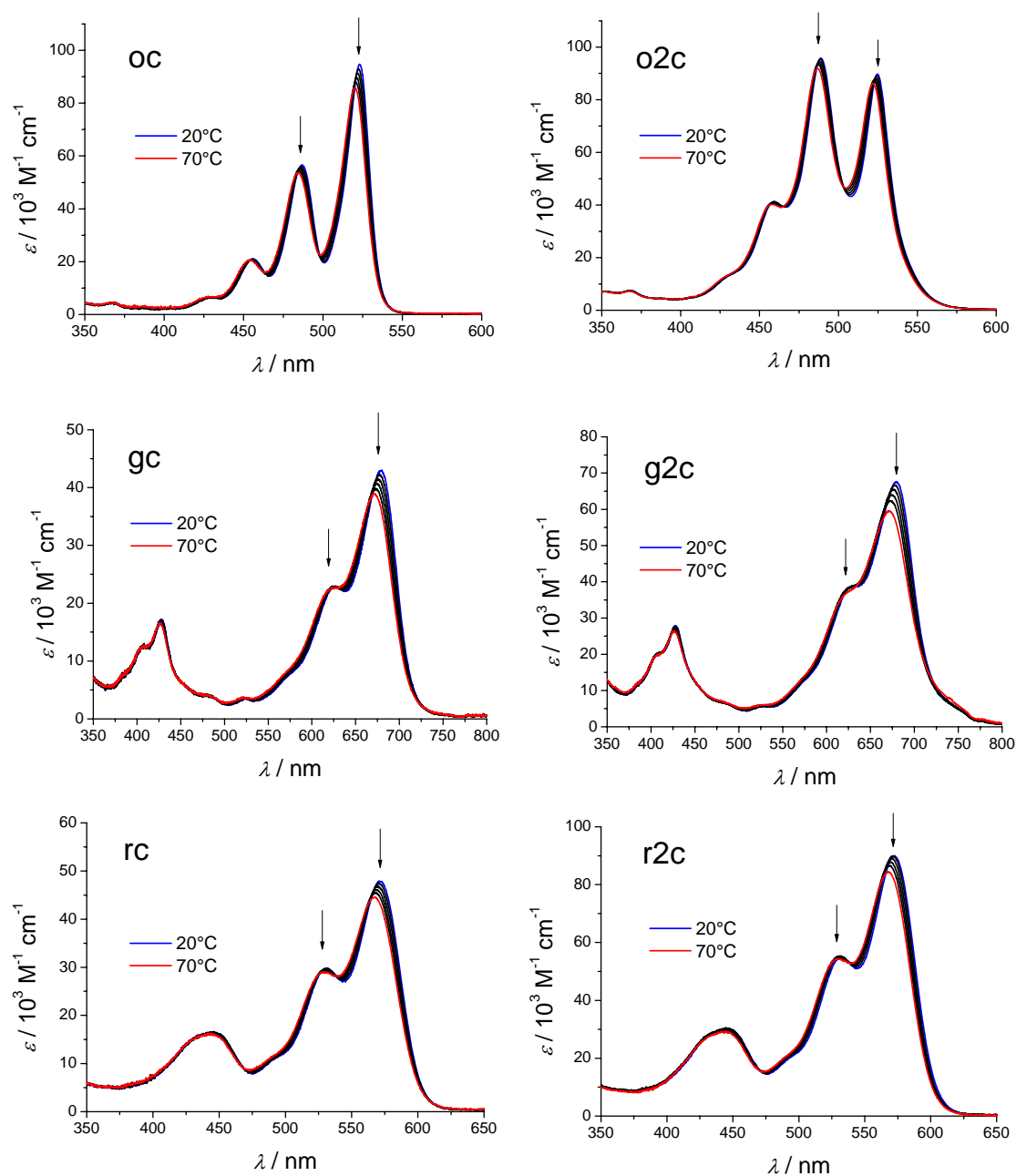
Figure 8. UV/vis absorption spectra of variable temperatures in CCl$_4$. Top: compounds **oc** (left, c = 4.56 x 10^{-6} M) and **o2c** (right, c = 5.83 x 10^{-6} M). Middle: compounds **gc** (left, c = 5.09 x 10^{-6} M) and **g2c** (right, c = 5.84 x 10^{-6} M). Bottom: compounds **rc** (left, c = 5.09 x 10^{-6} M) and **r2c** (right, c = 4.70 x 10^{-6} M). Concentrations given at 20°C. Arrows indicate trends upon rising temperature. Spectra are corrected for density changes due to rising temperature.

please refer to the broadened band shape observed in the spectra of **g2c** compared to the narrow spectral features observed for compound **gc**). This π–stacking can only be attributed to an intramolecular aggregation of the PBI chromophores because an *inter*molecular aggregate would show strong concentration dependence in the UV/vis spectra.[30] No substantial change in band shape upon increasing temperature is observed for the red systems **rc** and **r2c**, respectively.

Notably, all UV/vis absorption spectra show a small blue shift with increasing temperature, and a slightly reduced intensity of the absorption bands. These spectral changes are observed for both the monomeric and dimeric series **oc**, **gc**, **rc** and **o2c**, **g2c**, **r2c**, respectively, as well as for their respective reference compounds without calix[4]arene substitution **oref**, **gref** and **rref** (for spectra see Figures 8 and 9). Accordingly, the observed effects are independent of the respective PBI unit as well as of the calix[4]arene substitution of the chromophore. This hypsochromic shift is thus attributed to a decrease of the dielectric constant CCl_4 with increasing temperature,[ii] and the reduced absorption coefficient to the broadening of the absorption band is due to the population of more conformations at higher temperature.

[ii] This is supported by the fact, that for compound **oref** a hypsochromic shift of the band maximum from 523 nm in CCl_4 (with a relative permittivity of ε@293K = 2.24) to 517 nm in MCH (ε@293K = 2.02) is observed. Hence, lowering the solvent polarity of Δε ≈ 0.2 leads to a spectral shift of about 6 nm. For the permittivity value in CCl_4 at 343 K a value of ε = 2.14 is found, and accordingly an increase of temperature between 293 K and 343 K as shown in Figures 8 and 9 leads to a reduced permittivity of Δε ≈ 0.1, resulting in a hypsochromic shift of the band maximum of 3 nm from 523 nm (T = 293 K) to 520 nm (T = 343 K). Similar behavior is also found for compound **gref** (with 17 nm shift upon solvent change from CCl_4 to MCH with Δε ≈ 0.2, and with 8 nm shift upon temperature variation in CCl_4 with Δε ≈ 0.1) and compound **rref** (with 11 nm shift upon solvent change from CCl_4 to MCH with Δε ≈ 0.2, and with 5 nm shift upon temperature variation in CCl_4 with Δε ≈ 0.1). For permittivity values and related temperature dependence see: *CRC Handbook of Chemistry and Physics*; Lide, D. R. Ed.; CRC Press: Boca Raton, USA, 1995, 76th Edition.
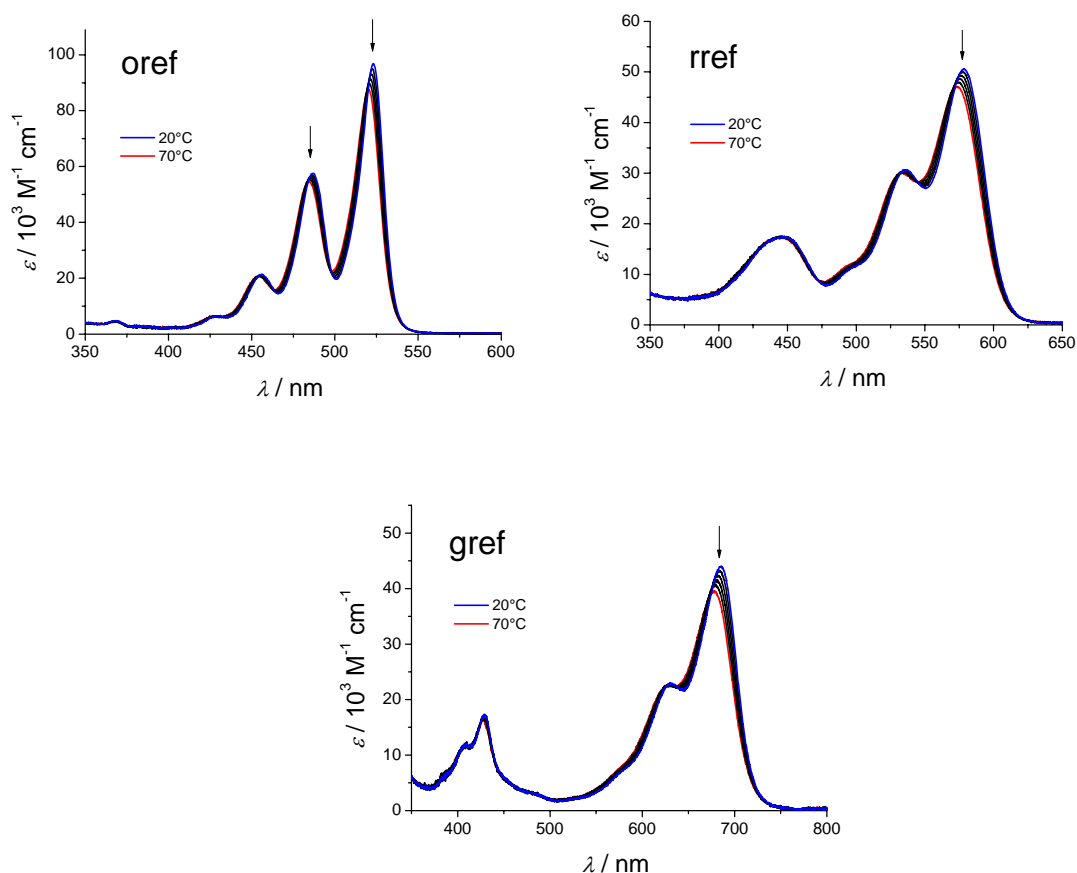
Figure 9. UV/vis absorption spectra of variable temperatures in CCl$_4$. Top left: compound **oref** (c = 4.96 x 10^{-6} M). Top right: compound **rref** (c = 4.89 x 10^{-6} M). Bottom: compound **gref** (c = 3.83 x 10^{-6} M). Concentrations are given at 20°C. Arrows indicate trends upon rising temperature. Spectra are corrected for density changes due to rising temperature.

5.6 Steady State Fluorescence Emission Properties

All compounds have been investigated by steady state fluorescence spectroscopy, and the values obtained for quantum yields and band maxima in the various solvents are summarized in Table 1. The fluorescence emission spectra in the various solvents are shown in Figure 10. The emission spectra of compound **oc** show the characteristic vibronic progressions of a non-aggregated orange PBI being in good agreement with those of the orange reference compound **oref** (for the respective emission maxima see Table 1); they are showing a hypsochromic shift of 17 nm from 537 nm in benzonitrile to 520 nm in
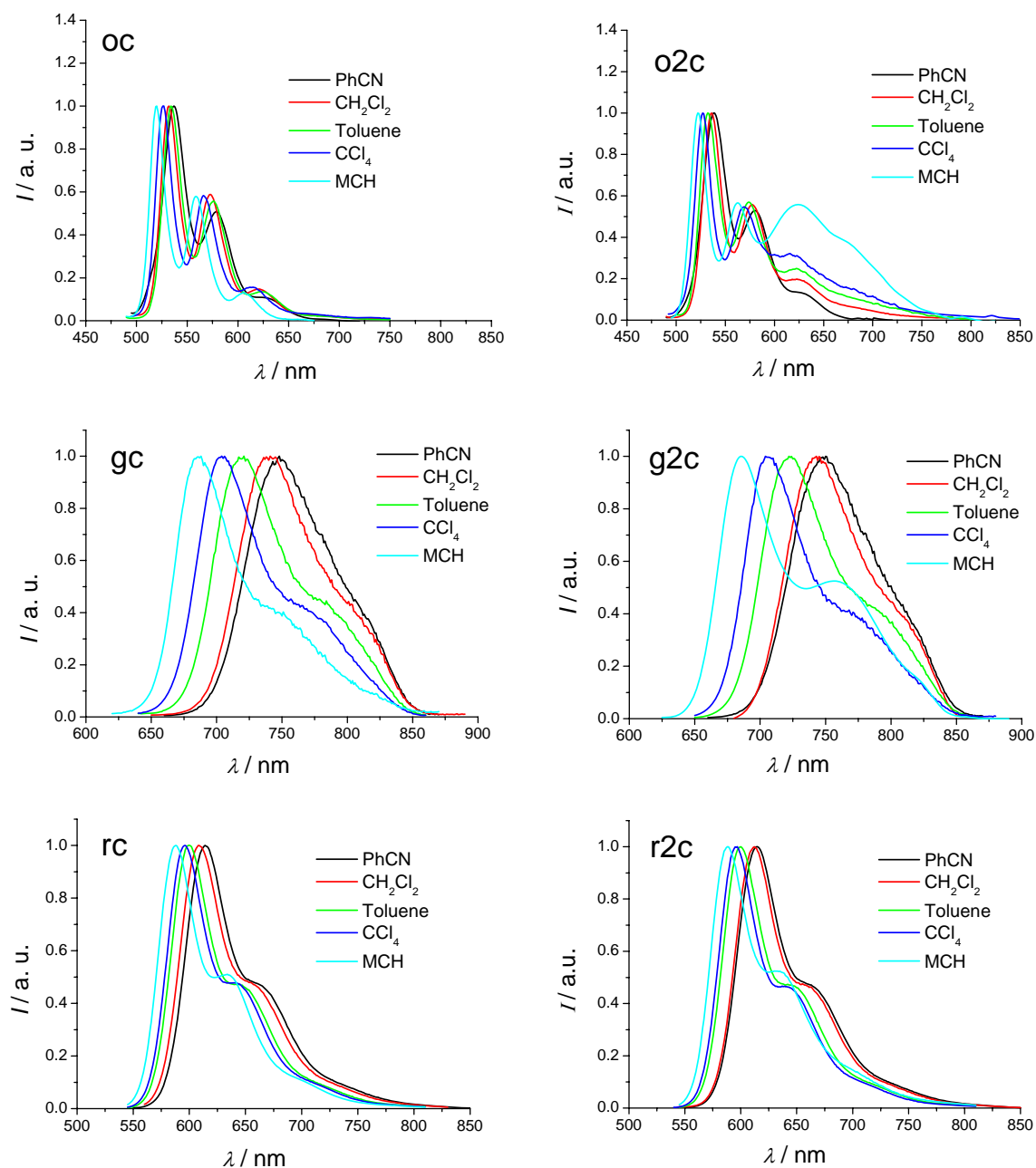
Figure 10. Normalized steady state fluorescence emission spectra in benzonitrile (PhCN, black line), CH$_2$Cl$_2$ (red line), toluene (green line), CCl$_4$ (blue line) and methylcyclohexane (MCH, cyan line) under dilute conditions (OD of the respective solution < 0.05). Top: compound **oc** (left) and compound **o2c** (right). Middle: compound **gc** (left) and compound **g2c** (right). Bottom: compound **rc** (left) and compound **r2c** (right).

MCH for compound **oc** due to solvatochromic effects similar like already observed in the UV/vis absorption spectra (see Table 1). In contrast, the spectra of the dimeric compound **o2c** depicted in Figure 10 reveal an additional broad red-shifted emission band at around 650 nm for all solvents, accompanied by a hypsochromic shift of the band maximum of 16 nm when changing from benzonitrile to MCH (see Table 1). The broad emission feature is increasing in intensity upon lowering the solvent polarity and becomes most pronounced in MCH. Furthermore, the values for the fluorescence quantum yields for the dimeric compound **o2c** decrease in solvents of lower polarity (values of or $\Phi_{fl} = 0.03$ in both benzonitrile and CH_2Cl_2; and $\Phi_{fl} = <0.01$ in toluene, CCl_4, and MCH, respectively, are observed for compound **o2c**; see Table 1), whereas for the respective monomeric compound **oc** comparably higher values are found (see Table 1).[iii] The observed broad spectral features can be attributed to an "excimer-type" emission resulting from π−stacked PBI chromophores.[28] Hence, also in the steady state fluorescence spectra a solvent polarity dependent competition between the emission from "monomeric" and π−stacked arrangement of the PBI units is observed, which was found already for the UV/vis absorption spectra. This again confirms the presence of an equilibrium between the two possible *pinched cone* conformations of the calix[4]arene unit (one π−stacked and one non-stacked arrangement of the PBI units, see above). The fluorescence quantum yields (given in Table 1) also support this trend, as solvent polarity dependent fluorescence quenching is observed, being typical for π−stacked sandwich aggregates of H-type arrangement.

The emission spectra of both the monomeric and dimeric *green* compounds **gc** and **g2c** show the characteristic fluorescence spectral features of a monomeric green PBI chromophore in benzonitrile, CH_2Cl_2, toluene, CCl_4 (for the respective emission maxima see Table 1), which are in reasonable agreement with the respective emission maxima of the green reference compound **gref** (see Table 1). Furthermore, a hypsochromic shift of 63 nm is found for compound **gc** (from 748 nm in benzonitrile to 685 nm in MCH) and of 66

[iii] Note, that due to the efficient photoinduced electron transfer process discussed in Chapter 3 between the electron-poor orange PBI unit and the electron-rich calix[4]arene substituent the quantum yield of the orange PBI chromophore is strongly quenched already for the non-aggregates species for both compounds **o2c** and **oc**, respectively. In contrast, the non calix[4]arene-substituted orange reference compound **oref** reveals quantum yields of almost unity in all five solvents (see Table 1 and Chapter 3).

nm for compound **g2c** (from 750 nm in benzonitrile to 684 nm in MCH), respectively, due to the pronounced solvatochromie of this charge transfer transition (compare UV/vis absorption spectra, and see Table 1). Only the spectrum of compound **g2c** in MCH reveals a distinct additional broad emission band at around 756 nm. Furthermore, the fluorescence quantum yields determined for compound **g2c, gc** and **gref** (given in Table 1) show very similar values in benzonitrile (Φ_{fl} = 0.17 – 0.18), in CH_2Cl_2 (Φ_{fl} = 0.19 – 0.22) and in toluene (Φ_{fl} = 0.24 – 0.27), but very different values in CCl_4 and MCH. Thus, a strong fluorescence quenching is observed for compound **g2c** in CCl_4 and MCH (Φ_{fl} = 0.12 in CCl_4 and Φ_{fl} < 0.01 in MCH) compared to those for the respective monomeric compound **gc** (Φ_{fl} = 0.37 in CCl_4 and Φ_{fl} = 0.41 in MCH) and to those of the green reference compound **gref** without calix[4]arene substitution (Φ_{fl} = 0.34 in CCl_4 and Φ_{fl} = 0.39 in MCH). These findings corroborate the presence of an equilibrium between the two possible *pinched cone* conformations of the calix[4]arene unit (one π−stacked and one non-stacked arrangement of the PBI units) for compound **g2c** in MCH, and these results thus closely mirror the observations made for the UV/vis absorption spectra of **g2c**. The π−π-stacking in the green system is, however, only observed for the spectra in MCH and to a lesser extend in CCl_4 which is most likely due to the increased sterical hindrance of the substituents in the *bay*-positions of the PBI chromophore (see above), that destabilize the close van der Waals contact between the two π−surfaces.

In accordance with this notion almost no changes in the emission spectra as a function of solvent polarity of the *red* monomeric and dimeric compounds **rc** and **r2c**, respectively, are observed. As for the UV/vis absorption spectra, also for the fluorescence emission spectra only for the lowest polarity solvent MCH a small spectral change is observed, leading to a slight band enhancement at 534 nm for the red dimeric compound **r2c** (see Figure 10). Furthermore, this trend is mirrored in the values for the fluorescence quantum yields. Accordingly, the quantum yields for compound **r2c** and **rc** show very similar values in benzonitrile (Φ_{fl} = 0.81 – 0.82), in CH_2Cl_2 (Φ_{fl} = 0.79 – 0.80), in toluene and in CCl_4 (around unity for both compounds), whereas for the red reference compound **rref** for all five solvents quantum yields around unity are observed (see Table 1). Only in MCH, a strong fluorescence quenching is observed for compound **r2c** indicating the formation of

the π−stacked conformer (Φ_{fl} = 0.29) in comparison to those of compounds **rc** and **rref**, respectively (for both compounds around unity).

5.7   Time-resolved Emission Spectroscopy

The fluorescence lifetimes of all compounds have been determined and the respective data are summarized in Table 2. For the *orange* reference compound **oref** fluorescence lifetimes between 3.9 ns and 4.9 ns have been determined, showing no dependence on solvent polarity. For both compounds **oc** and **o2c**, a drastically shortened fluorescence lifetime compared to the value of the orange reference compound **oref** is found which has been attributed to a very efficient photoinduced electron transfer process (k_{CT} = 3.1 x 10^{10} s^{-1} in CH_2Cl_2) between the electron-poor orange PBI unit and the electron-rich calix[4]arene substituent (see Chapter 3). The observed lifetimes for **oc** are thus reduced to values lower than the system response of approximately 150 ps, whereas for compound **o2c** lifetime values in the range of the system response of about 150 ps are measured (see Chapter 3). Notably, the fluorescence lifetime data of compound **o2c** reveal biexponential decays in all solvents. Accordingly, a fraction of the total amplitude corresponds to a much longer-lived emission component of 3.0 ns in benzonitrile, 2.9 ns in both CH_2Cl_2 and toluene, respectively, and of 2.6 ns in CCl_4. These findings again suggest the presence of an equilibrium between the π−stacked and the non-stacked *pinched cone* conformer of the calix[4]arene unit (see above), as emissive properties of both species – a drastically quenched lifetime due to PET for the non-stacked form and an additional longer-lived component due to PBI-excimer formation related to the π−stacked form[31] – are observed. However, the amplitude of this longer-lived component does not dominate the decay because the quantum yield of the π−stacked species is expected to be much smaller than that of the residual species in the non-stacked conformation. Accordingly, amplitude values of 0.5% are found in benzonitrile, and values of 2% in both CH_2Cl_2 and toluene, respectively and of 25% in CCl_4 are observed. This trend again shows that the equilibrium between the two *pinched cone* conformations is shifted towards the π−stacked species upon lowering the solvent polarity, and is hence closely relating to the findings from the steady state spectra (see above).

Table 2. Fluorescence lifetimes in various solvents.[a]

Cmpd	τ (ns) MCH	τ (ns) CCl$_4$	τ (ns) Toluene	τ (ns) CH$_2$Cl$_2$	τ (ns) Benzonitrile
oref[b]	4.2	4.1	4.0	4.9	3.9
oc	---[c]	---[c]	---[c]	---[c]	---[c]
o2c	---[d]	0.15	0.15	0.14	0.16
		2.6 (25%)	2.9 (2%)	2.9 (2%)	3.0 (0.5%)
gref[e,f]	5.9	5.6	4.3	3.1	2.5
gc[e]	6.1	5.6	4.4	3.3	2.7
g2c[e]	---[d]	---[g]	4.4	3.3	2.8
rref[h]	6.3	6.9	6.1	6.9	6.3
rc	5.9	6.3	6.3	5.6	4.7
r2c	7.4	6.3	5.8	5.7	4.9

[a] All spectra recorded at room temperature. [b] Data are in good agreement with the literature value of $\tau = 3.7$ ns for a similar orange PBI compound in CHCl$_3$, see ref. 8 and 12a [c] Values could not be determined as the signal falls into the system response of the instrument of ca. 150 ps. [d] Precipitation of the sample during the time frame of the experiment. [e] Note, that for all lifetimes determined for compounds **g2c**, **gc** and **gref** biexponential decays were observed. Accordingly, additional small components are found which are considered to be inherent to the green PBI chromophore itself (values given in ns with the respective amplitudes in brackets): For compound **gref**: 0.4 (10%) in MCH, 0.6 (12%) in CCl$_4$, 0.7 (5%) in toluene, 0.4 (8%) in CH$_2$Cl$_2$, 0.3 (30%) in benzonitrile, respectively. For compound **gc**: 0.7 (12%) in MCH, 0.3 (30%) in CCl$_4$, 0.5 (20%) in toluene, 0.4 (15%) in CH$_2$Cl$_2$, 0.2 (30%) in benzonitrile, respectively. For compound **g2c**: 0.5 (15%) in toluene, 0.8 (8%) in CH$_2$Cl$_2$, 0.6 (8%) in benzonitrile, respectively. [f] Data are in good agreement with the literature value of $\tau = 4.5$ ns for a similar green reference in toluene, see ref. 8. [g] Degradation of the sample during the time frame of experiment. [h] Data are in good agreement with literature values in CHCl$_3$ of $\tau = 6.5$ ns in ref. 11, and of $\tau = 7.4$ ns in ref. 12b.

For the *green* reference compound **gref** a fluorescence lifetime of 2.5 ns is found in the most polar solvent benzonitrile. With decreasing solvent polarity this value continuously increases up to 5.9 ns in MCH. The fluorescence lifetimes of both the green calix[4]arene substituted compounds **gc** and **g2c**, respectively, closely relate to those obtained for the reference compound **gref**: fluorescence lifetime values of 2.7 – 2.8 ns are found for compounds **gc** and **g2c** in benzonitrile which continuously increase for less polar solvents and reach a maximum value in MCH with 6.1 ns for compound **gc**.[iv] Likewise, for the *red*

[iv] Notably, for all lifetimes determined for compounds **g2c**, **gc** and **gref** biexponential decays are observed. Accordingly, additional small components of ca. 0.5 ns are found for each compound independent of the

reference compound **rref** fluorescence lifetime values between 6.1 ns and 6.9 ns are found in benzonitrile, CH_2Cl_2, toluene, CCl_4, and in MCH. The fluorescence lifetimes of both the red calix[4]arene substituted compounds **rc** and **r2c**, respectively, show values that are in good agreement with those obtained for the red reference compound **rref** and accordingly fluorescence lifetimes between 4.7 ns and 7.4 ns were determined in benzonitrile, CH_2Cl_2, toluene, CCl_4, and in MCH.

Accordingly, the changes in the fluorescence lifetimes depending on the solvent polarity for the respective orange, green and red PBI monomeric, dimeric and reference systems thus relate to the general trends already observed for the UV/vis absorption and fluorescence emission data: only for the orange compound **o2c** a π–stacked *pinched cone* species with an increased lifetime value could be identified in the equilibrium upon lowering the solvent polarity, whereas the measured lifetime values of the green and red systems **g2c** and **r2c**, respectively, are dominated by the emission of the non-stacked system.

5.8   Electrochemistry

The dimer compounds **o2c**, **g2c** and **r2c** as well as their respective monomeric counterparts **oc**, **gc** and **rc** were investigated by cyclic voltammetry in CH_2Cl_2 (vs. Fc/Fc^+); the obtained cyclic voltammograms (CVs) of the dimeric compounds are shown in Figure 11 and the respective data are summarized in Table 3. For the cyclic voltammograms of the monomeric compounds **oc**, **gc**, and **rc** see Chapter 3. The CV of compound **o2c** reveals two reversible reduction potentials at –1.10 V and –1.31 V that can be attributed to radical monoanion and dianion formation, respectively, of the orange perylene bisimide chromophore,[11] thus showing values very similar to compound **oc** (see Chapter 3). The first irreversible oxidation wave at +1.15 V for compound **o2c** can be attributed to the oxidation of the calix[4]arene moiety (see Chapter 3). No waves due to the oxidation of the

solvent polarity and of the calix[4]arene substitution of the chromophore. The latter components are thus considered to be independent of the calix[4]arene substitution of the dye unit and are assumed to be inherent to the green PBI chromophore itself (for details refer to Table 1.)

PBI units are observed. The values for the redox potentials found here agree with data from literature for the non-calix[4]arene substituted reference compound **oref**.[8,11]

For the green compound **g2c** redox potential values of −1.37 V and −1.48 V upon reduction (formation of radical anion and dianion, respectively) and of +0.19 V and +0.33 V upon oxidation (formation of radical cation and dication, respectively) are examined. Similar values are determined for compounds **gc** and **gref** (see Table 3 and Chapter 3).

The red compound **r2c** shows two reversible waves in the reductive cycle at −1.25 V and −1.38 V due to formation of the red PBI radical monoanion and dianion, and one reversible wave in the oxidative cycle at +0.82 V (formation of the radical monocation of the red PBI unit),[11] accompanied by an irreversible oxidation process above +1.12 V, which is again assigned to the oxidation of the calix[4]arene moiety (see Chapter 3). Similar potential values are found for compound **rc** (see Chapter 3) and again, a close match of the observed redox potentials with literature data is observed for compound **rref**.[8,11]

Table 3. Redox properties in CH_2Cl_2 (in V *vs.* Fc/Fc^+). Values of reference compounds **oref**, **gref**, and **rref** and of compounds **oc**, **gc**, and **rc** are given for comparison (see also Chapter 3).

	E_{red} (PBI$^-$/PBI^{2-})	E_{red} (PBI/PBI$^-$)	E_{ox} (PBI/PBI$^+$)	E_{ox} (PBI$^+$/PBI^{2+})	*Onset of irrev. oxidation*
oref[a]	−1.24	−1.01	+1.29		
oc	−1.32	−1.01	n. det.[b]		+1.10
o2c	−1.31	−1.10	n. det.[b]		+1.15
gref	−1.47	−1.33	+0.23	+0.36	
gc	−1.48	−1.36	+0.18	+0.32	+1.15
g2c	−1.48	−1.37	+0.19	+0.33	
rref[a]	−1.35	−1.15	+0.86		
rc	−1.35	−1.20	+0.81		+1.12
r2c	−1.38	−1.25	+0.82		+1.12

[a] See ref. 11. [b] Value could not be determined owing to the irreversible oxidation process of the calix[4]arene moiety.
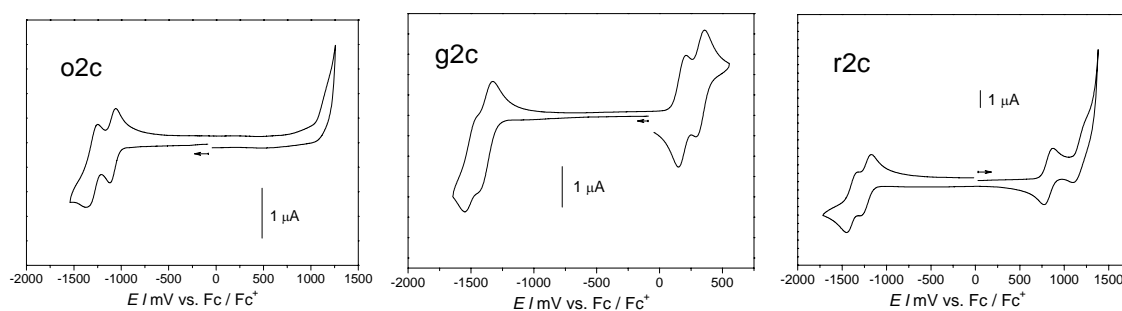
Figure 11. Cyclic voltammograms in CH_2Cl_2 of compound **o2c** (left), of compound **g2c** (middle), and of compound **rc** (right). Concentration = 2.0 x 10^{-4} M. Scan rate 100 mV s^{-1}. Working electrode: Pt disc, $\varnothing$ 1 mm; auxiliary electrode: Pt wire; reference electrode: Ag/AgCl; supporting electrolyte TBAHFP (0.1 M).

5.9 Femtosecond Transient Absorption Spectroscopy

The photophysical properties of the supramolecular building block **oc** in comparison to those of the non calix[4]arene-substituted reference compound **oref** were discussed in detail in Chapter 3. It has been found that the fluorescence quantum yield of compound **oc** (Φ_{fl} = 0.03) is almost completely quenched compared to the highly emissive reference compound **oref** (Φ_{fl} = 0.99) due to fast electron-transfer processes from the calix[4]arene moieties to the perylene bisimide chromophore leading to a short-lived charge-separated state consisting of the reduced perylene bisimide unit and the oxidized calix[4]arene moiety (see Chapter 3). For the present systems additionally the photophysical properties in less polar solvents such as CCl_4 and methylcyclohexane are of interest. Accordingly, femtosecond transient absorption studies in the solvents benzonitrile, CH_2Cl_2, toluene, CCl_4, and MCH were conducted to investigate the excited state properties of the dimeric arrays **o2c**, **g2c** and **r2c**, as well as their monomeric counterparts **oc, gc,** and **rc,** and their related reference compounds without calix[4]arene substitution **oref**, **gref** and **rref**, respectively. Exemplarily, the spectra of compounds **o2c**, **oc** and **oref** in CCl_4 are depicted in Figure 12.[v] For compounds **oc** and **oref** upon photoexcitation at 530 nm in CCl_4 an

---

[v] Note, that for solutions of **o2c** and **oc** in the lowest polarity solvent MCH precipitation of the compounds from solution was observed.

intense bleaching due to the depopulation of the ground state molecules in the probe area is observed at both 530 nm and 485 nm (see spectra in Figure 12). These bands are typical for $S_0 \rightarrow S_1$ transitions of the orange PBI chromophore.[10a,32] Furthermore, an intense negative signal is present at around 530 nm and 570 nm in the spectra of both compounds, respectively, which can be assigned to the stimulated emission of the orange PBI chromophore. These features are accompanied by a strong positive absorption band with a maximum centered at 715 nm assigned to the excited state absorption of the orange perylene chromophore. Upon increasing solvent polarity only slight changes in band shapes and general features of the spectra of the orange systems **oc** and **oref** have been observed in all other solvents (for spectra refer to Figures 15–17 in the Appendix of this Chapter). In contrast, for compound **o2c** an enhanced bleach signal at 485 nm is present in the spectra in CCl$_4$, that vanishes upon increasing solvent polarity (see for comparison the spectra of compound **o2c** in toluene, CH$_2$Cl$_2$ and benzonitrile in Figure 15 in the Appendix of this Chapter). The band at 485 nm is attributed to the π–stacked *pinched cone* conformation of the calix[4]arene, and the femtosecond transient absorption spectra thus relates to the trends already observed for the UV/vis absorption and fluorescence emission data.

Photoexcitation of the green compound **gc** in toluene at 640 nm leads to ground state bleaching below 715 nm and to the stimulated fluorescence emission between 715–740 nm, observed as a combined negative signal.[vi] Furthermore, the spectra show a small broad and positive absorption feature that extends from 470 nm to 570 nm, and a higher energy transition centered at 430 nm (bleach), which is likely due to the higher excited state transition of the perylene unit. The transient absorption spectra of the green reference compound **gref** and **g2c** reveal very similar features and are also in good agreement with spectral data reported in the literature (for spectra see Figures 18–20 in the Appendix of this Chapter).[33] Accordingly, no excited state interaction of the green PBI units has been observed in the spectra; and upon varied solvent polarity only minor changes in band shapes and general features have been found (for spectra refer to Figures 18–20 in the Appendix of this Chapter).

[vi] Note, that for solutions of **g2c** in MCH precipitation of the compounds was observed after ca. 30 minutes, and that for solutions of compounds **gc** and **g2c** in CCl$_4$ substantial light-induced degradation takes place.
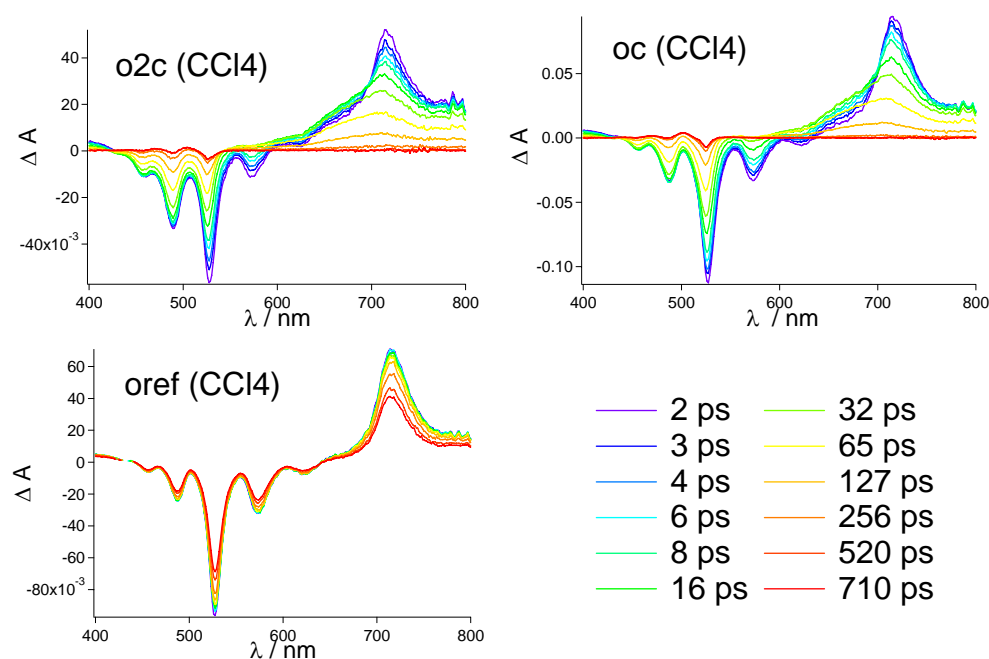
Figure 12. Femtosecond transient absorption spectra and corresponding time delays in CCl_4 after photoexcitation at 530 nm of compounds **o2c** (top left), **oc** (top right), and **oref** (bottom). Note, that due to low solubility of compound **o2c** in MCH for the solvent of lowest polarity CCl_4 was chosen.

The femtosecond transient absorption spectra of the red compounds **rc** and **r2c** in MCH (lowest polarity solvent, hence strongest interaction of dye units expected) following photoexcitation at 530 nm both display a broad absorption centered at 700–740 nm due to excited state absorption, a strong bleach of the ground state below 590 nm, and a band between 600–640 nm due to the stimulated emission from the lowest excited singlet state of the perylene unit (see Figures 21–23 in the Appendix of this Chapter). These bands are in very good agreement with the excited state properties of the red reference compound **rref** in MCH (see Figure 23 in the Appendix of this Chapter) and with those reported in the literature.[34] Within the time frame of the experiment, the negative band at 590 nm slightly shifts the position of its maximum to 610 nm which might be attributed to conformational changes of the red perylene bisimide dye.[vii] However, no excited state interaction of the red PBI units has been observed in the spectra; and upon varied solvent polarity only slight

---

[vii] Similar behavior is also known from single molecule spectroscopy for the red perylene bisimides bearing phenoxy substituents at the bay positions that were immobilized in a polymer matrix. It is known that local reorganizations in the vicinity of the molecule have an impact on the orientation of the phenoxy substituents for these red PBIs. For details, see ref. 35. For a recent study for processes in solution, see ref. 25.

changes in band shapes and general features have been found (for spectra refer to Figures 21–23 in the Appendix of this Chapter).

Accordingly, the femtosecond transient absorption spectra for the respective orange, green and red PBI monomeric, dimeric and reference systems thus relate to the general trends already observed in the UV/vis absorption and fluorescence emission spectroscopy: only for the orange dimeric **o2c** compound in CCl$_4$ spectral features due to the π–stacked *pinched cone* conformation could be observed, in all other solvents the prevalence of the non-stacked form can be assumed. For the respective green and red systems **g2c** and **r2c** no distinct spectral patterns due to the π–stacked arrangement have been found for all solvents studied.

5.10 Global and Target Analysis[viii]

To further analyze the formation of the π–stacked *pinched cone* conformation of the calix[4]arene especially found for the orange dimeric array **o2c**, the obtained data-matrices in the various solvents were analyzed with spectrotemporal parameterization. The latter technique is an advanced global and target analysis method that has been developed in particular to elucidate photoinduced processes in complex biological systems.[36] Here *global* refers to a simultaneous analysis of all measurements, whereas *target* refers to the applicability of a particular target model (see below and Chapters 2 and 3). Because the time information at all wavelengths is analyzed, this analysis gives a more in-depth view of the occurring photoinduced processes. As a final result, the so-called Species Associated Difference Spectra (SADS) are obtained, which are revealing the lifetimes and also the true spectra of the individual excited state species.

The data-matrices of the orange dimeric compound **o2c** and also those of the monomeric reference compound **oc** in CCl$_4$, toluene, CH$_2$Cl$_2$, and benzonitrile have been analyzed and the obtained SADS for compound **o2c** in CCl$_4$ and toluene are depicted in Figure 13A and 13B, respectively, and all other SADS are shown in Figure 24 in the Appendix of this

---

[viii] The femtosecond transient absorption data analysis by spectrotemporal parametrization was accomplished by Dr. I. H. M. van Stokkum at the Vrije Universiteit van Amsterdam, The Netherlands.

Chapter. For compound **o2c** the kinetic scheme shown in Figure 14 has been employed under the assumption of both the π−stacked and non-stacked conformation being present in the ground state. For compound **o2c** in CCl_4 five decay components are observed. The very first lifetime of 1.2 ps (black line in Figure 13A) is attributed to fast solvent reorganization processes[37] (for comparison see femtosecond transient absorption spectra of compound **oref** in Figure 17 in the Appendix of this Chapter). This spectrum is converted into two SADS representing the excited states of the π−stacked and the non-stacked conformation, respectively (red and cyan lines in Figure 13A, respectively). A lifetime of 192 ps is observed for the excited singlet state of the π−stacked conformer that shows the spectral patterns owing to the excited state interaction of the two chromophoric PBI units, *i.e.* a strongly enhanced band at 490 nm. The SADS representing the excited states of the non-stacked conformation decays significantly faster within 9 ps forming a deactivation pathway via a charge transfer state involving the formation of the orange PBI monoanion (represented by the blue line in Figure 13A). The latter SADS reveals a lifetime of 30 ps, and its spectral features show the complete loss of the stimulated emission at 580 nm and a significant broadening of the band at around 700 nm. This behavior has already been elucidated for compound **oc** and is due to a very efficient photoinduced electron transfer process between the electron-poor orange PBI unit and the electron-rich calix[4]arene substituent (see Chapter 3). Furthermore, the detailed analysis of the late time gated spectra reveals that a small amount (< 2%) of long-lived triplet is created for compound **o2c** (green line in Figure 13A), which is also observed for compound **oc** (for details see Chapter 3). An excited state charge transfer process resulting in a CT state of the π−stacked form could not be unambiguously confirmed by global and target analysis.
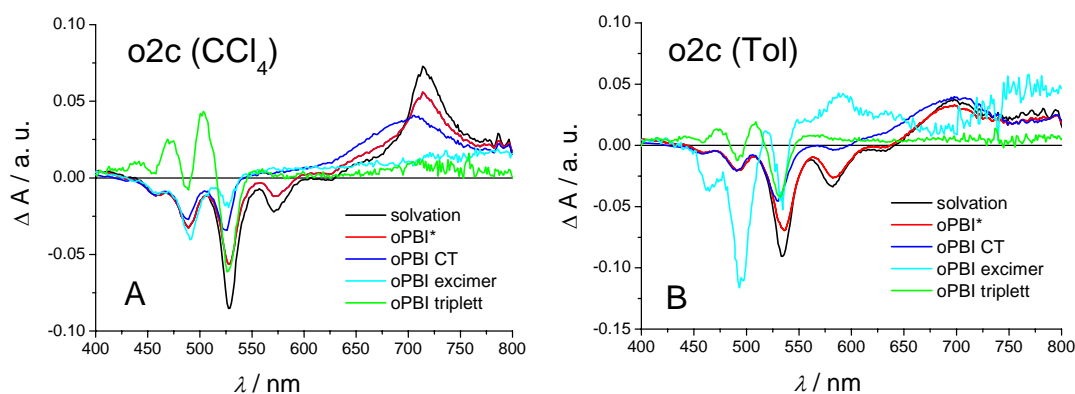
Figure 13. Species-associated difference spectra (SADS) of compound **o2c** resulting from the global and target analysis of femtosecond transient absorption data employing the kinetic scheme depicted in Figure 14 (**A**) in CCl_4 and (**B**) in toluene. Shown are processes after photoexcitation at 530 nm, features due to Raman scattering were omitted for clarity.

For the target analysis of compound **o2c** in toluene (see Figure 13B) similar spectral species including those of the π–stacked *pinched cone* conformation are observed. Accordingly, in toluene four decay components of 1.2 ps (fast solvent reorganization processes), of 18 ps (orange excited state), of 53 ps (CT state formation) and of 111 ps (excimer formation) are found (see Figure 13B), together with a minor component due to triplet state formation. The orange excimer state in toluene shows a smaller lifetime value of 111 ps compared to the one obtained in CCl_4 of 192 ps, due to the lesser stabilization resulting from higher solvent polarity. Accordingly, this state is less stable in toluene which relates to the findings from the steady state optical properties. For both the solvents CH_2Cl_2 and benzonitrile no spectral features attributable to the formation of an excimer-like state could be found by global analysis, for the respective SADS see Figure 24 in the Appendix of this Chapter. As already discussed for the time-resolved emission data, the observed lifetimes of the excimer state are significantly lower than those for other PBI aggregates reported in the literature,[31] which is most likely due to the fast quenching of the excited state of the orange PBI due to the competitive PET process involving the calix[4]arene electron donor. For the green and red systems **g2c** and **r2c** in the various solvents no excimer formation could be confirmed by global analysis, which again relates to the steady state optical results.
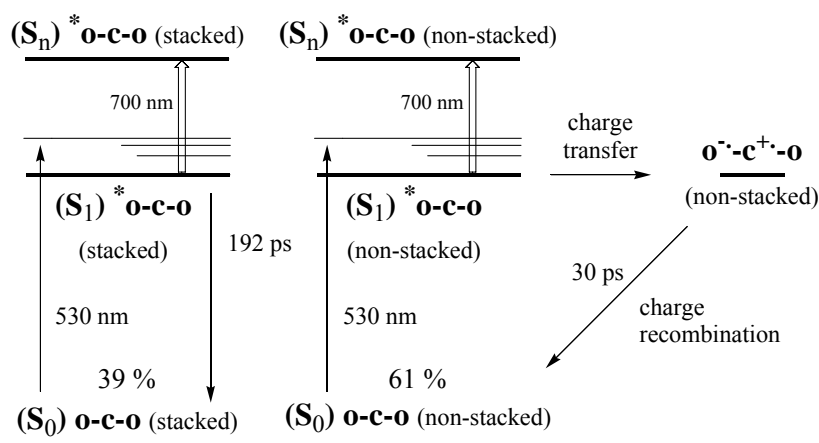
(S_n) *o-c-o (stacked) (S_n) *o-c-o (non-stacked)

700 nm   700 nm

charge transfer

$o^{-\cdot}\text{-}c^{+\cdot}\text{-}o$
(non-stacked)

(S_1) *o-c-o (S_1) *o-c-o

(stacked)   192 ps   (non-stacked)

30 ps

charge recombination

530 nm   530 nm

39 %   61 %

(S_0) o-c-o (stacked) (S_0) o-c-o (non-stacked)

Figure 14. Energy level diagram of compound **o2c** in CCl$_4$ showing deactivation pathways obtained with global and target analysis, together with the main decay times corresponding to the states.

5.11   Conclusions

The calix[4]arene scaffold has been utilized to preorganize each two identical orange, green and red PBI chromophoric units. An equilibrium between the two possible *pinched cone* conformations of the calix[4]arene unit, giving rise to the presence of a π−stacked conformation and a non−stacked *pinched cone* conformation, is clearly observed for the orange and green derivatives **o2c** and **g2c** as well as for compound **r2c** to a very slight extend. It has been shown that the two PBI units interact electronically in the π−stacked conformation and hence the latter species exhibits spectral features known from sandwich type aggregates with hypsochromically shifted absorption maxima and an excimer-type emission at long wavelength. The amount of π−stacked *pinched cone* conformation in the equilibrium is affected, first, by the sterical demand of the substituents in the *bay*-positions of the PBI chromophore, and second, by decreasing solvent polarity. With increasing sterical demand and the concomitant distortion of the chromophore out of planarity the π−stacked conformation is destabilized. Lowering the solvent polarity shifts the equilibrium towards the π−stacked form, and accordingly the amount of the stacked conformation is substantially increased in the solvents CCl$_4$ and MCH.

5.12 Experimental Section

Materials and Methods

Compounds **oref** and **rref**,[18] *N*-(1-pentyl-hexyl)-1,6,7,12-perylene-3,4:9,10-tetracarboxylic acid monoanhydride monoimide,[38] *N*-(butyl)-1,6,7,12-tetra(4-*tert*-butylphenoxy)-perylene-3,4:9,10-tetracarboxylic acid monoanhydride monoimide,[39] *N*-(cyclohexyl)-1,7-bis(pyrrolidinyl)perylene-3,4:9,10-tetracarboxylic acid monoanhydride monoimide[40] and 5,17-Diamino-25,26,27,28-tetrakis(propyloxy)-calix[4]arene[41] were synthesized according to literature procedures, for the synthesis of compounds **oc**, **gc**, **rc**, and **gref** refer to Chapter 3. All compounds were characterized by ^{1}H NMR spectroscopy, high resolution mass spectrometry, and compounds **o2c**, **g2c**, and **r2c** additionally by elemental analysis. Solvents were purified and dried according to standard procedures. Column chromatography was performed with silica gel 60 (0.035–0.070 mm); preparative TLC on 20 x 20 cm plates, height 1 mm, silica gel 60 (0.035–0.070 mm). NMR spectra were recorded on a Bruker 400 MHz and 600 MHz spectrometer. Mass spectra were performed on a Finnigan MAT MS 8200 or on a Bruker microTOF$_{LC}$.

UV/vis absorption spectra were measured on a Perkin-Elmer Lambda 40P UV/vis absorption spectrophotometer.

Steady state fluorescence emission spectra were recorded on a PTI QM4-2003 fluorescence spectrometer and are corrected against photomultiplier and lamp intensity. A long wavelength range emission corrected photomultiplier R928 was used. Fluorescence quantum yields were determined in CH_2Cl_2 vs. *N,N'*-(2,6-diisopropylphenyl)-1,6,7,12-tetraphenoxyperylene-3,4:9,10-tetracarboxylic acid bisimide (Φ_{fl} = 0.96 in $CHCl_3$) or Fluorescein (Φ_{fl} = 0.92 in 0.1N NaOH) as reference.[12b,42] The given quantum yields are averaged from values measured at three different excitation wavelengths with OD 0.02–0.05 in the absorption maximum (standard deviation σ = 1–3%).

Fluorescence lifetimes were measured with a streak camera system at the Universiteit van Amsterdam, The Netherlands, under the guidance of Dr. R. Williams. Details are described in Chapter 2 and in the literature.[43]

Femtosecond transient absorption spectra were measured at the Universiteit van Amsterdam, The Netherlands, under the guidance of Dr. R. Williams. Experimental details are described in Chapter 2 and in the literature.[44]

Global and target analysis was performed by Dr. I. H. M. van Stokkum at the Vrije Universiteit van Amsterdam, The Netherlands. For details of the method refer to Chapter 2 and to the literature.[36]

Data collection for **Crystal Structure** determination were carried out at the X-ray diffraction beam line of the Elettra Synchrotron, Trieste (Italy), using the rotating crystal method with the monochromatic wavelength of 1.000 Å. Data were collected on a CCD MAR detector. Measurements were performed at 100 K using a nitrogen stream cryo-cooler. Cell refinement, indexing and scaling of the data sets were carried out using Denzo and Scalepack.[45] The structures was solved by direct methods using SHELXS[46] and refined by the full-matrix least-squares method based on F^2 with all observed reflections.[46] The hydrogen atoms were placed at geometrically calculated positions. ΔF map of compound **r2c** revealed disordered $CHCl_3$ solvent accounting for 6 molecules for asymmetric unit. The propane chain at O4 and a *tert*-butylphenoxy group were found disordered (two positions, 50% each). All the calculations were performed using the WinGX System, Version 1.70.01.[47] Crystal data for compound **r2c**: $C_{176}H_{176}N_4O_{20}.6(CHCl_3)$, M = 3383.42, triclinic; space group $P\bar{1}$, a = 16.634(4), b = 17.396(4), c = 33.549(5) Å, α = 92.05(3), β = 96.55(2), γ = 93.72(3)°, V = 9615(4) Å^3, Z = 2, ρ_{calcd} = 1.169 g/cm^3, $F(000)$ = 3536. Final R = 0.1234, $wR2$ = 0.3272, S = 1.193 for 2066 parameters and 95672 reflections, 18991 unique [R(int) = 0.0250], of which 15274 with I > 2σ(I).

Cyclic voltammetry (CV) was performed by A.-M. Krause at the University of Würzburg, Germany, experimental details are described in Chapter 2.

## Synthesis and chemical characterization

Compound o2c
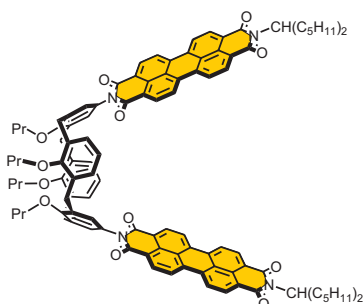
A suspension of 100 mg (1.61×10^{-4} mol, 1 equiv.) of 5,17-Diamino-25,26,27,28-tetrakis(propyloxy)-calix[4]arene, 351 mg (6.43×10^{-4} mol, 4 equiv.) of *N*-(1-pentyl-hexyl)-1,6,7,12-perylene-3,4:9,10-tetracarboxylic acid monoanhydride monoimide and 118 mg (6.43×10^{-4} mol, 4 equiv.) of $Zn(OAc)_2$ (H_2O-free) was heated in 2 mL distilled quinoline at 165 °C for 14 h under an argon atmosphere. The cooled reaction mixture was poured into 2N HCl and stirred for 30 minutes at 40 °C. To the solution 50 mL of CH_2Cl_2 were added and the resulting organic phase was washed with water and brine and dried over $MgSO_4$. The crude product was purified by column chromatography with CH_2Cl_2 and CH_2Cl_2/ethyl acetate 97:3 and successively by precipitation from CH_2Cl_2/methanol. Compound **o2c** was obtained as a light-red powder (146 mg, 8.70×10^{-5} mol, yield 55%). $C_{110}H_{108}N_4O_{12}$ (1678.05). Mp = 319–326 °C. TLC CH_2Cl_2; R_f = 0.01. **^{1}H NMR** (400 MHz, $CDCl_3$, 25 °C): δ (ppm) = 8.76 (bd, 4H, ^3J = 7.7 Hz; Per-*H*); 8.66 – 8.61 (m, 12H; Per-*H*); 7.12 (s, 4H; Ar-*H*); 6.46 (t, 2H, ^3J = 7.5 Hz; Ar-*H*); 6.33 (bd, 4H, ^3J = 7.0 Hz; Ar-*H*); 5.21 – 5.17 (m, 2H, N-C*H*); 4.55 and 3.22 (AX, each 4H, ^2J = 13.4 and 13.8 Hz; Ar-C*H₂*-Ar); 4.14 (bt, 4H, ^3J = 8.2; O-C*H₂*); 3.71 (t, 4H, ^3J = 6.6 Hz; O-C*H₂*); 2.30 – 2.21 (m, 4H; Alkyl-*H*); 2.07 – 2.01 (m, 4H; Alkyl-*H*); 1.92 – 1.85 (m, 8H, Propyl-*H*), 1.39 – 1.18 (m, 24H, Alkyl-*H*), 1.12 (t, 6H, ^3J = 7.5 Hz; Alkyl-*H*); 0.95 (t, 6H, ^3J = 7.5 Hz; Alkyl-*H*); 0.89 – 0.82 (m, 12H; Alkyl-*H*). **HR-MS** (ESI in $CHCl_3$/acetonitrile): calcd for $C_{110}H_{108}N_4NaO_{12}$ (m/z) 1699.7861 [M+Na]$^+$; found 1699.7856. **Analysis**: calcd (%) for $C_{110}H_{108}N_4O_{12}$ x H_2O (1696.07): C 77.90; H 6.54; N 3.30; found: C 77.95; H 6.68; N 3.24. **UV/vis** (CH_2Cl_2): λ (nm) [ε ($M^{-1}cm^{-1}$)] = 526 [164200], 490 [106700]. **Fluorescence** (CH_2Cl_2): λ_{max} (nm) = 536, 577; Φ_{Fl} = 0.03.

*Compound **r2c***
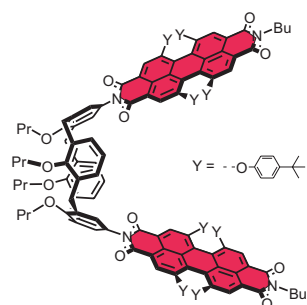
Under an argon atmosphere 40 mg (6.42×10^{-5} mol, 1 equiv.) of 5,17-Diamino-25,26,27,28-tetrakis(propyloxy)-calix[4]arene, 167 mg (1.61×10^{-4} mol, 2.5 equiv.) of *N*-(butyl)-1,6,7,12-tetra(4-*tert*-butylphenoxy)perylene-3,4:9,10-tetracarboxylic acid monoanhydride monoimide and 5-6 drops of triethylamine in toluene (1.0 mL) were heated to 125 °C for 24 h. The solvent was evaporated, the remaining crude product precipitated from CH_2Cl_2/methanol and the resulting solid purified by column chromatography with CH_2Cl_2/hexane 75:25 and successively precipitated from CH_2Cl_2/methanol. Compound **r2c** was obtained as a dark-red powder (140 mg, 5.25×10^{-5} mol, yield 82%). $C_{176}H_{176}N_4O_{20}$ (2667.30). Mp = 322–324°C. TLC CH_2Cl_2/hexane 80:20; R_f = 0.81. **^{1}H NMR** (400 MHz, CDCl$_3$, 25 °C): δ (ppm) = 8.28 and 8.24 (bs and s, 8H; Per-*H*); 7.25 – 7.21 (m, 16H; Phen-*H*); 7.00 (s, 4H; Ar-*H*); 6.87 – 6.83 (AX, 16H; Phen-*H*); 6.29 – 6.24 (m, 2H; Ar-*H*); 6.09 (d, 4H, ^3J = 7.7 Hz; Ar-*H*); 4.43 and 3.10 (AX, 8H, ^2J = 13.6 Hz; Ar-C*H$_2$*-Ar); 4.12 and 4.05 (t and m, 8H, ^3J = 7.5 Hz; O-C*H$_2$*); 3.60 (t, 4H, ^3J = 6.6 Hz; N-C*H$_2$*); 1.94 – 1.78 (m, 8H; Propyl-*H*); 1.70 – 1.63 (m, 4H, Butyl-*H*); 1.45 – 1.36 (m, 4H, Butyl-*H*); 1.29 and 1.27 (each s, 72H, *tert*-Butyl-Phen-*H*); 1.06 (t, 6H, ^3J = 7.4 Hz; Propyl-*H*); 0.94 (t, 6H, ^3J = 7.3 Hz; Butyl-*H*); 0.83 (t, 6H, ^3J =7.5 Hz; Propyl-*H*). **HR-MS** (ESI in CHCl$_3$/acetonitrile): calcd for $C_{176}H_{180}N_5O_{20}$ (m/z) 2683.3220 $[M+NH_4]^+$; found 2683.3216. **Analysis**: calcd (%) for $C_{176}H_{176}N_4O_{20}$ x H_2O (2685.31): C 78.72; H 6.68; N 2.09; found: C 78.55; H 7.00; N 1.93. **UV/vis** (CH_2Cl_2): λ (nm) [ε ($M^{-1}cm^{-1}$)] = 580 [92200]. **Fluorescence** (CH_2Cl_2): λ_{max} (nm) = 612; Φ_{Fl} = 0.79.

*Compound **g2c***
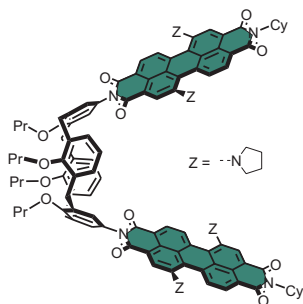
A suspension of 100 mg ($1.38 \cdot x \ 10^{-4}$ mol, 1 equiv.) of 5,17-Diamino-25,26,27,28-tetrakis(propyloxy)-calix[4]arene, 169 mg (2.76×10^{-4} mol, 2 equiv.) *N*-(cyclohexyl)-1,7-bis(pyrrolidinyl)perylene-3,4:9,10-tetracarboxylic acid mono-anhydride monoimide and 51 mg (2.76×10^{-4} mol, 2 equiv.) of $Zn(OAc)_2$ (H_2O-free) was heated in 1.5 mL distilled quinoline at 130 °C for 20 h under an argon atmosphere. The cooled reaction mixture was poured into 40 mL 2N HCl and stirred for 40 minutes at 50 °C. The resulting precipitate was filtered and dissolved in CH_2Cl_2. The solution was washed with water and brine and dried over $MgSO_4$. The crude product was purified by column chromatography with CH_2Cl_2 and successively by precipitation from CH_2Cl_2/hexane. Compound **g2c** was obtained as a dark-green powder (81 mg, 4.48×10^{-5} mol, yield 32%). $C_{116}H_{112}N_8O_{12}$ (1810.18). Mp = 351 °C (decomposition). TLC CH_2Cl_2/ethyl acetate 98:2; $R_f = 0.20$. **^{1}H NMR** (400 MHz, CDCl$_3$, 25 °C): δ (ppm) = 8.61 (bs, 2H; Per-*H*); 8.52 and 8.49 (d and s, 4H; Per-*H*); 8.39 (d, 2H, ^3J = 7.7 Hz; Per-*H*); 7.76 – 7.73 (m, 4H; Per-*H*); 7.14 (s, 4H; Ar-*H*); 6.44 (t, 2H, ^3J = 7.5 Hz; Ar-*H*); 6.29 (d, 4H, ^3J = 7.5 Hz; Ar-*H*); 5.11 – 5.06 (m, 2H; Cy-*H*); 4.54 and 3.21 (AX, 8H, ^2J = 13.5 and 13.7 Hz; Ar-C*H$_2$*-Ar); 4.17 – 4.13 (m, 4H; O-C*H$_2$*); 3.78 and 3.68 (bs and t, 12H, ^3J = 6.5 Hz; Pyrr-*H* and O-C*H$_2$*); 2.88 (bs, 8H; Pyrr-*H*); 2.66 – 2.57 (m, 4H; Cy-*H*); 2.09 – 1.74 (m, 34H; Pyrr-*H*, Propyl-*H*, Cy-*H*); 1.50 – 1.34 (m, 6H; Cy-*H*); 1.13 (t, 6H, ^3J = 7.4 Hz; Propyl-*H*); 0.93 (t, 6H, ^3J = 7.5 Hz; Propyl-*H*). **HR-MS** (ESI in CHCl$_3$): calcd. for $C_{116}H_{112}N_8O_{12}$ (m/z) 904.4199 $[M]^{2+}$; found 904.4194. **Analysis**: calcd (%) for $C_{116}H_{112}N_8O_{12}$ (1810.18): C 76.97; H 6.24; N 6.19; found C 77.28; H 6.87; N 5.85. **UV/vis** (CH_2Cl_2): λ (nm) [ε ($M^{-1}cm^{-1}$)] = 706 [92400]. **Fluorescence** (CH_2Cl_2): λ_{max} (nm) = 744; Φ_{Fl} = 0.22.

199

5.13   Appendix

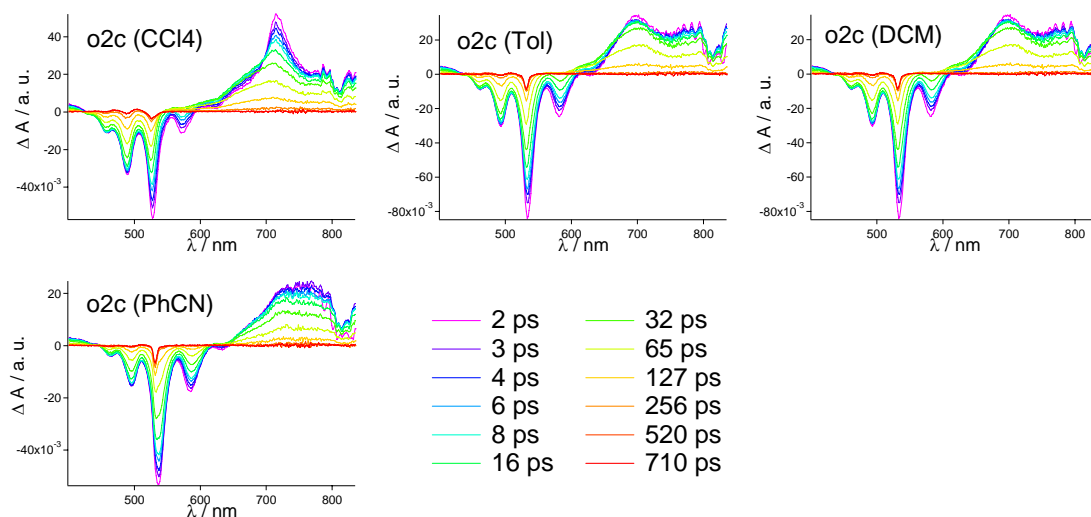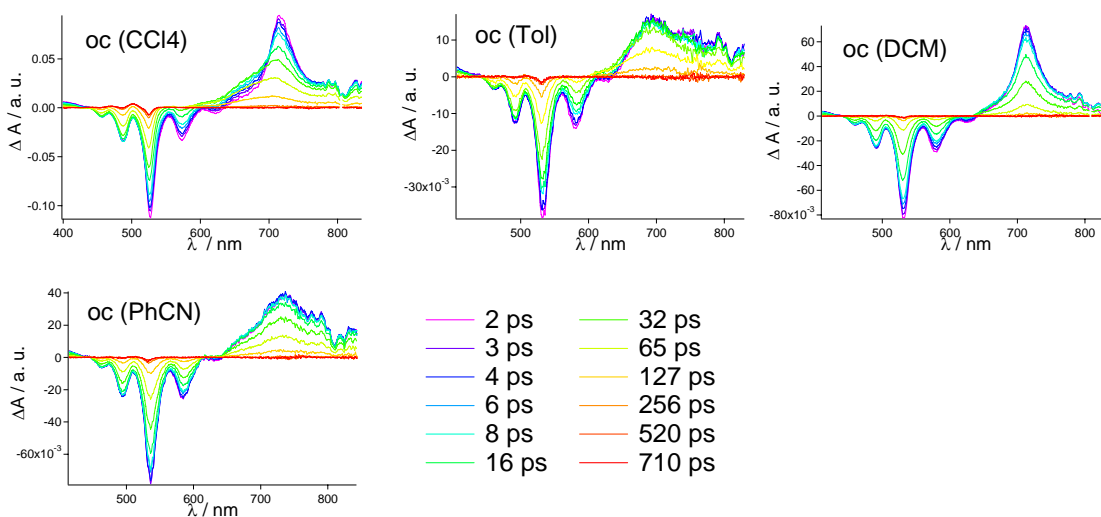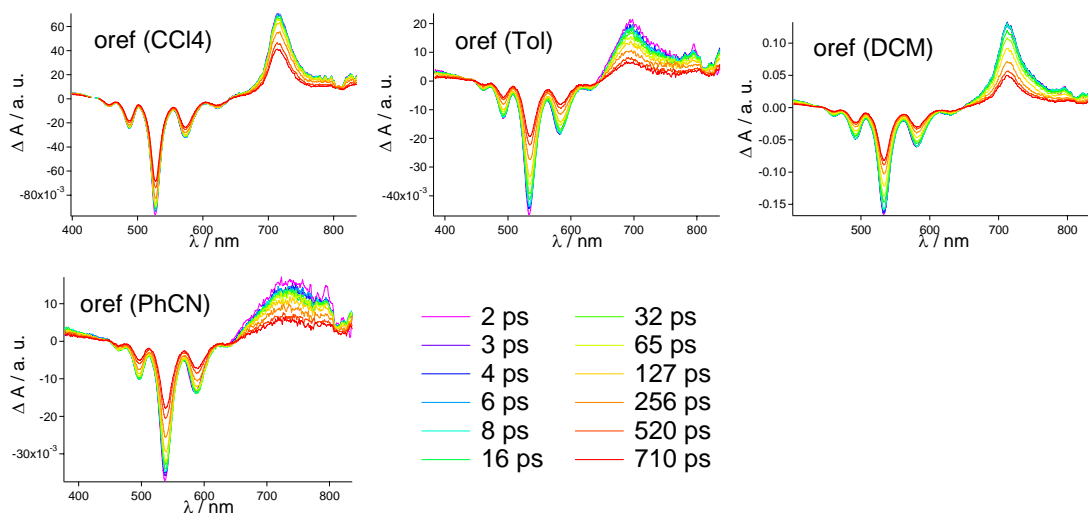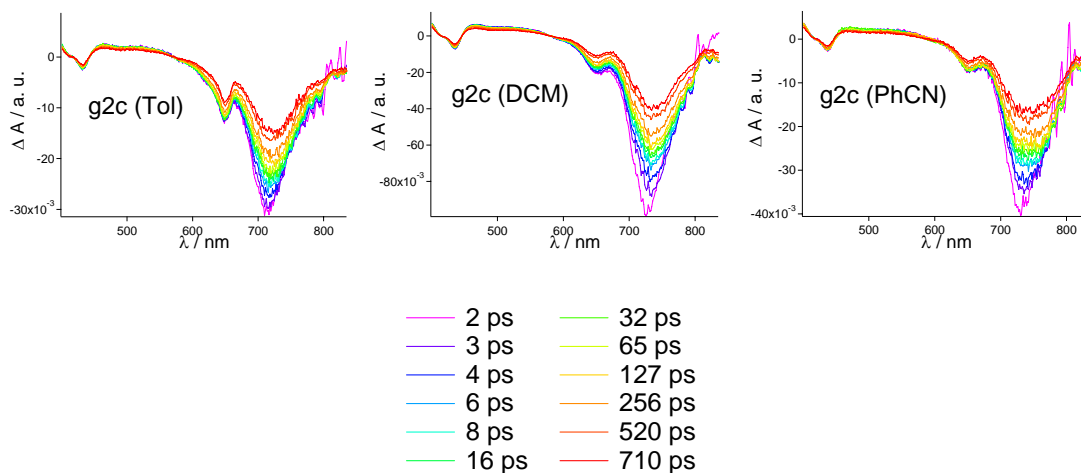### Femtosecond Transient Absorption Data of Compound o2c

Figure 15. Femtosecond transient absorption spectra and corresponding time delays of compound **o2c** after photoexcitation at 530 nm. Top Left: in CCl$_4$. Top Middle: in toluene (Tol). Top Right: in CH$_2$Cl$_2$ (DCM). Bottom Left: in benzonitrile (PhCN). Note, that compound **o2c** in MCH precipitates from solution after approximately 30 minutes. The scattered laser pulse is observed for all measurements.

Femtosecond Transient Absorption Data of Compound oc
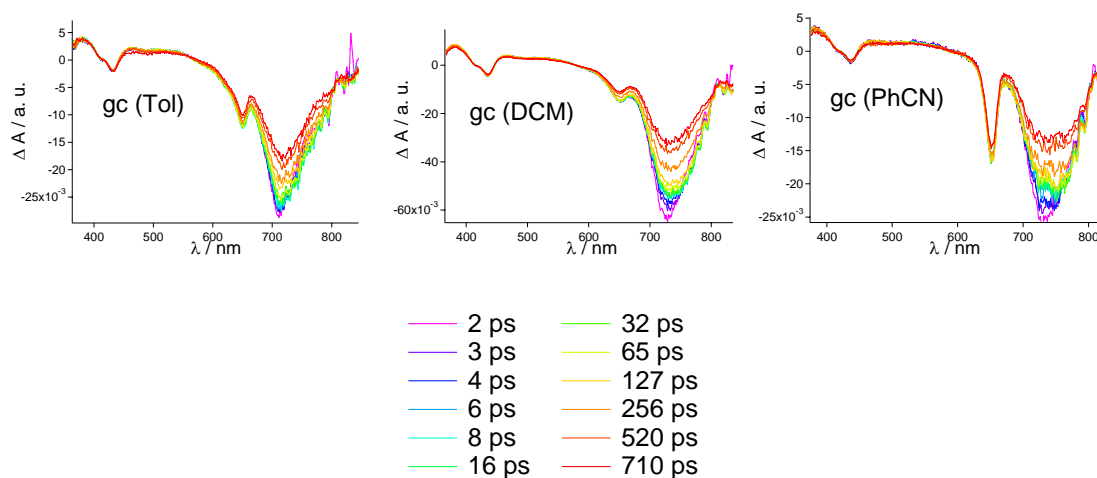

Figure 16. Femtosecond transient absorption spectra and corresponding time delays of compound **oc** after photoexcitation at 530 nm. Top Left: in CCl$_4$. Top Middle: in toluene (Tol). Top Right: in CH$_2$Cl$_2$ (DCM). Bottom Left: in benzonitrile (PhCN). Note, that compound **oc** in MCH precipitates from solution after approximately 30 minutes.

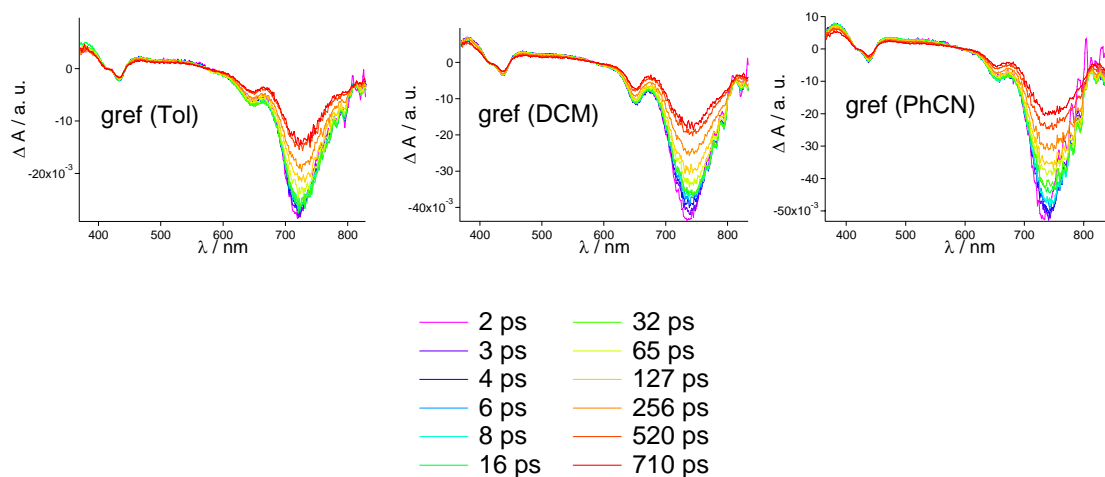## Femtosecond Transient Absorption Data of Compound oref

Figure 17. Femtosecond transient absorption spectra and corresponding time delays of compound **oref** after photoexcitation at 530 nm. Top Left: in CCl$_4$. Top Middle: in toluene (Tol). Top Right: in CH$_2$Cl$_2$ (DCM). Bottom Left: in benzonitrile (PhCN). Note, that compound **oref** in MCH precipitates from solution after approximately 30 minutes.
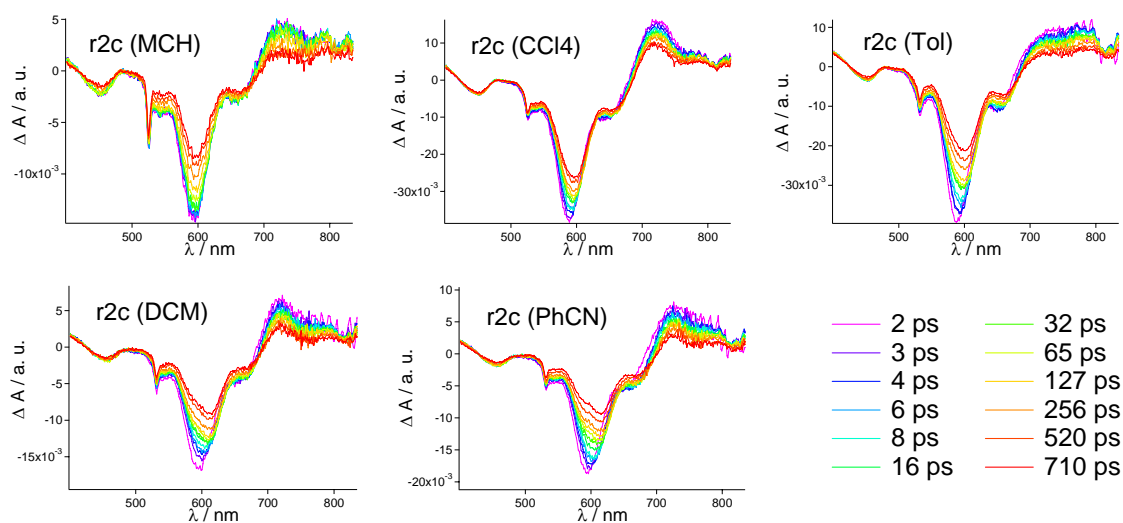
Femtosecond Transient Absorption Data of Compound g2c

Figure 18. Femtosecond transient absorption spectra and corresponding time delays of compound **g2c** after photoexcitation at 640 nm. Left: in toluene (Tol). Middle: in CH$_2$Cl$_2$ (DCM). Right: in benzonitrile (PhCN). Note, that the solution of compound **g2c** in CCl$_4$ shows substantial degradation of the UV/vis absorption spectrum after the measurement. Furthermore, compound **g2c** in MCH precipitates from solution after approximately 30 minutes. The scattered laser pulse is observed for the measurement in toluene.

Femtosecond Transient Absorption Data of Compound gc

Figure 19. Femtosecond transient absorption spectra and corresponding time delays of compound **gc** after photoexcitation at 640 nm. Left: in toluene (Tol). Middle: in CH_2Cl_2 (DCM). Right: in benzonitrile (PhCN). Note, that compound **gc** in CCl_4 shows substantial degradation of the UV/vis absorption spectrum after the measurement. Furthermore, compound **gc** in MCH precipitates from solution after approximately 30 minutes. The scattered laser pulse is observed for the measurements in toluene and benzonitrile.

Femtosecond Transient Absorption Data of Compound gref

Figure 20. Femtosecond transient absorption spectra and corresponding time delays of compound **gref** after photoexcitation at 640 nm. Left: in toluene (Tol). Middle: in CH_2Cl_2 (DCM). Right: in benzonitrile (PhCN). Note, that compound **gref** in CCl_4 shows substantial degradation of the UV/vis absorption spectrum after the measurement. Furthermore, compound **gref** in MCH precipitates from solution after approximately 30 minutes.

Femtosecond Transient Absorption Data of Compound r2c

Figure 21. Femtosecond transient absorption spectra and corresponding time delays of compound **r2c** after photoexcitation at 530 nm. Top Left: in methylcyclohexane (MCH). Top Middle: in CCl₄. Top Right: in toluene (Tol). Bottom Left: in CH$_2$Cl$_2$ (DCM). Bottom Middle: in benzonitrile (PhCN). The scattered laser pulse is observed for all measurements.
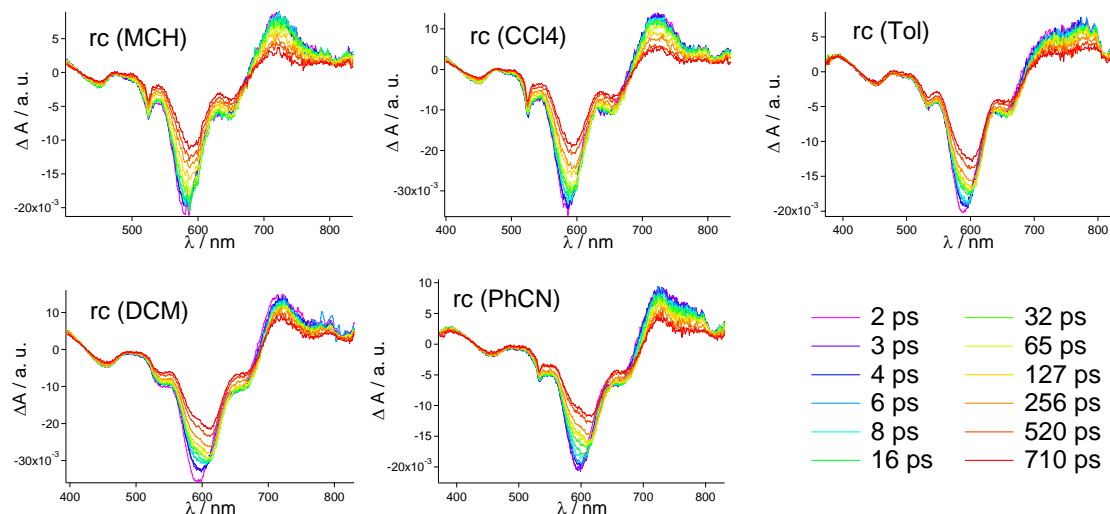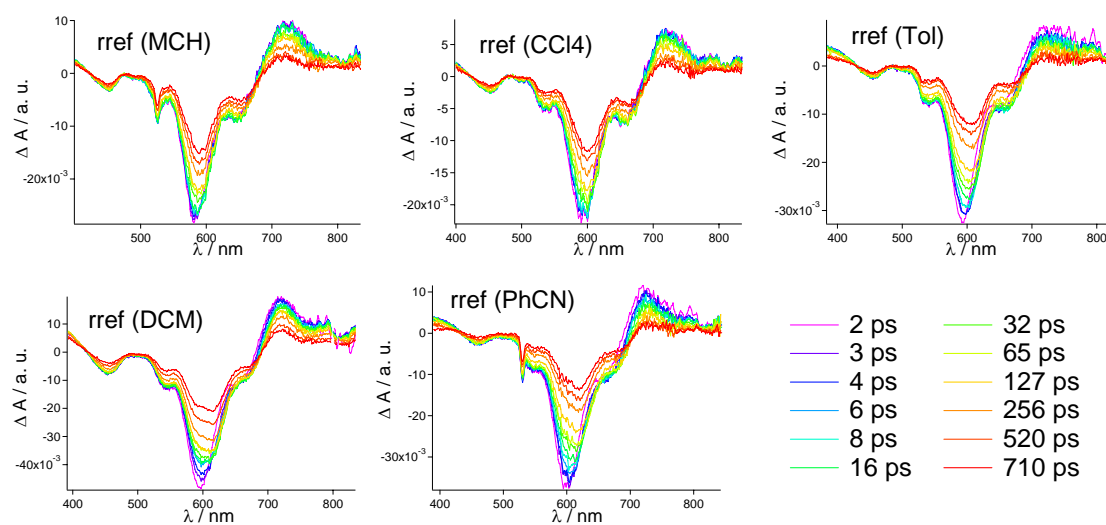
Femtosecond Transient Absorption Data of Compound rc

Figure 22. Femtosecond transient absorption spectra and corresponding time delays of compound **rc** after photoexcitation at 530 nm. Top Left: in methylcyclohexane (MCH). Top Middle: in CCl₄. Top Right: in toluene (Tol). Bottom Left: in CH$_2$Cl$_2$ (DCM). Bottom Middle: in benzonitrile (PhCN). The scattered laser pulse is observed for the measurements in methylcyclohexane, CCl₄, toluene and benzonitrile.
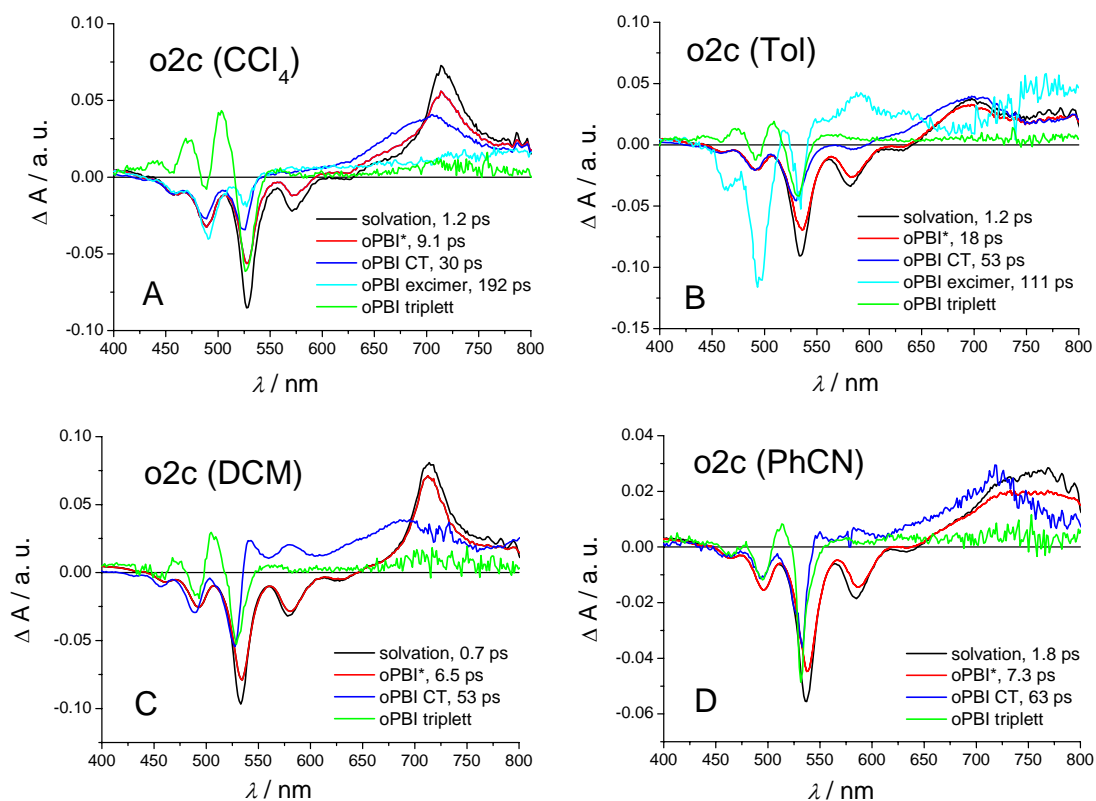
Femtosecond Transient Absorption Data of Compound rref

Figure 23. Femtosecond transient absorption spectra and corresponding time delays of compound **rref** after photoexcitation at 530 nm. Top Left: in methylcyclohexane (MCH). Top Middle: in CCl₄. Top Right: in toluene (Tol). Bottom Left: in CH₂Cl₂ (DCM). Bottom Middle: in benzonitrile (PhCN). The scattered laser pulse is observed for the measurements in methylcyclohexane and benzonitrile.

Global and Target Analysis

Figure 24. Species-associated difference spectra (SADS) of compound **o2c** in various solvents resulting from the global and target analysis of femtosecond transient absorption data using the kinetic scheme depicted in Figure 14. Shown are processes after photoexcitation at 530 nm, features due to Raman scattering were omitted for clarity. A (top left): in CCl$_4$. B (top right): in toluene (Tol). C (bottom left): in CH$_2$Cl$_2$ (DCM). D (bottom right): in benzonitrile (PhCN). SADS in CCl$_4$ and toluene are repeated for comparison from Figure 13.

5.14   References

(1)   (a) *Calixarenes 2001*; Asfari, Z., Böhmer, V., Harrowfield, J., Eds.; Kluwer Academic Publishers: Dordrecht, 2001. (b) *Calixarenes*; Gutsche, C. D.; The Royal Society of Chemistry: Cambridge, 1993. (c) *Calixarenes Revisited*; Gutsche, C. D.; The Royal Society of Chemistry: Letchworth, 1998. (d) Böhmer, V.; *Angew. Chem., Int. Ed. Engl.* **1995**, *34*, 713–745. (e) *Calixarenes in Action*; Mandolini, L., Ungaro, R., Eds.; Imperial College Press: London, 2000.

(2)   Kenis, P. J. A.; Noordman, O. F. J.; Houbrechts, S.; van Hummel, G. J.; Harkema, S.; van Veggel, F. C. J. M.; Clays, K.; Engbersen, J. F. J.; Persoons, A.; van Hulst, N. F.; Reinhoudt, D. N. *J. Am. Chem. Soc.* **1998,** *120,* 7875–7883.

(3)   (a) Zhao, B.-T.; Blesa, M.-J.; Mercier, N.; Le Derf, F.; Sallé, M. *J. Org. Chem.* **2005**, *70*, 6254–6257. (b) Yu, H.-h.; Pullen, A. E.; Büschel, M. G.; Swager, T. M. *Angew. Chem., Int. Ed.* **2004**, *43*, 3700–3703. (c) Yu, H.-h.; Xu, B.; Swager, T. M. *J. Am. Chem. Soc.* **2003**, *125*, 1142–1143. (d) Scherlis, D. A.; Marzari, N. *J. Am. Chem. Soc.* **2005,** *127,* 3207–3212.

(4)   (a) Schazmann, B.; Alhashimy, N.; Diamond, D. *J. Am. Chem. Soc.* **2006**, *128*, 8607–8614. (b) Souchon, V.; Leray, I.; Valeur, B. *Chem. Comm.* **2006**, 4224–4226. (c) Lee, S. H.; Kim, S. H.; Kim, S. K.; Jung, J. H.; Kim, J. S. *J. Org. Chem.* **2005**, *70*, 9288–9295. (d) Leray, I.; Lefevre, J.-P.; Delouis, J.-F.; Delaire, J.; Valeur, B. *Chem. – Eur. J.* **2001**, *7*, 4590–4598. (e) van der Veen, N.; Flink, S.; Deij, M. A.; Egberink, R. J. M.; van Veggel, F. C. J. M.; Reinhoudt, D. N. *J. Am. Chem. Soc.* **2000**, *122*, 6112–6113. (f) Ji, H.-F.; Dabestani, R.; Brown, G. M.; Sachleben, R. A. *Chem. Comm.* **2000**, 833–834. (g) Beer, P. D.; Timoshenko, V.; Maestri, M.; Passaniti, P.; Balzani, V. *Chem. Commun.* **1999**, 1755–1756. (h) Jin, T.; Monde, K. *Chem. Commun.* **1998**, 1357–1358. (i) Aoki, I.; Sakaki, T.; Shinkai, S. *J. Chem. Soc., Chem. Comm.* **1992**, 730–732. (j) Jin, T.; Ichikawa, K.; Koyama, T. *J. Chem. Soc., Chem. Comm.* **1992**, 499–501.

(5)   (a) Araki, K.; Iwamoto, K.; Shinkai, S.; Matsuda, T. *Chem. Lett.* **1989**, 1747–1750. (b) Iwamoto, K.; Araki, K.; Shinkai, S. *J. Org. Chem.* **1991**, *56*, 4955–4962.

206

(6)   (a) Conner, M.; Janout, V.; Regen, S. L. *J. Am. Chem. Soc.* **1991**, *113*, 9670–9671. (b) Scheerder, J.; Vreekamp, R. H.; Engbersen, J. F. J.; Verboom, W.; van Duynhoven, J. P. M.; Reinhoudt, D. N. *J. Org. Chem.* **1996**, *61*, 3476–3481. (c) Grootenhuis, P. D. J.; Kollman, P. A.; Groenen, L. C.; Reinhoudt, D. N.; van Hummel, G. J.; Ugozzoli, F.; Andreetti, G. D. *J. Am. Chem. Soc.* **1990**, *112*, 4165–4176. (d) Harada, T.; Rudzinski, J. M.; Osawa, E.; Shinkai, S. *Tetrahedron Lett.* **1993**, *49*, 5941–5954.

(7)   (a) Arduini, A.; Fabbi, M.; Mirone, L.; Pochini, A.; Secchi, A.; Ungaro, R. *J. Org. Chem.* **1995**, *69*, 1454–1457. (b) Ikeda, A.; Tsuzuki, K.; Shinkai, S. *J. Chem. Soc., Perkin Trans. 2* **1994**, 2073–2080. (c) Timmerman, P.; Nierop, K. G. A.; Brinks, E. A.; Verboom, W.; van Veggel, F. C. J. M.; van Hoorn, W. P.; Reinhoudt, D. N. *Chem. J. Eur.* **1995**, *1*, 132–143. (d) Matoušek, J.; Kulhánek, P.; Čajan, M.; Koča, J. *J. Phys. Chem.* A **2006**, *110*, 861–867.

(8)   Würthner, F. *Chem. Comm.* **2004**, 1564–1579.

(9)   (a) *Supramolecular Chemistry: Concepts and Perspectives*; Lehn, J.-M., Ed; VCH: Weinheim, 1995. (b) *Supramolecular Dye Chemistry*; Würthner, F., Ed.; Topics in Current Chemistry 258, Springer-Verlag: New-York, 2005.

(10)   (a) Hoeben, F. J. M.; Jonkheijm, P.; Meijer, E. W.; Schenning, A. P. H. J. *Chem. Rev.* **2005**, *105*, 1491–1546. (b) Simpson, C. D.; Wu, J.; Watson, M. D.; Müllen, K.; *J. Mater. Chem.* **2004**, *14*, 494–504. (c) Würthner, F.; Thalacker, C.; Diele, S.; Tschierske, C. *Chem. – Eur. J.* **2001**, *7*, 2245–2253.

(11)   You, C.-C.; Dobrawa, R.; Saha-Möller, C. R.; Würthner, F. *Top. Curr. Chem.* **2005**, *258*, 39–82.

(12)   (a) Ford, W. E.; Kamat, P. V. *J. Phys. Chem.* 1987, *91*, 6373–6380. (b) Gvishi, R.; Reisfeld, R.; Burshtein, Z. *Chem. Phys. Lett.* **1993**, *213*, 338–344.

(13)   (a) De Schryver, F. C.; Vosch, T.; Cotlet, M.; Van der Auweraer, M.; Müllen, K.; Hofkens, J. *Acc. Chem. Res.* **2005**, *38*, 514–522. (b) Sautter, A.; Kaletas, B. K.; Schmid, D. G.; Dobrawa, R.; Zimine, M.; Jung, G.; Van Stokkum, I. H. M.; De Cola, L.; Williams, R. M.; Würthner, F. *J. Am. Chem. Soc.* **2005**, *127*, 6719–6729.

(14)   (a) O'Neil, M. P.; Niemczyk, M. P.; Svec, W. A.; Gosztola, D.; Gaines III, G. L.; Wasielewski, M. R. *Science* **1992**, *257*, 63–65. (b) Beckers, E. H. A.; Meskers, S. C. J.; Schenning, A. P. H. J.; Chen, Z.; Würthner, F.; Janssen, R. A. J. *J. Phys. Chem. A* **2004**, *108*, 6933–6937. (c) Prodi, A.; Chiorboli, C.; Scandola, F.; Iengo, E.; Alessio, E.; Dobrawa, R.; Würthner, F. *J. Am. Chem. Soc.* **2005**, *127*, 1454–1462.

(15)   (a) Kraft, A.; Grimsdale, A. C.; Holmes, A. B. *Angew. Chem., Int. Ed. Engl.* **1998**, *37*, 402–428. (b) Karapire, C.; Zafer, C.; Icli, S. *Synth. Met.* **2004**, *145*, 51–60. (c) Pan, J.; Zhu, W.; Li, S.; Zeng, W.; Cao, Y.; Tian, H. *Polymer* **2005**, *46*, 7658–7669.

(16)   (a) Malenfant, P. R. L.; Dimitrakopoulos, C. D.; Gelorme, J. D.; Kosar, L. L.; Graham, T. O. *Appl. Phys. Lett.* **2002**, 2517–2519. (b) Dimitrakopoulos, C. D.; Malenfant, P. R. L. *Adv. Mater.* **2002**, *14*, 99–117. (c) Jones, B. A.; Ahrens, M. J.; Yoon, M.-H.; Facchetti, A.; Marks, T. J.; Wasielewski, M. R. *Angew. Chem., Int. Ed. Engl.* **2004**, *116*, 6363–6366. (d) Würthner, F.; Schmidt, R. *ChemPhysChem* **2006**, *7*, 793–797.

(17)   (a) Tang, C. W. *Appl. Phys. Lett.* **1986**, *48*, 183–185. (b) Schmidt-Mende, L.; Fechtenkötter, A.; Müllen, K.; Moons, E.; Friend, R. H.; MacKenzie, J. D. *Science* **2001**, *293*, 1119–1122. (c) Breeze, A. J.; Salomon, A.; Ginley, D. S.; Gregg, B. A.; Tillmann, H.; Hörhold, H.-H. *Appl. Phys. Lett.* **2002**, *81*, 3085–3087.

(18)   Seybold, G.; Stange, A. (BASF AG), *Ger. Pat.* DE 35 45 004, 1987 (*Chem. Abstr.*, 1988, **108**, 77134c).

(19)   Zhao, Y.; Wasielewski, M. R. *Tetrahedron Lett.* **1999**, *40*, 7047–7050.

(20)   Langhals, H. *Heterocycles*, **1995**, *40*, 477–500.

(21)   For examples with rigid spacer units containing perylene bisimides, see: (a) Giaimo, J. M.; Gusev, A. V.; Wasielewski, M. R. *J. Am. Chem. Soc.* **2002**, *124*, 8530–8531. (b) Ahrens, M. J.; Sinks, L. E.; Rybtchinski, B.; Liu, W.; Jones, B. A.; Giaimo, J. M.; Gusev, A. V.; Goshe, A. J.; Tiede, D. M.; Wasielewski, M. R. *J. Am. Chem. Soc.* **2004**, *126*, 8284–8294. (c) Rybtchinski, B.; Sinks, L. E.; Wasielewski, M. R. *J. Phys. Chem. A* **2004**, *108*, 7497–7505. (d) Van der Boom, T.; Hayes, R. T.; Zhao, Y.; Bushard, P. J.; Weiss, E. A.; Wasielewski, M. R. *J. Am. Chem. Soc.* **2002**, *124*, 9582–9590.

(22)   For other bichromophoric systems, see: (a) Jokic, D.; Asfari, Z.; Weiss, J. *Org. Lett*. **2002**, *4*, 2129–2132. (b) Yu, H.-H.; Pullen, A. E.; Büschel, M. G.; Swager, T. M. *Angew. Chem., Int. Ed.* **2004**, *43*, 3700–3703. (c) Kadish, K. M.; Frémond, L.; Ou, Z.; Shao, J.; Shi, C.; Anson, F. C.; Burdet, F.; Gros, C. P.; Barbe, J.-M.; Guilard, R. *J. Am. Chem. Soc.* **2005**, *127*, 5625–5631. (d) Scherlis, A. S.; Marzari, N. *J. Am. Chem. Soc.* **2005**, *127*, 3207–3212. (e) Pognon, G.; Boudon, C.; Schenk, K. J.; Bonin, M.; Bach, B.; Weiss, J. *J. Am. Chem. Soc.* **2006**, *128*, 3488–3489. (f) Van der Boom, T.; Evmenenko, G.; Dutta, P.; Wasielewski, M. R. *Chem. Mater.* **2003**, *15*, 4068–4074.

(23)   (a) Neuteboom, E. E.; Meskers, S. C. J.; Meijer, E. W.; Janssen, R. A. J. *Macromol. Chem. Phys.* **2004**, *205*, 217–222. (b) Wang, W.; Wan, W.; Zhou, H.-H.; Niu, S.; Li, A. D. Q. *J. Am. Chem. Soc.* **2003**, *125*, 5248–5249. (c) Wang, W.; Li, L.-S.; Helms, G.; Zhou, H.-H.; Li, A. D. Q. *J. Am. Chem. Soc.* **2003**, *125*, 1120–1121. (d) Hernando, J.; De Witte, P. A. J.; Van Dijk, E. M. H. P.; Korterik, J.; Nolte, R. J. M.; Rowan, A. E.; Garcia-Parajó, M. F.; Van Hulst, N. F. *Angew. Chem., Int. Ed. Engl.* **2004**, *43*, 4045–4049.

(24)   (a) Staab, H. A.; Riegler, N.; Diederich, F.; Krieger, C.; Schweitzer, D. *Chem. Ber*. **1984**, *117*, 246–259. (b) Langhals, H.; Ismael, R. *Eur. J. Org. Chem.* **1998**, 1915–1917.

(25)   Osswald, P.; Leusser, D.; Stalke, D.; Würthner, F. *Angew. Chem., Int. Ed. Engl.* **2005**, *44*, 250–253.

(26)   Kasha, M.; Rawls, H. R.; El-Bayoumi, M. A. *Pure Appl. Chem.* **1965**, *11*, 371–392.

(27)   (a) *Electronic Processes in Organic Crystals and Polymers*; Pope, M.; Swenberg, C. E.; Oxford University Press: New York, 1999. (b) Kazmaier, P. M.; Hoffmann, R. H. *J. Am. Chem. Soc.* **1994**, *116*, 9684–9691.

(28)   For examples containing perylene bisimide dyes see ref. 21, 23f and (a) Li, X.; Sinks, L. E.; Rybtchinski, B.; Wasielewski, M. R. *J. Am. Chem. Soc.* **2004**, *126*, 10810–10811. (b) Langhals, H.; Jona, W. *Angew. Chem., Int. Ed. Engl.* **1998**, *37*, 952–955. (c) Li, A. D. Q.; Wang, W.; Wang, L.-Q. *Chem. – Eur. J.* **2003**, *9*, 4594–4601.

(29)   Würthner, F.; Ahmed, S.; Thalacker, C.; Debaerdemaeker, T. *Chem. Eur. J.* **2002**, *20*, 4742–4750.

(30)   Chen, Z.; Stepanenko, V.; Dehm, V.; Prins, P.; Siebbeles, L. D. A.; Seibt, J.; Marquetand, P.; Engel, V.; Würthner, F. *Chem. – Eur. J.* **2007**, *13*, 436–449.

(31)   Longer-lived excited states due to PBI-excimer formation have been reported in the literature, see: (a) Katoh, R.; Sinha, S.; Murata, S.; Tachiya, M. *J. Photochem Photobiol., A* **2001**, *145*, 23–34. (b) Gómez, U.; Leonhardt, M.; Port, H.; Wolf, H. C. *Chem. Phys. Lett.* **1997**, *268*, 1–6. (c) Puech, K.; Fröb, H.; Leo, K. *J. Lumin.* **1997**, *72–74*, 524–525.

(32)   Ford, W. E.; Hiratsuka, H.; Kamat, P. V. *J. Phys. Chem.* **198**9, *93*, 6692–6696.

(33)   (a) Lukas, A. S.; Zhao, Y.; Miller, S. E.; Wasielewski, M. R. *J. Phys. Chem. B*, **2002**, 106, 1299–1306. (b) Shibano, Y.; Umeyama, T.; Matano, Y.; Tkachenko, N. V.; Lemmetyinen, H.; Imahori, H. *Org. Lett*. **2006**, *8*, 4425–4428.

(34)   Prodi, A.; Chiorboli, C.; Scandola, F.; Iengo, E.; Alessio, E.; Dobrawa, R.; Würthner, F. *J. Am. Chem. Soc.* **2005**, *127*, 1454–1462.

(35)   Hofkens, J.; Vosch, T.; Maus, M.; Köhn, F.; Cotlet, M.; Weil, T.; Herrmann, A.; Müllen, K.; De Schryver, F. C. *Chem. Phys. Lett*. **2001**, *333*, 255–263.

(36)   (a) van Stokkum, I. H. M.; Larsen, D. S.; van Grondelle, R. *Biochim. Biophys. Acta* **2004**, *1657*, 82–104. (b) van Stokkum, I. H. M.; Lozier, R. H. *J. Phys. Chem. B* **2002**, *106*, 3477–3485. (c) Mullen, K. M.; van Stokkum, I. H. M. *J. Statistical Software* **2007,** 18 (3). URL http://www.jstatsoft.org/v18/i03/ (d) Global and target analysis can be performed with e.g., the R package TIMP, see http://cran.r-project.org/doc/packages/TIMP.pdf

(37)   (a) Schweitzer, G.; Gronheid, R.; Jordens, S.; Lor, M.; De Belder, G.; Weil, T.; Reuther, E.; Müllen, K.; De Schryver, F. C. *J. Phys. Chem. A* **2003**, *107,* 3199–3207. (b) De Belder, G.; Jordens, S.; Lor, M.; Schweitzer, G.; De, R.; Weil, T.; Herrmann, A.; Wiesler, U. K.; Müllen, K.; De Schryver, F. C. *J. Photochem. Photobiol. A* **2001**, *145*, 61–70.

(38)   (a) Kaiser, H.; Lindner, J.; Langhals, H. *Chem. Ber.* **1991**, *124*, 529–535. (b) Nagao, Y.; Naito, T.; Abe, Y.; Misono, T. *Dyes Pigm.* **1996**, *32*, 71–83.

(39)   Würthner, F.; Sautter, A.; Schmid, D.; Weber, P. J. A. *Chem. Eur. J.* **2001**, *7*, 894–902.

(40)   (a) Würthner, F.; Stepanenko, V.; Chen, Z.; Saha-Möller, C. R.; Kocher, N.; Stalke, D. *J. Org. Chem.*, **2004**, *69*, 7933–7939. (b) Lukas, A. S.; Zhao, Y.; Miller, S. E.; Wasielewski, M. R. *J. Phys. Chem. B* **2002**, *106*, 1299–1306.

(41)   Prins, L. J.; Jollife, K. A.; Hulst, R.; Timmerman, P.; Reinhoudt, D. N. *J. Am. Chem. Soc.* **2000**, *122*, 3617–3627.

(42)   (a) Gvishi, R.; Reisfeld, R.; Burshtein, Z. *Chem. Phys. Lett.* **1993**, *213*, 338–344. (b) Demas, J. N.; Grosby, G. A. *J. Phys. Chem.* **1971**, *75*, 991–1024.

(43)   Lauteslager, X. Y.; van Stokkum, I. H. M.; van Ramesdonk, H. J.; Brouwer, A. M.; Verhoeven, J. W. *J. Phys. Chem. A*, **1999**, *103*, 653.

(44)   Vergeer, F. W.; Kleverlaan, C. J.; Stufkens, D. J. *Inorg. Chim. Acta* **2002**, *327,* 126–133.

(45)   Collaborative Computational Project, Number 4. *Acta Crystallogr.* **1994**, *Sect. D 50*, 760–763.

(46)   SHELX97 Programs for Crystal Structure Analysis (Release 97-2). G. M. Sheldrick, University of Göttingen, Germany, **1998**.

(47)   Farrugia, L. J. *J. Appl. Crystallogr.* **1999**, *32*, 837–838.

211

6

Summary

Artificial light-harvesting structures mimicking the basic principles in photosynthesis are of high scientific interest. However, within systems containing multiple chromophores that are realizing sequential energy transfer processes the optimization of both efficiency and directionality remains a challenging task.

The present work deals with the synthesis and the investigation of the photophysical properties of covalently constructed calix[4]arene–perylene bisimide dye arrays containing various PBI units. The obtained conjugates are characterized with respect towards their application in a new, zigzag-type architecture of artificial light-harvesting systems. For this purpose, orange (core-unsubstituted), red (6,7,11,12-*tert*-butylphenoxy-functionalized) and green (1,7-pyrrolidino-substituted) perylene bisimide building blocks have been attached to the calix[4]arene scaffold. First, the monochromophoric reference systems have been studied, and second, the photophysical properties of a comprehensive series of newly synthesized, multichromophoric calix[4]arene–perylene bisimide conjugates showing efficient energy transfer processes between the individual dye subunits have been investigated. Furthermore, a series of bichromophoric compounds containing identical chromophoric units has been obtained. Towards this goal, a variety of spectroscopic techniques such as UV/vis absorption, steady state and time-resolved fluorescence emission, and femtosecond transient absorption spectroscopy as well as a spectrotemporal analysis of the obtained data has been applied.

The *first Chapter* gives a short overview of several architectures of artificial light-harvesting systems containing perylene bisimides. Furthermore, an introduction into the field of calix[4]arenes is given as well as important concepts of photoinduced processes are discussed.

The *second Chapter* shortly describes the experimental techniques that have been applied.

In *Chapter 3* the syntheses and photophysical properties of a series of perylene bisimide–calix[4]arene conjugates, consisting of three different types of perylene bisimide (PBI) chromophores (orange, red and green) either substituted with one or two calix[4]arene moieties in the N-imide position, are described (for chemical structures see
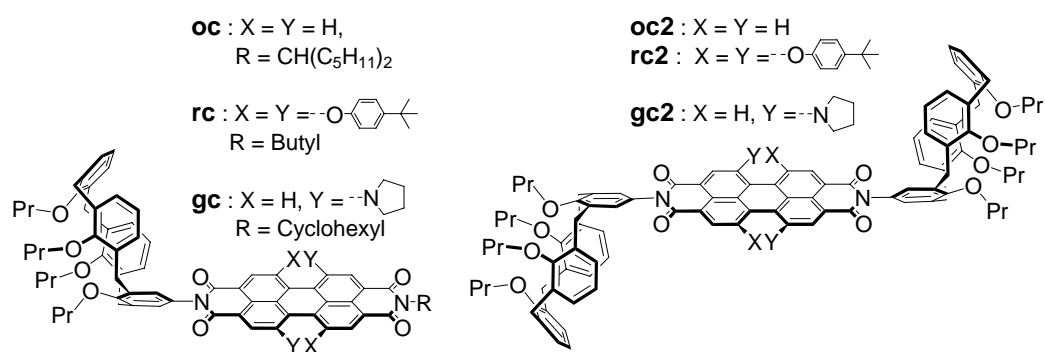
Figure 1. Chemical structures of the newly synthesized monochromophoric PBI-calix[4]arene conjugates (for details see Chapter 3).

Figure 1). A complete picture of the processes taking place after photoexcitation in toluene, CH_2Cl_2 and benzonitrile was obtained. It has been shown that calix[4]arene functionalization does not influence the photophysical properties of the red and the green PBI unit, but in contrast, substantially changes the properties of the orange fluorophore. Accordingly, the fluorescence quantum yields of the orange compounds **oc** and **oc2** are almost completely quenched compared to the highly emissive reference compound **oref** due to fast electron transfer processes from the calix[4]arene moieties to the perylene bisimide chromophore (k_{CS} = 3 x 10^{10} s^{-1} for compound **oc** and k_{CS} = 9 x 10^{10} s^{-1} for compound **oc2** in CH_2Cl_2, respectively) leading to a short-lived charge-separated state consisting of the reduced perylene bisimide unit and the oxidized calix[4]arene moiety (for a schematic representation see Figure 2). The latter CT state is characterized by the absence of stimulated emission and the presence of absorption features in the 600–750 nm region attributable to the formation of a radical anion of the perylene bisimide unit. The charge recombination kinetics show a clear solvent dependence that can be attributed to Marcus inverted region behavior. No such effects are observed for the red and green conjugates **rc**, **r2c**, **gc**, and **g2c**, respectively, which is rationalized by their more electron rich perylene bisimide cores.

Chapter 4 deals with perylene bisimide–calix[4]arene arrays composed of different orange, red and green types of perylene bisimide chromophores where the calix[4]arene scaffolds are applied to organize the chromophores in zigzag-type arrangements providing defined distances and angles between the PBI units (for chemical structures see Figure 3).
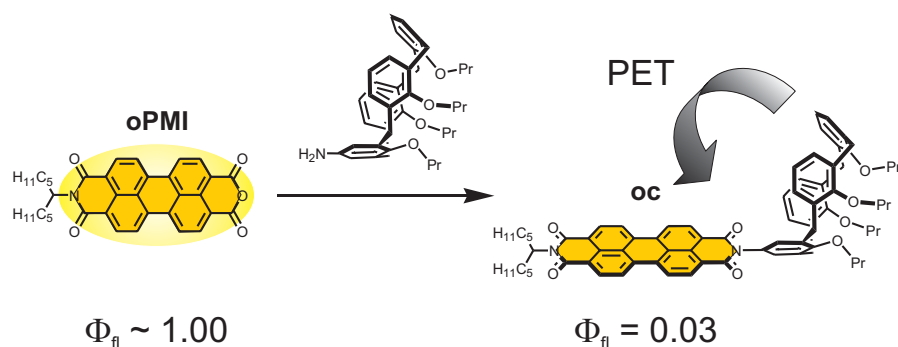
Figure 2. Schematic representation of the fluorescence quenching due to photoinduced electron transfer observed for compound **oc** upon calix[4]arene substitution of the orange PBI chromophore in CH$_2$Cl$_2$ (for details see Chapter 3).
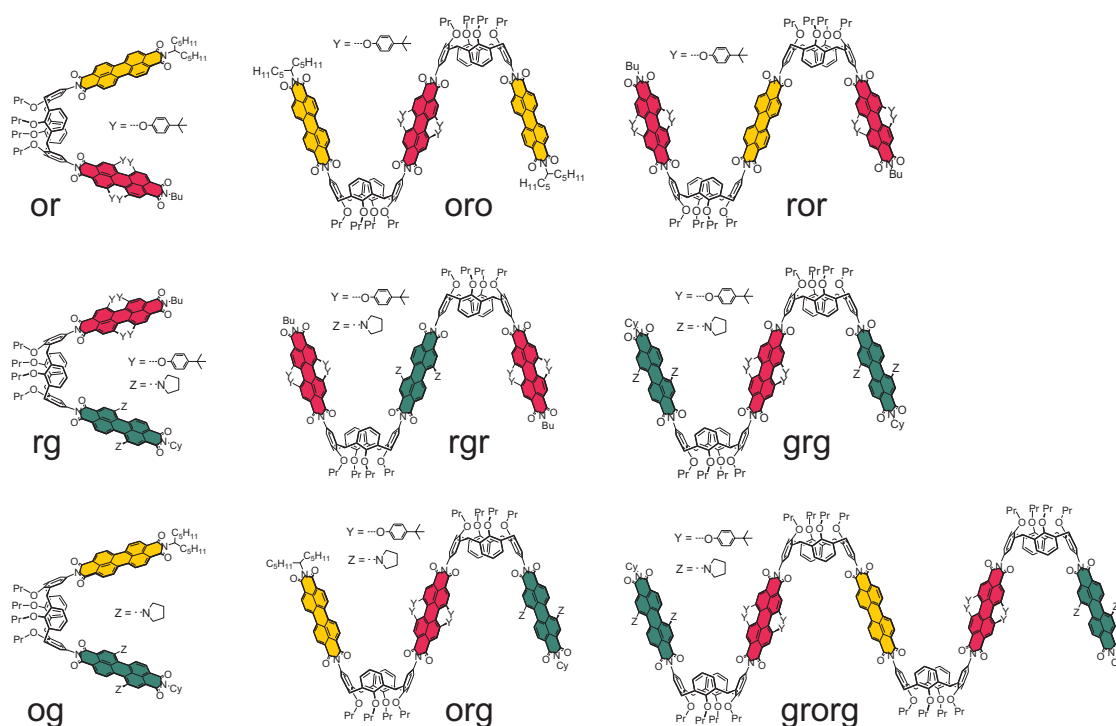

Figure 3. Chemical structures of the newly synthesized multichromophoric PBI-calix[4]arene energy transfer cascades (for details see Chapter 4).

The as such constructed arrays possess the characteristic feature that the individual chromophoric building blocks can be easily replaced by each other as well as their optical properties can be fine-tuned without influencing the overall geometric arrangement of the supramolecular system. Owing to the excellent spectral overlap of the individual dye units, these arrays display very efficient sequential energy transfer processes from the *orange* perylene bisimide chromophoric unit to the *red* chromophoric unit ($k_{ET} = 6.4 \times 10^{11}$ s^{-1} for

compound **or**), from the *red* PBI moiety to the *green* dye unit (k_{ET} = 4.0 x 10^{11}s^{-1} for compound **rg**), and slightly less efficient from the *orange* to the *green* PBI chromophore (k_{ET} = 1.5 x 10^{11}s^{-1} for compound **og**) within these systems (for a schematic representation see Figure 4). The experimentally obtained rate constants are in very good agreement with those calculated according to the Förster theory as k_{ET} = 5.9 x 10^{11} s^{-1}, k_{ET} = 4.0 x 10^{11} s^{-1}, and k_{ET} = 1.9 x 10^{11} s^{-1} for compounds **or**, **rg**, and **og**, respectively. Notably, these zigzag-type dye arrays can even harvest the photons absorbed by the orange perylene bisimide dye unit, despite the almost non-fluorescent nature of the parent calix[4]arene–perylene bisimide building block **oc**.
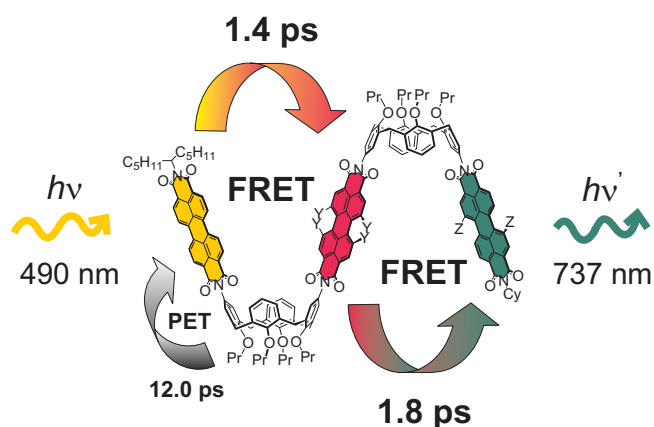
Figure 4. Schematic representation of the newly synthesized PBI-calix[4]arene light-harvesting array **org** and the excited state processes occurring after photoexcitation (for details see Chapter 4).

Finally, in *Chapter 5* a series of bichromophoric compounds **o2c**, **g2c** and **r2c**, respectively, afforded by the connection of each two identical orange, green or red PBI units via a calix[4]arene spacer unit is discussed. For all three compounds an equilibrium between the two possible *pinched cone* conformations of the calix[4]arene unit is observed, with one conformation showing a π–stacked sandwich arrangement of the PBI units and the second revealing a non-stacked conformation with the chromophores pointing away from each other. The amount of the π–stacked *pinched cone* calix[4]arene conformation in the equilibrium enhances upon decreasing the sterical encumbering of the respective PBI unit as well as upon lowering the solvent polarity, in thus increasing π–π–interactions between the PBI units. Accordingly, the presence of the π–stacked calix[4]arene conformation is most pronounced for compound **o2c** in MCH, CCl$_4$, and toluene; and to a lesser extend for compound **g2c** in MCH. Almost no π–stacked conformation is found for

217

the most sterically hindered red system **r2c**. Femtosecond transient absorption spectra of compound **o2c** in CCl$_4$ and toluene clearly reveal the spectral features of the π−stacked sandwich aggregate. Lifetime values of the excimer-like state have been determined to be 192 ps in CCl$_4$ and of 111 ps in toluene, respectively.

In conclusion, this work presents a new concept for an artificial light-harvesting system positioning the dye units by means of calix[4]arene spacers along a zigzag chain. The investigations start with the syntheses and optical properties of the monochromophoric building blocks and result in an elaborate study on the energy and electron transfer processes occurring after photoexcitation in a comprehensive series of multichromophoric calix[4]arene–perylene bisimide conjugates. Finally, the photophysical properties of a series of compounds containing each two identical PBI units are discussed.

7

Zusammenfassung

Künstliche Lichtsammelsysteme, die multiple Farbstoffeinheiten enthalten und gerichtete Energietransferprozesse zwischen den einzelnen Bausteinen realisieren, sind von hohem wissenschaftlichen Interesse, jedoch stellt die gleichzeitige Gewährleistung von Effizienz und Direktionalität immer noch eine große Herausforderung dar.

Die vorliegende Arbeit hat die Synthese und die Untersuchung der photophysikalischen Eigenschaften kovalent verknüpfter Calix[4]aren–Perylenbisimid(PBI)-Farbstoffkaskaden zum Thema, die verschiedenartige PBI-Chromophore enthalten. Dazu wurden orange (kernunsubstituierte), rote (6,7,11,12-*tert*-butylphenoxy-funktionalisierte) und grüne (1,7-pyrrolidino-substituierte) Perylenbisimid-Bausteine an ein Calix[4]arengerüst geknüpft. Zunächst wurden die monochromophoren Referenzverbindungen bezüglich ihrer photophysikalischen Eigenschaften untersucht. Im Anschluss daran wurde eine umfassende Serie von Calix[4]aren–Perylenbisimid-Farbstoffkaskaden hinsichtlich der nach Photoanregung im angeregten Zustand stattfindenden Prozesse charakterisiert. Die erhaltenen Kaskaden weisen hocheffiziente und gerichtete Energietransferprozesse zwischen den einzelnen Untereinheiten auf, deren Transferraten sich unter Annahme einer Zickzack-Anordnung der Chromophoreinheiten gemäß der Förstertheorie erklären lassen. Weiterhin wurde eine Serie von Farbstoffkaskaden, die jeweils zwei identische PBI-Chromophore enthalten, bezüglich ihrer photophysikalischen Eigenschaften untersucht. Zur Charakterisierung wurden jeweils verschiedene spektroskopische Techniken wie UV/vis-Absorptions-, stationäre und zeitaufgelöste Fluoreszenzemissions-, sowie femtosekunden-zeitaufgelöste transiente Absorptionsspektroskopie herangezogen, sowie zusätzlich eine spektrotemporale Analyse der erhaltenen Daten durchgeführt.

Das *erste Kapitel* gibt einen kurzen Überblick über unterschiedliche Konstruktionsprinzipien künstlicher Lichtsammelsysteme, die Perylenbisimideinheiten enthalten, sowie eine kurze Einführung in das Gebiet der Calix[4]arenchemie und abschließend eine Übersicht über wichtige theoretische Konzepte photoinduzierter Prozesse.

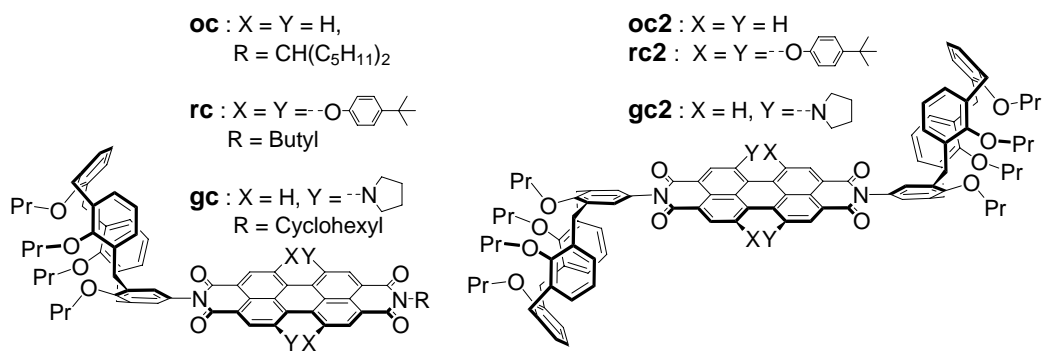Im *zweiten Kapitel* werden kurz die verwendeten spektroskopischen Techniken beschrieben.

Abbildung 1. Chemische Strukturen der neu synthetisierten monochromophoren Perylenbisimid–Calix[4]arenkonjugate (siehe Kapitel 3).

In *Kapitel 3* werden die Synthese und die photophysikalischen Eigenschaften einer Serie monochromophorer Perylenbisimid–Calix[4]arenkonjugate beschrieben, die durch Substitution dreier verschiedener PBI-Farbstoffeinheiten (orange, rot und grün) mit entweder einem oder zwei Calix[4]aren-Bausteinen in der N-Imidposition des Perylenbisimid-chromophores erhalten wurden (siehe Abbildung 1). Die vollständige Charakterisierung der Prozesse im angeregten Zustand nach Photoanregung erfolgte in Toluol, CH_2Cl_2 und Benzonitril. Bemerkenswerterweise beeinflusst die Calix[4]aren-Funktionalisierung die optischen Eigenschaften des roten sowie des grünen PBI-Chromophors nur unwesentlich, wohingegen jene des orangen Bausteins substanziell verändert werden. Es wurde gefunden, dass die Fluoreszenzemission in den orangen Verbindungen **oc** und **oc2** durch einen photoinduzierten Elektronentransfer von der Calix[4]areneinheit auf den elektronenarmen orangen PBI-Chromophor nahezu vollständig gelöscht ist (mit Transferraten von $k_{CS} = 3 \times 10^{10}$ s^{-1} für Verbindung **oc** und $k_{CS} = 9 \times 10^{10}$ s^{-1} für Verbindung **oc2** in CH_2Cl_2), wohingegen der entsprechende unsubstituierte Referenzchromophor **oref** eine Fluoreszenzquantenausbeute nahe 100% aufweist (siehe schematische Darstellung in Abbildung 2). Dieser Elektronentransferprozess führt zur Ausbildung eines ladungsgetrennten Zustandes bestehend aus dem Radikalmonoanion der Perylenbisimid-Einheit und dem Radikalmonokation des Calix[4]aren-Gerüsts, der in den transienten Absorptionsspektren zum einen durch das vollständige Fehlen der stimulierten Emission um 580 nm und zum anderen durch für das PBI-Monoanion typische Banden im Bereich von 600–750 nm charakterisiert ist. Die Kinetik der Ladungsrekombination zeigt eine Lösungsmittelabhängigkeit wie sie für die Marcus-inverse Region erwartet wird. Für die entsprechenden roten und grünen Derivate **rc**, **r2c**, **gc** und **g2c**

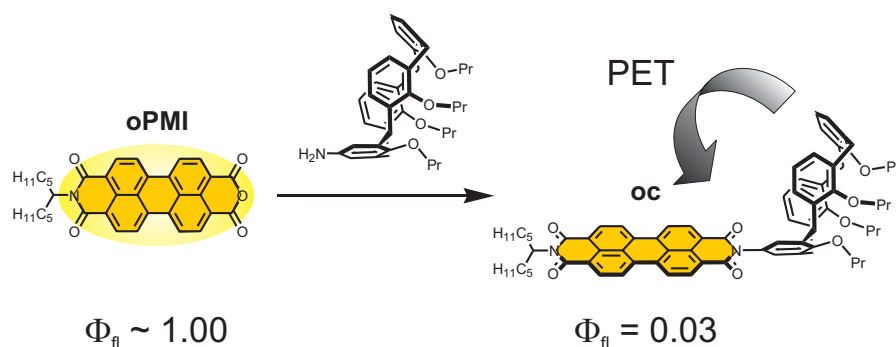$\Phi_{fl} \sim 1.00$ $\Phi_{fl} = 0.03$

Abbildung 2. Schematische Darstellung der Fluoreszenzlöschung aufgrund des photoinduzierten Elektronentransfers von der Calix[4]aren-Einheit auf den orangen PBI-Chromophor in Verbindung **oc** (siehe Kapitel 3).

wurden aufgrund der jeweils elektronenreicheren Farbstoffeinheit und der damit geringeren Begünstigung eines Elektronentransferprozesses keine solchen fluoreszenzlöschenden Effekte beobachtet.

Kapitel 4 beschreibt eine umfangreiche Serie neuartiger, multichromophorer Perylenbisimid-Calix[4]arenkaskaden bestehend aus bis zu drei unterschiedlichen PBI-Einheiten (orange, rot und grün), bei denen die einzelnen Chromophor-Bausteine durch das Calix[4]arengerüst in einer zickzack-Anordnung in definierten Abständen und Winkeln zwischen den PBI-Gruppierungen vorliegen (chemische Strukturen siehe Abbildung 3). Charakteristisch für die auf diese Weise erhaltenen Architekturen ist, dass die einzelnen Bausteine des Systems leicht gegeneinander ausgetauscht sowie ihre optischen Eigenschaften variiert werden können, ohne die räumliche Gesamtstruktur des Systems zu verändern. Aufgrund der exzellenten spektralen Überlappung der Einzelchromophore werden zwischen den einzelnen Farbstoffeinheiten hocheffiziente Energietransferprozesse vom orangen PBI-Baustein zum roten ($k_{ET} = 6.4 \times 10^{11}$ s^{-1} für Verbindung **or**), vom der roten PBI-Farbstoffeinheit zur grünen ($k_{ET} = 4.0 \times 10^{11}$s^{-1} für Verbindung **rg**), und geringfügig weniger effizient, vom orangen PBI-Baustein zur grünen Farbstoffeinheit ($k_{ET} = 1.5 \times 10^{11}$s^{-1} für Verbindung **og**) gefunden (schematische Darstellung siehe Abbildung 4). Diese experimentell erhaltenen Energietransferraten stimmen sehr gut mit den nach der Förster-Theorie berechneten Werten von $k_{ET} = 5.9 \times 10^{11}$ s^{-1} für Verbindung **or**, $k_{ET} = 4.0 \times 10^{11}$ s^{-1} für Verbindung **rg**, und $k_{ET} = 1.9 \times 10^{11}$ s^{-1} für Verbindung **og** überein. Bemerkenswerterweise können demnach die hier vorgestellten Perylenbisimid-Calix[4]arenkaskaden auch die von der orangen PBI-Komponente absorbierten Photonen nutzen, obwohl der zugrunde
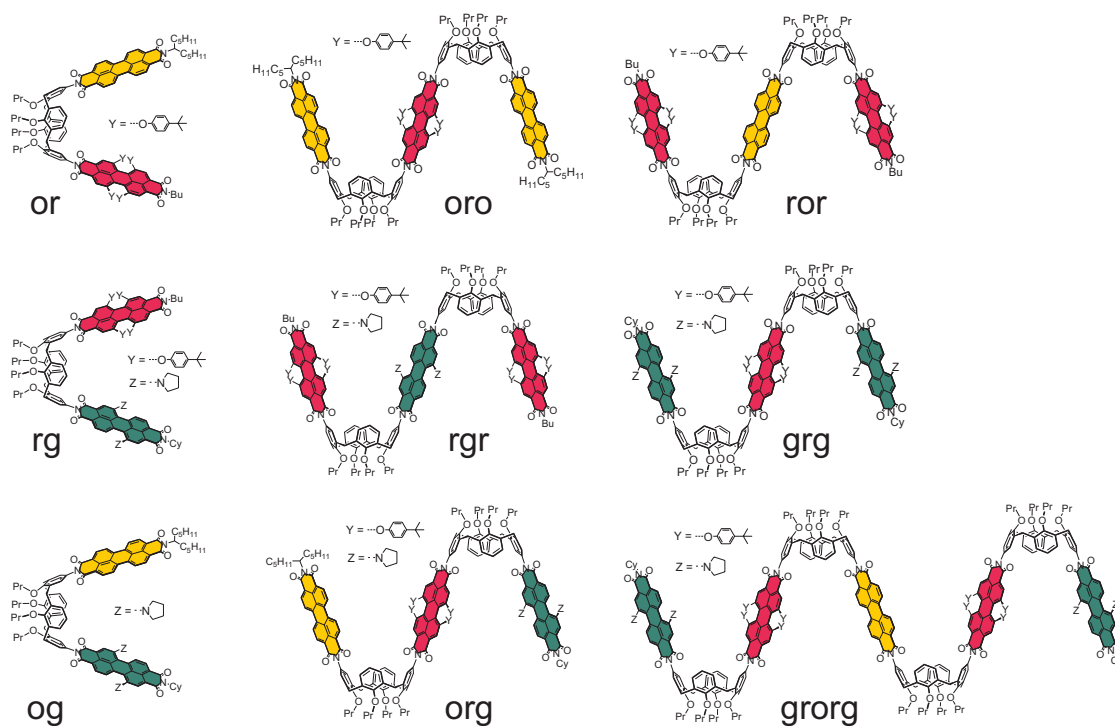
Abbildung 3. Übersicht über die neu synthetisierten multichromophoren Perylenbisimid-Calix[4]aren-Kaskaden (siehe Kapitel 4).
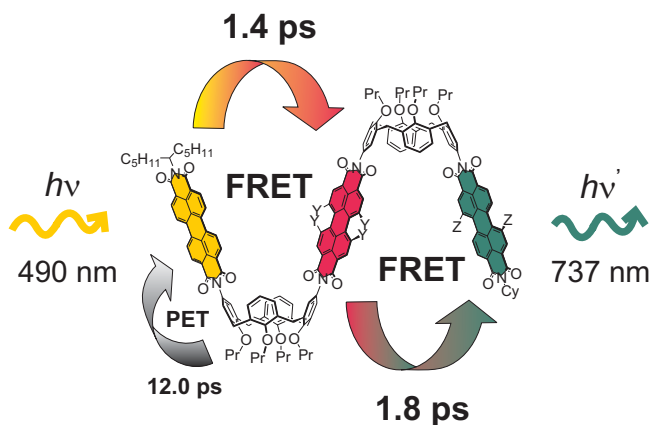

Abbildung 4. Schematische Darstellung der Prozesse nach Photoanregung der orangen PBI-Einheit in der multichromophoren Perylenbisimid-Calix[4]aren-Kaskade **org** (siehe Kapitel 4).

liegende Perylenbisimid-Calix[4]aren-Baustein **oc** nahezu keine Fluoreszenzemission aufweist. Dies ist durch eine etwa zehnfach höhere Rate für den Energietransfer- im Vergleich zum konkurrierenden Elektronentransferprozess bedingt.

223

Abschließend wird in *Kapitel 5* eine Serie bichromophorer Verbindungen **o2c**, **g2c** und **r2c** behandelt, die durch Verknüpfen von je zwei identischen orangen, roten und grünen PBI Einheiten über eine Calix[4]aren-Einheit erhalten wurde. Für alle drei Verbindungen wird ein Gleichgewicht zwischen zwei möglichen „*pinched cone*" Konformationen der Calix[4]aren-Einheit beobachtet, wobei die erste konformere Spezies eine π–π-gestapelte Geometrie der PBI-Chromophore aufweist, während in der zweiten Konformation die Perylenbisimid-Reste voneinander weg weisen. Der Anteil des π–π-gestapelten Konformers nimmt mit abnehmendem sterischen Anspruch des PBI-Substituenten sowie sinkender Lösungsmittelpolarität zu. Demnach liegt ein signifikanter Anteil des π–π-gestapelten Konformers für Verbindung **o2c** in MCH, CCl_4 und Toluol, und ein geringerer auch für Verbindung **g2c** in MCH und CCl_4 vor. Für das am stärksten sterisch gehinderte rote System **r2c** wird nahezu kein spektraler Hinweis für die π–π-gestapelte Konformation gefunden. Die femtosekundenzeitaufgelösten transienten Absorptionsspektren von Verbindung **o2c** in CCl_4 und Toluol zeigen deutlich die Ausbildung eines Excimer-artigen Zustandes, für den Fluoreszenzlebensdauern von 192 ps in CCl_4 und von 111 ps in Toluol gefunden werden.

Zusammenfassend beschreibt die vorliegende Arbeit eine neue Architektur von künstlichen Lichtsammelsystemen, deren wesentliches Merkmal eine zickzack-Anordnung der Chromophoreinheiten ist. Zunächst wurden die Synthese und die optischen Eigenschaften der monochromophoren Bausteine diskutiert, und anschließend die Energie- und Elektronentransferprozesse nach Photoanregung in einer umfangreichen Serie von multichromophoren Perylenbisimid–Calix[4]arenkaskaden untersucht. Abschließend wurden die photophysikalischen Eigenschaften einer Serie von Calix[4]aren–PBI-Konjugaten diskutiert, die jeweils zwei identische PBI Chromophore enthalten.

Acknowledgement/Danksagung

- Dörte Nowak, Marco Holzapfel, Dr. Rainer Stahl und Herrn Prof. Dr. Christoph Lambert für die vielen hilfreichen Diskussionen und helfenden Hände bei Spektroelektrochemie und Fluoreszenzmessungen.

- Herrn Dr. Matthias Grüne und Frau Elfriede Ruckdeschel für die motivierte und kompetente Messung der Tieftemperatur-NMR-Spektren.

- Herrn Dr. Michael Büchner und Herrn Fritz Dadrich für die Aufnahme der Massenspektren.

- Herrn Dipl.-Ing. Bernd Brunner für die kompetente Hilfe bei allen Computerfragen.

- Allen Mitarbeitern des Instituts für Organische Chemie der Universität Würzburg für die stete und freundliche Hilfe bei vielen kleinen und größeren Fragen.

- Frau Lieselotte Michels für die Durchführung der Elementaranalysen.

- Herrn Dr. Volker Böhmer für die gute Zusammenarbeit, die freundliche und familiäre Aufnahme in Mainz, die vielen gewinnbringenden Diskussionen zur Calix[4]arenchemie, die stete Unterstützung – und natürlich für die Einführung in die Pfälzer Weine.

- Herrn Dr. Myroslav O. Vysotsky für die gute Zusammenarbeit und Unterstützung und für seine beispielhafte Geduld bezüglich meiner unzähligen Fragen zu Calix[4]aren-NMR-Spektren.

- Frau Dr. Crenguta Dordea für die gute Zusammenarbeit, die synthetische Unterstützung bei der Calix[4]arenchemie und die schöne Zeit in Mainz.

- Allen Mitarbeitern des AK Böhmer der Universität Mainz für die freundschaftliche Aufnahme in Mainz, die stete Hilfsbereitschaft im Labor, die vielen hilfreichen Diskussionen zur Calix[4]arenchemie und für die schöne Zeit in Prag.

- Dr. René M. Williams from the Universiteit van Amsterdam for the scientific support, the fruitful discussions and for the nice stay in Amsterdam.

- Dr. Ivo H. M. van Stokkum from the Vrije Universiteit Amsterdam for the Global Analysis of the spectral data, for his scientific support and his patience.

- Prof. Dr. A. M. (Fred) Brouwer from the Universiteit van Amsterdam for the fruitful discussions, the introduction into molecular modeling and the nice time in the Molecular Photonics Group.

- John van Ramesdonk and Michiel M. Groeneveld for their help with any laser setup and for their endless patience with the impatient German girl.

- Dr. Anouk M. Rijs for everything.

- Alessandro, Deniz, Emile, Joana, Pablo, Simon and Tanzeela for the very nice time we spent together.

- Professor Dr. Ennio Zangrando and Dr. Elisabetta Iengo from the University of Trieste for the very fruitful collaboration and the crystal structure determination.

- Herrn Dr. Markus Wunderlin von der Universität Ulm für die Messung der Massenspektren.

- Dem 4. Stock, dem 2. Stock und dem ÖHC für die schöne Zeit in Würzburg.

- Meiner Familie.

Curriculum Vitae

Catharina Hippius

Date of birth: May 15th 1979

Nationality: German

PhD thesis

Since 07/2003	PhD thesis at the Julius-Maximilian-University Würzburg, Germany, Institute of Organic Chemistry, Group Prof. Dr. F. Würthner
09-12/2006	Research stay at the Universiteit van Amsterdam, The Netherlands, Molecular Photonics Group, Prof. Dr. A. M. Brouwer

Education

10/1997-09/2002	Studies in **Chemistry** at the Friedrich-Schiller-University Jena, Germany
11/2001-09/2002	**Diploma thesis** at the Friedrich-Schiller-University Jena, Institute of Organic and Macromolecular Chemistry, Group Prof. Dr. R. Beckert
09/2002	**Diploma** in Chemistry
06/1997	**Abitur**; Gymnasium „Carl Zeiss", Jena

Grants

01/2004-12/2005	**Kekulé-Scholarship** of the *"Stiftung Stipendien-Fonds des Verbandes der Chemischen Industrie e.V."* (VCI)
05/1999-09/2002	Member of the *"**Stiftung der Deutschen Wirtschaft** Klaus Murmann"* (sdw)

List of Publications

- *Sequential FRET Processes in Calix[4]arene-Linked Orange-Red-Green Perylene Bisimide Dye Zigzag Arrays*: **Hippius, C.**; van Stokkum, I. H. M.; Gsänger, M.; Groeneveld, M. M.; Williams, R. M.; Würthner, F. *J. Am. Chem. Soc.* submitted.

- *Excited State Interactions in Calix[4]arene–Perylene Bisimide Dye Conjugates: Global and Target Analysis of Supramolecular Building Blocks*: **Hippius, C.**; van Stokkum, I. H. M.; Zangrando, E.; Williams, R. M.; Würthner, F. *J. Phys. Chem. C.* **2007**, in press.

- *Photophysical Characterization of a Light-Harvesting Tetra Naphthalene Imide/Perylene Bisimide Array*: Flamigni, L.; Ventura, B.; You, C.-C.; **Hippius, C.**; Würthner, F. *J. Phys. Chem. C.* **2007**, *111*, 622–630.

- *Energy Transfer in Calixarene-Based Cofacial Positioned Perylene Bisimide Arrays*: **Hippius, C.**; Schlosser, F.; Vysotsky, M. O.; Böhmer, V.; Würthner, F. *J. Am. Chem. Soc.* **2006**, *128*, 3870–3871.

- *Light-Harvesting Metallosupramolecular Squares Composed of Perylene Bisimide Walls and Fluorescent Antenna Dyes*: You, C.-C.; **Hippius, C.**; Grüne, M.; Würthner, F. *Chem. Eur. J.* **2006***, 12,* 7510–7519.

- *Syntheses and Properties of Cycloamidines based on 4H-Imidazoles*: Beckert, R.; **Hippius, C.**; Gebauer, T.; Stöckner, F.; Lüdigk, C.; Weiss, D.; Raabe, D.; Günther, W.; Görls, H. *Z. f. Naturforsch. B* **2006**, *6*, 437–447.